

University of Nottingham



School of Mathematical Sciences

The Influence of Autocorrelation on Extremal Properties of Gaussian Random Processes, Correlated Randomness and Stochastic Periodicity

Alessandro Ogunshemi
4257690

A thesis submitted to the University of Nottingham for the degree of
Doctor of Philosophy

February 2022

ABSTRACT

Characterising the behaviour of a random process with respect to returns to previous states is a perennial concern of stochastic process theory, with applications of results spanning the applied sciences—from reliability in physical systems and networks, to the detection of surfaces in image analysis. The Gaussian stochastic process is entirely specified by its autocorrelation, a function that measures memory or time dependence in the process and whose form can lead to changes in higher order properties of the process. For a zero-mean Gaussian process the most common returns are to the zero-level, meaning an exploration of the zero-crossings—as influenced by the autocorrelation function—is a route for studying the interplay between randomness and dependence.

In this thesis, autocorrelation with two forms of periodic modulation is used to study changes in the zero-crossings of stationary Gaussian processes when the frequency of periodicity is increased. Realisations of the process are simulated for a variety of autocorrelations with either exponential or power-law decay, and the time intervals between zero-crossings are shown to be well-approximated by either finite or compound mixture distributions—the latter formulation pertaining to cases of strong dependence in crossings. Sufficient conditions for observing three different kinds of zero-crossing behaviour are determined and tested through a combination of simulation and modelling tools. Critical values of the autocorrelation's frequency and respective modulations result in three distinct power spectrum profiles, particularly so at extremely small/large cases of that dominant frequency. (1) Without the periodic modulation, power is concentrated at small frequencies, with zero as the peak frequency, so that crossing intervals have a large variance and are weakly correlated. (2) With a cosine modulation the origin is a minimum point, and the power spectrum is maximal away from the origin, resulting in wave-like sample functions with strongly correlated crossings. (3) With a cosine-squared modulation the spec-

trum contains at least three maxima including the origin, and at least two minima, leading to long sequences of regular crossings punctuated by rare but significantly large periods of no axis crossings.

Mixture distributions provide an alternative to using Markov chains and stochastic integrals to model the dependence between crossings. This approach provides the added benefit for tail estimation that expressions are all either explicit or asymptotically integrable. A closer investigation of the behaviour at extreme cases when the autocorrelation's periodicity parameter $a \geq 0$ is either zero or very large further reveals patterns in the zero-crossing sequence reminiscent of stochastic periodicity in random dynamical systems. Lacunarity, a measure of spatial heterogeneity of the crossings, reveals that at very small and large timescales there is Poisson-like behaviour, and within that range, non-Poissonian features are observed. These are moderately dissimilar when $a = 0$, but for $a \gg 1$ the deviations are significant, persist at large timescales relative to the correlation length, and contain oscillations typical of a deterministic process. Further proof of the proposed tripartite classification and ensuing analyses is demonstrated in a case study involving magnetoencephalography signal data that are approximately Gaussian distributed; level-crossings of the mean values recognise a change between two brain states associated with before and after trial participants perform a voluntary action.

ACKNOWLEDGEMENTS

My supervisors Keith Hopcraft and Simon Preston have been exceptional in their support throughout my PhD. Conceiving the project and steadying my wanderings; providing insightful suggestions that led to weeks of fruitful investigation; and displaying generosity, patience, amiability, and faith, even when things have slowed. From meeting one to final submission, it has been my privilege as supervisee. Because of you both, I emerge an even more eager budding mathematician. Perhaps even a statistician...

Salutations to my zero-crossing progenitors, those also previously shepherded by Keith; my gratitude for your theses and other massively helpful material.

This research was funded by the University of Nottingham. I am additionally grateful for the library and computing resources; I take great pride in the tower of books (many single-copy) I amassed and guarded for years. More than these, I would like to thank university staff—both those with and without welfare in their job title—that have truly cared for my welfare during my time here. I am especially indebted to my attentive and trusting doctor at Cripps Health Centre for years of calm reassurance, assistance, dedication, and just generally being a great person.

My family (brother, dad and mum), though separated by distance for long stretches of time, have still blessed me: deep conversations; home-made cake and other scrumptious delights; replays of precious moments; companionship from shared entertainment choices; continual prayers; being cool in their individual ways. Where I am today is strongly correlated and influenced by the years my loving parents spent raising me and investing in my future, so: e ʒeun fun gbogbo. To all my friends (both young and old-er than me), and my caring extended family: I am thankful for the kindness and optimism repeatedly demonstrated in word and deed, to the point of accelerating my achievements by addressing me with grand greetings.

Finally, and with sincerity, I thank God that my current studies are at an end.

Dedicato ai miei genitori — grazie per sempre ricordarmi di casa.

CONTENTS

List of Tables	xii
List of Figures	xiii
Glossary of Symbols and Terms	xvi
1 INTRODUCTION	1
1.1 The Level-Crossing Problem	3
1.2 Applications of The Level-Crossing Problem	4
1.3 Case Studies	6
1.3.1 Case Study 1: Wave Periods in Combined Sea States	6
1.3.2 Case Study 2: Geological Fractures	6
1.3.3 Case Study 3: Sleep States	7
1.4 Original Contributions	8
1.5 Publications	9
1.6 Thesis Outline	9
2 LITERATURE REVIEW	16
2.1 Gaussian Processes	16
2.1.1 On the Prevalence of Gaussian Processes	18
2.1.2 Stochastic Memory	19
2.2 Zero-Crossing Theory	20
2.2.1 Crossing Counts	20
2.2.2 Crossing Intervals	21
2.2.3 The Interval Density	24
2.2.3.1 Laplace Transform Method	26
2.2.3.2 Slepian Regression Method	27

2.3	Mixture Distributions	29
2.3.1	Finite Mixtures	29
2.3.2	Compound Mixtures	30
2.4	Parameter Estimation	32
2.4.1	Method of Moments	33
2.4.2	Maximum Likelihood Estimation	34
2.4.3	Comparison of MOM and MLE	35
2.5	Lacunarity	36
2.5.1	Origins	36
2.5.2	Computation	37
2.5.3	Lacunarity of Stationary Gaussian Processes	38
2.6	Roots of a Stochastic Time Series	38
2.7	Reference Processes	40
2.7.1	Random Telegraph-Wave	41
2.7.2	Random Cosine-Wave	42
2.7.3	Periodicities and Returns	42
2.8	Summary	44
3	SIMULATIONS OF OSCILLATORY CORRELATED GAUSSIAN PRO- CESSES	46
3.1	Autocorrelations and Power Spectra	46
3.2	Simulation Methods	50
3.2.1	Discretisation of Time	50
3.2.2	Generating a Random Process	51
3.2.3	Zero-Crossing Statistics	54
3.3	Simulation Results	56
3.3.1	Convergence of Algorithm	57
3.3.2	Sample Functions	58
3.3.3	Interval Moments	62
3.4	Stochastic Periodicity Revisited	64
3.5	Summary	67

4	FINITE MIXTURE MODELS FOR THE INTERVAL DENSITY	69
4.1	Preliminaries	70
4.1.1	Properties of Class 0 Processes	70
4.1.2	A Basis Distribution	72
4.1.3	Solution Methods	74
4.2	Results	75
4.2.1	Smooth Processes	76
4.2.1.1	Squared Exponential	76
4.2.1.2	Sinc Type 1	77
4.2.1.3	Power-Law	79
4.2.1.4	Sech	79
4.2.1.5	Sinc Type 2	80
4.2.2	Sub-Fractal Processes	80
4.2.2.1	Exponential Sum	81
4.2.2.2	Sine Convolution	83
4.2.2.3	Matérn	84
4.2.2.4	Cosine-Exponential Product	84
4.2.2.5	Butterworth	85
4.2.3	Dependence in Class 0 Processes	85
4.3	Summary	88
5	COMPOUND MIXTURE MODELS FOR THE INTERVAL DENSITY	90
5.1	Motivation	92
5.1.1	Power Spectrum Changes	92
5.1.2	Sample Function Changes	95
5.2	Generalised Random Variable for Crossing Intervals	96
5.2.1	Derivation	96
5.2.2	The Latency Density	98
5.2.3	Refinements for Sub-Fractal Processes	100
5.3	Results	101
5.3.1	Class 1 Processes	101

5.3.2	Class 2 Processes	105
5.4	Latency in Classes 1 and 2 Processes	105
5.5	Summary	111
6	PATTERNS AND OTHER PROPERTIES OF THE CROSSING SE- QUENCE	112
6.1	Zero-Crossing Trace	113
6.1.1	Class 0 Processes	113
6.1.2	Class 1 Processes	114
6.1.3	Class 2 Processes	115
6.2	Lacunarity	117
6.2.1	Poisson Process	120
6.2.2	Cosine Wave	120
6.2.3	Non-Oscillatory Gaussian Processes	121
6.2.4	Oscillatory Gaussian Processes	123
6.3	Counting Distributions	125
6.4	Zero-Crossing Orbits	128
6.4.1	Phase Space Diagrams	128
6.4.2	Correlation Coefficients	131
6.5	Summary	132
7	ZERO-CROSSING ANALYSIS IN PRACTICE	134
7.1	Lacunarity: Continuous vs Gliding Box Methods	134
7.1.1	Criticisms of Gliding Box Lacunarity	135
7.1.2	Comparisons in the Independent Case	136
7.1.3	Comparisons in the Dependent Case	137
7.2	Case Study 4: MEG Signals	139
7.3	Summary	141
8	CONCLUSION	144
8.1	Discussion	144
8.2	Chapter Summaries	147

8.3	Future Work	152
8.3.1	Additional Processes	152
8.3.2	Count Distributions	153
8.3.3	Stochastic Periodicity	155
A	POWER SPECTRA OF CLASS 0 PROCESSES	158
A.1	Special Functions	158
A.2	Smooth Processes	158
A.3	Sub-fractal Processes	159
B	PROBABILITY DISTRIBUTIONS	161
B.1	Normal Distribution	161
B.2	Uniform Distribution	162
B.3	Exponential Distribution	162
B.4	Gamma Distribution	162
B.5	Weibull Distribution	163
B.6	Exponential Product Distribution	163
B.7	Beta Distribution	164
B.8	Wong's Density Function	164
C	TAIL BEHAVIOUR OF THE INTERVAL DENSITY	166
D	HIGHER ORDER DISTRIBUTIONS	171
E	FORMULAE FOR CONTIGUOUS AND GLIDING BOX COUNT METHODS	175
E.1	Contiguous Boxes	175
E.2	Gliding Boxes	176
E.3	Relation to Counting Distributions	178
F	PARAMETER VALUES AND ADDITIONAL STATISTICS: CLASS 0 DENSITIES	180
G	PARAMETER VALUES: CLASSES 1 AND 2 DENSITIES	184

H	MATLAB CODE FOR SIMULATING A CORRELATED RANDOM PROCESS	187
I	MATLAB CODE FOR COMPUTING LACUNARITY	194
J	MATLAB CODE FOR COMPUTING THE INTERVAL DENSITY AND CROSSING COUNT DISTRIBUTIONS	198
	References	203

LIST OF TABLES

4.1	Summary of finite mixture models for class 0 smooth processes	77
4.2	Summary of finite mixture models for class 0 sub-fractal processes	82
5.1	Critical values of the periodicity parameter a for a class 1 process	93
F.1	Further statistics for class 0 smooth processes	182
F.2	Further statistics for class 0 sub-fractal processes	183

LIST OF FIGURES

1.1	Illustration of deterministic periodicity	2
1.2	Schematic for the level-crossing problem	3
3.1	Algorithm 1: iterative Fourier filtering method	53
3.2	Comparison of analytical and simulation estimates of correlation functions	59
3.3	Demonstration of convergence of the iterative Fourier filtering method	59
3.4	Realisations of the processes g_1 and g_2	60
3.5	Realisations of the processes ρ_{1j} and ρ_{2j}	62
3.6	Comparison of analytical and simulation estimates of the variance of crossing intervals for processes ρ_{1j} and ρ_{2j}	64
3.7	Comparison of analytical and simulation estimates of the correlation coefficient of crossing intervals for processes ρ_{1j} and ρ_{2j}	65
3.8	Plot showing changes to the periodicity density as the periodicity parameter a increases	66
4.1	Plots of the interval density for class 0 smooth processes	78
4.2	Plots of the interval density for class 0 sub-fractal processes	83
4.3	Plot illustrating the roles of mixture density components	86
4.4	Comparison of Laplace inversion and finite mixture models for the interval density	88
5.1	Plots demonstrating how the power spectrum $S_{ij}(\omega)$ changes as the periodicity parameter a increases	93
5.2	Sample function plots showing new crossings are introduced as a increases	96

5.3	Plots of the compound mixture model when the periodicity density is used as the mixing density	99
5.4	Plots illustrating changes to the interval density asymptotics as crossing dependence increases	100
5.5	Plots of the interval density and its models for the process ρ_{11} , for specific values of $a > 0$	103
5.6	Plots of the interval density and its models for the process ρ_{21} , for specific values of $a > 0$	104
5.7	Plots of the interval density and its models for the process ρ_{12} , for specific values of $a > 0$	106
5.8	Result of applying nonlinear regression to the compound mixture model for the process ρ_{12}	107
5.9	Plots of the latency density for processes ρ_{11} and ρ_{12} as a increases	108
5.10	Plots illustrating tail behaviour of the interval density for processes ρ_{1j} when $a = 10$	109
6.1	Plots of the normalized zero-crossing trace for processes g_1 and g_2	114
6.2	Plots illustrating clustering of zero-crossings for the process ρ_{11} when $a = 100$	116
6.3	Plots illustrating clustering of zero-crossings for the process ρ_{12} when $a = 100$	118
6.4	Plot showing high variability of crossing trace for the process ρ_{12} when $a = 100$	119
6.5	Plots of lacunarity and log-lacunarity slope for processes g_1 and g_2	122
6.6	Plots of lacunarity and log-lacunarity slope for oscillatory Gaussian processes when $a = 100$	124
6.7	Counting distributions for a Poisson process and a cosine wave	126

6.8	Counting distributions and maximum crossing counts from simulations of processes ρ_{1j}	127
6.9	Zero-crossing orbits for processes ρ_{1j}	130
6.10	Plots of Kendall's tau coefficient for processes ρ_{1j} and ρ_{2j}	132
7.1	Plots of contiguous and gliding box numerical lacunarity for a Poisson process	137
7.2	Plots of contiguous and gliding box numerical lacunarity for stationary Gaussian processes	138
7.3	Plots illustrating approximate normality of the MEG signals studied	140
7.4	Power spectrum plots for MEG signals	141
7.5	Results from a zero-crossing analysis of MEG signals . . .	143
8.1	Plots relating to absolute log returns of GBP:USD exchange data in April 2016.	154
8.2	Plots of the unwrapped phase for stationary Gaussian processes with strong oscillatory correlation	157
D.1	Finite mixture models applied to summed crossing intervals	173

GLOSSARY OF SYMBOLS AND TERMS

The lists below represent the main symbols and notation used throughout the thesis, contextualised to the zero-crossing problem and in keeping with related literature. In numerical simulations, Δt is the discretisation length, and n_{\max} is the sample length. Below, vectors are primarily included in element form.

Independent Variables

η	periodicity/latency variable
r	box size
t	time
T	crossing interval
τ	delay (time)
ω	angular frequency

Dependent Variables and Related Sets

$D_{x(t)}$	set of periodicities in sample function $x(t)$
D_c	set of time intervals between returns of $x(t)$ to level c
$f_S(\eta)$	periodicity density
$F(r)$	Fano factor at box size r
$\mathcal{N}(r)$	counting process at time-length r
$p(T)$	interval density
$P(T)$	cumulative density function of crossing intervals
$P_N(\mathcal{N}(r))$	probability mass function for counting process $\mathcal{N}(r)$
$S(\omega)$	power spectrum
$S_{ij}(\omega)$	model power spectrum
$U(T)$	Rice's interval density
$x(t)$	sample function
$\Lambda(r)$	lacunarity at box size r
$\lambda(r)$	log-lacunarity slope at box size r

$\zeta(t)$	sign of sample function $x(t)$
$\rho(\tau)$	autocorrelation
$\rho_{ij}(\tau)$	model oscillatory autocorrelation: $\rho_{ij}(\tau) = g_i(\tau) \cos^j(a\tau/\sqrt{j})$, for some autocorrelation $g_i(\tau)$, with $j = 1$ or 2

Vectors and Related Functions

$\ell(T; \alpha)$	loglikelihood function for simulation data T , given mixture parameters α
$M_j(r_n)$	j -th box mass of size $r = r_n$
N_n	total crossing count at time t_n
t_n	n -th discretised time point: $t_n = \Delta t(n - 1)$
τ_n	n -th discretised delay (time) point
T_k	k -th simulated crossing interval
r_n	n -th box size
x_n	n -th element of a realisation of $x(t)$
X_m	m -th element of discrete Fourier transform of x
z_n	crossing indicator of x for time interval $[t_{n-1}, t_n]$
ζ_n	sign of x_n
ω_n	n -th angular frequency

Averages and Derivatives

a_m	odd derivatives of $\rho_{ij}(\tau)$; $m = 0, 1, 2, \dots$
b_m	even derivatives of $\rho_{ij}(\tau)$; $m = 0, 1, 2, \dots$
c_v	coefficient of variation: $c_v = \sigma_T / \mu_T$
\bar{R}	rate of crossings in sample function $x(t)$
\bar{R}_M	rate of maxima in sample function $x(t)$
$\bar{\eta}$	modal periodicity
κ_1	correlation coefficient of adjacent crossing intervals
κ_τ	Kendall's tau correlation coefficient
μ_T	mean of crossing intervals: $\mu_T = \langle T \rangle$

σ_T^2 variance of crossing intervals

Parameters

a	periodicity parameter
$a_k, b_k, c_k, d_k, v_k, w_k$	scale and shape parameters for mixture component density k
L	correlation length
α_k	weight parameter for mixture component density k
Θ	persistence exponent

Operators

$\lceil \cdot \rceil$	ceiling function
$\langle \cdot \rangle, E[\cdot]$	expectation
$\lfloor \cdot \rfloor$	floor function
$\mathcal{F}[\cdot]$	Fourier transform
$\mathcal{L}[\cdot]$	Laplace transform
$\max\{\cdot\}$	maximum
$\min\{\cdot\}$	minimum
$\mathcal{O}(\cdot)$	big Oh
$\Pr\{\cdot\}$	probability
$\text{Var}[\cdot]$	variance

Abbreviations

CB	Contiguous Box
cdf	cumulative density function
CW	Cosine-Wave Process
DFT	Discrete Fourier Transform
DFT^{-1}	Inverse Discrete Fourier Transform
FFM	Fourier Filtering Method
FFT	Fast Fourier Transform

GB	Gliding Box
iFFM	Iterative Fourier Filtering method
LCP	Level-Crossing Problem
MATLAB	MATrix LABoratory: Programming and numeric computing platform by The MathWorks, Inc.
MLE	Maximum Likelihood Estimation
MOM	Method of Moments
pdf	probability density function
RNG	Random Number Generator
TW	Telegraph-Wave Process
ZCA	Zero-Crossing Analysis
ZCP	Zero-Crossing Problem

Other Notation

e	scientific notation: e.g. $1e-03 = 1 \times 10^{-3} = 0.001$
g_i	Gaussian process with autocorrelation $g_i(\tau)$
$H(t)$	Heaviside step function: $H(t) = 1 (t > 0), 0 (t \leq 0)$
$H_1(m)$	discrete Heaviside step function: $H_1(m) = 1 (m \geq 0), 0 (m < 0)$
\mathbf{i}	imaginary unit: $\mathbf{i} = \sqrt{-1}$
\mathbb{N}	set of natural numbers; \mathbb{N}_0 includes zero
\mathbb{R}	set of real numbers; $\mathbb{R}_{\geq 0}$ is the non-negative subset
\mathbb{Z}	set of integers
$\delta(t)$	Dirac delta function: $\delta(t) = \infty (t = 0), 0 (t \neq 0)$
$\delta_1(t)$	unit delta function: $\delta_1(t) = 1 (t = 0), 0 (t \neq 0)$
$\delta_{mn}, \hat{\delta}_m(n)$	Kronecker delta function: $\delta_{mn} = 1 (m = n), 0 (m \neq n)$
ρ_{ij}	Gaussian process with autocorrelation $\rho_{ij}(\tau)$
\in	in
\forall	for all
\exists	there exists

INTRODUCTION

The study of randomness has grown significantly since its foundations in 17th century games of chance [1]. The more formal idea of a random process now suffuses the applied sciences, playing a significant role in refining deterministic models (e.g. incorporating a stochastic dependent variable into a differential equation model of vibration in a mechanical system [2]), likewise in the simulation of discrete/continuous events (e.g. finding the waiting time for customers in queues [3]). Obtaining a characterisation of the random behaviour remains a central objective when analysing mathematical objects or data that are stochastic in nature, whereupon explanations and/or predictions are possible. One particular interest is the degree of correlation between states or values of a random process, and for realisations of that process the autocorrelation function provides a measurement of memory relative to previous values. The autocorrelation of a time-varying process usually has at least one time-scale, a correlation decay-length typifying the range of time over which dependence on the past persists. Long-term correlation has been shown to preclude the clustering of extremal events [4], and additional time-scales imbue further dependence in the process, for example: modulation of an autocorrelation with a periodic function serves to regularise extremal properties, demonstrated by increased frequency of zeros and turning points [5].

Periodic functions have also been applied in discrete and continuous dynamical systems where of interest is the evolution from an initial configuration into stable, cyclical or unstable behaviour [6]. In the discrete case, highly organized structures relative to equilibrium points and attractors are observed in two-dimensional plots

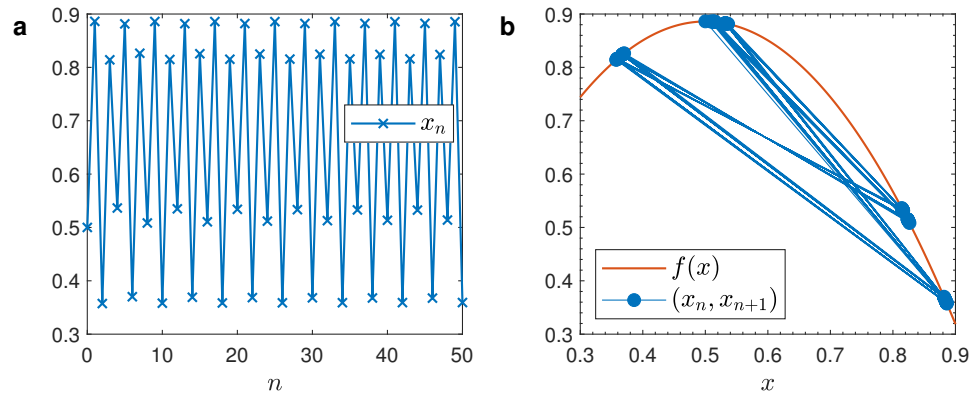


Figure 1.1.: Illustration of deterministic periodicity. Time series (plot a) and phase diagram (plot b) for the logistic map $x_{n+1} = f(x_n)$, where $x_0 = 0.5$, $f(x) = \gamma x(1 - x)$, and $\gamma \approx 3.545$ is such that as $n \rightarrow \infty$, the oscillations in x_n repeat every eight iterations [7].

of sequential mappings of the form $x_{n+1} = f(x_n)$, $n \in \mathbb{N}_0$; similarly in the continuous case, but for systems of differential equations like $\dot{x} = f(x, t)$, $t \in \mathbb{R}_{\geq 0}$, with attractors termed limit cycles. The logistic map (e.g.[6]) constrained to the interval $[0, 1]$ exemplifies deterministic periodicity (see Fig. 1.1) provided the growth rate γ satisfies $3 \leq \gamma \leq \gamma_\infty \approx 3.5699$; and for $\gamma > \gamma_\infty$ the evolution is chaotic, an exhibition suggestive of randomness and yet is completely deterministic. Stochastic periodicity has been investigated in dynamical systems prescribed by stochastic differential equations (e.g. [8]), and there equilibrium states are of two kinds: stationary solutions, which are random variables independent of shifts in time; random periodic solutions, which consist of an infinite family of curves traversed from one to the other as time progresses. The latter differs in the deterministic case for which a periodic solution is a closed curve such that if the system starts at such a curve its orbit remains on that curve. Thus, stochastic periodicity manifests differently from the deterministic kind, but there is still a boundedness to the behaviour.

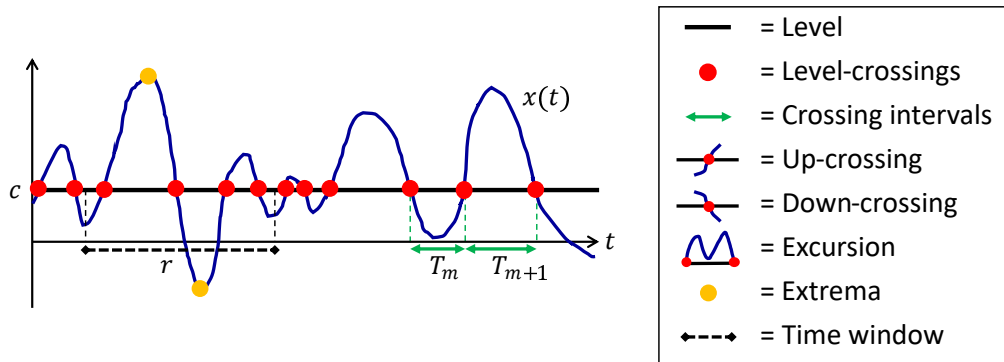


Figure 1.2.: Schematic for the level-crossing problem. Level crossings occur when the sample function $x(t) = c$, $c \in \mathbb{R}$, and the time duration between these points are termed crossing intervals. Up-/down-crossings are level-crossings with positive/negative slope. An excursion is the segment of the sample function between two level crossings. Also indicated are two extrema of $x(t)$, a maximum and a minimum point.

1.1 THE LEVEL-CROSSING PROBLEM

Degrees of randomness, correlation in time, and detection of patterns are represented in the 'level-crossing problem' (LCP), which studies the behaviour of random processes with respect to returns to a prescribed level, so as to establish the frequency and dependence structure of the time intervals between returns or crossings. Figure 1.2 illustrates some of the associated attributes that may be extracted from the sample function $x(t)$ of a random process: the time duration between crossings; the number of level-crossings and extrema in fixed time windows; the behaviour of excursions after a crossing. Each of these give rise to random variables that enable classification of extremal properties of the sample function as a whole. In the case where the level $c = 0$ either because the zero-level is of particular interest, or the prescribed level has been incorporated into the definition of $x(t)$, the research topic is then the 'zero-crossing problem' (ZCP), and this shall be the main phrasing in subsequent chapters.

1.2 APPLICATIONS OF THE LEVEL-CROSSING PROBLEM

Historical accounts of the LCP usually start with Rice's detailed study [9, 10] of noise arising as a result of random fluctuations in the flow of electrons in physical devices, and his presentation cemented the utility of the spectral representation of stochastic processes. Elsewhere in electronic engineering, zero-crossings have been pivotal in monitoring and decision making processes for various networks. Quality, continuous mobile communication is maintained by network algorithms that decide which base station handles incoming and outgoing radio signals, and switching (or handoff) occurs when the signal from another base station exceeds a critical value (see [11, 12]). Instability in power systems can be inferred from stability in the associated frequencies, as decline/increase from nominal frequency values is indicative of energy shortage/excess [13, 14].

Applications of the level-crossing problem in mechanical engineering include: finding the steady state distribution of the water level in a dam with a general release rule [15]; modelling the asymmetric distribution of ocean waves which exhibit both Gaussian and non-Gaussian characteristics [16]; examining statistics of the horizontal wind flow speed in wind power systems [17]; and intermittency, a natural environment for level-crossing perspectives, being the irregular shifting of a system in and out of less active states [18]. The zero-crossing rate (ZCR) has been a ubiquitous measure in textural analysis of image and speech data, [19, 20, 21]. There the task is to first represent the data as a curve, and then use a numerical algorithm to extract essential features, detect boundaries, and discard noisy data. Encoded information can be thought of as data with a correlation structure.

Machine learning is a modern computational tool in which numerical algorithms and statistical models are used to find and predict patterns in data sets. The two main categories are 'supervised learning' (data presented with labels) and 'unsupervised learning' (data presented unlabelled). Zero-crossings enter as a convenient method to simplify data, and through their summary statistics establish features of time series data. When this is repeated for other time-domain and frequency-

domain attributes, a vector of features is obtained, which acting as an identifier can then be used to establish associations that can only be accessed numerically [22]. These approaches are particularly useful in analysis of sound data, examples of which include: distinguishing between speech from a health or unhealthy (due to some pathology) individual [23]; determination of bat species from echolocation calls [24]; and earthquake source characterisation prior to seismic events [25].

Whilst the LCP usually involves a correlated random process, the crossing framework readily finds application in diverse fields of theoretical research. In ‘system point analysis’ a sample path is constructed such that its level-crossings represent state changes of a particular stochastic process [26]. Classical extreme value theory usually applies to the extrema of independent and identically distributed random variables; a comprehensive account of the theorems relating to extremal properties of random sequences and processes which puts the LCP in the extreme value context is given in [27]. Another related and major research area relating to stochastic processes is that of so called first-passage and escape times—the first and subsequent times that a process crosses and exists a barrier (see [28]). Closely connected is the idea of ‘persistence’ [29], which using the schematic in Fig. 1.2 is the probability that $x(t)$ has a long positive excursion; that is

$$\Pr \{x(t) > c \mid x(s) = c\} \quad \text{for } t \in (s, s + T), s \in \mathbb{R} \quad \text{as } T \rightarrow \infty. \quad (1.1)$$

The idealised framework of characterising a random process by returns to prescribed levels means developments in level-crossing theory enable further applications, as seen in possibly the most general contribution to date: the Wave Analysis for Fatigue and Oceanography numerical package (see [30] and references therein), which enables simulation of random processes, whether Gaussian or non-Gaussian, and accepting as inputs either empirical data or appropriate analytical functions. Also possible is corresponding numerical computation of marginal and joint probability density functions for intervals between level-crossings, and heights of extrema.

1.3 CASE STUDIES

Before outlining the work in this thesis, we shall briefly spotlight certain contemporary applications which especially embody the approaches we take in tackling the zero-crossing problem. A common theme is the launching of real-world data analysis after exploring a range of computer-generated data. Nomenclature relating to the analyses is expanded further in subsequent chapters.

1.3.1 *Case Study 1: Wave Periods in Combined Sea States*

Context [31]: In oceanography, a wave period is the time spent between the peaks of two ocean waves relative to a prescribed level. The wave period and its density are important in probabilistic descriptions of sea states. Real sea states can consist of wind waves and swells, and this dual nature makes difficult a combined statistical representation of the system. Mixture models are one way to capture the increased complexity in wave period distributions, and they avoid the unsuitable assumptions behind traditional theoretical distributions.

Analysis: The data consist of nine combined sea states simulated via a commonly used two-peaked power spectrum, and field data (collected by buoys) with two sea states. The analysis was performed on up-crossings of the zero-level, with the time intervals assigned mixture models that separated wind-sea and wind-swallow dominated sea states.

1.3.2 *Case Study 2: Geological Fractures*

Context [32]: The spacings within rock formations are collectively labelled fractures, and their structure affects fluid flow such that the rocks are either a barrier or a conduit. Fracture modelling is therefore critical for predicting fluid flow, and extracting fluids (e.g. water, gas and oil), and the first step is characterising existing fracture data. Scan lines are constructed by identifying points along a line where a

fracture is present or absent. (Under the ZCP nomenclature fracture locations are analogous to zero-crossing locations.) The concept of lacunarity is used to classify fracture randomness and clustering.

Analysis: Lacunarity based classification is applied both to synthetic data with known fractal features, and geological data on carbonate rocks. Significant breaks in the log-lacunarity slope match with critical spacings between fracture clusters, and these corresponded to length scales for both cluster and inter-cluster distance.

1.3.3 Case Study 3: Sleep States

Context [33]: The human electroencephalogram (EEG) enables monitoring of electrical activity in the brain. Taking measurements of potential difference from differently positioned electrodes, the activity from different areas integrate so intricately that the EEG may be regarded as a time series. Yet, because neural electrical signals in their function carry important physiological information, there will also exist short term structure and regularity. Whilst clinicians are trained to ascribe different EEG wave forms to brain states, it is convenient and efficient to automate the process using mathematical and computational tools. Zero-crossings can be used to assign frequencies to EEG signals and thereby detect rhythms, and lacunarity can reveal further details.

Analysis: Lacunarity is used to establish similarities and dissimilarities in the four phases of sleep that humans alternate through during the night. Comparing the lacunarity curves to a surrogate pure random process demonstrates that as sleep deepens, the EEG signals show more irregularity. Characteristic times obtained by finding the maximum lacunarity curvature are identifiable with each particular sleep phase.

1.4 ORIGINAL CONTRIBUTIONS

There are three essential frameworks through which this thesis adds to current zero-crossing literature.

1. Classification of stationary Gaussian processes. Analytical investigations into the ZCP seek to predict crossing behaviour directly from a process's governing equation (e.g. autocorrelation, power spectrum, differential/regression equation). Here we demonstrate that for a stationary Gaussian process, the behaviour can be divided into three classes which are attributable to three power spectrum forms. To the author's knowledge, only two of those classes are found in the literature, possibly due in part to historical application-driven analysis in the areas of telecommunications and oceanography.

2. Mixture models for crossing intervals. As will be evidenced in the literature review, the complex nature of dependent zero-crossing intervals is reflected in a long record of analytical results that shed light on non-trivial and surprising aspects of the ZCP. Here we pair data simulated from an exhaustive list of power spectrum forms, with the construction of different mixture models informed by established results. In this way, the usual direction of analysis is in a sense reversed. Furthermore, by setting up an optimisation problem, we align the discussion with the aforementioned machine learning perspective, in particular, regression which falls under supervised learning.

3. Lacunarity and crossing dependence. Zero-crossings of non-Markov, stationary Gaussian processes are dependent, and this long-standing result is further interrogated using the concept of lacunarity. We are keen to emphasise the geometrical nature of the ZCP—different from fractal processes, and imbued with non-trivial patterns captured by the lacunarity measure. The role of the tripartite classification is again well demonstrated. Another important contribution of this work is the detailed critique of the gliding-box algorithm used prolifically in numerical lacunarity computations, despite previous critiques. The zero-crossings of simulated one-dimensional processes provide a context to evaluate the algorithm and reliabil-

ity of the resulting statistic absent from issues relating to orientation and limited computing resources, each of importance in data of two dimensions and higher.

Supplementary to the frameworks just listed, the work here brings together ideas from different sub-disciplines of applied statistics: frequency-based analysis; Monte-Carlo simulation methods; point process theory; parametric inference; numerical optimisation; stochastic geometry; and, of course, Gaussian processes. It is hoped that these connections help expand the audience of thesis. Mixture models are not discussed in the publication related to this work, and the models provide a novel mechanism that by analogy tracks the effects of strong crossing dependence.

1.5 PUBLICATIONS

The paper “Lacunarity of the zero crossings of Gaussian processes” [34] arose out of the work covered in this thesis. Its main themes are: a critique of box-counting methods for lacunarity computation of time series; and a study of the various lacunarity signatures arising from oscillatory autocorrelation in stationary Gaussian processes. The contributions by the present author included numerical simulations and related computational aspects. Derivations and evaluation of the main ideas, together with the write-up, were jointly contributed with the other authors.

1.6 THESIS OUTLINE

Chapter 2: Literature Review

This chapter begins with a survey of pertinent results of zero-crossing theory, in particular for Gaussian processes and averages relating to attributes marked in Fig. 1.2. Next, two established methods for computing the probability density of time intervals between zero-crossings are described: (1) Markov chain and Laplace transform methods; (2) Slepian-regression models and evaluating conditional expectations. Following that, the two main analytical tools of the thesis—mixture modelling and

lacunarity—are summarised and shown to be useful for the ZCP. Finally, descriptions and elementary properties are given for two non-Gaussian stationary processes that represent extremes of crossing dependence: (1) a random telegraph-wave in which zero-crossings form a Poisson process, so that crossing intervals are independent; (2) a cosine-wave for which the length of all crossing intervals is the half-period of the cosine, so that crossing intervals are dependent. In later chapters Gaussian processes will be seen to exhibit similar behaviour depending on the autocorrelation function.

Chapter 3: Simulations of Oscillatory Correlated Gaussian Processes

As with many treatments in zero-crossing literature, our analysis begins with the autocorrelation. In this chapter, the governing autocorrelation function for the thesis is presented, its form chosen to explore different types of correlation decay, smoothness, and periodic modulation, the latter controlled by a periodicity parameter $a \geq 0$. The modulation is achieved using the functions $\cos(a\tau)$ and $\cos^2(a\tau/\sqrt{2})$, and as a increases, three distinct power spectrum profiles are observed, while the mean crossing interval is unchanged by the choice of cosine function. These enable a simple classification based on turning points of the power spectrum: (1) when $a = 0$, the origin is a maximum point, and power is concentrated around small frequencies; (2) when the cosine modulation is used, the origin becomes a minimum point, and maxima occur away from the origin; 3) when the cosine-squared modulation is used, the origin remains a maxima, and there are either two inflection points or two additional maxima, with minima occurring away from the origin.

Next, the algorithm used to generate realisations of each process is described and shown to converge such that the error in sample correlations is minimised. Further proof of the reliability of simulations is provided by comparison of crossing interval moments to analytical results from the previous chapter. Realisations show that as periodicity in the autocorrelation increases, sample functions begin to exhibit wave-like properties due to the increased frequency of zero-crossings and turning

points. The extent of this emergent regularity is determined by the type of periodic modulation, and less by the type of correlation decay, or smoothness of the process. All observed features agree with the subdivisions established using the power-spectrum, and thus we conclude subsequent analyses should be performed in view of the three classes.

Chapter 4: Finite Mixture Models for the Interval Density

Having validated simulation methods, this chapter considers the first class of stationary Gaussian processes, represented here by the absence of periodic modulation, and we label them as class 0. The similarity within this categorisation is further demonstrated using finite mixtures of a generalised exponential distribution to model the crossing intervals. The models incorporate known asymptotic forms for very small/large intervals, and parameter estimates are obtained via maximum likelihood estimation (MLE). Autocorrelations with either exponential or power-law correlation decay are investigated, most previously encountered in the literature, and almost all are either a summation of exponential functions, or part of a sequence that converges to the squared exponential function. Mixture models are shown to compare favourably and in some cases better than the Markov chain and Slepian-regression methods for computing the interval density.

Chapter 5: Compound Mixture Models for the Interval Density

This chapter investigates the effects of periodic modulation on the examples studied in the chapter 4, particularly the effects on the interval density. For the non-oscillatory part of the autocorrelation, we concentrate on the squared exponential, representative of smooth processes, and also Wong's exponential sum [35], representative of sub-fractal processes. Wong's process is the only case for which the interval density is known exactly; though the density is composed of elliptic integrals, the previous chapter informs us that a mixture of two exponential distributions

provides a satisfactory model. The periodic modulation introduces shifts and additions in the power spectrum, and a careful analysis identifies critical values of the periodicity parameter beyond which the aforementioned duality of spectrum profiles exist, distinct from the earlier class 0 case. We label those caused by $\cos(a\tau)$ as class 1, and those caused by $\cos^2(a\tau/\sqrt{2})$ as class 2.

For the crossing intervals resulting from the transformed spectra, a random variable is proposed to model additional crossings caused by increasing the periodic modulation—this construction influenced by discussions in the penultimate chapter of [36]. The associated distribution of the new random variable provides a way to transform the interval density in the class 0 case (where the periodicity parameter a is zero), to the densities for each of the other two classes (transitioned into beyond critical values of a). The transformation is achieved using a mixing density, itself constructed as a finite mixture, and the model parameters are again found using MLE. In addition to the generalised exponential distribution previously employed, beta distributions are used to capture new features in the density profile. Asymptotic forms are derived for the integral equation that defines the interval density, $p(T)$. According to the model, the right density-tail for a class 1 process decays like a beta density, whilst in the class 2 case the decay is like a gamma density.

Chapter 6: Patterns and Other Properties of the Crossing Sequence

Mixture models of the two previous chapters demonstrate that the long run or asymptotic behaviour of zero-crossing intervals is approximately analogous to sampling from a mixture distribution, with dependence attributable to either a discrete or a continuous mixing distribution. The crossing sequence itself is dependent in time, and so this chapter explores behaviour at extreme periodicities ($a = 0$ and $a = 100$) as determined by the counting process defined by the zero-crossings.

The lacunarity measure is used to reveal scale dependence in the crossing sequence. When $a = 0$, lacunarity signatures for the Gaussian processes are similar to that of a Poisson process. Whilst this is also true when $a = 100$ and the time scales are very

small/large relative to the mean crossing interval, at intermediary time scales, the lacunarity clearly separates the three classes of Gaussian process. Turning points in the log-lacunarity slope demonstrate more clearly the distinction from a Poisson process, for which the slope is constant. The differences are even more emphatic when $a = 100$. In the class 1 case, because the power spectra for the Gaussian and cos-wave processes are concentrated at the large frequencies $\sim \pm a/(2\pi)$, their lacunarity is also similar; however the oscillations in the Gaussian case gradually attenuate towards the Poisson limit. In the class 2 case, lacunarity decays significantly more slowly, indicative of the greater scale dependence caused by the presence of both slow and fast time scales, respectively caused by the power spectrum being concentrated at the origin as well as the larger frequencies $\sim \pm a/(\sqrt{2}\pi)$.

Following on from the lacunarity analysis, time series plots and phase diagrams of the sequence of crossing intervals are investigated more closely. At large a the crossing interval pairs encircle a diagonal line that reflect their correlation coefficient, and the display bears a strong resemblance to a stochastic dynamical system. The presentation is meant to highlight the geometric aspects of the ZCP, and expand on why a complete Markov-chain model for the crossings may be possible but will be particularly difficult.

Chapter 7: Zero-Crossing Analysis in Practice

This chapter first evaluates a common numerical method for calculating lacunarity based on gliding boxes, and identifies its limitations. The standard method of counting events which uses contiguous boxes is preferable as it allows reliable comparison with analytical results for random data sets. Following that discussion, the lacunarity measure (using contiguous boxes) is used to analyse magnetoencephalography signals for the purpose of differentiating the brain states before and after a button is pressed. After the button press, level-crossings of the mean-level occur with greater regularity and become positively correlated. Power spectrum estimates most resemble those belonging to the class 1 category. Consequently, the lacunarity

curves also contain oscillations similar to those previously observed. Informed by the analysis in chapter 5, finite mixtures of beta densities are used to model the interval density. Crossing intervals in the signal after the button press are bimodal, and the density shape is qualitatively similar to that for the periodically modulated version of Wong's process when the periodicity parameter is close to the critical value. This case study lends support to the utility of dividing stationary processes into three categories.

Chapter 8: Conclusion

A summary of the preceding chapters is given followed by examples for continuing research, namely: the behaviour of level- and curve-crossings of Gaussian and non-Gaussian processes; the connection to correlated Bernoulli trials as represented by the indicator function for zero-crossings; and stochastic periodicity in a dynamical system with finite variance.

Appendices

These contain additional details on formulae used throughout the thesis, and code for numerical simulations.

Appendix	Title
A	Power Spectra of Class 0 Processes
B	Probability Distributions
C	Tail Behaviour of the Interval Density
D	Higher Order Distributions
E	Formulae for Contiguous and Gliding Box Count Methods
F	Parameter Values and Additional Statistics: Class 0 Densities
G	Parameter Values: Classes 1 and 2 Densities
H	MATLAB Code for Simulating a Correlated Random Process
I	MATLAB Code for Computing Lacunarity

J MATLAB Code for Computing the Interval Density and Crossing
Count Distributions

2

LITERATURE REVIEW

This chapter presents key results on the zero-crossing statistics of stationary Gaussian processes, and summarises the two main analytical tools of the thesis, namely mixture modelling and lacunarity. Two non-Gaussian processes are also introduced as comparators for analysing crossing dependence: a switching process with jumps that are Poissonian; and a cosine wave that has a uniformly distributed random phase.

2.1 GAUSSIAN PROCESSES

Much of the progress concerning the zero-crossing problem (ZCP) has involved Gaussian processes. These have the property of being fully characterised by their mean vector and covariance matrix: for example, the probability density of a Gaussian vector-valued process $\mathbf{X} \in \mathbb{R}^d$ with mean $\boldsymbol{\mu}$ and covariance matrix $\Lambda_{\mathbf{X}}$ is [1]

$$f_{\mathbf{X}}(\mathbf{X}) = (2\pi \det[\Lambda_{\mathbf{X}}])^{-d/2} \exp\left(-\frac{1}{2}(\mathbf{X} - \boldsymbol{\mu})^T \Lambda_{\mathbf{X}}^{-1}(\mathbf{X} - \boldsymbol{\mu})\right), \quad (2.1)$$

and when the dimension $d=2$, the covariance matrix takes the form

$$\Lambda_{\mathbf{X}} = \begin{pmatrix} \sigma_X^2 & \rho_X \sigma_X \sigma_Y \\ \rho_X \sigma_X \sigma_Y & \sigma_Y^2 \end{pmatrix}, \quad (2.2)$$

where $\mathbf{X} = (X, Y)$, the respective components have means μ_X, μ_Y , and variances σ_X^2, σ_Y^2 , and their correlation is $\rho_X = \sigma_X^{-2} \sigma_Y^{-2} \text{Cov}[X, Y]$. The univariate Gaussian

distribution obtains from (2.1) when $d=1$, and properties of this case are listed in App. B.1. The simplicity of its definition gives a Gaussian process a completeness property that allows for various simplifying assumptions in the derivation of zero-crossing results, as do the twin concepts of ‘stationarity’ and ‘ergodicity’. A time dependent stochastic process with sample functions $x(t)$ is strictly stationary if distributions derived from it are independent of shifts in time; it is weakly stationary if its mean is constant and its covariance function, $\text{Cov}[x(t), x(t + \tau)]$, depends on the lag time τ alone [37]. The two types of stationarity are equivalent for a Gaussian process since it depends only on its mean and covariance function. A process is strictly ergodic if the behaviour of a single sample function within a suitably large time window is typical of the entire ensemble of possible sample functions observed at one or more instants in time [38]. This then implies that time averages along a sample function are equivalent to ensemble averages.

Theorem 2.1

A stationary Gaussian process with power spectrum $S(\omega)$ is ergodic if and only if its spectral distribution function $\bar{S}(\omega) = \int_{-\infty}^{\omega} S(w) dw$ is continuous everywhere [37].

Thus, it is enough to speak of the stationary Gaussian process $x(t)$ with mean μ and variance σ^2 , and normalised autocorrelation $\rho(\tau)$, a real-valued function defined as

$$\rho(\tau) = \left(\mathbb{E}[x(0)x(\tau)] - \mu^2 \right) / \sigma^2. \quad (2.3)$$

Its validity depends on four properties: symmetry, $\rho(-\tau) = \rho(\tau)$; boundedness, $|\rho(\tau)| \leq \rho(0)$; asymptotic decay, $\lim_{\tau \rightarrow \infty} \rho(\tau) \rightarrow 0$; a positive-definite spectrum $S(\omega)$. The latter function is easily obtained through the following theorem.

Theorem 2.2 (Wiener-Khinchin)

The Fourier transform of the autocorrelation $\rho(\tau)$ of a weakly stationary process is the power spectrum $S(\omega)$ [38].

The k -th derivative of the stationary process $x(t)$ has covariance function [37]

$$\rho_{x^{(k)}}(\tau) = (-1)^k \rho^{(2k)}(\tau) = \mathcal{F} \left[(2\pi\omega)^{2k} S(\omega) \right], \quad (2.4)$$

where $\mathcal{F} [f(t)] = 2 \int_0^\infty f(t) \cos(2\pi\omega t) dt$ is the Fourier transform of an even function $f(t)$. Consequently, the process's differentiability can be determined from its autocorrelation; it is k -times differentiable if $\left| \rho^{(2k-1)}(0) \right| = 0$. The process is labelled smooth if all the derivatives of $\rho(\tau)$ exist, sub-fractal if $\rho(\tau)$ is at least twice (but not infinitely) differentiable, and fractal otherwise. Equivalently, a process is smooth if and only if the integral in Eq. (2.4) exists for all $k \geq 0$. For sub-fractal processes, the integral exists for finitely many k .

Henceforth, it will be assumed the process $x(t)$ is continuous, differentiable, and has mean zero and variance unity; whence its autocorrelation is $\rho(\tau) = E[x(0)x(\tau)]$. Reference will also be made to quantities illustrated and labelled in Fig. 1.2.

2.1.1 On the Prevalence of Gaussian Processes

Gaussian processes are employed extensively in machine learning applications [39], again because of their definitional flexibility. They also arise naturally as a consequence of the 'central limit theorem'. The classical version of the theorem states [40]: given a sequence $\{X_1, X_2, \dots, X_n\}$ of independent and identically distributed random variables with mean μ and variance σ^2 , as $n \rightarrow \infty$, the distribution of the random variable

$$Y_n = \frac{\frac{1}{n} \sum_{i=1}^n X_i - \mu}{\sigma / \sqrt{n}} \quad (2.5)$$

tends to the standard normal distribution, which is a Gaussian distribution with mean 0 and variance 1. Therefore, Gaussian-like behaviour will be observed for example in the sample mean of any suitably long random experiment, or large data set. Oceanography furnishes us with a further example relevant to the zero-crossing problem, one model of ocean water being that of a moving incompressible fluid of infinite depth and obeying the Euler equations [41]. The limit of a super-

position of infinitely many elementary sea-waves is a random sea surface that can be modelled as a stationary Gaussian process $W(t, x, y)$. At each point (x, y) on the surface, there is then a time wave $W(t)$, from which obtains wave height and length/duration, and ultimately an analysis of the level-crossings.

2.1.2 Stochastic Memory

To further explicate what we mean by memory in a stochastic process, we provide the following definitions based on the power spectrum [42]. Firstly, a function $F(x)$ is slowly varying at infinity if for any $\gamma > 0$, $F(\gamma x) \sim F(x)$ as $x \rightarrow \infty$. The function $F(x)$ is slowly varying at the origin if $\tilde{F}(x) = F(x^{-1})$ is slowly varying at infinity. A stationary process $x(t)$ with power spectrum $S(\omega)$ is said to exhibit linear (a) long-range dependence, (b) intermediate dependence, (c) short-range dependence, or (d) antipersistence, if

$$S(\omega) = F(\omega) |\omega|^{-2q}, \quad \text{as } \omega \rightarrow 0, \quad (2.6)$$

where $F(\omega)$ is a symmetric function that is slowly varying at zero and

$$\begin{aligned} \text{(a)} & \quad q \in (0, 1/2), \\ \text{(b)} & \quad q = 0 \quad \text{and} \quad \lim_{\omega \rightarrow 0} F(\omega) = \infty, \\ \text{(c)} & \quad q = 0 \quad \text{and} \quad 0 \leq F(0) < \infty, \text{ or} \\ \text{(d)} & \quad q \in (-1/2, 0). \end{aligned} \quad (2.7)$$

Out of these four sub-definitions for stochastic memory, the third (short-range dependence) is the primary focus of this thesis. For alternative definitions of stochastic memory, particularly as extending to nonlinear or higher order dependence, non-stationary processes, and the prevalence of long-term correlation in time series, see further [42, 43, 44].

2.2 ZERO-CROSSING THEORY

2.2.1 Crossing Counts

In 1944 Rice [9] produced the seminal result that for a Gaussian process with autocorrelation $\rho(\tau)$, the mean number of zero-crossings in a time window r is

$$\langle \mathcal{N}(r) \rangle = \bar{R}r = \pi^{-1} \sqrt{-\rho''(0)}r, \quad (2.8)$$

and $\mu_T = \bar{R}^{-1}$ is the mean length of crossing intervals T . Rice further showed that the average number of maxima $\mathcal{N}_M(r)$ accrues similarly as

$$\langle \mathcal{N}_M(r) \rangle = \bar{R}_M r = (2\pi)^{-1} \sqrt{-\rho^{(4)}(0) / \rho''(0)}r, \quad (2.9)$$

and excursions above a large level behave according to a Rayleigh distribution (a type of Weibull distribution with shape parameter 2, see App. B.5). Generalizing Rice's work and with greater rigour was the tenor of results that followed; conditions were weakened for $\langle \mathcal{N}_c(r) \rangle$, the mean number of crossings of level $c \in \mathbb{R}$ by $x(t)$ [9, 27]:

$$\langle \mathcal{N}_c(r) \rangle = \pi^{-1} \sqrt{-\rho''(0)} r e^{-c^2/2} = \bar{R} r e^{-c^2/2}. \quad (2.10)$$

Leadbetter [45] computed corresponding quantities for crossings of arbitrary curves, i.e. zero-crossings of $x(t) - u(t)$, for some continuous function $u(t)$. The next major contribution, by Steinberg et al. [46], found the variance of zero-crossings in time r , which unlike (2.8)–(2.10) depends on the global properties of the autocorrelation $\rho(\tau)$:

$$\text{Var}[\mathcal{N}(r)] = \bar{R}r + 2\bar{R} \int_0^r (r - T)(U(T) - \bar{R}) dT, \quad (2.11)$$

where

$$\begin{aligned}
 U(T) &= \frac{1}{\pi^2 \bar{R} (1 - \rho^2(T))^{3/2}} \left(|A^2 - B^2|^{1/2} + B \arctan \left(\frac{B}{|A^2 - B^2|^{1/2}} \right) \right), \\
 A &= -\rho''(0) (1 - \rho^2(T)) - \rho'^2(T), \\
 B &= \rho''(T) (1 - \rho^2(T)) + \rho(T) \rho'^2(T),
 \end{aligned} \tag{2.12}$$

and $U(T)dT$ is the conditional probability of a zero occurring in the interval $(t+T, t+T+dT)$, given a crossing at time t [10]. Equations (2.8)–(2.11) were arrived at through construction of integrals involving $x(t)$ and its derivative(s), which are then evaluated by substitution of the multivariate Gaussian distribution (2.1).

The ‘Fano factor’ for a counting process $\mathcal{N}(r)$, defined as

$$F(r) = \text{Var}[\mathcal{N}(r)] / \langle \mathcal{N}(r) \rangle, \tag{2.13}$$

is a statistic used to compare fluctuations in the counts relative to a Poisson process, for which the variance and mean are equal, whereupon $F(r) = 1$. Smith [47] used simulation studies to show that for Gaussian processes, the zero-crossings at large time windows can be either sub-Poissonian ($F(r) < 1$, crossings are anti-bunched) or super-Poissonian ($F(r) > 1$, crossings are bunched). This depended on the smoothness of the process, and consequently there is memory in the crossing sequence. These results were echoed in [5], where variation of periodicity in the autocorrelation initiated a transition from slight anti-bunching of crossings to asymptotically deterministic characteristics demonstrated by oscillations in the Fano factor.

2.2.2 Crossing Intervals

The behaviour of the crossing intervals is even more complex and less amenable to exact derivation even when using properties of the Gaussian distribution. Thus,

a different approach was required, most prominently, McFadden's work on Markov chain models for the intervals [48]. The clipped process $\zeta(t)$,

$$\zeta(t) = \begin{cases} 1, & x(t) \geq 0, \\ -1, & x(t) < 0, \end{cases} \quad (2.14)$$

identifies the sign changes in $x(t)$. The product $\zeta(t)\zeta(t+\tau)$ is even if and only if an even number of zero-crossings occurs in time τ , so the autocorrelation of $\zeta(t)$ is given by

$$R(\tau) = \sum_{m=0}^{\infty} (-1)^m P_N(\mathcal{N}(\tau) = m). \quad (2.15)$$

This is related back to the autocorrelation of a stationary Gaussian process in the Van Vleck arcsine law [49]:

$$R(\tau) = (2/\pi) \arcsin(\rho(\tau)). \quad (2.16)$$

McFadden [48] derived the following identities relating the count distribution $P_N(\mathcal{N}(\tau) = m)$, and the density for intervals formed by $m+2$ zero-crossings, $p_m(T)$:

$$P_N''(\mathcal{N}(\tau) = m) = \bar{R} (p_m(\tau) - 2H_1(m-1)p_{m-1}(\tau) + H_1(m-2)p_{m-2}(\tau)), \quad (2.17)$$

where the function $H_1(m)$ is one if $m \geq 0$, and zero otherwise. Note: $p_0(T) = p(T)$, the density for successive intervals. Substituting (2.17) into the second derivative of (2.15) leads to

$$(4\bar{R})^{-1} R''(T) = \sum_{m=0}^{\infty} (-1)^m p_m(T). \quad (2.18)$$

A second infinite sum follows from the definition of $U(T)$ as the conditional density of observing additional intervals of length T :

$$U(T) = \sum_{m=0}^{\infty} p_m(T). \quad (2.19)$$

If successive crossing intervals are assumed independent, the convolution method for random variable sums enables computation of $p_m(T)$ through Laplace transforms:

$$\bar{p}_m(s) = \bar{p}_0^{m+1}(s), \quad (2.20)$$

where $\bar{p}_m(s) = \mathcal{L}[p_m(T)] = \int_0^\infty p_m(T) e^{-sT} dT$ denotes the Laplace transform of $p_m(T)$. Two further transforms can be made; from (2.18)&(2.19),

$$h(s) = \mathcal{L}\left[(4\bar{R})^{-1} R''(T)\right], \quad u(s) = \mathcal{L}[U(\tau)], \quad (2.21)$$

and substituting these into the model (2.20) yields two equations for $\bar{p}_0(s)$:

$$\bar{p}_0(s) = h(s) / (1 - h(s)), \quad (2.22)$$

$$\bar{p}_0(s) = u(s) / (1 + u(s)), \quad (2.23)$$

the which are identical if the independence assumption holds. Being the generating function of $p(T)$, $\bar{p}_0(s)$ may be expanded as a sum of interval moments:

$$\bar{p}_0(s) = 1 - \langle T \rangle s + \langle T^2 \rangle s^2 + \mathcal{O}(s^3). \quad (2.24)$$

As $T \rightarrow \infty$, $R''(T) \rightarrow 0$ and $U(T) \rightarrow \bar{R}$ [10], and so $h(s)$ and $v(s) = \mathcal{L}[U(\tau) - \bar{R}]$ both admit Taylor expansions about $s = 0$. The three expansions are then substituted into (2.22)&(2.23); each equation after matching coefficients of s^2 respectively produce two expressions for the interval variance:

$$\begin{aligned} \sigma_1^2 &= 4(\pi\bar{R})^{-1} \int_0^\infty \arcsin(\rho(\tau)) d\tau, \\ \sigma_2^2 &= \bar{R}^{-2} \left(1 + 2 \int_0^\infty (U(\tau) - \bar{R}) d\tau \right); \end{aligned} \quad (2.25)$$

matching coefficients of s returns Rice's result for the mean interval, i.e. $\mu_T = \bar{R}^{-1}$. The pair of equations in (2.25) will not be equal if the intervals are dependent, but in many examples [5, 34, 50] the geometric mean of σ_1^2 and σ_2^2 is a sufficiently

accurate estimate of the true interval variance, σ_T^2 .

The Markov chain model (2.20) implies the correlation coefficient between the m -th and $m+j$ -th intervals,

$$\kappa_{m,m+j} = \frac{\langle T_m T_{m+j} \rangle - \langle T_m \rangle^2}{\langle T_m^2 \rangle - \langle T_m \rangle^2} = \frac{\langle T_m T_{m+j} \rangle - \mu_T^2}{\sigma_T^2}, \quad (2.26)$$

factorises as $\kappa_{m,m+j} = \kappa_{m,m+1}^j \equiv \kappa_1^j$. Specific cases of j and refinements to McFadden's models were tested in [5, 50] using simulations of Gaussian processes with parametrised autocorrelation or power spectra. Increases of the controlling parameter result in the peak frequencies moving away from the origin, a decrease in interval variance, and the correlation coefficients $\kappa_{m,m+j}$ initially oscillate with j , before monotonically increasing towards 1. Power spectra that are narrow and concentrated at frequencies away from the origin are variously referred to as narrow-band [46, 48, 49, 50]. The Markov Chain models produce relatively accurate estimates of the interval variance, and also for the first correlation coefficient κ_1 when the power spectrum is concentrated around the origin. For higher order correlation coefficients, the signs do not always agree with that of simulations, implying that the Markov chain model breaks down. As the intervals become more correlated ($\kappa_1 \rightarrow 1$), the gap between predicted and simulated values of $\kappa_{m,m+j}$ widens.

2.2.3 The Interval Density

Devising a method that exactly determines $p(T)$, the probability density function (pdf) of zero-crossing intervals, has been the critical aspect of the ZCP since its inception by Rice. Referring to Rice's conditional density (2.12), McFadden [51] commented that $U(T)$ approximates $p(T)$ when T is small, and for a narrow-band spectrum the "range of agreement includes most of the practical range of axis-crossing intervals" since most of these are near μ_T . However, as $T \rightarrow \infty$, $U(T) \rightarrow \bar{R}$ and is therefore not a valid density function. Refinements that use more complicated Rice series have been used to obtain limiting forms of $p(T)$ [52].

Asymptotic results for $p(T)$ given the autocorrelation of a smooth or sub-fractal process have been derived [53, 54] based on the joint distribution of observing two crossings in an infinitesimally small interval, and bounds found by making comparison to related processes with known results; and the asymptotics depend on the autocorrelation. In particular, for the left-tail,

$$\begin{aligned}\rho'''(0) = 0 &\Rightarrow p(T) \sim \mathcal{O}(T) \quad \text{as } T \rightarrow 0, \\ \rho'''(0) \neq 0 &\Rightarrow p(T) \sim \mathcal{O}(1) \quad \text{as } T \rightarrow 0;\end{aligned}\tag{2.27}$$

and for the right tail, if $|\rho(\tau)| < \alpha\tau^{-d}$ for some $\alpha > 0$, $d > 1$, and all $\tau > 0$, then as $T \rightarrow \infty$,

$$1 - P(T) = \int_T^\infty p(t) dt \sim e^{-\Theta T}.\tag{2.28}$$

This particular result when $\rho(\tau)$ is oscillatory was interrogated in [5], and the persistence exponent Θ for a periodic autocorrelation was shown to approach infinity as the periodicity parameter increases. Therefore, we proceed with the following definition from [55] for a stationary Gaussian process: there exists a nonnegative, possibly infinite, limit

$$\Theta = - \lim_{T \rightarrow \infty} \frac{1}{T} \log \left(\Pr \left\{ \sup_{t \in [0, T]} x(t) < 0 \right\} \right);\tag{2.29}$$

and this is finite for nonnegative autocorrelations [56]. (Note: sup denotes the ‘supremum’, or least upper bound.) Analytical methods for obtaining $p(T)$ are examined in [48, 52, 57], and we now describe the two most capable in the sense of providing an estimate over a large range of interval sizes, and being easy to adopt with the aid of well-established numerical routines.

2.2.3.1 Laplace transform method

An approximation of the interval density may be obtained by Laplace inversion of the Markov chain model outlined above. From (2.21), and applying integration by parts,

$$\begin{aligned}
 h(s) &= \frac{1}{4\bar{R}} \int_0^\infty R''(T) e^{-sT} dT \\
 &= \frac{1}{4\bar{R}} \left(-R'(0+) + s \int_0^\infty R'(T) e^{-sT} dT \right) \\
 &= \frac{1}{2} + \frac{s}{2\pi\bar{R}} \int_0^\infty \frac{\rho'(T) e^{-sT}}{\sqrt{1-\rho^2(T)}} dT, \tag{2.30}
 \end{aligned}$$

the last line following from the arcsine law (2.16) and the result $\lim_{\tau \rightarrow 0+} R'(\tau) = -2\bar{R}$ [51]. Substituting this into (2.22) then allows computation of the interval density as

$$p(T) = \mathcal{L}^{-1}[h(s)/(1-h(s))]. \tag{2.31}$$

Depending on the autocorrelation $\rho(\tau)$ of the process, (2.31) can be inverted; numerical Laplace inversion is possible using for example the Talbot method [58].

The denominator in (2.31) means $\mathcal{L}[p(T)]$ has at least one pole. In the simplest case, this occurs once on the negative s -axis and prescribes the persistence exponent Θ (2.29), which can then be found by solving $h(-\Theta) = 1$. Wilson [5] performed a systematic study of the poles in (2.31) and revealed that for a periodic autocorrelation there are multiple poles, which in turn make the inversion particularly difficult to set-up and then evaluate. For small values of the periodicity parameter associated with the process, the first two poles are sufficient in predicting the persistence exponent. However, the estimate worsens as the frequency of oscillations in $\rho(\tau)$ increases, even with refinements to (2.20) in the form of correlated Markov chain models [5, 48]. Those refinements do produce improvements to the interval variance, but less so for the correlation coefficient, demonstrating that the Laplace transform method is correct up to $\mathcal{O}(s^2)$.

2.2.3.2 Slepian regression method

Unlike the previous method, here the distribution of zero-crossing intervals of $x(t)$ is obtained by conditioning on the process directly in a manner similar to derivations of crossing count moments [9, 46]. The following description is adopted from Sec. 8.4 of [37].

Suppose an up-crossing of the level $c \in \mathbb{R}$ by $x(t)$ occurs at time $t = t_0$, i.e. $x(t_0) = c$, $x'(t_0) > 0$. Define $\xi_c(t)$ as the excursion from t_0 to $t_0 + T$, at which a down-crossing of c occurs. Without loss of generality, set $t_0 = 0$. The length in time of the excursion, T , has probability density function

$$p(T) = f_{\xi_c(t)}(c) \mathbb{E} \left[\mathbb{I}_{\{\xi_c(s) > c, s \in (0, T)\}} \cdot \left(-\xi_c'(T)^- \mid \xi_c(T) = c \right) \right], \quad (2.32)$$

where $f_{\xi_c(t)}(\xi_c)$ is the density of $\xi_c(t)$, \mathbb{I}_A is the indicator function of the event A , and $\xi_c'(t)^- = \min\{0, \xi_c'(t)\}$ is the negative part of the derivative. The excursion is constructed as a Slepian model, which for a Gaussian process with normalised autocorrelation $\rho(\tau)$ is

$$\xi_c(t) = c\rho(t) + \zeta\rho'(t) / \rho''(0) + \kappa(t), \quad (2.33)$$

where $\zeta \geq 0$ has Rayleigh density $(z / |\rho''(0)|) \exp(-z^2 / (2|\rho''(0)|))$, and $\kappa(t)$ is a nonstationary, zero-mean Gaussian residual process, independent of ζ , and with covariance function

$$\rho_\kappa(\tau_1, \tau_2) = \rho(\tau_2 - \tau_1) - \rho(\tau_1)\rho(\tau_2) + \rho'(\tau_1)\rho'(\tau_2) / \rho''(0). \quad (2.34)$$

To obtain the interval density, the infinite-dimensional conditional expectation in (2.32) is approximated by discretisation of the interval $[0, T]$ and performing the ensuing numerical integration, which is now possible with high accuracy for normal distributions. If necessary, the regression approximation (2.33) is improved by including values of $\kappa(s)$ at additional points $s \in (0, T)$. The WAFO toolbox [30] implements the solution method for finding the distribution of level-crossings

and related quantities; only the power spectrum (or autocorrelation) of the original process is required, which can be supplied analytically or estimated numerically, making the procedure even more useful when analysing real world data. In [52] the method is described as exact, and examples of output level-crossing interval densities compared with their simulated counterparts are provided therein for differentiable Gaussian processes.

When the underlying assumptions of the Slepian regression method are revisited, the interpretative reliability appears less certain. The result (2.32) is an application of the more general formula by Durbin [37]:

Theorem 2.3

Let $\{y(t), 0 \leq t < \infty\}$ be a continuous process and define $T = \inf_{t>0} \{y(t) > 0\} < \infty$. If the conditional distribution of $y(s), 0 \leq s \leq t$, given $y(0)$, is non-degenerate, then T has density function

$$f_T(t) = f_{y(t)}(0) \mathbb{E} \left[\mathbb{I}_{\{y(s) < 0, s \in (0, t)\}} \cdot \max\{0, y'(t)\} \mid y(t) = 0 \right].$$

(Note: \inf denotes the ‘infimum’, or greatest lower bound.). Proving this theorem rests on the following connection between distributions of level-crossing intervals and the differentiable process $y(t)$: if, with probability one, $y(s)$ has no tangent of the level $c \in \mathbb{R}$, then

$$\Pr\{T \geq t\} = \Pr\{y(s), \forall s \in (0, t)\}.$$

From (2.27), this does not hold for sub-fractal processes; indeed, there may be no excursion since with probability greater than zero, crossings occur in time windows of arbitrary small extent—granted, these tangents are finite in any window of time by Rice’s result (2.8). Furthermore, since the correlation between $x(t)$ and $x(t + T)$ goes to zero as $T \rightarrow \infty$, the Slepian model becomes less appropriate. Crossings of other levels also become more likely because the average number of turning points increases with time (2.9). Thus, estimation of the tail behaviour will be particularly affected unless σ_T^2 is small. In spite of these points, the Slepian regression approach

is “more general, more accurate and relatively unknown” [57], compared to alternatives like the Laplace transform method, and simulation/optimisation studies, including for certain sub-fractal processes. In principle, tuning the input parameters for the WAFO toolbox should allow for the more complex cases.

2.3 MIXTURE DISTRIBUTIONS

2.3.1 *Finite Mixtures*

In the analysis of statistical data from an unknown distribution one approach is to combine different known distributions and fit the resulting distribution to the data. Given sample data $\mathbf{T} = \{T_m, m = 1, \dots, n_T\}$, a ‘finite mixture’ model proposes that the associated probability density function may be expressed as

$$p(T) = \sum_{k=1}^K \alpha_k g_k(T; \boldsymbol{\theta}_k), \quad (2.35)$$

where $K < \infty$, the mixing weights α_k satisfy $0 < \alpha_k < 1$, with $\alpha_K = 1 - \sum_{k=1}^{K-1} \alpha_k$, and $\boldsymbol{\theta}_k$ is a vector of parameters for the k -th component density function $g_k(T; \boldsymbol{\theta}_k)$. The component densities need not all be from the same distribution family, and the random variable under consideration may be either continuous or discrete (in which case $p(T)$ is a probability mass function).

A finite mixture model like (2.35) implicitly segments the data into K groupings, each group modelled by one of the component densities. In the analysis of failure time data, these groups may correspond to different but known causes of failure; whilst in cluster analysis the objective is to obtain optimal groupings as judged by a sequential procedure [59]. A comprehensive list of applications of finite mixtures is provided in Tab. 2.1.3 of [60], covering disciplines such as agriculture, economics, medicine, geology and engineering. In the literature, mixtures commonly use mem-

bers of the exponential family of distributions (*EXPF*) which have density functions of the form [61]

$$\exp(\mathbf{a}(T) \cdot \boldsymbol{\theta} - b(\boldsymbol{\theta}) - c(T)), \quad (2.36)$$

where $\boldsymbol{\theta}$ is a vector of parameters, $\mathbf{a}(T)$ and $c(T)$ are respectively vector and scalar functions of the independent variable, $b(\boldsymbol{\theta})$ is a scalar function of the parameters, and ' \cdot ' is the dot product operator. Examples from the exponential distribution family when the random variable T is continuous include the normal, exponential, gamma and Weibull distributions, and the latter three—being defined only for nonnegative values of the independent variable—are relevant when modelling data based on time records. Basic properties of these three special cases of (2.36) can be found in App. B.3–B.5.

2.3.2 Compound Mixtures

As an extension to (2.35), if the component densities are from the same distribution family, and all but one of the parameters are fixed (i.e. $\boldsymbol{\theta}_k \mapsto (\boldsymbol{\theta}, \eta_k)$, $g_k(T; \boldsymbol{\theta}_k) \mapsto g(T; \boldsymbol{\theta}, \eta_k)$) the weights α_k may be read as probabilities at a finite number of points η_k from an infinite set $\mathcal{D} \subseteq \mathbb{R}$, i.e. $\alpha_k \equiv f_k(\eta_k)$. In the limit where positive probabilities are assigned to all values $\eta \in \mathcal{D}$, the mixed pdf becomes

$$p(T) = \int_{\mathcal{D}} g(T; \boldsymbol{\theta}, \eta) f(\eta) d\eta; \quad (2.37)$$

$f(\eta)$ is the 'mixing density' and $g(T; \boldsymbol{\theta}, \eta)$ operates as a 'kernel function'. Models of the form (2.37) are 'compound mixtures', also referred to in the literature as continuous or general mixtures [62]. The random variable T can be interpreted as exhibiting behaviour due to some unobserved 'latency variable', η . Other generalisations from standard distributions are possible (see [63]); likewise, the compound mixture form can be specified directly as in 'Bayesian inference' [60]. We note that the density (2.32) is also defined as an integral equation.

A counting process $\{\mathcal{N}(t), t \geq 0\}$ represents the total number of events that have

occurred by time t for an associated stochastic process. Renewal theory studies counting processes where the times between successive events are ‘independent and identically distributed’, the canonical example being a Poisson process where the inter-event times, T , have an exponential distribution with mean $\langle T \rangle = \bar{R}$, and the event counts follow a Poisson distribution [64]:

$$P_N(\mathcal{N}(t) = n) = e^{-\bar{R}t} (\bar{R}t)^n / n!, \quad n = 0, 1, 2, \dots \quad (2.38)$$

The count distribution has also been derived for cases where the inter-event times have Erlang [65], Weibull [66] or hyperexponential [67] distributions. Models in renewal theory can be improved using ‘randomisation’; given a count distribution, a compound mixture is constructed by randomising (i.e. assigning a distribution to) a variable or parameter. One example is a group of independent sources of Poissonian renewals, each with different renewal rates; the rate \bar{R} in (2.38) appears as a random variable η with a density $f(\eta)$ [64], and the distribution of counts in a fixed time t becomes

$$P_N(\mathcal{N}(t) = n) = \int_0^\infty e^{-\eta t} \frac{(\eta t)^n}{n!} f(\eta) \, d\eta, \quad n = 0, 1, 2, \dots \quad (2.39)$$

The zero-crossing problem is concerned with crossing events that are correlated in time; when the random process is non-Markov and stationary, the times between successive crossings are ‘dependent and identically distributed’. This thesis seeks to align the study of zero-crossings to that of renewal processes by using similar analytical tools, particularly mixture modelling.

Further extensions of the mixture paradigm (e.g. mixtures using survival functions and regression models, incorporating dependence using latency and hidden Markov models) can be found in [59]; the forms outlined above prove sufficient for our purposes. Mixture modelling of zero-crossings is represented in the literature. In case study 1 (Sec. 1.3.1), the authors use finite mixtures of 2–4 Weibull and log-normal distributions to model zero-level up-crossings. The same authors develop a (bivariate) mixture copula model [68], which uses a Gaussian ‘copula function’ to

combine the marginal distributions of wave height and zero-up-crossing period. In [69], a coupled hidden Markov model based on zero-crossings of vibration signals is devised as a method for estimating bearing performance degradation.

2.4 PARAMETER ESTIMATION

To fit the finite mixture model (2.35), a form for the component densities $g_k(T; \theta_k)$ is chosen, usually from the same distribution family. To fit the compound mixture model (2.37), a kernel function $g(T; \theta, \eta)$ must be specified, as well as a mixing density $f(\eta)$, the latter of which may be selected from a known distribution family as a single or mixed density function, thereby contributing additional parameters. Let α now represent the full set of unknown parameters in a finite or compound mixture model $p(T; \alpha)$; the task of fitting the distribution then reduces to obtaining parameter estimates $\hat{\alpha}$. A primary concern is ‘identifiability’, and for a finite mixture, this means a unique characterisation of $p(T; \alpha)$ exists, subject to relabelling of indices. Various authors have stated that for continuous distributions involving finite mixtures, problems with identifiability seldom arise [59, 60, 70]. There is also a general rule that any probability density function can be approximated by a finite mixture model to an arbitrary degree of accuracy—allowing for negative mixing weights—and this was recently explored more concretely in [71]. Here we are equally interested in modelling distributions and interpreting models; thus, the number of finite mixture components should be minimised. Additional components can be added to account for multimodality and when the data suggests a heavier tail [63]. Most widely used as solution methods for parameter estimation are ‘method of moments’ (MOM) and ‘maximum likelihood estimation’ (MLE).

2.4.1 Method of Moments

In MOM, analytical moments as computed from the mixture model are equated to the corresponding sample moments of the data \mathbf{T} . For example: the raw moments $m_r(\boldsymbol{\alpha})$ and the central moments $\mu_r(\boldsymbol{\alpha})$ are respectively calculated as

$$m_r(\boldsymbol{\alpha}) = \int_{\mathbb{R}} T^r p(T; \boldsymbol{\alpha}) dT, \quad \mu_r(\boldsymbol{\alpha}) = \int_{\mathbb{R}} (T - m_1(\boldsymbol{\alpha}))^r p(T; \boldsymbol{\alpha}) dT, \quad (2.40)$$

and by the binomial theorem ([72], Eq. 1.37b) for $r \in \mathbb{N}$, the central and raw moments relate through

$$\mu_r(\boldsymbol{\alpha}) = \sum_{k=0}^r \binom{r}{k} (-1)^{r-k} m_k(\boldsymbol{\alpha}) (m_1(\boldsymbol{\alpha}))^{r-k}; \quad (2.41)$$

likewise for the corresponding sample moments $\hat{\mu}_r$ and \hat{m}_r . (When working with sample data, the mean \hat{m}_1 and central moments $\hat{\mu}_r$, $r \geq 2$, are usually relied upon.)

A system of equations for the parameters then arises:

$$m_r(\boldsymbol{\alpha}) = \hat{m}_r, \quad \text{for } r = 1, \dots, |\boldsymbol{\alpha}|, \quad (2.42)$$

where \hat{m}_r denotes the corresponding r -th sample moment, and $|\boldsymbol{\alpha}|$ is the total number of parameters. At least one solution exists when the number of equations matches the total number of parameters. For the finite mixture model composed of K exponential distributions, (2.42) is a system of polynomial equations of degree at most $2K$. This can be simplified further by eliminating some of the variables, and when $K \leq 3$ the system can be solved analytically. In cases where the left-hand side of (2.42) cannot be inverted due to the presence of non-linear functions and/or irreducible integrals, a solution may be sought using numerical methods.

2.4.2 Maximum Likelihood Estimation

The simplest version of MLE begins by assuming the sample data \mathbf{T} are independent observations from the proposed mixture density $p(\mathbf{T}; \boldsymbol{\alpha})$, and treating their joint probability density as a function of the parameters $\boldsymbol{\alpha}$. This produces the ‘likelihood function’, a measurement of the relative likelihood that parameters $\boldsymbol{\alpha}$ give rise to the sample data. Taking the logarithm leads to the ‘log-likelihood function’

$$\ell(\mathbf{T}; \boldsymbol{\alpha}) = \log \left(\prod_{m=1}^{n_T} p(\mathbf{T}_m; \boldsymbol{\alpha}) \right) = \sum_{m=1}^{n_T} \log(p(\mathbf{T}_m; \boldsymbol{\alpha})). \quad (2.43)$$

The goal is to then find the particular $\hat{\boldsymbol{\alpha}}$ that maximises $\ell(\mathbf{T}; \boldsymbol{\alpha})$, which then means the sample data is most likely to have come from $p(\mathbf{T}; \boldsymbol{\alpha})$ with $\boldsymbol{\alpha} = \hat{\boldsymbol{\alpha}}$ compared to any other $\boldsymbol{\alpha}$. The logarithm is a monotone function meaning the location of turning points are the same for both the likelihood and log-likelihood functions, and the latter is easier to work with.

The traditional method of maximizing multivariate functions—i.e. solving first-order partial differential equations for the $\boldsymbol{\alpha}$, and using the second-order derivatives to verify the maxima—is not as easily performed due to the form of (2.43). Therefore, parameter estimates are typically arrived at through numerical minimisation of the negated log-likelihood function, and this thesis relies on the ‘Nelder-Mead algorithm’ [73]. As a direct-search method, it does not require computation of the objective function’s gradient. Rather, the domain is explored at each iteration using a ‘simplex’ with vertices formed of the working guestimates based on various function evaluations. This leads to reflection/expansion/contraction/shrinkage transformations of the simplex, and in the ideal situation the simplex contracts iteratively to the unique minimiser. Behaviour of the algorithm when the objective function depends on more than two variables is relatively unknown [74], analytically speaking; the method yet enjoys a pragmatism repeatedly reinforced in practical problems, a key advantage over other methods being it requires in most cases only two function evaluations at each iteration. We note that in probabilistic modelling

the so-called ‘Expectation-Maximisation’ or ‘EM algorithm’ is the preferred strategy of statisticians [31, 59, 60] as it does have better convergence properties than solely performing numerical optimisation of the log-likelihood function, and accounts for the data being incomplete (since the mixture grouping for each of the sample data is unknown). However, the setup is more intricate, convergence can be slow, and, crucially, we did not require that approach here.

2.4.3 Comparison of MOM and MLE

Both MOM and MLE become asymptotically consistent as the sample size n_T goes to infinity. The MOM has the advantage of being easy to setup and the approximate solutions to the equations can usually be found. However, if the original mixture model is not appropriate, the MOM can produce inadmissible parameters. Furthermore, equations for unbiased sample moments exist for only the first four central moments [75]. Thus, we make use of it mainly for obtaining initial parameter estimates. The MLE method is a better choice for parameter estimation as it uses the target distribution directly, has the smallest asymptotic variance, and not all the models we propose are mixtures of exponential distributions. Initiating numerical procedures from different starting values can lead to multiple admissible solutions. When this occurs, other properties can be used to decide the most suitable solution: higher-order moments; distance measures that compare empirical and model-predicted cumulative density functions; known properties of the data, which for us includes existing zero-crossing theory; location of turning points in histograms of the data; and others discussed in [59, 60].

An independence assumption led to the log-likelihood function (2.43), and independence of zero-crossing intervals has been critiqued and indeed demonstrated to not strictly be true [5, 57]. However, as in the case of computing the interval variance [51], a qualified independence can produce satisfactory results. Implicit to any mixture model is the dependence encapsulated in the mixing density; and it

will be shown in chapters 4 and 5 to be sufficient for obtaining the parameters of both finite and compound mixture models.

2.5 LACUNARITY

2.5.1 *Origins*

Definitions of lacunarity include: “a multiscaled method for describing patterns of spatial dispersion ” [76]; it “quantifies the degree of translational invariance of the analyzed objects” [77]. The concept was introduced by Mandelbrot [78] as a complementary tool for analysing objects that exhibit ‘fractal’ behaviours, and more generally, it created a new dialogue for describing deterministic and stochastic geometries. Fractal objects possess distinct features that are similar at different scales. Deterministic fractals can be generated iteratively, and often lead to geometrically complex structures. Random fractals have been used to describe a variety of objects in nature [78]—from ferns and snowflakes, to coastlines and galaxy clusters; and they have also found application in stochastic modelling of financial markets [44] and turbulence in fluids [18].

A stochastic process is a random fractal if it has the same statistics at different scales. From these descriptions arise the concept of self-similarity or self-affinity; only mathematically constructed fractals are infinitely self-similar. The power spectra of a random stationary fractal signal $x(t)$ is proportional to $1/\omega^q$, $q > 0$ [79], and as in Sec. 2.1.2, such processes have long term memory. A fractal Gaussian process requires a different level-crossing analysis to the approach taking in this thesis. The associated autocorrelation of such processes are not twice differentiable at the origin, equation Eq. (2.8) implying the average number of crossings in any time window is infinite; however, the crossing count distribution (and therefore also the lacunarity measure) can in fact be related directly to the autocorrelation [80]. In this sense, crossings of differentiable stationary Gaussian processes exhibit a different kind of complexity.

The ‘box dimension’ of a fractal process is $\log(N)/\log(r)$ where N is the number of nonempty boxes relative to a scale size r . The lacunarity measure provided a way to distinguish between fractal objects with the same box dimension, but differing degrees of translational invariance. Lacunarity was then later advocated by Plotnick et al. [76] for any data set in one, two or three dimensions, including imaging data.

Properties such as correlated randomness, deterministic regularity, and clustering relate to variability with respect to scale, and each have distinct lacunarity signatures as outlined in case studies 2 and 3, Sec. 1.3. Derivatives of the lacunarity measure can be used to detect scale dependent changes. A process that is the same at all scales has a lacunarity slope that does not change significantly, and it is possible to identify a decay exponent for the lacunarity by taking logarithms. (This relates back to the box dimension under the concept of a Hurst exponent [79, 80], also used when analysing fractal processes.) A periodic process has an oscillating lacunarity slope. These two behaviours can be used to evaluate periodic and aperiodic dependence as measured by lacunarity, in particular whether they are preserved at different length scales.

2.5.2 Computation

The computation of lacunarity involves boxes $b(\mathbf{r})$ of size \mathbf{r} based on a discretisation spanning the data set, and the $b(\mathbf{r})$ can be closed intervals, squares or cubes, depending on the data’s dimension. Within each box the occurrence of a particular feature is counted as the box moves through the data; these counts $\mathcal{N}(\mathbf{r})$ are then averaged to produce the lacunarity measure:

$$\Lambda(\mathbf{r}) = \langle \mathcal{N}^2(\mathbf{r}) \rangle / \langle \mathcal{N}(\mathbf{r}) \rangle^2 = 1 + \text{Var}[\mathcal{N}(\mathbf{r})] / \langle \mathcal{N}(\mathbf{r}) \rangle^2. \quad (2.44)$$

The standard ‘contiguous-box’ method uses non-overlapping boxes, and is the form traditionally used when describing counting processes (e.g. [3]). Discussions of lacunarity often involve the ‘gliding-box’ method [76, 81] which involves sliding the boxes through the data one discretisation length at a time, resulting in more

contributions to the lacunarity statistic. The calculation becomes computationally costly when the discretisation of the data is large, and therefore also the total number of possible box sizes. This necessitates methods that still produce accurate estimates but more efficiently, ostensibly by limiting the number of times the data is scanned for the box counting—refer to App. E, and to [82] for higher dimensions.

2.5.3 *Lacunarity of Stationary Gaussian Processes*

In [34], lacunarity of the zero-crossings of one-dimensional Gaussian processes with periodic autocorrelation demonstrates the scale-dependent nature of crossings and the strength of dependence in the crossing sequence. The dependence is particularly complex in that at very small/large scales compared with the mean length of crossing intervals, the behaviours resemble a Poisson process, whilst at intermediate time scales there are significant departures that are determined by the process's smoothness. Additionally, when the periodic correlation is strong, oscillations in the lacunarity and its slope demonstrate the similarity at those intermediate time scales to deterministic signals. The oscillations eventually decay as the box size increases.

2.6 ROOTS OF A STOCHASTIC TIME SERIES

The zero-crossing problem can be seen as a subset-cum-reformulation of the general task of solving the equation $f(x) = 0$. If $f(x)$ is a polynomial, the algebraic theorem states that every polynomial of degree n with real or complex coefficients has n real or complex roots [40]; that is,

$$f(x) = x^n + a_{n-1}x^{n-1} + \dots + a_0 = A(x - x_1) \cdots (x - x_n) = 0, \quad (2.45)$$

where a_j are the coefficients, x_j are the roots, and $A \in \mathbb{R}$ is a scaling factor. For non-trivial cases where $n > 5$, or when $f(x)$ is non-invertible, general algebraic solutions are not possible, though there is a diverse range of numerical methods (e.g. [83]) for obtaining approximate solutions.

Fourier analysis involves the decomposition of an input function as a linear combination of sine and cosine functions, and in so doing identifying the periodicity (i.e. returns to zero) of a function. Specifically, a function $f(x)$ with period $2T$ has the ‘Fourier series’ expansion [79]

$$f(x) = \frac{\alpha_0}{2} + \sum_{m=1}^{\infty} \alpha_m \cos(\pi mx/T) + \sum_{m=1}^{\infty} \beta_m \sin(\pi mx/T), \quad (2.46)$$

the coefficients α_m, β_m computed as

$$\alpha_m = \frac{1}{T} \int_{-T}^T f(x) \cos(\pi mx/T) dx, \quad \beta_m = \frac{1}{T} \int_{-T}^T f(x) \sin(\pi mx/T) dx. \quad (2.47)$$

Fourier series have always featured prominently in signal processing [9, 79].

Now let $f(x) = x$ (i.e. the identity function), and suppose $x(t) \in \mathbb{R}$, $t \geq 0$, represents a continuous random variable. By definition, there are infinitely many zeros, and strictly speaking $\Pr\{x(t)=0\}=0$. It is then needful to speak in terms of the probability of a zero-crossing occurring in a time window $[t+T, t+T+dt]$, as described above. A further extension is the ‘auto-regressive process’ $\text{AR}(p)$, a simple version of which is [39]

$$x(t) = \sum_{i=1}^p c_i x(t-i) + \epsilon(t) + c_0, \quad (2.48)$$

for constants $c_i \in \mathbb{R}$, and uncorrelated Gaussian noise $\epsilon(t)$. Such processes are ‘discrete-time signals’ and ‘Markovian’. They are used widely in time series analysis; indeed, it could be argued that time series analysis is concerned with ascribing models to the fluctuations (i.e. crossings) in random signals.

Given a real signal $x(t)$, the corresponding ‘analytical signal’ is [79]

$$x_a(t) = x(t) + \mathbf{i}x_q(t) \equiv A(t) \exp(\mathbf{i}\varphi(t)), \quad (2.49)$$

where $A(t)$ and $\varphi(t)$ are respectively the amplitude and phase modulations, and $x_q(t)$, also termed the quadrature, is the Hilbert transform, computed as

$$x_q(t) = \hat{H}[x(t)] = \frac{1}{\pi} \text{p.v.} \int_{-\infty}^{\infty} \frac{x(\tau)}{t - \tau} d\tau, \quad (2.50)$$

where p.v. stands for principal value. The analytic signal $x_a(t)$ is completely specified by its real and complex zero-crossings, the which are encoded in the amplitude and phase modulations. Real zeros are those instances of time where $A(t)$ vanishes, while complex zeros co-occur with more subtle changes in which $A(t)$ does not change sign. A real zero converted (RZC) signal can be constructed by adding a sine wave $\Omega \sin(\omega_0 t)$ of known frequency ω_0 greater than the highest frequency in the data. Changing the amplitude Ω affects the number of complex zeros that are converted into real zeros. Information in the original signal can be assessed through the perturbations of the regular sine wave, particularly displacement of the real zeros. When applied to an image, this can highlight features such as strong scattering.

Knowledge of the full set of zeros additionally provides an alternative way of representing signals [84], similar to Eq. (2.45). Encoding of information in interspike intervals of neural spike trains has been regarded as a mechanism for the auditory system. Given a particular type of narrow band power spectrum (i.e. power concentrated at large frequencies), and certain refinements, reconstruction of a signal from level-crossings is possible [84]. This further highlights the importance of research on the level-crossing problem.

2.7 REFERENCE PROCESSES

In the analysis to follow, two stationary, ergodic, non-Gaussian processes will be useful references in terms of dependence in a zero-crossing sequence. They have previously featured in the literature alongside results for Gaussian processes [9, 48], ideal because they possess relevant and easy to derive properties.

2.7.1 Random Telegraph-Wave (TW)

Consider the process $x_{TW}(t)$ that jumps between values $+1$ and -1 such that the number of jumps occurring in a time interval of length $|\tau|$ follow a Poisson distribution (2.38) with rate \bar{R} [38]. By analogy, the zero-crossings of this process are the instantaneous jumps. In computing the autocorrelation we need only consider pairs of time points t_1, t_2 . Without loss of generality, suppose $x_{TW}(t_1) = 1$. This then equals $x_{TW}(t_2)$ if and only if there is an even number of jumps in time $|\tau| = |t_2 - t_1|$; else $x_{TW}(t_2) = -1$. It follows that the autocorrelation of the process is

$$\begin{aligned}
 \rho_{TW}(\tau) &= \langle x_{TW}(t_1) x_{TW}(t_2) \rangle \\
 &= 1 \cdot \Pr\{x_{TW}(t_1) = x_{TW}(t_2)\} + (-1) \cdot \Pr\{x_{TW}(t_1) \neq x_{TW}(t_2)\} \\
 &= \sum_{m \text{ even}} \frac{(\bar{R} |\tau|)^m}{m!} e^{-\bar{R} |\tau|} - \sum_{m \text{ odd}} \frac{(\bar{R} |\tau|)^m}{m!} e^{-\bar{R} |\tau|} \\
 &= e^{-\bar{R} |\tau|} \sum_{m=0}^{\infty} \frac{(-\bar{R} |\tau|)^m}{m!} = e^{-2\bar{R} |\tau|}, \tag{2.51}
 \end{aligned}$$

substituting (2.38). The the power spectrum is then

$$S_{TW}(\omega) = \mathcal{F} \left[e^{-2\bar{R} |\tau|} \right] = \bar{R} / \left(\bar{R}^2 + \pi^2 \omega^2 \right). \tag{2.52}$$

Since the jump counts are Poisson distributed, the time intervals between them have an exponential density function with mean \bar{R} [3]; and because by definition they are independent, their correlation coefficient κ_1 is zero. The converse of this last statement is not necessarily true. McFadden [85] was interested in the similarity of the clipped Gaussian process (2.14) to a Poisson process in relation to computing the fourth product moment $\mathbb{E}[x(t) x(t + \tau_1) x(t + \tau_2) x(t + \tau_3)]$, for delay times τ_1, τ_2, τ_3 . When $\zeta(t)$ has the autocorrelation (2.51), the arcsine formula (2.16) implies $x(t)$ has autocorrelation $\rho(\tau) = \sin\left(\pi e^{-2\bar{R}\tau} / 2\right)$. The higher order properties of this process are not Poissonian, as demonstrated by its lacunarity [34].

2.7.2 Random Cosine-Wave (CW)

The process described by

$$x_{CW}(t) = \sqrt{2} \cos(at + \phi), \quad \phi \sim UNIF(0, 2\pi), \quad (2.53)$$

(where *UNIF* denotes the uniform distribution, App. B.2), has autocorrelation

$$\begin{aligned} \rho_{CW}(\tau) &= (2\pi)^{-1} \int_0^{2\pi} x_{CW}(t) x_{CW}(t + \tau) \, d\phi \\ &= (2\pi)^{-1} \int_0^{2\pi} (\cos(a\tau) + \cos(2at + a\tau + 2\phi)) \, d\phi = \cos(a\tau). \end{aligned} \quad (2.54)$$

The corresponding power spectrum is computed using the properties $\cos(a\tau) = (e^{-ia\tau} + e^{ia\tau}) / 2$ and $\mathcal{F}[1] = \delta(\omega)$, and the full form of the Fourier transform, $\mathcal{F}[f(t)] = \int_{-\infty}^{\infty} f(t) e^{-i2\pi\omega t} \, dt$:

$$S_{CW}(\omega) = \mathcal{F}[\cos(a\tau)] = \frac{1}{2} \left(\delta\left(\omega + \frac{a}{2\pi}\right) + \delta\left(\omega - \frac{a}{2\pi}\right) \right). \quad (2.55)$$

The zeros of $x_{CW}(t)$ occur when the argument of the cosine is an odd multiple of $\pi/2$, and the crossing intervals are all of length π/a , resulting in a degenerate distribution, $\delta(T - \pi/a)$; and thus the correlation coefficient κ_1 is one. The density for crossing intervals of a Gaussian process with periodic autocorrelation does resemble a delta-function [5], and the asymptotic similarity to the CW process is replicated in the lacunarity [34] within intermediate time scales.

2.7.3 Periodicities and Returns

A probabilistic definition for the set of periodicities $\eta > 0$ of a random function $x(t)$, $t \in \mathbb{R}$, is

$$D_{x(t)} = \{\eta : \Pr\{x(t) = x(t + \eta)\} > 0, \forall t \in \mathbb{R}\}. \quad (2.56)$$

This differs from the set of time intervals $T > 0$ between level-crossing returns:

$$D_c = \{T : \Pr\{x(t) = c = x(t+T)\} > 0, t \in \mathbb{R}\}. \quad (2.57)$$

These should be treated as the supports for distributions of the periodicities and crossing intervals, with respective densities $f_S(\eta)$ and $p(T)$, where S denotes the associated power spectrum $S(\omega)$. Both sets apply only to times between exactly two returns, and their distinction can be demonstrated by the TW and CW processes defined above. Our primary interest is in the zero-crossings, and for the CW process, $D_{x(t)} = \{2\pi/a\}$, with $D_0 = \{\pi/a\}$, i.e. $D_{x(t)} \cap D_0 = \emptyset$. For the TW process, the switches from 1 to -1 , and vice versa, occur independently, so that $D_{x(t)} = D_1 = D_{-1} = [0, \infty)$.

For a stationary process $x(t)$, the probability density function of positive frequencies can be obtained from the power spectrum as $2S(\omega)$; and correspondingly for the periodicities, under the variable transformation $\omega = 1/\eta$,

$$f_S(\eta) = 2 \left| \frac{d\omega}{d\eta} \right| S(\omega(\eta)) = \frac{2}{\eta^2} S\left(\frac{1}{\eta}\right). \quad (2.58)$$

The maximum periodicity (i.e. the supremum of $D_{x(t)}$) is necessarily an upper-bound for the level-crossing intervals since the periodicities hold at every point in time, for every value in the domain of $x(t)$, and the crossing intervals have been defined to span no more than two crossings. There are no such restrictions on the smallest possible crossing interval, as demonstrated by the CW process. From (2.52)&(2.55), the density functions for periodicities in the TW and CW processes are, respectively,

$$2S_{TW}(\omega) = \frac{2}{\eta^2} \frac{\bar{R}}{(\bar{R}^2 + \pi^2/\eta^2)} = \frac{2\bar{R}}{\pi^2 + \bar{R}^2\eta^2}, \quad (2.59)$$

$$2S_{CW}(\omega) = \frac{2}{\eta^2} \delta\left(\frac{1}{\eta} - \frac{a}{2\pi}\right) = \delta\left(\eta - \frac{2\pi}{a}\right), \quad (2.60)$$

For the essentially deterministic crossings of the cos-wave process, $f_S(\eta)$ and $p(T)$ have the same form; whereas for the telegraph-wave process the decay in $f_S(\eta)$ is

power-law, and for $p(T)$ exponential.

For a stationary Gaussian process with mean zero and variance 1, within every suitably long time window r ($10\mu_T$, say), $\Pr\{|x(t)| > 3\} \sim 10^{-3}$, so that returns to levels large in magnitude though correlated are quite rare. More formally, (2.10) implies all returns in r are finite in counts. Additionally, the following result is recorded in the literature ([27, 37]) for cases where the process's autocorrelation $\rho(\tau)$ satisfies $\lim_{\tau \rightarrow \infty} \log(\tau)\rho(\tau) \rightarrow 0$. From (2.10), set $\bar{N}_C = \bar{R}e^{-C^2/2}$, for $C = |c|$, $c \in \mathbb{R}$. If $r, C \rightarrow \infty$ so that $r\bar{N}_C \rightarrow \tilde{N}_C$, then

$$\lim_{C \rightarrow \infty} P_N(\mathcal{N}_C(r) = m) = \exp(-\tilde{N}_C) \tilde{N}_C^m / m!. \quad (2.61)$$

Nguyen [86] verified this result through simulations when $\rho(\tau) = e^{-\tau^2/2}$ and $C = 1$. Our main concern is with crossings of the zero-level, but given the symmetry of the process, (2.61) would suggest runs of large crossing intervals ($> 3\mu_T$, say) are rare, and that the interval density never skews to the right.

2.8 SUMMARY

This chapter has described why a Gaussian process is a helpful launch-point for characterising random zero-crossings. A fair amount of general results and analyses relating to crossing averages exist, and these remain important benchmarks for any future modelling. The task of finding the interval density has been solved numerically speaking and subject to certain conditions, but there are still few analytic expressions. As an alternative, the mixture model approach for approximating distributions was outlined, and in particular, the use of parametric forms reduces the problem to one of optimisation—provided underlying assumptions are valid. Lacunarity is a particularly powerful tool in the analysis of counting processes, and it too can provide information on the degree of dependence in crossing intervals. Finally, elementary properties were given for two non-Gaussian processes that will be reference points in the analysis to follow, their respective crossing sequences exemplars of two extremes of dependence. The next chapter introduces a type of Gaussian

process with periodic autocorrelation, and via simulations will begin exploration of the effects on sample functions, and by extension the zero-crossings.

3

SIMULATIONS OF OSCILLATORY CORRELATED GAUSSIAN PROCESSES

This chapter describes simulation methods for generating a correlated process and extracting its zero-crossings. Examples of Gaussian process are simulated to illustrate the foundational numerical procedures, and validate statistical results using existing zero-crossing theory. The notion of oscillatory correlation is introduced and shown to suggest a categorisation for stationary Gaussian processes such that distinct zero-crossing behaviours can be expected. Here the emphasis is on moments of the crossing intervals to benchmark the simulation methods. Subsequent chapters will explore the distributions of random variables relating to the intervals. In this thesis all numerical computations (integrations, simulations, optimisations, etc.) are performed in the programming environment MATLAB®.

3.1 AUTOCORRELATIONS AND POWER SPECTRA

Let $x(t)$, $-\infty < t < \infty$, be a real stationary, ergodic, Gaussian process, with mean $\langle x(t) \rangle = 0$, variance $\text{Var}[x(t)] = \langle x^2(t) \rangle = 1$, and zero-crossing intervals having random variable T . The normalized autocorrelation of processes we shall consider take the form

$$\rho_{ij}(\tau; a, L) = g_i(\tau; L) \cos^j(a\tau / \sqrt{j}), \quad j = 1, 2, \quad (3.1)$$

where $g_i(\tau; L)$ is itself an autocorrelation, $a \geq 0$ is the periodicity parameter, and $L > 0$ is the correlation length. Notionally, L^{-1} gives the rate of decay in the autocorrelation; increasing the value of L means the influence of previous values persists over a longer range in time. Similarly, increasing a gives the process more periodic dependence, and this will be used to explore dependence in the zero-crossings. The index j allows us to test two kinds of oscillatory correlation, the $j = 2$ case being the non-negative type. For convenience, we shall at times refer to a process by its autocorrelation without any argument; likewise, the parameters a, L may be suppressed in $\rho_{ij}(\tau; a, L)$ and $g_i(\tau; L)$.

Our focus is on processes that are either smooth or sub-fractal, meaning they are at least once differentiable and the mean crossing count (2.8) is finite. We prescribe $g_i(\tau)$ in (3.1) to expand as $1 - \tau^2 / (2L^2) + \mathcal{O}(|\tau|^3)$. The full autocorrelation (3.1) then has expansion

$$\rho_{ij}(\tau) = \sum_{m=0}^{\infty} \left(2m\alpha_m |\tau|^{-1} + \ell_m \right) \frac{\tau^{2m}}{(2m)!}, \quad (3.2)$$

and the smoothness of the process is determined by the form of $g_i(\tau; L)$. Using the formula for the product of two power series ([72], Eq. 0.316) leads to

$$\begin{aligned} \alpha_0 &= 0, & \ell_0 &= 1; \\ \alpha_1 &= 0, & \ell_1 &= g_i''(0) - a^2 = -(L^{-2} + a^2); \\ \alpha_2 &= g_i'''(0), & \ell_2 &= g_i^{(4)}(0) + 6a^2L^{-2} + ja^4; \quad \text{etc.} \end{aligned} \quad (3.3)$$

We are explicit in these expansions because they relate to higher order properties of the process and its zero-crossings, and therefore relevant to the simulation method and validation. The coefficients α_m and ℓ_m respectively give the value of odd and even derivatives of $\rho_{ij}(\tau)$. Only for smooth processes is $\alpha_m = 0$ for all m ; additionally, for sub-fractal process $\alpha_2 \geq 0$, independent of the periodicity parameter a . By definition, $\rho_{ij}(\tau) = \langle x(t)x(t+\tau) \rangle$, so $\ell_0 = \rho_{ij}(0) = \langle x^2(t) \rangle$; ℓ_0 is the

variance of $x(t)$. Rice's result (2.8) gives the mean crossing count in time window r as $\bar{R}r$, where

$$\bar{R} = \sqrt{-\varrho_1}/\pi = \sqrt{L^{-2} + a^2}/\pi \equiv \langle T \rangle^{-1}, \quad (3.4)$$

$\langle T \rangle$ being the mean crossing interval. Likewise, the expected number of maxima in the path traced by $x(t)$ is $\bar{R}_M r$, (2.9), where

$$\sqrt{-\varrho_2/\varrho_1}/(2\pi) = \sqrt{(g_i^{(4)}(0) + ja^4 + 6a^2)/(L^{-2} + a^2)}/2\pi =: \bar{R}_M, \quad (3.5)$$

and unlike (3.4), here there is dependence on the type of oscillatory correlation ($j = 1$ or 2). Note that if $\varrho_2 > 0$, \bar{R}_M does not strictly exist for the process, and so for consistency of interpretation one may use the Wiener-Khinchin theorem (Thm. 2.2) with $S_{ij}(\omega)$ as the power spectrum:

$$\begin{aligned} \rho_{ij}(\tau) &= 2 \int_0^\infty S_{ij}(\omega) \cos(2\pi\omega\tau) d\omega, \\ \Rightarrow \varrho_m &= \rho_{ij}^{(2m)}(0) = 2(-1)^m \int_0^\infty (2\pi\omega)^{2m} S_{ij}(\omega) d\omega. \end{aligned} \quad (3.6)$$

If the integral exists then \bar{R}_M exists, thereby providing a test for the sub-fractality of the process [48]. Indeed, turning points of $x(t)$ occur at zero-crossings of its derivative $x'(t)$.

There are of course an infinity of stationary Gaussian processes, but as for the behaviour of their associated power spectra $S(\omega)$, in particular relating to the maxima, there are only three forms: spectra with (1) a maximum at the origin alone, (2) maxima displaced from the origin, and (3) a combination of these two. By design, the choices we make for $g_i(\tau)$ will have a power spectrum $G_i(\omega)$ that is either maximal at the origin alone, or equals a positive constant on a closed interval including the origin and is zero outside that interval. The associated spectra of the

full autocorrelation $\rho_{ij}(\tau)$ are easily calculated using the following properties of the Fourier Transform. For $b_1, b_2 \in \mathbb{R}$, and scalar, real-valued functions $f_1(t), f_2(t)$,

$$\mathcal{F}[b_1 f_1(t) + b_2 f_2(t)] = b_1 \mathcal{F}[f_1(t)] + b_2 \mathcal{F}[f_2(t)], \quad (3.7)$$

$$\mathcal{F}[f_1(t) \cos(b_1 t)] = \frac{1}{2} \left(F_1 \left(\omega + \frac{b_1}{2\pi} \right) + F_1 \left(\omega - \frac{b_1}{2\pi} \right) \right), \quad (3.8)$$

where $F_1(\omega) = \mathcal{F}[f_1(t)] = 2 \int_0^\infty f_1(t) \cos(2\pi\omega t) dt$ gives the Fourier transform of an even function $f_1(t)$. Given $G_i(\omega) = \mathcal{F}[g(\tau)]$, the Fourier transforms of $\rho_{ij}(\tau)$, $j=1, 2$ are, respectively,

$$\begin{aligned} S_{i1}(\omega) &= \mathcal{F}[g_i(\tau) \cos(a\tau)] \\ &= \frac{1}{2} \left(G_i \left(\omega + \frac{a}{2\pi} \right) + G_i \left(\omega - \frac{a}{2\pi} \right) \right), \end{aligned} \quad (3.9)$$

$$\begin{aligned} S_{i2}(\omega) &= \mathcal{F} \left[g_i(\tau) \cos^2 \left(a\tau / \sqrt{2} \right) \right] = \frac{1}{2} \mathcal{F}[g_i(\tau)] + \frac{1}{2} \mathcal{F} \left[g_i(\tau) \cos \left(\sqrt{2} a\tau \right) \right] \\ &= \frac{1}{2} G_i(\omega) + \frac{1}{4} \left(G_i \left(\omega + \frac{a}{\sqrt{2}\pi} \right) + G_i \left(\omega - \frac{a}{\sqrt{2}\pi} \right) \right), \end{aligned} \quad (3.10)$$

where the cosine double-angle formula is used to compute $S_{i2}(\omega)$. Now, $S_{ij}(\omega)$ is an even function, and for all values of a ,

$$0 \leq S_{i1}(0) \leq G_i(0), \quad G_i(0) / 2 < S_{i2}(0) \leq G_i(0); \quad (3.11)$$

and as $a \rightarrow \infty$,

$$S_{i1}(0) = G_i \left(\frac{a}{2\pi} \right) \rightarrow 0, \quad (3.12)$$

$$S_{i2}(0) = \frac{1}{2} \left(G_i(0) + G_i \left(\frac{a}{\sqrt{2}\pi} \right) \right) \rightarrow \frac{1}{2} G_i(0). \quad (3.13)$$

Evaluating the power spectrum at frequencies indicated by the shifts to $G_i(\omega)$ seen in (3.9)&(3.10) gives

$$S_{ij} \left(\pm \frac{a}{\sqrt{2}^{3-j}\pi} \right) \rightarrow \frac{1}{2^j} G_i(0), \quad \text{as } a \rightarrow \infty. \quad (3.14)$$

Equations (3.12)&(3.13) imply that at large a , $S_{i1}(\omega)$ has a minimum point at the origin and is maximal at frequencies $\pm\omega_0$, for some $\omega_0 \sim a/(2\pi)$. The function $S_{i2}(\omega)$ instead retains a maximum point at the origin and develops two additional maxima at the frequencies $\pm\omega_0$, for some $\omega_0 \sim a/(\sqrt{2}\pi)$. Thus our chosen formulation will exemplify the aforementioned trio of forms as the periodicity parameter a is varied, and the effects of this categorisation are central to this thesis. Recall that the power spectrum of the cos-wave process is a sum of delta functions, each centred at frequencies $\pm a/(2\pi)$, (2.55), and this form of power spectrum accompanies deterministic oscillations in sample functions. Equation (3.14) shows that as $a \rightarrow \infty$, the power spectrum never becomes a delta function, meaning that even at large a there is still some randomness in the sample functions and zero-crossings of the Gaussian process $x(t)$.

3.2 SIMULATION METHODS

3.2.1 Discretisation of Time

A random process may be simulated by constructing a finite numerical sequence with the required distribution and correlation properties. These ‘realisations’ represent sample functions of the process with time infinite in the past and future. Specifically, the function $x(t)$ is sampled at time points

$$\mathbf{t}_n = (n - 1) \Delta t, \quad n = 1, 2, \dots, n_{\max}, \quad (3.15)$$

leading to a realisation x . The notation \mathbf{t}_n should be understood as the n -th element of the vector \mathbf{t} , the boldface used for vectors to differentiate between parameters used elsewhere in the thesis.

The discretisation step Δt and sampling length n_{\max} must be chosen such that the correct frequency of zero-crossings is observed, and there are three length scales to bear in mind: a^{-1} , L and $\langle T \rangle$, respectively corresponding to periodicity, memory and zero-crossing intervals. We require that $\Delta t/L \ll \langle T \rangle$, as well as $\Delta t/L \propto a^{-1}$ at

large a since from (3.4), larger a leads to a smaller mean interval. Without loss of generality, we set $L=1$ and choose

$$\Delta t = 1/\text{round} \left\{ 200\sqrt{1+a^2} \right\} \approx \langle T \rangle / (200\pi), \quad (3.16)$$

where the function ‘round’ gives the nearest integer to its argument. For convenience, we set $n_{\max} = 3.1416 \times 10^6$. It follows that for each realisation,

$$\begin{aligned} \langle \text{no. of crossings} \rangle &\approx \frac{\text{total time}}{\text{average time between crossings}} \approx \frac{n_{\max}\Delta t}{\langle T \rangle} \\ &\approx 5 \times 10^3, \end{aligned} \quad (3.17)$$

3.2.2 Generating a Random Process

According to Thm. 2.1, all we require is a procedure that suitably produces a discrete-time Gaussian process, and then by ergodicity, each realisation will possess the average statistical properties of a sample function of the process. Adapted from [4], Fig. 3.1 contains the algorithm we use to produce a single realisation of the random process $x(t)$, and it supersedes the standard Fourier filtering method (FFM) for generating a process described in [87] and elsewhere.

The discrete Fourier transform (DFT) of the sequence of values x_n , $n = 1, \dots, n_{\max}$, can be calculated using

$$\mathbf{X}_{m+1} = \sum_{n=0}^{n_{\max}-1} x_{n+1} e^{i2\pi mn/n_{\max}}, \quad m = 0, \dots, n_{\max} - 1, \quad (3.18)$$

and this relates to the x_n through the inverse DFT

$$x_{n+1} = \frac{1}{n_{\max}} \sum_{m=0}^{n_{\max}-1} \mathbf{X}_{m+1} e^{i2\pi mn/n_{\max}}, \quad n = 0, \dots, n_{\max} - 1, \quad (3.19)$$

$\mathbf{i} = \sqrt{-1}$ being the imaginary unit. Below, the expression $\text{DFT}\{x\}$ is used to denote the DFT of the elements of x according to (3.18); likewise, $\text{DFT}^{-1}\{\mathbf{X}\}$ denotes the inverse DFT of \mathbf{X} according to (3.19).

Let $\boldsymbol{\tau}$ and $\boldsymbol{\omega}$ respectively be vectors of the delay times and frequency points associated with the above time discretisation; then for symmetric forms of autocorrelation and power spectrum,

$$\boldsymbol{\tau}_n = \Delta t \times |n - n_{\max}/2 - 1|, \quad \boldsymbol{\omega}_n = (\Delta t)^{-2} \boldsymbol{\tau}_n / n_{\max}, \quad n = 1, \dots, n_{\max}. \quad (3.20)$$

The following relations (see [88], Sec. 7-9) are central to both the standard and iterative Fourier filtering methods:

$$(\Delta t)^{-1} S(\bar{\boldsymbol{\omega}}) \approx \text{DFT}\{\rho(\boldsymbol{\tau})\} \approx n_{\max}^{-1} \mathbf{X} \odot \mathbf{X}^*, \quad (3.21)$$

where \mathbf{X}^* is the complex conjugate of \mathbf{X} , the operator ' \odot ' denotes element-wise multiplication, and in order to match values of the theoretical and discrete Fourier transforms, the frequencies $\boldsymbol{\omega}$ are shifted circularly using

$$\bar{\boldsymbol{\omega}}_n = \begin{cases} \boldsymbol{\omega}_n, & n = n_{\max}/2, \\ \boldsymbol{\omega}_{(n+n_{\max}/2) \bmod n_{\max}}, & \text{otherwise.} \end{cases} \quad (3.22)$$

The first approximation in (3.21) is the numerical analogue of the Wiener-Khinchin theorem (2.2), with equality in the limit $n_{\max} \rightarrow \infty$ and $\Delta t \rightarrow 0$. The second approximation gives the power spectrum estimate as obtained from a realisation x and its DFT, \mathbf{X} . In the notation of Fig. 3.1, the FFM stops at step 3, defining a realisation through $x = \text{DFT}^{-1}\{\mathbf{W} \odot \mathbf{Y}\}$. We found the FFM to almost always yield a realisation that failed the Kolmogorov-Smirnov test for normality at the 5% significance level [89]. It also required significantly increasing the sample length n_{\max} to obtain reliable zero-crossing statistics when the periodicity parameter a was very large ($a > 30$), thereby requiring additional computing time and memory resources.

The iterative Fourier filtering method (iFFM) uses the fact that correlation in time for a discrete-time process is encoded in ranking of data values. After generating an initial sequence of uncorrelated variates from a target distribution, this same

**Iterative Fourier filtering method (iFFM) for generating
a realisation x of a correlated random process**

1. Calculate S , the power spectrum at frequency points ω , or calculate ρ , the autocorrelation at delay times τ , then compute weight function W using

$$W_m^2 = (\Delta t)^{-1} S_m \quad \text{or} \quad W_m^2 = |\rho_m|.$$

2. Generate uncorrelated sequence of random numbers y from target distribution.
3. Compute Fourier transform of y , enforce desired power spectrum using weight function and compute inverse Fourier transform:

$$Y = \text{DFT}\{y\}; \quad X_m = W_m Y_m |Y_m|^{-1}; \quad x = \text{DFT}^{-1}\{X\}.$$

4. Compute ranks (in decreasing order) of x and y , rank-replace x with the current y , then redefine y as x :

$$RX = \text{rank}\{x\}, \quad RY = \text{rank}\{y\}; \quad x_{n \rightarrow RX_n} = y_{n \rightarrow RY_n}; \quad y = x.$$

5. Repeat steps 3–4 until x_n (satisfactorily) has the target correlation properties.

Figure 3.1.: Algorithm 1. DFT refers to the discrete Fourier transform, and DFT^{-1} to its inverse, respectively defined in (3.18, 3.19). In step 2 we use the standard normal distribution, with random variates generated by MATLAB. We find 29 iterations at step 5 to be acceptable.

sequence is permuted recursively to have the required ranking (i.e. correlation), and so the target distribution is preserved throughout. The rank-replacement in step 4 slightly alters the long-term correlation, and so it and the filtering step are repeated. These further iterations lead to convergence of the ranks RX , and since these determine the magnitudes of DFT contributions (3.18) they invariably lead to convergence in the realisation x . Consequently, the iFFM can produce reliable realisations for arbitrary large a without adjusting the sample length n_{\max} as a increases. The quality of the standard normal variates (used at step 2) depends only on the accuracy of MATLAB's (or other software's) pseudorandom number generators.

A description of how computers produce pseudorandom numbers is given in [90], and in particular, standard normal variates are obtained as transforms of standard

uniform variates, themselves the result of a ‘multiplicative congruential algorithm’, or similar method. Except where indicated, we use MATLAB’s implementation of the ‘Mersenne Twister’ random number generator (RNG) [91], combined with the ‘Ziggurat algorithm’ [92] for the distribution transformation, yielding an exactly normally distributed sequence [90]. Given a seed or starting value for the RNG, one obtains a cycle of numbers termed the ‘random number stream’. For the Mersenne Twister, the stream has length (i.e. periodicity) $2^{19937} - 1$. Choosing different seeds leads to different streams, which in our context leads to independent realisations of the random process. Specifically, 10^3 realisations will use $10^3 n_{\max} = 3.1416 \times 10^9 \lesssim 2^{32}$ different pseudorandom numbers.

3.2.3 Zero-Crossing Statistics

Having generated a realisation x , the zero-crossings are obtained as follows. First define $\xi := \text{sign}\{x_n\}$. A zero-crossing occurs in the time interval $[t_{n-1}, t_n]$ if x_{n-1} and x_n have opposite signs, i.e. $\xi_{n-1}\xi_n = -1$. Thus, identify all the zero-crossings of x through

$$z_n := \begin{cases} (1 - \xi_{n-1}\xi_n) / 2, & n = 2, \dots, n_{\max}, \\ 0, & n = 1, \end{cases} \quad (3.23)$$

and $z_n = 1$ denotes a crossing in the interval $[t_{n-1}, t_n]$. Next, from the values of n such that $nz_n \neq 0$, form a new sequence l_k , $k = 1, \dots, N$, the locations immediately after the crossings. Given the time discretisation (3.15), the crossings are (approximately) located at times $l_k^\Delta := \Delta t(l_k - 1) - \Delta t/2$, and zero-crossing intervals are given by

$$T_k := l_{k+1}^\Delta - l_k^\Delta = \Delta t(l_{k+1} - l_k), \quad k = 1, \dots, N - 1. \quad (3.24)$$

The smallest possible value of T_k is Δt , meaning there is potentially some simulation error, particularly when the principal mode of the interval density is zero. This corresponds to tangent-type zero-crossings (instances of time where the process and

its derivative are zero) being more frequent than up-/down-crossings. Numerical operations performed by MATLAB (with the default precision of 32 digits after the decimal place) mean the standard normal variates it generates are unlikely to be exactly zero, so x_n is almost always nonzero. Furthermore, the discretisation (3.16) ensures the appropriate number of crossings are observed for each realisation, and in all cases we expect

$$P(T \leq \Delta t) \approx P\left(T \leq (200\pi)^{-1}\langle T \rangle\right) \ll 1, \quad (3.25)$$

$P(T)$ being the analytical cumulative density function for crossing intervals. For simulation estimates of the interval density, we use the frequency binning method with a bin size of $\max\left\{2, \sqrt{1 + a^2}/2\right\}$ —refer to App. J.

From (3.24) simulation estimates for zero-crossing interval moments can be computed, and over multiple realisations the domain of crossing intervals (given a particular autocorrelation function) is better sampled; then averaging over realisations improves the moment estimation. McFadden's work [48] predicts the interval variance σ_T^2 for a Gaussian process with autocorrelation $\rho(\tau)$ as

$$\begin{aligned} \sigma_T^2 &= \sigma_1 \sigma_2, \\ \sigma_1^2 &= 4(\pi\bar{R})^{-1} \int_0^\infty \arcsin(\rho(\tau)) d\tau, \\ \sigma_2^2 &= \bar{R}^{-2} \left(1 + 2 \int_0^\infty (U(\tau) - \bar{R}) d\tau \right), \end{aligned} \quad (3.26)$$

where

$$\begin{aligned} U(\tau) &= \frac{1}{\pi^2 \bar{R} (1 - \rho^2(\tau))^{3/2}} \left(\left| A^2 - B^2 \right|^{1/2} + B \arctan \left(\frac{B}{\left| A^2 - B^2 \right|^{1/2}} \right) \right), \\ A &= -\rho''(0) (1 - \rho^2(\tau)) - \rho'^2(\tau), \\ B &= \rho''(\tau) (1 - \rho^2(\tau)) + \rho(\tau) \rho'^2(\tau). \end{aligned} \quad (3.27)$$

The variance and mean, μ_T , may be combined to give the coefficient of variation

$$c_v = \sigma_T / \mu_T, \quad (3.28)$$

a measure of dispersion in the distribution of the random variable relative to the mean. Each of the contributory estimates to σ_T^2 result from assuming the crossing intervals are statistically independent. The linear correlation coefficient for adjacent intervals is defined as

$$\kappa_1 = (\langle T_1 T_2 \rangle - \mu_T^2) / \sigma_T^2, \quad (3.29)$$

where $\langle T_1 T_2 \rangle$ is the product moment of adjacent intervals. By considering a Markov Chain model for the crossing intervals, McFadden also derived an analytic form for κ_1 [48]:

$$\kappa_1 = 1 - 2\sigma_1 / (\sigma_1 + \sigma_2), \quad (3.30)$$

where σ_1, σ_2 are defined in (3.26). These analytical results for the interval moments enable verification of the simulation method outlined above, and are therefore a foundation for subsequent investigations into the effect of correlation on zero-crossing statistics. Later chapters will consider distributions of the crossing intervals and of the counting process formed by the crossings, this secondary process represented in simulations as the cumulative sum of (3.23).

3.3 SIMULATION RESULTS

We now specify two forms for the function $g_i(\tau)$ in (3.1):

$$\begin{aligned} g_1(\tau) &= \exp(-\tau^2/2), \\ g_2(\tau) &= \frac{3}{2} \exp(-|\tau|/\sqrt{3}) - \frac{1}{2} \exp(-\sqrt{3}|\tau|), \end{aligned} \quad (3.31)$$

each prescribing processes previously studied in the literature [48, 35], the first a smooth process and the second sub-fractal. Substituting these forms into our general autocorrelation (3.1) gives four processes ($\rho_{11}, \rho_{21}, \rho_{12}, \rho_{22}$), and these are

sufficient at this juncture to check that simulations support the analytical results listed above, particularly with regards to the smoothness of the process and the type of oscillatory correlation. Equations for power spectra $G_{ij}(\omega)$ can be found in App. A.

3.3.1 Convergence of Algorithm

The simulation method as described in Fig. 3.1 guarantees that the output has the distribution specified at step 2, and so it remains to check convergence of the algorithm. In addition to the autocorrelation function $\rho(\tau) = \langle x(t) x(t + \tau) \rangle$ for a Gaussian process $x(t)$, the following higher order correlations [38] can be expressed in terms of $\rho(\tau)$: for delay times $\tau_1 \leq \tau_2 \leq \tau_3 \leq \tau_4$,

$$\begin{aligned} \langle x(\tau_1) x(\tau_2) x(\tau_3) x(\tau_4) \rangle &= \rho(\tau_1 - \tau_2) \rho(\tau_3 - \tau_4) + \rho(\tau_1 - \tau_3) \rho(\tau_2 - \tau_4) \\ &\quad + \rho(\tau_1 - \tau_4) \rho(\tau_2 - \tau_3), \end{aligned}$$

and so in particular,

$$\langle x(t) x^3(t + \tau) \rangle = 3\rho(\tau), \quad \langle x^2(t) x^2(t + \tau) \rangle = 1 + 2\rho^2(\tau). \quad (3.32)$$

Let \mathbf{y} be a realisation of a second process $y(t)$, and from (3.22) define $\bar{\tau} = n_{\max}(\Delta t)^2 \bar{\omega}$. Similar to (3.21), the cross-correlation of $x(t)$ and $y(t)$ at time $\tau = \bar{\tau}_n$ is

$$\langle x(t) y(t + \tau) \rangle \approx n_{\max}^{-1} \text{DFT}^{-1} \{ \text{DFT}\{x\} \odot \text{DFT}\{y\}^* \}, \quad (3.33)$$

By redefining $x(t)$ and $y(t)$ appropriately, (3.33) can be used to obtain simulation estimates for $\langle x(t) x(t + \tau) \rangle$, $\langle x(t) x^3(t + \tau) \rangle$, and $\langle x^2(t) x^2(t + \tau) \rangle$.

Figure 3.2 considers correlation functions for realisations of the process with autocorrelation $\rho_{11}(\tau; 10) = \exp(-\tau^2/2) \cos(10\tau)$. Plot (a) shows the error in the autocorrelation is reduced through repeated iterations of the filtering and rank-

replacement steps of the iFFM, and plots (b, c) respectively contain numerical estimates and corresponding analytical forms of $\langle x(t) x^3(t + \tau) \rangle$ and $\langle x^2(t) x^2(t + \tau) \rangle$. Each iteration of the iFFM (Fig. 3.1) produces a realisation x and its ranks \mathbf{RX} . Let $\mathbf{x}^{(k)}$ and $\mathbf{RX}^{(k)}$ denote the realisation and ranks after the k -th iteration, $k=1$ being the first pass of the algorithm and $k > 1$ the remaining reiterations at step 5. Define also unit-delta functions $\delta_1(t)$, $\bar{\delta}_1(t)$ through

$$\delta_1(t) = 1 - \bar{\delta}_1(t) = \begin{cases} 1, & t = 0, \\ 0, & \text{otherwise.} \end{cases} \quad (3.34)$$

Figure 3.3 compares x and \mathbf{RX} over successive iterations. The plots show that as the number of iterations k increases, changes in both the values of the realisation and their ranks (i.e. relative positions of the x_n with respect to magnitude, and therefore the correlation) decrease; that is,

$$\mathbf{x}^{(k)} - \mathbf{x}^{(k-1)} \rightarrow \mathbf{0}, \quad \sum_{n=1}^{n_{\max}} \bar{\delta}_1(\mathbf{RX}_n^{(k)} - \mathbf{RX}_n^{(k-1)}) \rightarrow 0 \quad \text{as } k \rightarrow \infty, \quad (3.35)$$

where $\mathbf{0}$ is the zero vector. Plot (b) includes rank changes up to 100 iterations of the algorithm to make the decline more apparent to the reader; however, the adjacent plot and the plots in Fig. 3.2 indicate 30 iterations are sufficient and the additional computer time not required. (Each iteration can last as long as 1 second, and crossing statistics are to be calculated from multiple realisations.) Recall that x was initially a sequence of uncorrelated normal variates, and since the correlation properties converge we can trust the method does simulate correlated Gaussian processes. Further validation of the simulation method are provided by subsequent comparisons to existing analytical results for zero-crossings of Gaussian processes.

3.3.2 Sample Functions

The sample function properties are intimately connected to those of the crossing intervals and provide a first look at how crossing behaviour is affected by the

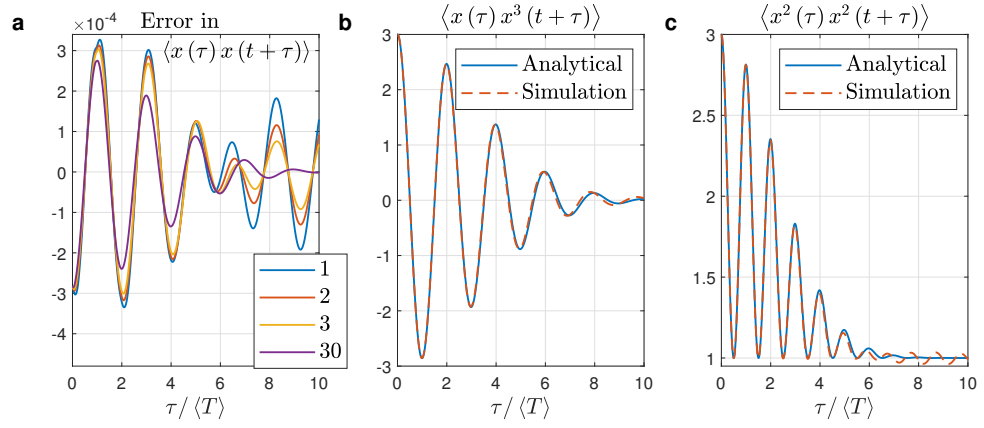


Figure 3.2.: Plots comparing analytical correlation functions with estimates given a single realisation of the process ρ_{11} when $a = 10$. The simulations use the iFFM (Fig. 3.1) with 2^{21} as the RNG seed. In (a) the legend refers to iterations of the algorithm. The error (simulation estimates minus analytical values) in the autocorrelation is seen to progressively decrease after each iteration. In plots (b, c) simulation estimates of (3.32) use the final realisation (30th iteration), and the simulation results match well with analytical curves.

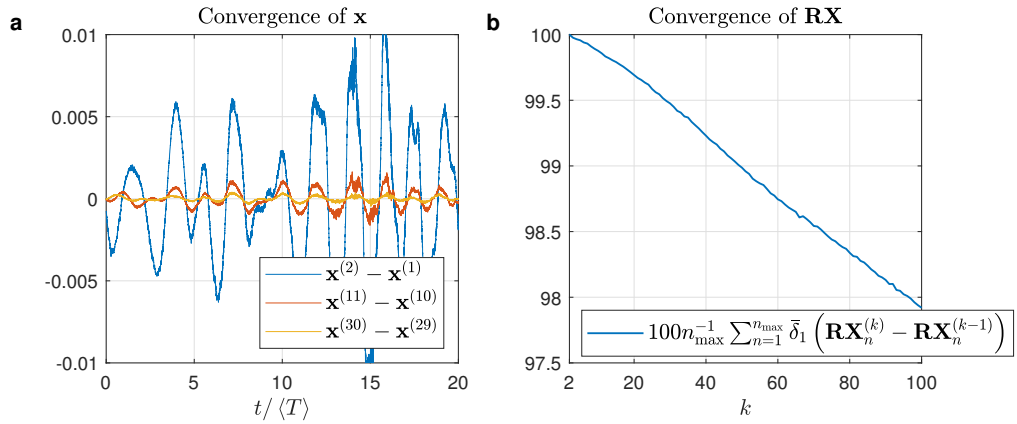


Figure 3.3.: Plots demonstrating convergence of the iFFM (Fig. 3.1), for simulations of the process with autocorrelation $\rho_{11}(\tau; 10)$ and 2^{21} as the RNG seed. Plot (a) demonstrates the values x_n make the realisation converge. Plot (b) shows as a percentage the proportion of ranks that are changed at each iteration; as k increases there are fewer changes, meaning the correlation in x also converges.

autocorrelation. The realisations in Figs. 3.4&3.5 are of processes ρ_{1j} and ρ_{2j} for different values of a (refer to Eq. (3.1)). Each realisation is generated using an RNG seed of 2^{21} , so the only difference (in terms of simulation input) is their respective power spectra. When $a = 0$, the autocorrelations reduce to $g_1(\tau)$ and $g_2(\tau)$

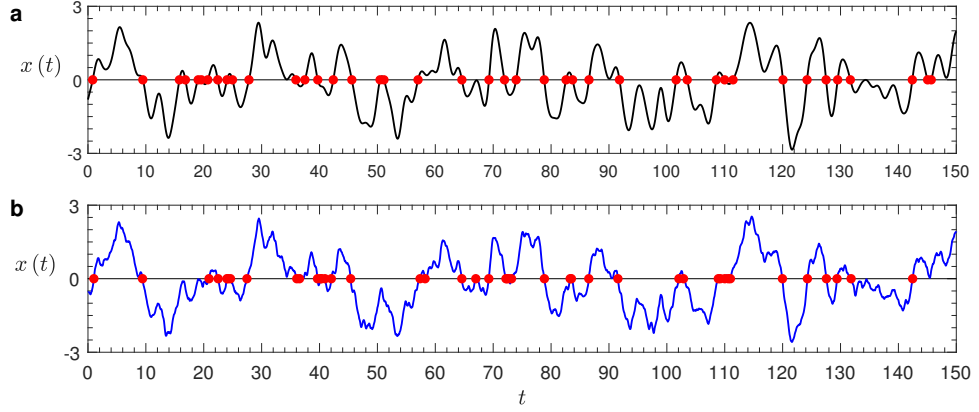


Figure 3.4.: Realisations of the processes g_1 (a) and g_2 (b), generated using the iFFM with the same RNG seed. The curves are similar but additional turning points in the g_2 case indicate g_1 is a smoother process. Zero-crossings are marked as red circles, and the time intervals between these show more variation in the g_2 case.

(defined in (3.31)), and their realisations are shown in Fig. 3.4, the differences clear. The g_1 case is smoother, crossings are at times bunched together, but crossing intervals do not vary a great deal. The g_2 realisation has additional rapid turning points away from the zero level, and here bunched crossings (i.e. short intervals) usually precede much larger crossing intervals. This is expected given the autocorrelation; the sub-fractality of $g_2(\tau)$ means in a sample function shorter crossings are more frequent, and the slower correlation decay ($e^{-|\tau|/\sqrt{3}}$ as opposed to $e^{-\tau^2/2}$ for $g_1(\tau)$) allows for larger crossing intervals. These two features balance out so that the mean interval length is the same for both processes.

There are distinct changes in sample function behaviour when oscillatory correlation is introduced. The number of zero-crossings and turning points both increase linearly in time, (2.8)&(2.9), and we shall make reference to the rates of crossings, \bar{R} , and of turning points, $2\bar{R}_M$: from (3.4)&(3.5),

$$\begin{aligned} \bar{R} &= \frac{\sqrt{1+a^2}}{\pi} \sim \frac{a}{\pi} \quad \text{as } a \rightarrow \infty; \\ 2\bar{R}_M &= \frac{\sqrt{(g_i^{(4)}(0) + 6a^2 + ja^4) / (1+a^2)}}{\pi} \sim \frac{\sqrt{ja}}{\pi} \quad \text{as } a \rightarrow \infty. \end{aligned} \quad (3.36)$$

Rice's result (3.5) is for expected maxima, and since a Gaussian process is distributed symmetrically about its mean value (here zero), the result must also apply to the minima; whence the average number of turning points in time t' is $2\bar{R}_M t'$. Note: for sub-fractal processes with autocorrelation $\rho_{2j}(\tau)$, \bar{R}_M exists when $a^2 > 13/(\sqrt{39j+81}-9)$.

The first four plots in Fig. 3.5 illustrate the 'cos' type of oscillatory correlation; the autocorrelation varies between ± 1 , so sample function values have positive and negative correlation. As a increases, there is greater periodic memory in the process and realisations begin to look more regular, almost sinusoidal due to the frequency of turning points approaching that of zero-crossings ($2\bar{R}_M \sim \bar{R} \sim a/\pi$). Additionally, plots (b, d) show the sub-fractal properties are suppressed, but not removed since from (3.3), α_2 is independent of a . There is little difference between plots (c, d), respectively smooth and sub-fractal cases with $a = 10$.

The remaining four plots in Fig. 3.5 are for the 'cos²' type of oscillatory correlation, for which the autocorrelation is non-negative. Again, as a increases we see similarity in sample function behaviour, irrespective of the degree of smoothness, and we label this effect as a 'homogenisation'. Likewise, sample functions are regularised towards wave-like forms, though less pronounced than in the $j = 1$ extreme a cases. Realisations in plots (e-h) resemble a slowly changing random process described by $g_i(\tau)$ upon which is superimposed a rapid sinusoidal modulation of frequency $a/(\sqrt{2}\pi)$. From (3.36), turning points in the $j = 2$ case occur more frequently than zero-crossings when a is large ($2\bar{R}_M \sim \sqrt{2}a/\pi > \bar{R}$). In the vein of the 'Bolzano Theorem'[40] (relating to roots of continuous functions on closed intervals), it follows from continuity and symmetry (of a Gaussian process) that there must be frequent bunched crossings as well as epochs during which no axis crossings occur (so as to match the average crossing number in the $j = 1$ case), and these are evidenced in plots (g, h).

In the above, not much has been said on sample functions when $a \in (0, 3)$. Contained in this interval are critical values of a which we shall argue are best determined by a spectral analysis (see Ch. 5). In essence, when a is below the critical value,

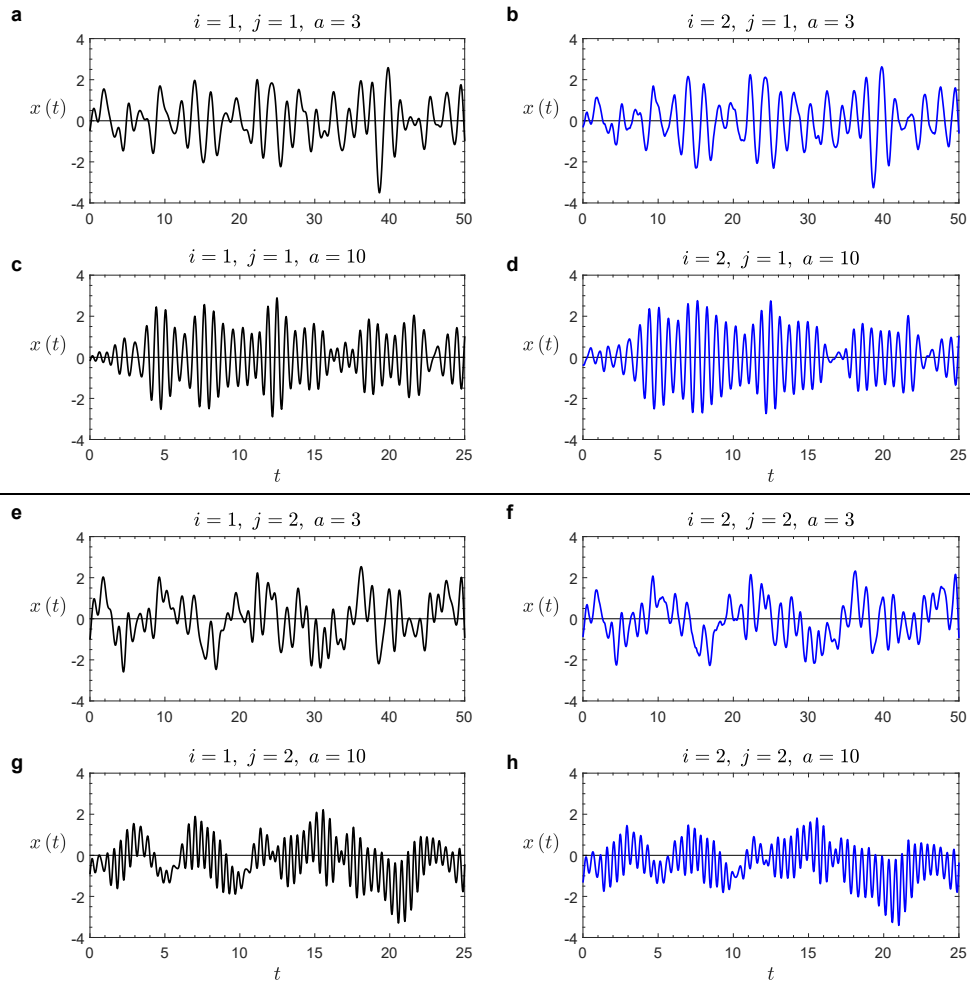


Figure 3.5.: Realisations of processes with autocorrelation $g_i(\tau) \cos^j(a\tau/\sqrt{j})$, for the choices of $g_i(\tau)$ given in (3.31). Plots (a–d) show that in $j = 1$ cases, the sample function regularises towards a sinusoidal function. Conversely, plots (e–g) show another kind of regularity wherein behaviour from the $a = 0$ case is preserved. As a increases, the type of oscillatory correlation ($j = 1$ or $j = 2$) is more significant than the choice of $g_i(\tau)$, and there is little difference between smooth (a, c, e, g) and sub-fractal (b, d, f, h) processes.

the behaviour of the power spectrum near the origin is relatively unchanged, and consequently neither are sample function and zero-crossing properties.

3.3.3 Interval Moments

From (3.4), the mean interval length is $\pi/\sqrt{1+a^2}$, so as a increases the mean interval length decreases, in line with crossings occurring with greater frequency.

This result holds for both sub-fractal and smooth choices of $g_i(\tau)$ in (3.1), and independent of the type of oscillatory correlation. By contrast, the variance of the crossing intervals is impacted by both smoothness and periodicity. Figure 3.6 includes plots of the variance as computed from McFadden's equations (3.26), and they agree well with simulations. The similarity between smooth and sub-fractal processes as a increases is reflected in the interval variance, and identifying the asymptotic dependence on a is also useful in distinguishing between the two types of oscillatory correlation. For this a third curve is included in each of the four plots of Fig. 3.6, the values given in the legend found using nonlinear regression. The interval variance decays (approximately) like $a^{-7/2}$ for $j=1$ processes, and like a^{-1} when $j=2$. Since the mean decays like a^{-1} , for the coefficient of variation (3.28)

$$c_v \sim a^{(5(j-1)-3)/4} \quad \text{as } a \rightarrow \infty; \quad (3.37)$$

This implies that when $j=1$ the interval sizes become less dispersed relative to the mean as a increases, but when $j=2$ the reverse occurs, and both are glimpsed in Fig. 3.5. These forms of c_v prefigure modelling of the crossing interval distribution, especially evolution of tail behaviour, as will be revealed in chapter 5.

The correlation coefficient (3.29), as estimated from simulations and application of McFadden's result (3.30), are contained in Fig. 3.7. When a is small, κ_1 is similar for both types of oscillatory correlation and McFadden's model is in (approximate) agreement with simulation results. For the $j=1$ cases this agreement holds till $a=10$, and beyond this the underestimation grows, though κ_1 still approaches the same limit as the simulations. Note that for the smooth process ρ_{11} , κ_1 increases to 1 from a negative value, whilst for sub-fractal processes ρ_{21} , κ_1 is positive for all values of a . Conversely, for $j=2$ cases when $a=10$, McFadden's result converges to a much different value to that of simulations and with a significantly different gradient. Moreover, it is not immediately obvious how nonnegative correlation at large a in the process leads to negative correlation in the interval sequence. The coefficient κ_1 defined in (3.29) is Pearson's correlation coefficient, which measures

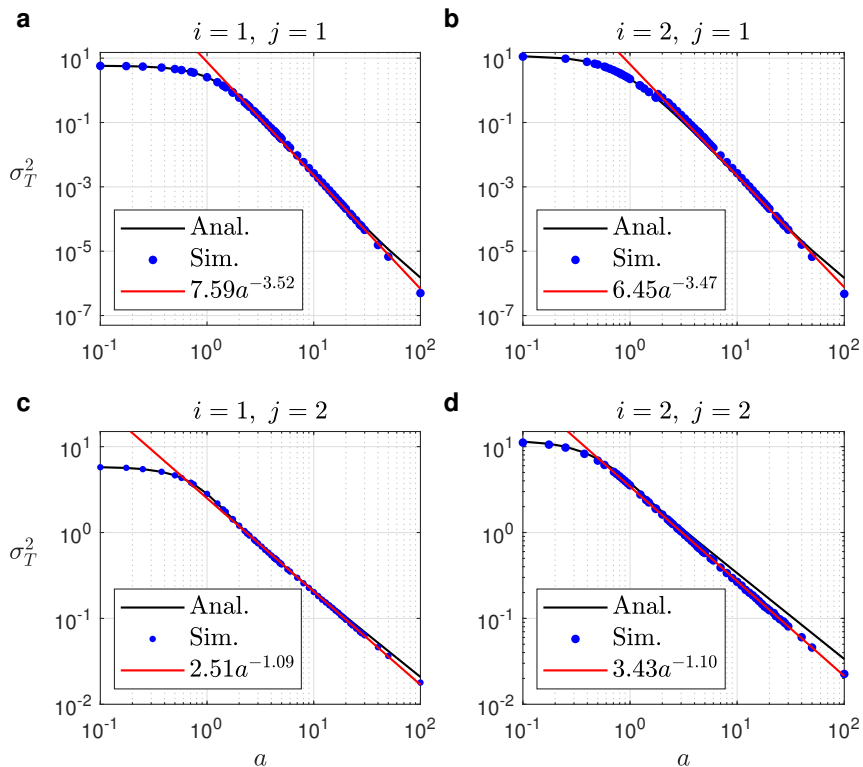


Figure 3.6.: Plots of the interval variance as a function of a for processes with autocorrelation $g_i(\tau) \cos^j(a\tau/\sqrt{j})$, for choices of $g_i(\tau)$ given in (3.31). Analytical results from McFadden's equations (3.26) are shown as black lines, simulation results (averaged over 10^2 realisations for each a) as blue circles, and the asymptotic dependence on a as red lines. Simulations were generated using the iFFM (Fig. 3.1) with RNG seeds chosen at random for each realisation.

linear dependence [40]. Therefore, exploring the behaviour of crossing intervals as a increases will require a closer look at dependence in the sequence of intervals.

3.4 STOCHASTIC PERIODICITY REVISITED

In section Sec. 2.7.3 we gave a definition of probabilistic periodicity, and we now discuss the density function $f_S(\eta)$ defined in (2.58); explicit expressions for the

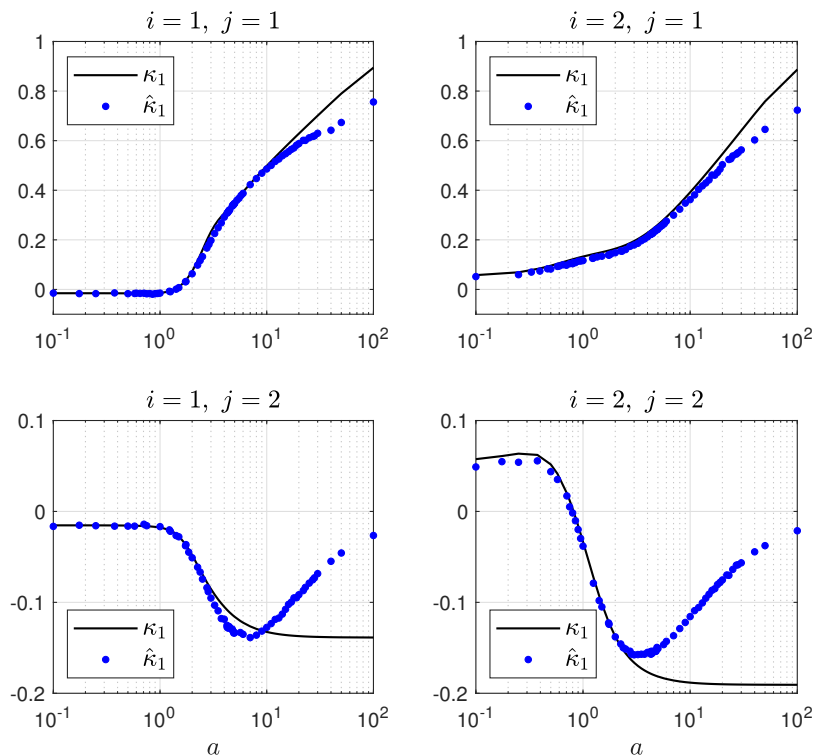


Figure 3.7.: Plots of the linear correlation coefficient as a function of a for processes with autocorrelation $g_i(\tau) \cos^j(a\tau/\sqrt{j})$, for choices of $g_i(\tau)$ given in (3.31). Analytical results from McFadden's equations (3.30) are shown as black lines and simulation results (averaged over 10^2 realisations for each a) as blue circles. Simulations were generated using the iFFM (Fig. 3.1) with RNG seeds chosen at random for each realisation

power spectra are found in App. A. Now, for any power spectrum $S(\omega)$ that decays to zero as $\omega \rightarrow 0$,

$$f_S(\eta) = \frac{2}{\eta^2} S\left(\frac{1}{\eta}\right) \sim 2\eta^{-2} S(0) \rightarrow 0, \quad (3.38)$$

as $\eta \rightarrow \infty$, and so the power-law decay at large η is the same for both Gaussian and Poisson processes. This is not the case for the cos-wave (CW) process which has no randomness in its periodicity density; $f_S(\eta)$ in that case is a delta function (2.60). In figure 3.8, we see that the periodicity density changes as a increases for Gaussian processes with power spectra $S_{ij}(\omega)$, defined in (3.9)&(3.10). The example of the random telegraph-wave (TW) which has Poissonian crossings is used to highlight similarities and differences; its periodicity density is (2.59), and this is plotted for

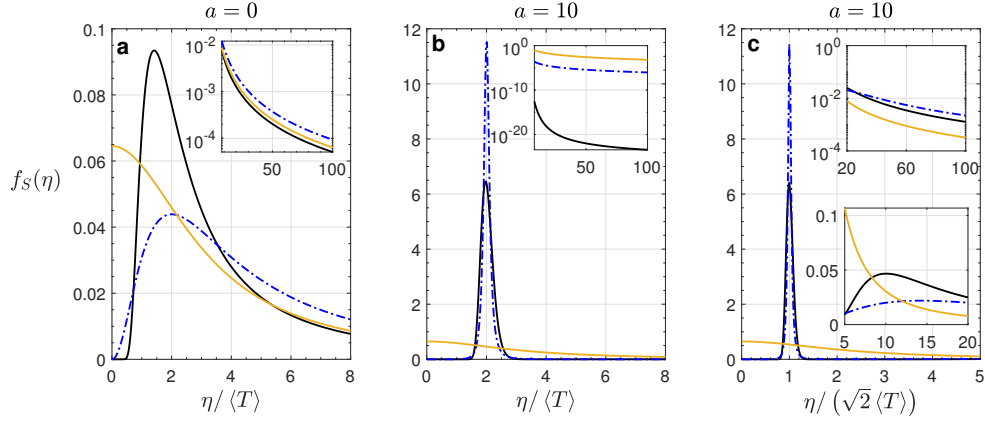


Figure 3.8.: Plots of the density function for sample function periodicities as a varies, where $f_S(\eta) = 2\eta^{-2}S(\eta^{-1})$, for respective power spectra $S(\omega)$. Insets show behaviour at larger values of η . Orange curves are used for the TW process with Poissonian crossings; solid black curves are used for the Gaussian processes ρ_{1j} , and dash-dot blue curves for ρ_{2j} . (a): The densities for processes g_1 and g_2 are quite different at small η , but the inset shows decay at large η is similar to the Poisson case. (b): The cosine modulation significantly narrows $f_S(\eta)$, particularly for the smooth process ρ_{11} ; the sub-fractal process ρ_{21} decays similar to that of the Poisson case. (c): The cosine-squared modulation also narrows $f_S(\eta)$, but there is a secondary, much larger mode; and in this instance the decay for both smooth and sub-fractal cases are bounded below by the Poisson case.

crossing rates $\bar{R} = \langle T \rangle^{-1}$.

From Fig. 3.8 it is possible to identify the modal periodicities $\bar{\eta}$, which are the time periods after which sample functions are most likely to exhibit similar behaviour. For the Poisson case, the mode is zero, in agreement with it being a memoryless process [3]. For all the Gaussian processes, $\lim_{\eta \rightarrow 0} f_S(\eta) = 0$. Plot (a) shows the variance is large when $a = 0$, the density is left-skewed, and the modal periodicity is approximately $\sqrt{2}\langle T \rangle$ for the g_1 process, and $2\langle T \rangle$ for the g_2 process. The Sub-fractality of g_2 means the probability of observing similar behaviour in time scales much less than $\langle T \rangle$ is greater than that for g_1 ; and smoothness has the opposite effect around the mode. As $\eta \rightarrow \infty$, the curves for g_1 and g_2 are located either side of the Poisson case. As a increases, $f_S(\eta)$ becomes more concentrated and symmetric around the mode. For the cosine modulation, plot (b), the modal periodicity is $\bar{\eta} \approx 2\langle T \rangle$, further demonstration of similarity to the cos-wave process. For the

cosine-squared modulation, plot (c), the periodicity density is bimodal from which we can identify a slow timescale $\bar{\eta}_1 \approx \sqrt{2}\langle T \rangle$, and a fast timescale $\bar{\eta}_2 \approx 10\sqrt{2}\langle T \rangle$. The cos-wave process typifies the crossing behaviour associated with a narrow periodicity density function. For the Gaussian processes, when a is large, since most of the variation happens at small time scales and the processes are symmetric, there will be an increased frequency of zero-crossings and turning points at all levels, in agreement with Rice's results (3.4)–(3.5), and the wave-like properties in Fig. 3.5. More formally, given a power spectrum $S(\omega)$, stationary points of $f_S(\eta)$ occur when

$$\begin{aligned} \frac{df_S}{d\eta} &= -\frac{2}{\eta^4} \left(2\eta S|_{\omega=\eta^{-1}} + S'|_{\omega=\eta^{-1}} \right) = 0 \\ \Rightarrow S|_{\omega=\eta^{-1}} &= -\frac{1}{2\eta} S'|_{\omega=\eta^{-1}} \\ \Rightarrow S(\omega) &= -\frac{\omega}{2} \frac{dS}{d\omega}. \end{aligned} \quad (3.39)$$

The modal periodicity is then either zero, or $\bar{\eta}$ such that $f_S(\eta)$ is maximal and $\omega = \bar{\eta}^{-1}$ satisfies (3.39). Thus, the number of time scales in a stationary process is determined by the number of maxima in its spectrum.

3.5 SUMMARY

This chapter introduced the types of Gaussian processes we study and expected behaviour given their autocorrelation functions. Simulating processes was shown to be straightforward and the output reliable; given the three inputs of RNG seed, distribution, and autocorrelation (or associated power spectrum), the iFFM converges to a unique realisation that minimises correlation error and has the correct distribution. Existing analytical results further validated simulations, and the plots produced helped with visualising the influence of the autocorrelation on extremal properties of the random processes considered. In particular, the type of oscillatory correlation (governed by the periodicity parameter a) led to different sample function and zero-crossing properties, a recognition that we shall argue is vital to

any proposed models of crossing behaviour. Increasing periodicity homogenises processes towards forms almost independent of their smoothness, and the periodicity regularises the zero-crossings.

The general form of autocorrelation (3.1) will enable further exploration of the subtleties of the zero-crossing problem, particularly as it applies to dependence in the crossing sequence. Traditionally, the correlation coefficient (3.29) when close to zero is interpreted as representing independent behaviour, which here applies to the crossing intervals, and a Markov chain dependence is sufficient for predicting the interval variance [48]. The next chapter investigates these interpretations as they concern the case $a=0$; subsequent chapters will further interrogate the underlying assumptions when $a > 0$ and interval dependence is clear. We will also seek to establish general results for zero-crossings of Gaussian processes, and continue to look at the ZCP through the lens of probabilistic or stochastic periodicity.

4

FINITE MIXTURE MODELS FOR THE INTERVAL DENSITY

Simulation results in the preceding chapter showed the evolution of a stationary Gaussian processes and its zero-crossings as oscillatory correlation is increased. The zero-crossings are representative of statistical dependence in the process, and modelling associated distributions such as that of crossing intervals remains an important aspect. Sections 2.2.3.1 and 2.2.3.2 described and critiqued two key methods that express the interval density as an integral. For stationary Gaussian processes, simulation estimates for the interval variance are well predicted by those models that assume a Markov chain dependence amongst the intervals [5, 48]. However, this assumption does not necessarily carry over to computation of the interval density, particularly when intervals are strongly correlated (see [5]).

The next two chapters will present an alternative perspective using mixture models, the focus being less on composite functions of the autocorrelation and more on samples of the crossing intervals. The goal is to demonstrate that for processes which fall into a specific category (as determined by their power spectrum), their interval densities can be modelled using a finite set of basis functions. These estimates provide explicit formulas with tail behaviour as predicted by existing theory [5, 93]. Our approach of informed modelling directly from the data speaks to the connection to other contexts involving point processes and sequences of events, such as reliability and queueing theory [59]. By definition, finite mixture modelling implicitly assigns a structure to the data; in practice, this may correspond to a known grouping as in survival analysis, or an emergent property as in cluster analysis. The latter case would seem a reasonable perspective on long term behaviour of the crossing interval

sequence of a stationary process given the crossings occur linearly in time.

This chapter focuses on example processes with our general autocorrelation (3.1) when $a = 0$. Reflected in plots of the correlation coefficient, Fig. 3.7, such cases may be treated as having approximately independent intervals, with effect that both Markov chain and Slepian regression methods produce reasonable estimates for the interval density, though only so far as existing numerical integration methods allow for particular autocorrelations. We contend that the intervals can also be modelled with finite mixtures of two or more density functions, and this is tested using a range of smooth and sub-fractal processes, most of which have been examined in the nearly six decades of literature on zero-crossings and studies of certain physical systems. In the same spirit as [85], this chapter addresses the question of how similar crossing intervals of Gaussian processes are to inter-event times of a Poisson point process, a case in which the interval density is a one parameter exponential function.

4.1 PRELIMINARIES

4.1.1 Properties of Class 0 Processes

In Sec. 3.1 the observation was made that based on properties of the power spectrum, there are three kinds of stationary Gaussian processes, and we now label these as classes, the first of which has the following definitional properties.

Proposition 1 (Class 0 Process)

A process with autocorrelation function $g(\tau)$ and power spectrum $G(\omega)$ such that

$$(I) \quad g(\tau) = \sum_{m=0}^{\infty} \left(2m\alpha_m |\tau|^{-1} + \ell_m \right) \frac{\tau^{2m}}{(2m)!}, \quad \alpha_0 = \alpha_1 = 0, \ell_0 = -\ell_1 = 1;$$

$$(II) \quad \forall \omega, G(\omega) \leq G(0), G(0) > 0;$$

(III) *Either $\omega = 0$ is the only maximum point of $G(\omega)$, or $G(\omega)$ is a positive constant for $|\omega| < \omega_*$ and zero for $|\omega| \geq \omega_*$, for some $\omega_* > 0$.*

For a smooth process, $\alpha_m = 0, \forall m$, and the process is infinitely differentiable [37]; but for a sub-fractal process not all of the α_m are zero, and the process is m -times differentiable if and only if $\alpha_m = 0$, for $m \in \mathbb{N}$ [37]. These properties influence the distribution of the crossing intervals $p(T)$, particularly near the origin [35, 53]:

$$\begin{aligned} \alpha_2 = 0 &\Rightarrow p(T) \sim \mathcal{O}(T), \quad p(0) = 0; \\ \alpha_2 \neq 0 &\Rightarrow p(T) \sim \mathcal{O}(1), \quad \frac{\alpha_2}{6} \leq p(0+) \leq \frac{\alpha_2}{4}. \end{aligned} \quad (4.1)$$

In the former case, $p(T)$ can be found using the Slepian regression method [2] up to some $\hat{T} \gg \langle T \rangle$, the magnitude of which depends heavily on the interval variance σ_T^2 . The reliability of the method when $\alpha_2 \neq 0$ was discussed in Sec. 2.2.3.2. The Laplace inversion method was also shown to have limitations, Sec. 2.2.3.1. To the author's knowledge, Wong's process [35] has the only autocorrelation for which the interval density has been derived explicitly. The derivation is similar to the Slepian regression method but it starts from an exact explicit representation of the random process $x(t)$.

The large T behaviour of the interval density has similarly been predicted [54] for a process $x(t)$ with autocorrelation $\rho(\tau)$, and processes in this chapter all have a finite persistence exponent Θ , earlier defined in (2.29), and here means

$$p(T) \sim e^{-\Theta T}, \quad \text{as } T \rightarrow \infty. \quad (4.2)$$

Slepian's comparison theorem [93] says that given two processes $x(t), y(t)$ respectively having autocorrelations $\rho_x(\tau), \rho_y(\tau)$, if $\rho_x(\tau) \leq \rho_y(\tau)$ for $0 \leq \tau \leq T'$, then

$$1 - P_x(T) \leq 1 - P_y(T), \quad (4.3)$$

for $0 \leq T \leq T'$ where $P_x(T), P_y(T)$ are the respective cumulative density functions (cdfs) of the crossing intervals. Class 0 processes all have mean interval π , so if the inequality $\rho_x(\tau) \leq \rho_y(\tau)$ holds as $T' \rightarrow \infty$, then the persistence exponent Θ will be smaller for the process $y(t)$ and the variance of the intervals σ_T^2 larger, regardless of the smoothness of the process. Further inequalities relating to the asymptotics of

$p(T)$ have been derived [53], but for our purposes those listed above are sufficient, and represented in the finite mixture models we now describe.

4.1.2 A Basis Distribution

The interval density $p(T)$ will be modelled as

$$p(T) = \sum_{k=1}^K \alpha_k f_k(T; \boldsymbol{\theta}_k), \quad (4.4)$$

where $K < \infty$, $\alpha_k < 1$, $\alpha_K = 1 - \sum_{k=1}^{K-1} \alpha_k$, and $\boldsymbol{\theta}_k$ is a vector of parameters for the k -th component density function, $f_k(T; \boldsymbol{\theta}_k)$. The general aim is to demonstrate using basis functions that the similarity of class 0 processes is reflected in the interval density. We define a new distribution family, the 'generalized exponential product distribution', $GEXPP(c, d, a, b)$, with probability density function (pdf)

$$\frac{d(a^d + b^d)^{c/d}}{b^c \Gamma(c/d) \left((a^d + b^d)^{c/d} - a^c \right)} T^{c-1} \exp\left(-\left(\frac{T}{b}\right)^d\right) \left(1 - \exp\left(-\left(\frac{T}{a}\right)^d\right)\right), \quad (4.5)$$

for (positive) shape parameters c, d , and (nonnegative) scale parameters a, b . The $GEXPP$ distribution¹ allows for all possible polynomial forms at small T , and exponential decays at large T . It incorporates three well-known exponential-type distribution families. In the limit $a \rightarrow 0$, (4.5) becomes

$$\frac{d}{b^c \Gamma(c/d)} T^{c-1} \exp\left(-\left(\frac{T}{b}\right)^d\right). \quad (4.6)$$

When $c = d$, the Weibull distribution, $WEIB(c, b)$, obtains. It is used widely in reliability theory (e.g. [94]) for its flexibility and the simplicity of its cdf. The case $d = 1$ gives the gamma distribution, $GAM(c, b)$, which also has a long tradition in reliability theory, and in other contexts involving sequences of events. If $c = d = 1$ the exponential distribution, $EXP(b)$, results, again with broad applications, in

¹ This differs from the exponentiated Weibull distribution [95], though the two are equivalent for certain values of the shape parameters.

particular as the distribution of intervals between Poisson distributed events [64].

The choice of parameters should respect the asymptotics at the left tail (4.1) and right tail (4.2), thereby requiring $c, d \geq 1$ in (4.5). For sub-fractal processes with $p(0) > 0$, the mixture model would need at least one *EXP* distribution. The other cases when $p(0) = 0$ could be dealt with using either of the *GAM* or *WEIB* distributions; however the shape parameter would need to be fixed ($c = 2$) for the pdf to be $\mathcal{O}(T)$ as $T \rightarrow 0$, leaving only one unspecified parameter and therefore less flexibility for the associated density contributions in (4.4). Alternatively, the *GEXPP* distribution with $c = d = 1$ and $a, b > 0$ gives the ‘exponential product distribution’, *EXPP*(a, b), which from (4.5) has pdf

$$\frac{a+b}{b^2} \exp\left(-\frac{T}{b}\right) \left[1 - \exp\left(-\frac{T}{a}\right)\right]. \quad (4.7)$$

This function is $\mathcal{O}(T)$ as $T \rightarrow 0$; and as $T \rightarrow \infty$ the function is essentially exponential with parameter b .

From (4.1), the interval density is at least once differentiable when $p(0) = 0$, and as the mixture components $f_k(T; \theta_k)$ each have the form (4.5), we require

$$c_k \geq 2 \quad \text{if} \quad a_k = 0, \quad (4.8)$$

for *GAM* or *WEIB* densities. We shall extend this condition to cases where $p(0) > 0$, and doing so does not suggest a loss of interpretation. According to (4.2), the mixture component with the slowest decay should be strictly exponential, which is achieved by either *EXP* or *EXPP*, the latter being necessary if $p(0) = 0$. Given the mixture (4.4) with each $f_k(T; \theta_k)$ having the form (4.5), the persistence exponent is estimated as

$$\Theta = \max_k \{b_k : d_k = 1\}. \quad (4.9)$$

With the exception of results concerning the tails of $p(T)$, it is not immediately

obvious what are suitable parameter values. Specifying only a few parameter constraints allow for improvements to the estimation without necessarily increasing K , the number of mixture components in (4.4).

A summary of the four distributions (EXP , GAM , $WEIB$, $EXPP$) is included in App. B. Note that the EXP distribution is a specific case of the other three distributions; in particular, $EXPP(a, b)$ approaches $EXP(b)$ as $a \rightarrow 0$. Again, we emphasise that these should be compared to the random telegraph-wave process in which intervals are given by one EXP distribution.

4.1.3 Solution Methods

The goal is to use simulation data to find parameters such that the model (4.4) is satisfactory according to tail behaviour outlined above and other criteria to follow. As discussed in Sec. 2.4, parameter estimates are primarily found using maximum likelihood estimation (MLE). The input data consists of crossing intervals $\mathbf{T} = \{\mathbf{T}_m; m=1, \dots, n_T\}$, the result of 10^3 realisations of the process $x(t)$, each giving $\approx 5 \times 10^3$ intervals (3.17).

The underlying assumption is that for sufficiently large n_T , the mixture model is identifiable; that is, a unique characterisation of $p(\mathbf{T})$ exists (subject to relabelling of indices), important because we have proposed a basis distribution $GEXPP$, (4.5), for crossing intervals of class 0 processes. When the model's component densities $f_k(\mathbf{T}; \boldsymbol{\theta}_k)$ each have the form (4.6) (i.e. for GAM , $WEIB$ or EXP distributions) identifiability of the mixture has been established [60]. The $EXPP$ and EXP distributions only use scale parameters; other than the stretching or shrinking from parameters prescribing different decay rates, the general shape of their density functions remain the same for all parameter choices. This would advise against having too many component densities from either the $EXPP$ or EXP distributions, both in terms of parameter estimation and what the models say about zero-crossings of the original process.

The problem can be stated as follows: to find parameters that maximise the log-likelihood function [60]

$$\ell(\mathbf{T}; \boldsymbol{\alpha}) = \sum_{m=1}^{n_T} \log(p(\mathbf{T}_m; \boldsymbol{\alpha})) = \sum_{m=1}^{n_T} \log\left(\sum_{k=1}^K \alpha_k f_k(\mathbf{T}_m; c_k, d_k, a_k, b_k)\right), \quad (4.10)$$

and as outlined above, constraints for the parameters are determined by the choice of $f_k(T; \boldsymbol{\theta}_k)$, chosen prior to the optimisation. The form of loglikelihood function assumes the \mathbf{T}_m are independent. Nevertheless, the intervals are dependent, but for class 0 processes this dependence is sufficiently weak that the above form of likelihood function is an acceptable approximation. The parameter estimates are found by minimizing the negated loglikelihood function in MATLAB, primarily using the implementation of the Nelder-Mead simplex method [73], and imposing that at inadmissible parameter values $\ell(\mathbf{T}; \boldsymbol{\alpha}) = -\infty$. The solution process as outlined here is of a supervised nature. It is advantageous to fit the data with a single density function that captures the persistence exponent, and then add extra component densities based on additional characteristics of $p(T)$ such as skewness, inflections and turning points. Estimates for additional parameters are then found either by observation or solving moment equations. The mixture parameters α_k are such that $p(T)$ is dominated by one of the component densities, so that with reasonable estimates of the other parameters the solution procedure will converge. More importantly, the processes we consider are strongly connected so that estimates for one process can be used as initial estimates for another process. Given two different probability models, the one with the smaller error in moments and cdf (as compared with the data) is selected.

4.2 RESULTS

A variety of class 0 processes g_i are now explored, where for the index i , odd values will denote a smooth process, whilst even i will denote a sub-fractal process. A representative list of parameter estimates is given in App. F for reference. Each Gaussian process is first described, followed by its interval density. Equations for

power spectra are provided in App. A. Tables 4.1&4.2 summarise the density models, and Figs. 4.1–4.4 contain plots of the interval density that compare simulation results and various models. We restrict the analysis to cases where McFadden’s variance equations [48] give comparable results to simulation estimates, which invariably translates to $\sigma_T^2 < 30$ and $G_i(0) < 20$.

4.2.1 Smooth Processes

Class 0 smooth processes are in fact more complicated than their sub-fractal counterparts, indicated by the range of correlation decay and the forms of interval density. We consider processes with the following autocorrelations:

$$g_1(\tau) = \exp(-\tau^2/2); \quad (4.11)$$

$$g_3(\tau, \gamma) = \left(\frac{\sin(\sqrt{3}\tau/\sqrt{\gamma})}{\sqrt{3}\tau/\sqrt{\gamma}} \right)^\gamma, \quad \gamma \in \mathbb{N}; \quad (4.12)$$

$$g_5(\tau, \gamma) = \left(1 + \frac{\tau^2}{2\gamma} \right)^{-\gamma}, \quad \gamma \in \mathbb{R}_{>1/2}; \quad (4.13)$$

$$g_7(\tau, \gamma) = \operatorname{sech}\left(\sqrt{1 + \gamma^2\tau}\right) \cosh(\gamma\tau), \quad \gamma \in \mathbb{R}; \quad (4.14)$$

$$g_9(\tau) = \frac{3\left(\sin(\sqrt{5}\tau) - \sqrt{5}\tau \cos(\sqrt{5}\tau)\right)}{5\sqrt{5}\tau^3}. \quad (4.15)$$

4.2.1.1 g_1 : Squared Exponential

Figure 4.1(a). The prototypical Gaussian process, and the limiting form of certain smooth and sub-fractal processes, it has the fastest autocorrelation decay possible for a differentiable process [39]. The crossings intervals have been identified as anti-bunched, that is, repelled from each other [5, 47], and the Laplace inversion method gives the persistence exponent as ≈ 0.4009 [5]. Figure 1(a) shows the interval density, composed of one *WEIB* and one *GAM* pdf which capture behaviour near

Process	γ	Decay	Mixture	Persistence
g_1	-	$e^{-\tau^2/2}$	<i>WEIB, GAM, EXPP</i>	0.4256
g_3	1	τ^{-1}	<i>WEIB</i> \times 3, <i>GAM</i> \times 5, <i>EXPP</i>	0.4709
	2	τ^{-2}	<i>WEIB</i> \times 2, <i>GAM</i> \times 3, <i>EXPP</i>	0.4162
	3	τ^{-3}	<i>WEIB</i> \times 2, <i>GAM, EXPP</i>	0.4389
	4	τ^{-4}	<i>WEIB, GAM, EXPP</i>	0.4296
g_5	1	τ^{-2}	SAA	0.3281
	2	τ^{-4}	SAA	0.3778
	3	τ^{-6}	SAA	0.3949
	4	τ^{-8}	SAA	0.4019
g_7	0	$e^{-\tau}$	<i>GAM</i> \times 2, <i>EXPP</i>	0.3748
	1	$e^{-\tau(\sqrt{2}-1)}$	SAA	0.2829
	2	$e^{-\tau(\sqrt{5}-2)}$	<i>GAM</i> \times 3, <i>EXPP</i>	0.1928
	3	$e^{-\tau(\sqrt{10}-3)}$	<i>GAM</i> \times 4, <i>EXPP</i>	0.1442
g_9	-	τ^{-2}	<i>WEIB</i> \times 2, <i>GAM</i> \times 2, <i>EXPP</i>	0.4581

Table 4.1.: Summary of class 0 smooth processes, their correlation decay, finite mixture density models, and estimates of the persistence exponent Θ , (4.2). SAA means “Same As Above”.

the mode of $p(T)$, and the *EXPP* pdf describes the left and right tails. The three mix together to give an inflection point just before the exponential tail takes over.

4.2.1.2 g_3 : *Sinc Type 1*

Figures 4.1(b)–(d) and 4.3. This type of process shows the effect of a power spectrum that is nonzero on an open interval that includes the origin, and zero otherwise. With reference to Sec. 2.7.3, the periodicity density (2.58) in this case is bounded below owing to the Heaviside functions (see App. A.2). The $\gamma=1$ case is referred to as low frequency white noise (e.g. [49, 52]), and in signal communication the range of frequencies for which the power spectrum is nonzero has a physical interpretation, such as the range of detectable sound frequencies. We note that this type of oscillatory correlation is different from the class 1 and 2 type because the power spectra are maximal and centred at the origin. Interval densities of the sinc type 1 process are complex, as evidenced by the number of mixture components, and the complexity is caused by the additional time scales given by zeros of the autocorrelation. From (4.12) these occur at delay times $(\sqrt{3/\gamma}/\pi) \tau \in \mathbb{Z}$, and

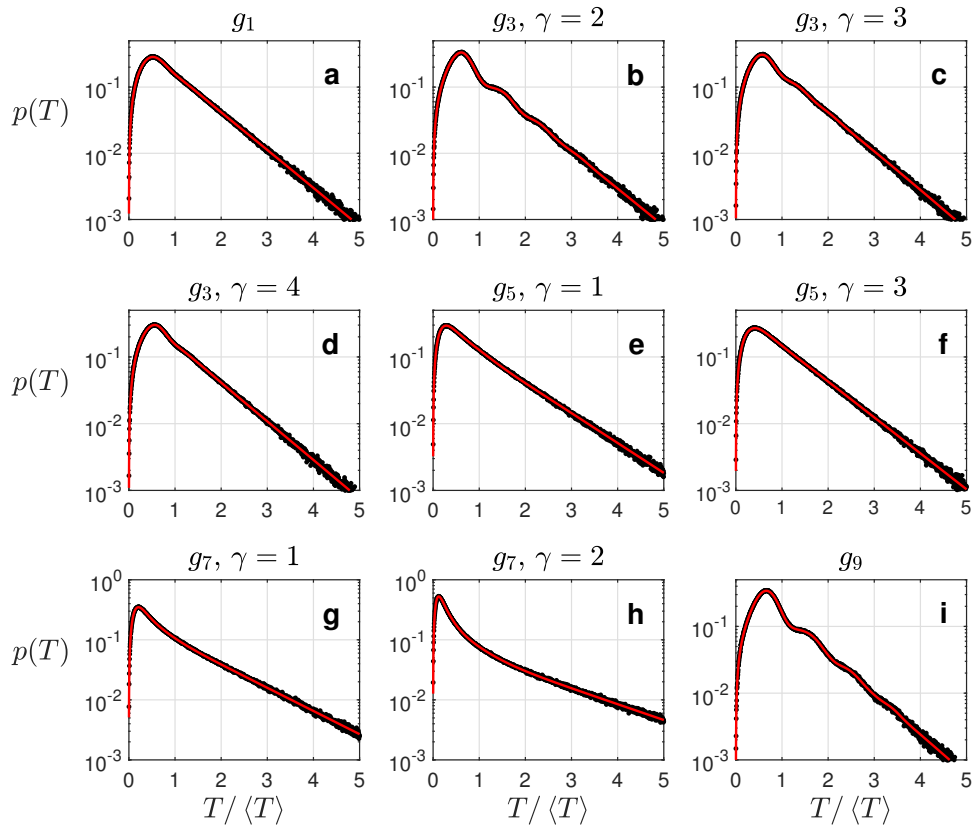


Figure 4.1.: Plots of the interval density for class 0 smooth processes. Simulation estimates for $p(T)$ are displayed as black dots and the finite mixture models as red lines.

these translate into multi-modality in the zero crossings. This complexity reduces as the parameter γ increases. In fact, if we let γ tend to positive integer infinity so that $g_3(\tau, \gamma)$ is a valid autocorrelation, then

$$\begin{aligned}
 \lim_{\gamma \rightarrow \infty} \log(g_3(\tau, \gamma)) &= \lim_{\gamma \rightarrow \infty} \gamma \log\left(\text{sinc}\left(\sqrt{3/\gamma}\tau\right)\right) \\
 &= \lim_{\gamma \rightarrow \infty} \gamma \log\left(1 - \tau^2\gamma^{-1}/2\right) \\
 &= \lim_{Y \rightarrow 0} \frac{\log(1 - \tau^2 Y/2)}{Y} \\
 &= \lim_{Y \rightarrow 0} \frac{-\tau^2/2}{1 - \tau^2 Y/2} = -\tau^2/2, \quad (4.16)
 \end{aligned}$$

where the Taylor expansion of the ‘sinc’ function was used, followed by L’Hôpital’s rule [40]; hence the limiting form of $g_3(\tau, \gamma)$ is $\exp(-\tau^2/2) = g_1(\tau)$. Thus, the $\gamma = 4$ case has the same form of interval density as the g_1 process. For the three

other cases the extra *WEIB* and *GAM* pdfs are required to capture the extra turning/inflection points in $p(T)$ due to zeros of $g_3(\tau, \gamma)$.

A plot of the density in the $\gamma=1$ case is given in Fig. 4.3 and oscillations in the tail appear to persist as $T \rightarrow \infty$. It has been shown [96] that $p(T)$ is bounded above and below by exponential functions, and so the process still has a finite persistence exponent. We note that although the power spectrum mimics a uniform distribution (A.2), the periodicity density (2.58) does not have finite support.

4.2.1.3 g_5 : Power-law

Figure 4.1(e)&(f). This type of process provides another extension from an invalid power spectrum since if $\gamma \leq 1/2$, the value at the origin goes to infinity (see App. A.2); the power spectrum is not positive definite. Here we only consider integer values of the parameter γ for which the form of the power spectrum simplifies to a polynomial-exponential product. Like the g_3 process, as $\gamma \rightarrow \infty$, the g_5 autocorrelation (4.13) converges to the squared exponential case, and Wilson [5] showed that for valid values of γ , the g_5 process behaves similar to the g_1 process. Thus, the density models use the same mixture form as the g_1 process, the component densities playing similar roles.

Slepian's comparison theorem [93] applied here means there is always more memory in such a power-law process compared to the $\gamma=\infty$ limit. Moreover, since the autocorrelation function is non-negative, more variability is observed than in a sinc type 1 process with the same autocorrelation decay. Thus the convergence to the g_1 case is here from a larger interval variance and smaller persistence exponent, in agreement with (4.3).

4.2.1.4 g_7 : Sech

Figures 4.1(g)&(h) and 4.4(a). The $\gamma=0$ case for this process maps onto to the one dimensional 'diffusion equation' [97], achieved by transforming time t through $\tau = \log(t)$, the delay time in the Gaussian process. Other values of γ serve to show that the autocorrelation decay for a smooth process can be made arbitrarily

small; the mean crossing interval remains fixed at π whilst the variance grows. The impact is that more mixture components are required in the density model, and exclusively using *GAM* densities for the small T tempers the decay. Small T must be understood relative to the variance which when $\gamma=3$ is approximately 26.0788. Rewriting the autocorrelation function as

$$g_7(\tau, \gamma) = \frac{e^{-(\sqrt{1+\gamma^2}-\gamma)\tau}}{1 + e^{-2\sqrt{1+\gamma^2}\tau}} + \frac{e^{-(\sqrt{1+\gamma^2}+\gamma)\tau}}{1 + e^{-2\sqrt{1+\gamma^2}\tau}}$$

gives a kind of exponential sum, but prescribing a smooth process, unlike the autocorrelation $g_2(\tau, \gamma)$ below.

4.2.1.5 g_9 : Sinc Type 2

Figure 4.1(i). This process was found by assuming a simple parabolic form of power spectrum, taking the inverse Fourier transform, and adjusting coefficients to conform to the class 0 Taylor expansion (Prop. 1). Additionally, it exemplifies oscillatory correlation with two sinusoidal functions separated by phase alone. The interval density is similar to those of the sinc type 1 process, and the autocorrelation function can be generalized by considering faster power-law decay $\tau^{-\gamma}$, $\gamma > 2$, with $\gamma-2$ as the power on the sinusoids. This would enable the first turning point of the autocorrelation function away from the origin to occur above the τ -axis. Unlike $g_3(\tau, \gamma)$, this family of functions cannot converge to the squared exponential as both sinusoidal functions are required for the power spectrum to be valid. The two types of sinc processes illustrate the point that oscillatory correlation must create additional turning points and shifts in the power spectrum in order to observe new features in the interval density.

4.2.2 *Sub-Fractal Processes*

The sub-fractal process is ostensibly a convolution of the ‘Ornstein-Uhlenbeck process’ (OUP), which has autocorrelation $\rho(\tau) = e^{-|\tau|}$. The OUP is the only Markov

stationary Gaussian process [29], but it is non-differentiable so the mean interval does not exist. The sub-fractal process is also recognisable from its power spectrum $S(\omega)$: there exists a $J > 2$ such that for any $j > J$, the integral $\int_0^\infty \omega^j S(\omega) d\omega$ is divergent. We consider the following forms of autocorrelation:

$$g_2(\tau, \gamma) = \frac{\gamma^2}{\gamma^2 - 1} \exp\left(-\frac{|\tau|}{\gamma}\right) - \frac{1}{\gamma^2 - 1} \exp(-\gamma |\tau|), \quad \gamma \in \mathbb{R}_{>1}; \quad (4.17)$$

$$g_4(\tau) = \sin\left(\frac{\pi}{2} \exp\left(-\frac{2\tau}{\pi}\right)\right); \quad (4.18)$$

$$g_6(\tau, \gamma) = \exp\left(-\sqrt{2\gamma - 1} |\tau|\right) \sum_{j=0}^{\gamma} \frac{(\gamma + j)!}{(2\gamma)!} \binom{\gamma}{j} \left(2\sqrt{2\gamma - 1} |\tau|\right)^{\gamma - j}, \quad \gamma \in \mathbb{N}; \quad (4.19)$$

$$g_8(\tau) = \sqrt{2} \cos\left(\frac{|\tau|}{\sqrt{2}} - \frac{\pi}{4}\right) \exp\left(-\frac{|\tau|}{\sqrt{2}}\right); \quad (4.20)$$

$$g_{10}(\tau) = \sin\left(\frac{\pi}{14}\right) \left(\exp(-\bar{\gamma} |\tau|) + 2 \sum_{j=1}^3 \exp\left(-\bar{\gamma} |\tau| \cos\left(\frac{j\pi}{7}\right)\right) \cos\left(\frac{j\pi}{7} - \bar{\gamma} |\tau| \sin\left(\frac{j\pi}{7}\right)\right)\right),$$

$$\bar{\gamma}^{-2} = -\left(\sin\left(\frac{\pi}{14}\right) \left(1 + 2 \sum_{j=1}^3 \cos\left(\frac{3j\pi}{7}\right)\right)\right). \quad (4.21)$$

Appendix A contains exact expressions for the corresponding power spectra, except for the g_4 process, though an approximate form is given. These set of processes are closer to the telegraph-wave (TW) process, which has an exponential autocorrelation and an exponential interval density—refer to 2.7.1.

4.2.2.1 g_2 : Exponential Sum

Figure 4.2(a)–(c). At first glance this process would seem the simplest class 0 sub-fractal process. For γ close to 2, the autocorrelation and the density model are both an exponential sum. The $\gamma = \sqrt{3}$ case stands unique as the only non-trivial example of a stationary Gaussian process for which $p(T)$ is known explicitly [35], given in App. B. A plot of this function, $p_w(T)$, is included in Fig. 4.2(b), and the three parameters for the exponential mixture were found using known properties of

Process	γ	Decay	Mixture	Persistence
g_2	$\frac{(1+\sqrt{3})}{2}$	$e^{-2\tau/(1+\sqrt{3})}$	<i>EXP, EXPP</i>	0.3093
	$\sqrt{3}$	$e^{-\tau/\sqrt{3}}$	<i>EXP</i> \times 2	0.2893
	2	$e^{-\tau/2}$	SAA	0.2737
	$2\sqrt{3}$	$e^{-\tau/(2\sqrt{3})}$	<i>EXP</i> \times 3	0.2032
g_4	-	$e^{-2\tau/\pi}$	<i>EXP</i> \times 2	0.3037
g_6	1	$e^{-\tau}$	<i>EXP, EXPP</i>	0.3193
	2	$e^{-\sqrt{3}\tau}$	<i>GAM, EXPP</i>	0.3804
	3	$e^{-\sqrt{5}\tau}$	SAA	0.3929
	4	$e^{-\sqrt{7}\tau}$	<i>WEIB, GAM, EXP</i>	0.4019
g_8	-	$e^{-\tau/\sqrt{2}}$	<i>WEIB, GAM, EXP</i>	0.3524
g_{10}	-	$e^{-0.3725\tau}$	<i>WEIB</i> \times 2, <i>GAM</i> \times 2, <i>EXP</i>	0.5203

Table 4.2.: Summary of class 0 sub-fractal processes, their autocorrelation decay, finite mixture density models, and estimates of the persistence exponent Θ , (4.2). SAA means Same As Above.

the density function (B.1): $p_w(0)$, μ_T and σ_T^2 . The value of the persistence exponent given in Tab. 4.2 compares well with Wong's result of $(2\sqrt{3})^{-1} \approx 0.2887$. Additionally, the third and fourth central moments of the exponential mixture both have relative errors of order 10^{-3} , and at the discretisation length $\Delta t = 1/200$, the absolute error in the cdf is $\sim 10^{-7}$, the true value found by integrating Wong's pdf. These results show that using mixture models is a good choice. As $\gamma \rightarrow 1$ the autocorrelation approaches $(1 + \tau) e^{-\tau}$, which is a Matérn process described below; and for parameters values close to 1 the density model is better estimated by the *EXP-EXPP* mixture.

In the opposite direction, similar to the sech process, g_7 , as γ grows, the interval density for the g_2 autocorrelation necessitates more mixture components since although the mean remains the same, $p(0)$ increases and the persistence exponent decreases. Miroshin [98] has studied the exponential sum process, and labelled it a Wong-type. It can be shown that adding additional exponential functions to the autocorrelation, and requiring the standardized Taylor expansion above (Prop. 1) and non-negativity of power spectrum, leads to a smooth process for which $p(T) = 0$. Indeed, the 'sech' function can be expanded as an infinite series of exponential functions ([72], Eq. 1.232.2). Interestingly, Miroshin's goal was to use the g_2 pro-

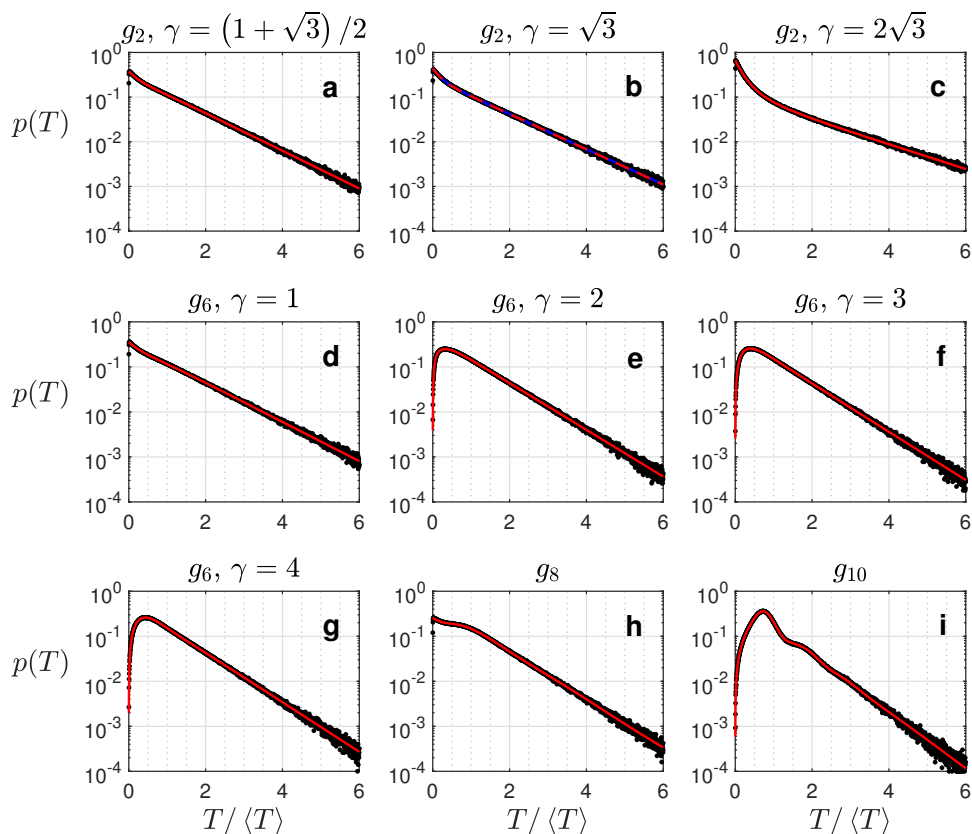


Figure 4.2.: Plots of the interval density for class 0 sub-fractional processes. Simulation estimates for $p(T)$ are displayed as black dots and the finite mixture models as red lines. Additionally, Wong's density function (B.1) is included in (b) as a solid blue line.

cess to show that Rice's results on crossing moments apply to the OUP, effected through the transformation $\tau \mapsto \gamma\tau$ and taking the limit $\gamma \rightarrow \infty$. Wong's process which relates to Brownian motion remains a special case, though it is conceivable that a similar analysis to that of Wong could yield a result. Based on the above discussion, such a solution is likely to be of greater complexity if γ is not close to 2.

4.2.2.2 g_4 : Sine Convolution

Figure 4.2(d). As mentioned in the discussion of the TW process, Sec. 2.51, a Gaussian autocorrelation can be constructed by assuming the accompanying clipped process (2.14) has the same autocorrelation as a non-Gaussian process with Poissonian crossings. Inverting the arcsine rule (2.16) and substituting for $R(\tau)$ the form

(2.51) leads to (4.18). Figure 4.2(d) shows crossing intervals are well described by a mixture of two exponential distributions, and unlike in a Poisson process the intervals are dependent.

4.2.2.3 g_6 : Matérn

Figure 4.2(d)–(g). Strictly speaking, we investigate the half-integer Matérn process; the full form of autocorrelation can be found in [39], which also shows the Matérn process to be solutions to homogeneous stochastic differential equations relating to autoregressive processes. The general $g_6(\tau, \gamma)$ function which allows for non-integer values of the parameter has the same form as $G_5(\omega, \gamma)$, the power spectrum for the power-law process. Thus, as the parameter γ tends to infinity, the Matérn process also converges to the squared exponential case. Moreover, successive values of $\gamma \in \mathbb{N}_{>1}$ serve to remove odd terms in the Taylor expansion of the autocorrelation, and so the process is γ -times differentiable.

Table 4.2 demonstrates the approach of the Matérn process towards smoothness. Method of moments for an exponential mixture produces negative parameter values when $\gamma = 1$, so we instead model the left tail using an *EXP* pdf, and the right tail using a *EXPP* pdf. As γ increases, the autocorrelation becomes thrice differentiable so that $p(0) = 0$, reflected in the change in density mixture. By $\gamma = 4$, it has inherited the characteristics of the g_1 process, their persistence exponents now within 2% of each other.

4.2.2.4 g_8 : Cosine-Exponential Product

Figure 4.2(h). This process arises in ‘linear filter theory’ as the linear oscillator driven by white noise [37]. Analytically, the process is a soft modification to the OUP, and this is reflected in the density model. The *WEIB* and *GAM* pdfs are used to incorporate the inflection point near the mean. The *EXP* pdf describes the limit at both the origin and the tail, its dominance demonstrated by the value of the associated mixture parameter, $\alpha_3 \approx 0.7233$. The process is sub-fractal and so short intervals occur with high probability. However, this is balanced by the

oscillatory part of the autocorrelation (4.20). This effect of oscillatory correlation enforcing bi-modalities and inflection points in the density profile near the origin will again be encountered in the next chapter. By expanding the cosine in $g_8(\tau)$ it is seen to have two sinusoids separated by phase alone; hence the power spectrum is concentrated at the origin.

4.2.2.5 g_{10} : *Butterworth*

Figure 4.1(i). The full name of this process is the 'low-pass seventh-order Butterworth' process, and it was used by Mimaki [50] in constructing models for the correlation coefficient when a scale parameter is varied such that the power spectrum evolves out of a class 0 classification. The power spectrum is continuous and decays like ω^{-14} , thereby closely resembling the $g_3, \gamma = 1$ case, and here too the interval density has multi-modalities. Note that for the g_{10} process, the density mixture in Tab. 4.2 has four less components than that g_3 case, and the density tail does not have persistent oscillations. Both distinctions are a consequence of the power spectrum being fully, rather than piecewise, continuous. Again, we emphasise that oscillatory correlation does not necessarily cause non-class 0 crossing interval behaviour, and that the prediction depends on the form of power spectrum near the origin.

4.2.3 *Dependence in Class 0 Processes*

The finite mixture model assumes the sample data can be partitioned into independent sub-populations governed by a single distribution. A physical example would be a stock of different electrical products, each with different failure rates. The hyperexponential (mixture of two exponentials) random variable then arises when a product is selected at random. One could pursue such an interpretation, for example: the autocorrelation of a g_2 process has two correlation decay scales, one of which dominates at large delay times, and this duality is reflected in the zero-crossings. It could also be said that the symmetry of a Gaussian process causes

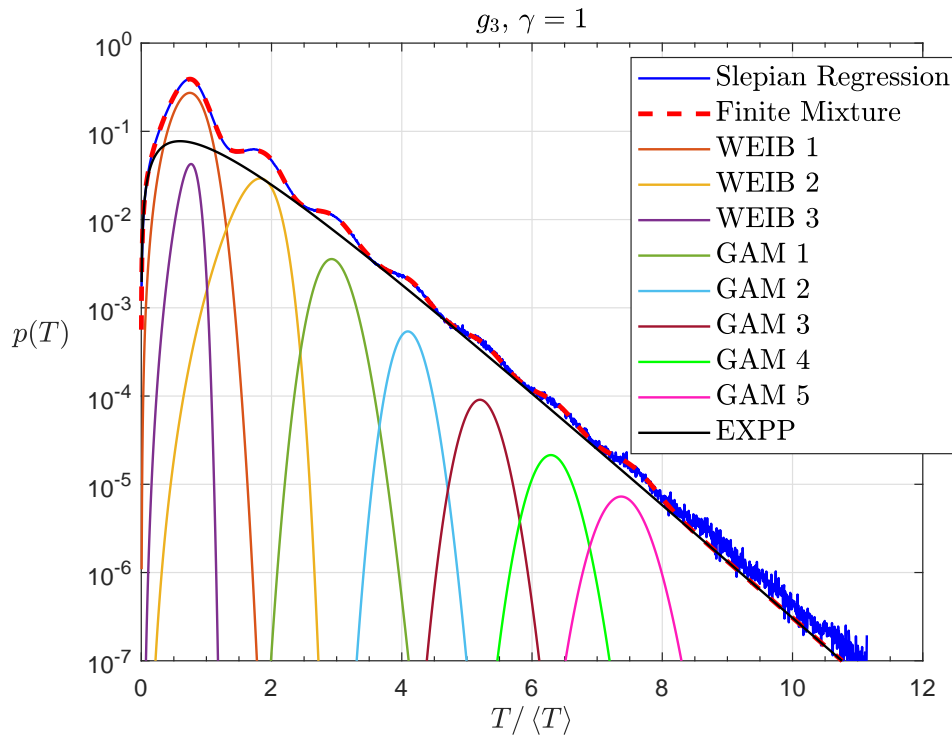


Figure 4.3.: Plot illustrating the important roles of the component densities for the g_3 process with $\gamma=1$. In order to better resolve the tail of the density function, 2000 realisations were simulated. The Slepian regression solution was computed using the MATLAB toolbox WAFO [30].

intervals of varying lengths, and then stationarity of the process means some property of the interval sequence is preserved so that the distribution is independent of shifts in time. Given the difficulty of obtaining the analytic interval density, there is the mathematical convenience of using different distributions to obtain a simple but capable description in the aggregate. The sinc type 1 process with parameter one is a perfect example of this, and displayed in Fig. 4.3. The *EXPP* pdf gives the foundational structure of the density function, particularly the skewness. The remaining pdfs cover the turning points of the interval density; the ‘peakedness’ at those points determine whether a *WEIB* or *GAM* pdf is more appropriate. The figure includes the result from applying the Slepian regression method, Sec. 2.2.3.2, and so the finite mixture model provides a useful, approximate decomposition of an integral equation (2.32) with additional elements that must themselves be evaluated numerically.

Dependence in the sequence of crossing intervals modelled using Markov chains was described in Sec. 2.2.2 and we now test the accompanying Laplace transform method for class 0 processes. From (2.31)

$$p(T) = \mathcal{L}^{-1}[\bar{p}(s)] = \mathcal{L}^{-1}[h(s)/(1-h(s))], \quad (4.22)$$

where from (2.30), and with $\bar{R} = \langle T \rangle^{-1} = \pi^{-1}$,

$$h(s) = \frac{1}{2} + \frac{s}{2} \int_0^\infty \frac{\rho'(T) e^{-sT}}{\sqrt{1-\rho^2(T)}} dT; \quad (4.23)$$

$\rho(\tau)$ is the autocorrelation. For the g_4 process, (suppressing the argument) the autocorrelation (4.18) satisfies $\rho' = -e^{-2\tau/\pi} \sqrt{1-\rho^2}$, so

$$h(s) = \frac{1}{2} - \frac{s}{2} \mathcal{L}[e^{-2T/\pi}] = \frac{1}{2} - \frac{\pi s}{2(\pi s + 2)} = \frac{1}{\pi s + 2} \Rightarrow \bar{p}(s) = \frac{1}{\pi s + 1},$$

which from App. B.3 is the generating function for the *EXP* distribution with mean π .

Another example where the integral (4.23) may be evaluated directly is the g_7 process with $\gamma=0$. This case of the autocorrelation (4.14) satisfies $\rho' = -\rho \sqrt{1-\rho^2}$. Substitution into (4.23) gives ([99], Eq. 4.9.7)

$$h(s) = \frac{1}{2} - \frac{s}{2} \mathcal{L}[\operatorname{sech}(t)] = \frac{1}{2} \left[1 - s\beta\left(\frac{s+1}{2}\right) \right], \quad (4.24)$$

where

$$\beta(z) = \frac{1}{2} \left[\psi\left(\frac{z+1}{2}\right) - \psi\left(\frac{z}{2}\right) \right], \quad z > 0, \quad (4.25)$$

and $\psi(z) = d(\log(\Gamma(z)))/dz$ is the digamma function. The form that results upon substitution into (4.22) can be inverted numerically using Talbot inversion as implemented in MATLAB by McClure [58]. Results for both processes are found in Fig. 4.4 and compared with the previous finite mixture models. The estimate from the Laplace inversion is better for the smooth 'sech' process. The correlation coefficients for the g_7 case are $\hat{\kappa}_1 \approx -0.0043$ and $\kappa_1 = -0.0053$, where the accented

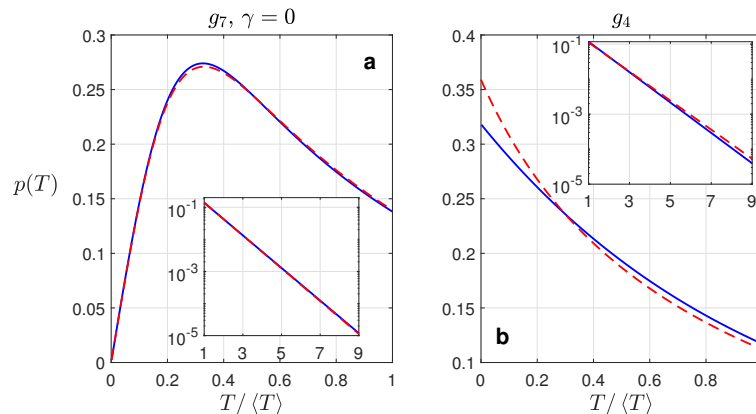


Figure 4.4.: Plots comparing Laplace inversion (blue curves) and finite mixture (dashed red curves) methods for the interval densities given autocorrelations (a) $\text{sech}(\tau)$ and (b) $\sin(\pi \exp(-2|\tau|/\pi)/2)$. The g_7 case uses a *GAM-GAM-EXPP* mixture, and the g_4 case an *EXP-EXP* mixture.

coefficient is the simulation estimate and the other from the model (3.30). For the g_4 process $\hat{\kappa}_1 \approx 0.0416$ and $\kappa_1 = 0.0492$. It could be said that in the g_7 case interval dependence is weaker, and therefore the Markov chain assumption is closer to being true. What we will say is that the Markov chain model, and also the Slepian regression approach, are more accurate for smooth processes, one reason being that there are fewer turning points between zero-crossings and therefore less correlation in the crossing sequence. Also related to this is the correlation decay, which is $e^{-\tau}$ for g_7 , and $e^{-2\tau/\pi}$ for g_4 ; a slower correlation decay means there is more memory over a longer range, thereby limiting the Markov chain assumption.

4.3 SUMMARY

A variety of class 0 processes have been presented and their interval densities modelled using a small selection of distributions. That such a representation is possible is supported by the fact that most of the processes are related, the relations extending across the smooth/sub-fractal divide. Mixture models demonstrate the changing nature of the interval density for each Gaussian process; the right tail may be exponential as $T \rightarrow \infty$, and the left tail approach a constant or be linear as $T \rightarrow 0$, but many other characteristics may be observed in-between. The two

determining factors from the autocorrelation are magnitude of the autocorrelation's third derivative at zero, and the absence/presence of oscillatory correlation. The selection of processes that have been considered are representative of those encountered in the long history of the zero-crossing problem, and thus provides information on expected behaviour.

The next chapter will extend the mixture perspective to cases where crossing intervals are strongly correlated and the power spectral density is no longer concentrated at small frequencies. The goal is to map from the class 0 case, the underlying principle being that knowing the interval density of the class 0 case almost determines the corresponding classes 1 and 2 forms—advantageous because finding the density for the former is comparatively simpler.

5

COMPOUND MIXTURE MODELS FOR THE INTERVAL DENSITY

In the previous chapter, a basis function was used to construct interval density models for families of class 0 processes that have a “simple” kind of interval dependence. It is conceivable that finite mixture models also exist for classes 1 and 2 processes; more interesting is whether the relationships between power spectra as derived in equations (3.9)–(3.10), translate to the interval density. We seek a connecting mechanism different from Markov Chain models (e.g.[5]), informed by the discussion of sample function periodicity (Sec. 3.4), and preserving the analytical flexibility of the previous chapter. To this end, we introduce compound mixture models, which as described in Sec. 2.3.2 can model the transformation of a parameter into a random variable.

Stochastic periodicity was discussed in Sec. 2.7.3, and we stated that level-crossing intervals T are necessarily bounded above by periodicities η . From this we may conjecture that a kernel function $K(T, \eta)$ exists such that the periodicity density $f_S(\eta)$, (2.58), is related to the interval density $p(T)$ through

$$p(T) = \int_T^\infty K(T, \eta) f_S(\eta) d\eta. \quad (5.1)$$

For the telegraph wave process which has exponentially distributed intervals, we have from (2.59)

$$p(T) = \bar{R}e^{-\bar{R}T} = \int_T^\infty \bar{R}^2 e^{-\bar{R}\eta} d\eta$$

$$\begin{aligned} &\equiv \int_T^\infty K(T, \eta) f_S(\eta) d\eta = \int_T^\infty \frac{2\bar{R}K(T, \eta)}{\pi^2 + \bar{R}^2\eta^2} d\eta, \\ \Rightarrow K(T, \eta) &= \frac{1}{2}\bar{R}e^{-\bar{R}\eta} \left(\pi^2 + \bar{R}^2\eta^2 \right), \end{aligned} \tag{5.2}$$

and note the kernel is independent of T . The cos-wave process suggests another approach: using random variables, since the zero-crossing intervals are all half the period of the process; that is $T = \eta/2$, also indicating the two are dependent. For a Gaussian process, the choice of kernel or random variable is less obvious. The models we propose combine the two approaches.

We start by exploring changes in the power spectrum caused by increases to the periodicity parameter a , and then show they provide critical values for the transition out of a class 0 process. Thereafter, sample functions and their crossings are used to illustrate the transformation principle from the class 0 interval density to that of classes 1 or 2; crossings simulated with the same RNG seed but different power spectra overlap within certain time scales. This is then formalized by the derivation of a generalized random variable for crossing intervals, and its distribution found from its generating function. The model is tested on representative processes for varying a , and various consequences of the model are discussed—in particular, manifestation of the parameter a as a distribution embedded in zero-crossing intervals.

Our focus shall be on the classes 1 and 2 forms of the smooth process g_1 , (4.11), and the sub-fractal process g_2 with $\gamma = \sqrt{3}$, (4.17), the latter providing an example of how behaviour of the interval density near the origin evolves with a . The power spectra are given by

$$S_{ij}(\omega; a) = \frac{(j-1)}{2}G_i(\omega) + \frac{1}{2j} \left(G_i\left(\omega + \frac{a}{\pi\sqrt{2^{3-j}}}\right) + G_i\left(\omega - \frac{a}{\pi\sqrt{2^{3-j}}}\right) \right), \tag{5.3}$$

where

$$G_1(\omega) = \sqrt{2\pi} \exp\left(-2\pi^2\omega^2\right), \quad G_2(\omega) = \frac{8\sqrt{3}}{(3 + 4\pi^2\omega^2)(1 + 12\pi^2\omega^2)}. \tag{5.4}$$

The density models will again be validated using simulation data, but the preceding analysis aims to be general in its description, so that the categorisation of classes 0, 1 and 2 readily transfers to other processes encountered in the literature.

5.1 MOTIVATION

5.1.1 Power Spectrum Changes

We have said that classes 1 and 2 processes are best distinguished by their power spectra, and Figs. 5.1(a)&(b) show how the power spectrum $S_{1j}(\omega; a)$ changes as a increases, a visualisation of the analytic results of equations (3.11)–(3.14). In the class 1 case, only one maxima exists and is at the origin when $a \leq 1$; and for larger a , two maxima form, with the value at the origin going to zero as $a \rightarrow \infty$. As was shown in Sec. 3.3.2, increases to a lead to a gradual regularisation in the sense that sample functions tend towards a sinusoidal wave-form (Fig. 3.5). In the class 2 case, Fig. 5.1(b), the departure from the class 0 profile is much slower owing to the extra contribution near the origin (5.3). When $a = \sqrt{3}$ there is one maxima at the origin and two inflection points, and by $a = 3$, these have become minima and there are two additional maxima. The origin remains the global maximum, and so the regularisation at extreme a does not lead to approximately sinusoidal sample functions as in the class 1 case. These observations relate back to the point on time scales relating to the power spectrum, Sec. 3.4.

The changes to the power spectrum naturally define critical values of a that lead to significant changes in sample function and zero-crossing behaviours. Consider the value of the power spectrum at the origin as a function of a . Being an even function, of particular interest are values of a such that second and higher order derivatives of $S_{ij}(0; a)$ are equivalently zero. From (5.3), this reduces to finding zeros of the function

$$S_0(a, k; i, j) = G_i^{(k)} \left(\frac{a}{\pi \sqrt{2^{3-j}}} \right), \quad (5.5)$$

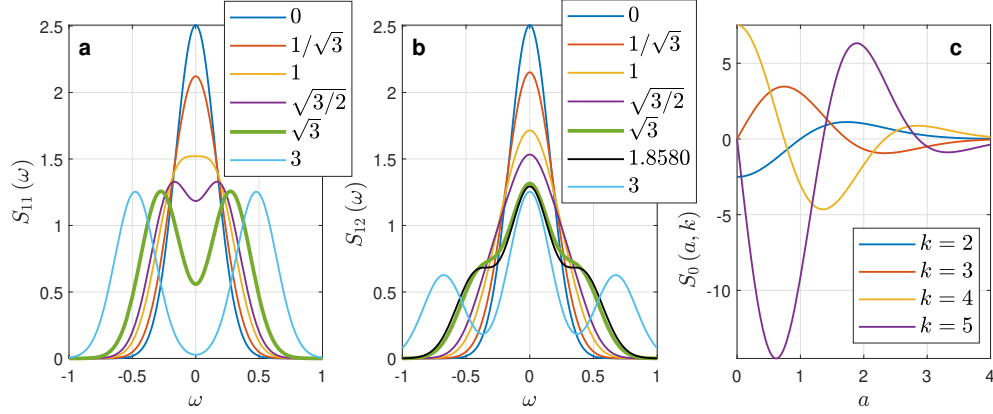


Figure 5.1.: Plots demonstrating changes to the power spectra $S_{1j}(\omega; a)$. The legends in plots (a)&(b) represent values of the periodicity parameter a . Provided in plot (c) are the first few curves resulting from equation (5.5) when $i = j = 1$.

where the bracketed superscript notation is used for the k -th order derivative. Specialising now to the squared exponential case, Fig. 5.1 (c) contains plots of $S_0(a, k; 1, j)$ for $k = 2, \dots, 5$ when $j = 1$, and since (5.5) is monotone in j , the curves for $j = 2$ are identical up to a rescaling of the axes. The zeros of $S_0(a, k; 1, j)$ satisfy polynomials in a , and for $k \leq 5$ the nonzero solutions are:

k	2	3	4	5
a	$\sqrt{2^{1-j}}$	$\sqrt{2^{1-j} \cdot 3}$	$\sqrt{2^{1-j} (3 \pm \sqrt{6})}$	$\sqrt{2^{1-j} (5 \pm \sqrt{10})}$

Table 5.1.: Critical values of the periodicity parameter, found by solving $S_0(a, k; 1, j) = 0$, from Eq. (5.5).

In agreement with the plots in Fig. 5.1 (a)&(b), the most important values in terms of dissimilarity to $G_1(\omega)$ are

$$a_0 := \sqrt{(1+j)/2}. \quad (5.6)$$

Let a_u denote values of a where $S_{1j}(\omega)$ has an undulation point (first and second order derivatives equal to zero). When $j = 1$, $a_u = 1$, and for $a > a_u$ the origin is a minimum point of the spectrum. When $j = 2$ the origin is always the global maximum and $a_u \approx 1.8580$. The spectrum either has two inflection points

($\sqrt{3/2} < a < a_u$) or two additional maxima ($a > a_u$). There is therefore an interval I_0 containing values of a such that the oscillatory process ρ_{ij} in fact has the properties of a class 0 process. The key determiner of class categorisation is not non-negativity of the autocorrelation, but the number of changes in first and second order derivatives of the power spectrum $S_{ij}(\omega)$. Therefore, we list the following classification properties, supplementary to Prop. 1, for a stationary process with power spectrum $S(\omega)$:

Proposition 2 (Process Classification)

- *Class 0: $S(\omega)$ has a maximum at the origin, and either has no additional stationary/inflection points or is a rectangular function centred at the origin;*
- *Class 1 process: $S(\omega)$ has a minimum at the origin and additional stationary/inflection points away from the origin, including at least two maxima;*
- *Class 2: $S(\omega)$ has a maximum at origin and additional stationary/inflection points away from the origin.*

The above analysis to identify significant changes in the power spectrum $S_{ij}(\omega)$ can be repeated for any modified class 0 process provided the derivative of the original spectrum exists at the origin, meaning roots of Eq. (5.5) exist. One such exception is the power-law process (4.13) with $\gamma = 1$ for which $G_i(\omega)$ is an exponential function with a cusp discontinuity at the origin. In this case $I_0 = \{0\}$, so $\rho_{5j}(\tau; \gamma = 1, a > 0)$ is always a class 1 or 2 process. When the class 0 autocorrelation is already periodic such as in the g_3 case, (4.12), one critical value of a is readily obtained from the oscillatory part of the autocorrelation, the effect on the process being that there are competing periodicities either side of that critical value.

5.1.2 Sample Function Changes

Changes in the power spectrum are reflected in sample functions. Recall that for the Gaussian process ρ_{ij} , the mean interval between zero-crossings is

$$\langle T \rangle = \pi / \sqrt{1 + a^2}, \quad (5.7)$$

and this may be used as a time-scale for tracking sample function changes. If we generate realisations for different values of a using the same random number generator (RNG) seed, and then (with time rescaled) overlay their sample function curves, we obtain plots as in Figs. 5.2(a)&(b). In both we see that the sample function at the critical values $a_0 = \sqrt{(1+j)/2}$ is almost identical to the $a = 0$ case; zero-crossings and turning points virtually coincide and so we expect the interval densities to be similarly related. For values of a above these critical values, the realisations are less comparable to the $a = 0$ case, and certain of the crossings (in rescaled time) are either removed or added, in accordance with asymptotic regularity of the process. Note that the changes are slower (i.e. require larger a) for the ρ_{12} process which has a larger critical value a_0 . For $a > 3$ the differences are far more than a contraction of time, and the oscillatory correlation starts to dominate. In Fig. 5.2 (c)&(d) we once again overlay the sample functions but without rescaling time. Let $x_0(t)$ be the realisation when $a = 0$, and $x_{1j}(t)$ the realisation when $a = 5$. We observe that if two adjacent crossings r_1, r_2 of $x_0(t)$ are “matched” with crossings of $x_{1j}(t)$, between r_1 and r_2 there is almost always a series of extra crossings. This suggests a sampling or mixing of a ‘base state’ of crossings due to $g_i(\tau)$, and a regulatory or ‘latent state’ due to the periodic modulations in ρ_{ij} . Such a mixing idea is better indicated by the plot for the class 1 case; nevertheless, both plots (c)&(d) of Fig. 5.2 clearly display the extra crossings as highly correlated, as though belonging to a sub-population. We now formalize our observations into compound mixture models.

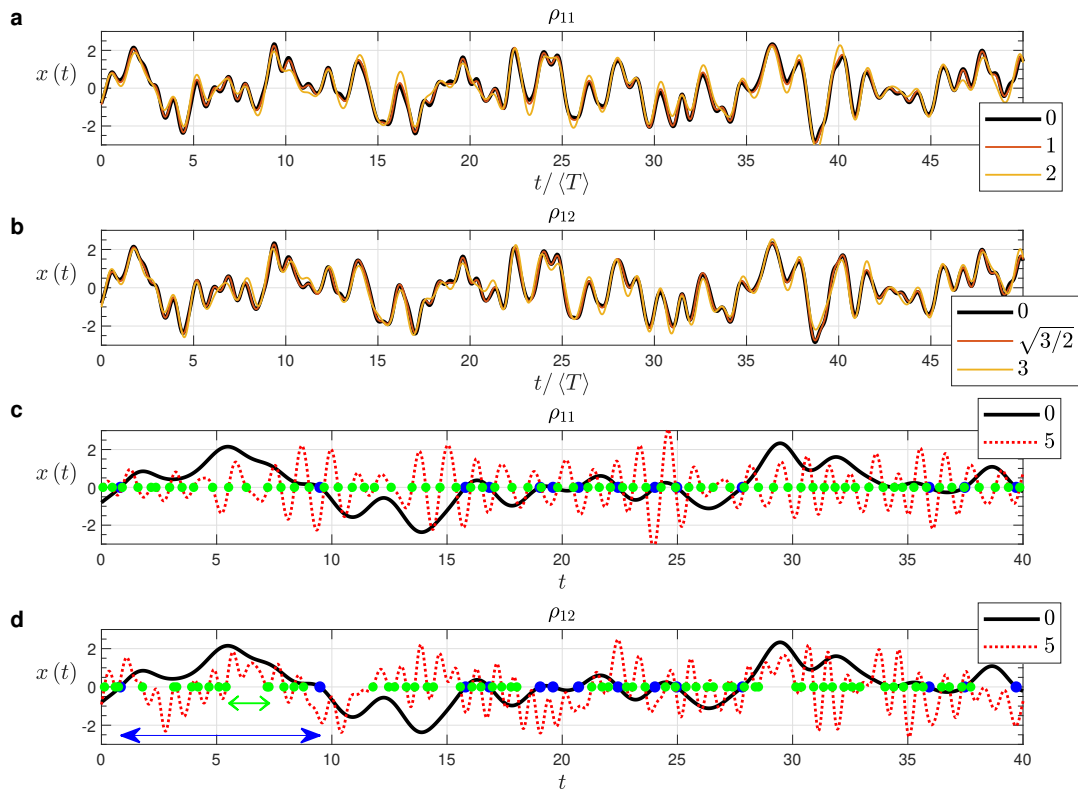


Figure 5.2.: (a)&(b): Sample function plots for processes ρ_{11} (a) and ρ_{12} (b) with time rescaled by the mean interval length to highlight the similarity in profiles when a is small and close to the critical values $\sqrt{(1+j)}/2$. (c)&(d): Plots comparing sample functions and zero-crossing locations for the ρ_{1j} process when $a=0$ (solid black line, with crossings as blue circles) and when $a=5$ (dotted red line, with crossings as green circles), illustrating the mixing idea of zero-crossings when $a > 0$. In all four plots, the legend indicates the value of a for each curve.

5.2 GENERALISED RANDOM VARIABLE FOR CROSSING INTERVALS

5.2.1 Derivation

Consider an arbitrary interval of length τ with distribution $p_0(\tau)$ and spanning two consecutive random crossings r_1, r_2 of a base random process, as signified by a blue double arrow in Fig. 5.2(d). Suppose modification of the base process leads to a new process with “additional” crossings. Let η represent the intervals between

these extra crossings, as signified in Fig. 5.2(d) by a green double arrow. The number of intervals of length η after r_1 up to and including r_2 is $1 + \beta_1(\tau/\eta)$, for some $\beta_1 \geq 0$, and the size of each interval between r_1 and r_2 is thus approximately $T = \tau / (1 + \beta_1(\tau/\eta))$. From this construction, if the change to the base process is small, we expect $T \sim \tau$, whilst if the change is large we expect $T \sim \eta$. In the zero-crossing context described above, these two extremes respectively correspond to small and large values of the periodicity parameter a . We proceed with a more general form of random variable for crossing intervals of the new process:

$$T(\tau, \eta) = \tau / \left(1 + \beta_1(\tau/\eta)^{\beta_2}\right)^{1/\beta_2}, \quad \beta_1, \beta_2 > 0. \quad (5.8)$$

Here as in the literature on compound mixtures (e.g. [63]) we refer to η as the 'latency variable' having some density $f(\eta)$. The compound variable T will have density $p(T)$ which we seek to model via a transformation from the distribution of the base random variable τ .

From (5.8), τ can be expressed as

$$\tau = T / \left(1 - \beta_1(T/\eta)^{\beta_2}\right)^{1/\beta_2}, \quad (5.9)$$

and the maximum length of a crossing interval T of the new process is

$$T_M = \max \left\{ \lim_{\tau \rightarrow \infty} T(\tau, \eta) \right\} = \beta_1^{-1/\beta_2} \max\{\eta\} \equiv \beta_1^{-1/\beta_2} \eta_M. \quad (5.10)$$

The generating function of $T(\tau, \eta)$ is then

$$\begin{aligned} \mathcal{L}[p(T)] &= \int_0^{T_M} e^{-sT} p(T) dT \\ &\equiv \int_0^{\eta_M} \int_0^\infty e^{-sT(\tau, \eta)} p_0(\tau) f(\eta) d\tau d\eta, \quad d\tau = dT \left(1 - \beta_1(T/\eta)^{\beta_2}\right)^{-1-1/\beta_2} \\ &= \int_0^{\eta_M} \int_0^{\beta_1^{-1/\beta_2} \eta} \frac{e^{-sT}}{\left(1 - \beta_1(T/\eta)^{\beta_2}\right)^{1+1/\beta_2}} p_0 \left(\frac{T}{\left(1 - \beta_1(T/\eta)^{\beta_2}\right)^{1/\beta_2}} \right) f(\eta) dT d\eta \end{aligned}$$

$$= \int_0^{T_M} \int_{\beta_1^{1/\beta_2} T}^{\eta_M} \frac{e^{-sT}}{\left(1 - \beta_1(T/\eta)^{\beta_2}\right)^{1+1/\beta_2}} p_0 \left(\frac{T}{\left(1 - \beta_1(T/\eta)^{\beta_2}\right)^{1/\beta_2}} \right) f(\eta) d\eta dT,$$

where we have substituted (5.9) and reversed the order of integration. It follows from equivalence of definition that

$$p(T) = \int_{\beta_1^{1/\beta_2} T}^{\eta_M} \frac{1}{\left(1 - \beta_1(T/\eta)^{\beta_2}\right)^{1+1/\beta_2}} p_0 \left(\frac{T}{\left(1 - \beta_1(T/\eta)^{\beta_2}\right)^{1/\beta_2}} \right) f(\eta) d\eta. \quad (5.11)$$

For zero-crossings of Gaussian processes ρ_{ij} defined in Sec. 3.1, we have found the model with $\beta_1 = 1$, $\beta_2 = 2$ to be sufficient to capture the principle features of the interval density function, whereupon (5.11) reduces to

$$p(T) = \int_T^{\eta_M} \left(\frac{\tau}{T}\right)^3 p_0(\tau) f(\eta) d\eta, \quad \tau = T / \left(1 - (T/\eta)^2\right)^{1/2}. \quad (5.12)$$

Appendix C details the tail behaviour predicted by the model (5.11), discussed further below.

5.2.2 The Latency Density

We choose to refer to $f(\eta)$ as the ‘latency density’, rather than the mixing density, because even though the latter describes its role, latency better preserves the notion of embeddedness of the periodicity parameter a . It remains to specify a form for $f(\eta)$, and for a first approximation we use the power spectrum. If η were the length between zero-crossings of a cosine function, 2η would be the period and the frequency $\omega = 1/(2\eta)$. Using this transformation gives

$$f_s(\eta) = 2f_s(2\eta) = \frac{1}{\eta^2} S_{ij} \left(\frac{1}{2\eta}; a \right), \quad (5.13)$$

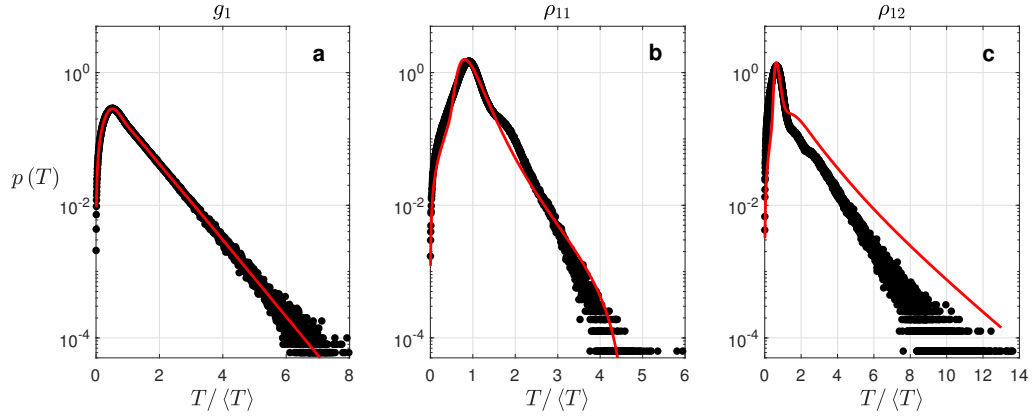


Figure 5.3.: Plots of the interval density obtained from 1000 realisations (black circles) of the process ρ_{1j} when (a) $a = 0$, (b) $j = 1$, and $a = 3$ (c) $j = 2$, $a = 3$, with corresponding mixture models shown as solid red lines. The model in (a) is a finite mixture (4.4), whilst (b) and (c) contain the compound mixture model (5.12) that uses (5.13) as the latency density.

a rescaled version of the periodicity density (2.58). The results are shown in Fig. 5.3 (b)&(c) when $a = 3$ for the process ρ_{1j} , and we include $p_0(\tau)$ for comparison. The plots demonstrate the transformation principle, particularly for small intervals T (which follows from expanding (5.12) near the origin) and around the mode. The power spectrum $S_{ij}(\omega)$ has a maximum at $\omega \approx a/(2\pi)$, so that the mode of $f_s(\eta)$ is $\eta \approx \pi/a$ (the asymptotic form of the mean interval length), and we would like to have $T \sim \eta$ as $a \rightarrow \infty$. There are other properties required by the mixture model (5.12) which $f_s(\eta)$ simply does not have, and this is because on its own it does not exclusively filter out zero-crossing returns (refer to Sec. 2.7.3).

Taking the same approach as the previous chapter, we further specify finite mixture models for the latency density, the choice of which is largely informed by the different tail behaviours. In particular, Fig. 5.4 (a)&(b) demonstrate the range of the crossing intervals as a increases. For a class 1 process, increasing a suggests a truncation of the support of $p(T)$ towards twice the mean interval, and so we shall use *BETA* density components in $f(\eta)$. Conversely, for a class 2 process the variation relative to the mean interval grows linearly with a , alongside the increase in the rate of crossings. We shall therefore use a combination of *BETA* and *GEXPP* density components for $f(\eta)$, thereby combining features analogous to

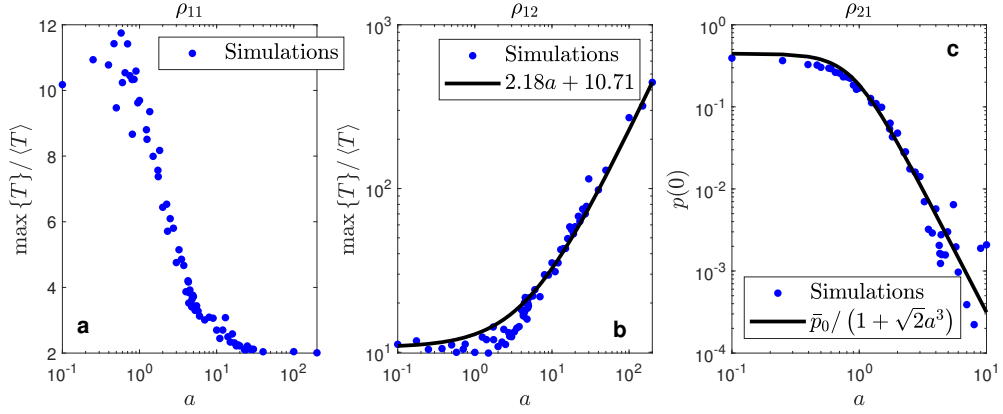


Figure 5.4.: (a)&(b): Plots illustrating asymptotics of the maximum interval obtained in simulations as a increases for the process ρ_{1j} . (c) Plot of estimates for $p(T=0)$ as a increases for the process ρ_{21} .

how the power spectrum (5.3) in this case combines classes 0 and 1 behaviours. The *GEXPP* density was given in Eq. (4.5), and further details for the *BETA* distribution are found in App. B.7. In terms of the construction, a mixture of at least three distributions is necessary to capture the interval variance, the curvature of $p(T)$, and other properties described below.

5.2.3 Refinements for Sub-Fractal Processes

As a final note, when the base process is sub-fractal and its interval density is nonzero at the origin, for the new process, the density $p(T)$ tends to zero at the origin as $a \rightarrow \infty$; that is, periodicity suppresses sub-fractal effects. Here we only deal with the ρ_{21} process, and a plot of $p(0)$ as a function of a is included in Fig. 5.4 (c). A simple way to deal with this property is to change the base density:

$$p_0(\tau) \mapsto \epsilon p_0(\tau) + (1 - \epsilon) p_\epsilon(\tau), \quad 0 \leq \epsilon \leq 1, \quad (5.14)$$

for some function $p_\epsilon(\tau)$ that is zero at the origin; then (5.12) implies $p(0) = \epsilon p_0(0)$. The continuity condition (C.4) jointly constrains $p_\epsilon(\tau)$ and $f(\eta)$, and so $p_\epsilon(\tau)$ is chosen such that it has mean π and approaches the origin like $\mathcal{O}(\tau)$. This is achieved using a mixture density similar to the g_1 density model, so that with

$\lim_{a \rightarrow \infty} \epsilon(a) = 0$, it in effect defines a surrogate smooth process approached by a sub-fractal process as oscillatory correlation increases.

The model (5.12) is now completely specified, and once again we use maximum likelihood estimation (MLE) to find the parameters. The solution method remains unchanged if we assume that we need not modify the loglikelihood function to account for dependence amongst the intervals. Each evaluation of the loglikelihood function now requires integration at every T_m from the interval data:

$$\begin{aligned} \ell(\mathbf{T}; \boldsymbol{\alpha}, \epsilon) &= \sum_{m=1}^{n_T} \log(p(\mathbf{T}_m; \boldsymbol{\alpha}, \epsilon)) \\ &= \sum_{m=1}^{n_T} \log \left(\int_{\mathbf{T}_m}^{\eta_M} (\tau_m / T_m)^3 p_0(\tau_m; \epsilon) f(\eta; \boldsymbol{\alpha}) d\eta \right), \\ \tau_m &= T_m / \left(1 - (T_m / \eta)^2 \right)^{1/2}, \end{aligned} \quad (5.15)$$

where $\epsilon = 0$ for a smooth process. The optimisation can be sped up by using fewer realisations (and therefore, fewer crossing intervals) than in the $a = 0$ case, and also by making use of mex functions¹.

5.3 RESULTS

5.3.1 Class 1 Processes

Figure 5.5 compares the interval density obtained from simulations and the compound mixture model (5.12) for the process ρ_{11} . Here the class 0 regime is $I_0 = [0, 1]$, and for values of a in this interval, the density is better represented by the finite mixture model *WEIB-GAM-EXPP*—the same form as that of the g_1 process (Tab. 4.1), and this similarity supports the time-contraction property (Fig. 5.2). When $a > 1$, the right tail of the density is clearly not exponential and resembles a multinomial (according to $f(T)$). As a grows, the density becomes more symmetric in line with the increased regularity of the crossings. The mode approaches

¹ <https://uk.mathworks.com/help/matlab/call-mex-file-functions.html>.

the mean interval length, and at either side, inflection points or shoulders develop, specifically at 1.5 standard deviations from the mean. This agrees with earlier comments on crossings being bounded by the modal periodicity (Sec. 2.7.3), and so the density profiles are a demonstration of narrow randomness, à la a cos-wave process, Sec. 2.7.2. At large a ($a \geq 3$), the shape of the distribution mirrors the latency density $f(\eta)$, here a *BETA* mixture. More than one beta pdf is needed so as to capture the symmetry, the peakedness, the tails and the width ($\langle T \rangle \pm 1.5\sigma_T$). When the component density curves intersect an inflection point can present in $f(\eta)$, depending on the shape parameters. These properties make the *BETA* mixture a suitable latency density for the transformation to $p(T)$.

Results for the sub-fractal process ρ_{21} are given in Fig. 5.6 and similar features to its class 1 counterpart are observed, though at a much slower rate owing to the larger interval variance (see Fig. 3.5). Here $I_0 = [0, 0.3295]$, and plots (a) and (b) show both the density model (5.12) and a mixture of two exponentials, the latter providing a better estimate and having the same form as that of the g_2 process (with $\gamma = \sqrt{3}$, Tab. 4.2). As mentioned above, increasing a leads to a gradual suppression of sub-fractal effects, particularly as the “most common” interval goes from zero, a tangent-type crossing, to the mean interval. To estimate when these changes occur a second sequence of critical a values may be obtained by considering terms in the Taylor expansion of $\rho_{21}(\tau; a)$, specifically when there are sign changes. From equations (3.1) and (3.31).

$$\rho_{21}(\tau; a) = 1 - \frac{(1 + a^2)}{2} \tau^2 + \frac{2\sqrt{3}}{9} |\tau|^3 + \frac{(3a^4 + 18a^2 - 13)}{72} \tau^4 - \frac{(3a^2 - 1)}{9\sqrt{3}} \tau^5 + \dots \quad (5.16)$$

For a smooth process the expansion would contain only even terms, each nonzero and with alternating sign; therefore when this is resembled by the expansion for a sub-fractal process it indicates a smoothening of the process. The fifth term of the expansion (5.16) is zero when $a = 1/\sqrt{3}$, and the corresponding density

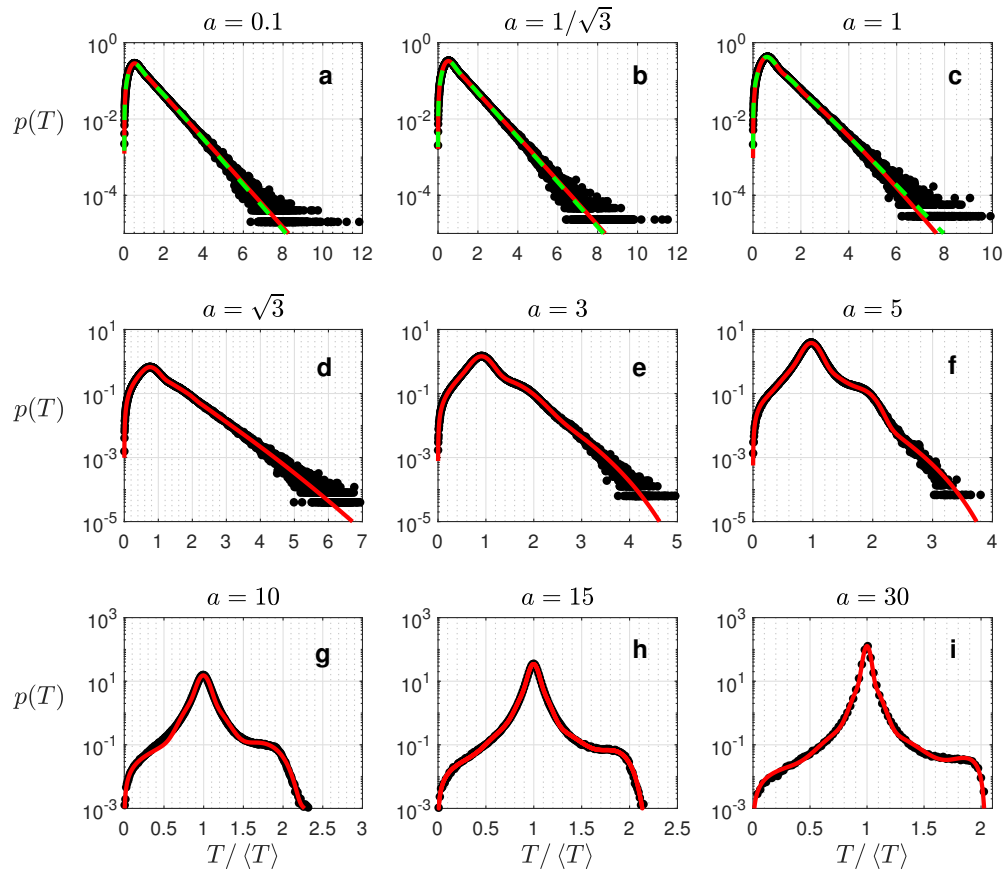


Figure 5.5.: Plots of the interval density for zero-crossings of the process ρ_{11} for values of the periodicity parameter $a > 0$. Histogrammed data are shown as black dots, and density models as solid red lines. In plots (a)&(b) the solid red lines represent the rescaled density $\sqrt{1+a^2}p_0(\sqrt{1+a^2}T)$ for when a is below the critical value, $a=1$. The density model (5.12) is displayed as a solid red line in plots (c)–(f). Also included as dashed green lines are plots of a finite mixture model *WEIB-GAM-EXPP* which are similar to the rescaled $p_0(\tau)$ density.

is shown in plot (c): the profile is largely a more exaggerated version of that in the plot prior, except the tail is not exponential. The fourth term of the expansion (5.16) is positive for $a > \sqrt{\sqrt{40/3} - 3}$, and at this value (shown in plot(d)) $p(T)$ is approximately equal at the origin and at the mode—sub-fractal effects are balanced by the periodicity. For still larger values of a , $p(T)$ becomes less distinguishable in shape from that of the smooth process (compare Fig. 5.6 (i) and Fig. 5.5 (g)), as captured in the density model that uses the revised base density (5.14). Note: the

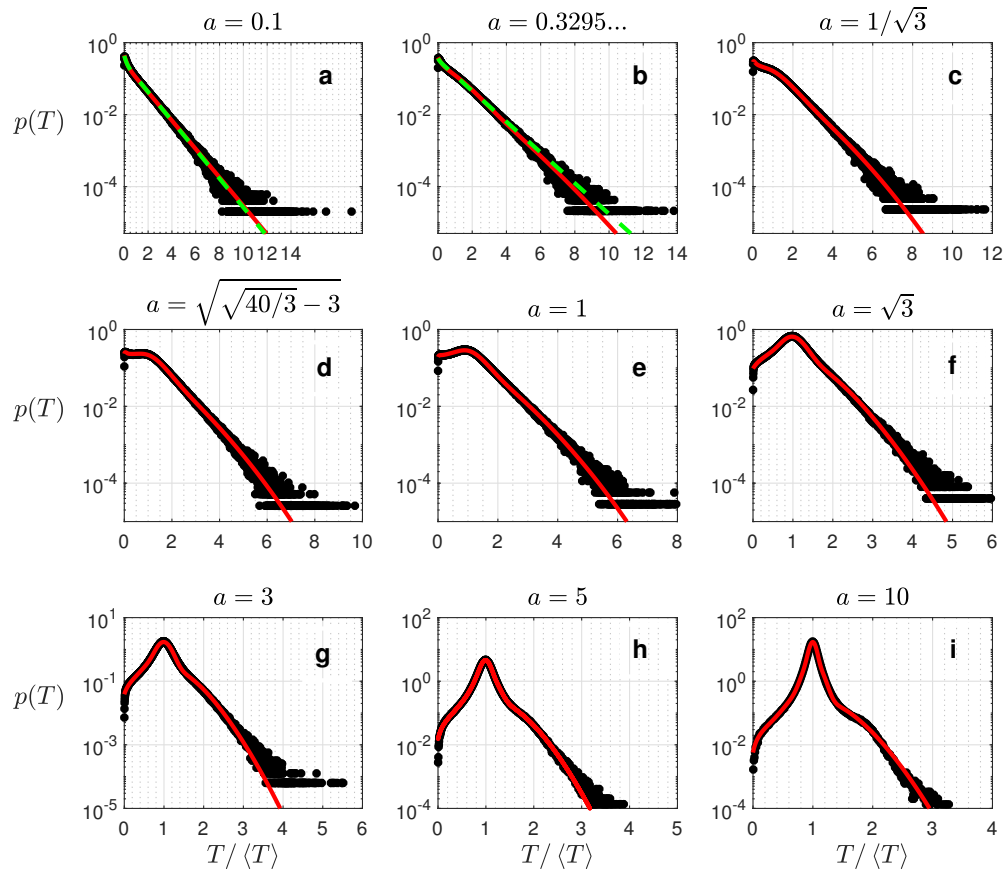


Figure 5.6.: Plots of the interval density for zero-crossing of the process ρ_{21} for values of the periodicity parameter $a > 0$. Histogrammed data are shown as black dots, and density models as solid red lines. In plot (a), the solid red line represents the rescaled density $\sqrt{1+a^2}p_0(\sqrt{1+a^2}T)$ for when a is below the critical value, $a \approx 0.3295$. The density model (5.12) is displayed as a solid red line in plots (b)–(f). Also included as dashed green lines are plots of a finite mixture model *EXP-EXP* which in plot (a) is similar to the rescaled $p_0(\tau)$ density.

third term in (5.16) is independent of a meaning $p(0) > 0$, always. Notwithstanding, the dominance of the periodicity parameter at large a makes the density increasingly dissimilar to the $a=0$ case.

5.3.2 Class 2 Processes

Figure 5.7 portrays the greater complexity of interval density for the class 2 process ρ_{12} . The density is approximately exponential at large T , and the mode tends to $\langle T \rangle / \sqrt{2}$ as $a \rightarrow \infty$. This symmetry is again a reflection of the strong correlation in the interval sequence (see Fig. 6.3), very different from the class 1 case. Here the class 0 regime is $I_0 = [0, \sqrt{3/2}]$ and we include the g_1 mixture model form to highlight the similarity in this regime (plots (a)–(c)). For $a > \sqrt{3/2}$, $p(T)$ is partitioned into two forms at approximately $\sqrt{2}\langle T \rangle$, and this is encapsulated in the form of the latency density, $f(\eta)$: small intervals (near the mode) are governed by *BETA* distributions, and large intervals by *GEXPP* distributions. In addition, $p(T)$ develops oscillations with period $\propto \sqrt{2}\langle T \rangle$. The oscillations dampen as $T \rightarrow \infty$, and their maximum amplitude increases as $a \rightarrow \infty$.

We can demonstrate a higher order nonlinearity of the crossings by returning to the general form of the density model (5.11). If we allow β_1 to depend on T , the range of integration can then expand/contract, thereby allowing for scale changes that match the simulation estimate of $p(T)$. This is of course no longer a maximum likelihood problem, but more akin to ‘least squares estimation’. One approach is to first smooth the density as estimated numerically by a histogram of the data, giving $\hat{p}(T)$, and then find $\beta_1(T)$ that solves $p(T) = \hat{p}(T)$. Figure 5.8 proves the added variation in β_1 can account for the extra features in the density, and in spite of our crude approach, β_1 is close to 1 for most values of T . Our choice to keep β_2 constant at 2 preserves the symmetry to Rice’s result (5.7). This extra nonlinearity explains why the matching of crossings in Fig. 5.2 (c)&(d) is less apparent for the class 2 process.

5.4 LATENCY IN CLASSES 1 AND 2 PROCESSES

How apposite is the label “latency”, and what does the latency density do for us?

The latency density models regularity. Figure 5.9 demonstrates how $f(\eta)$

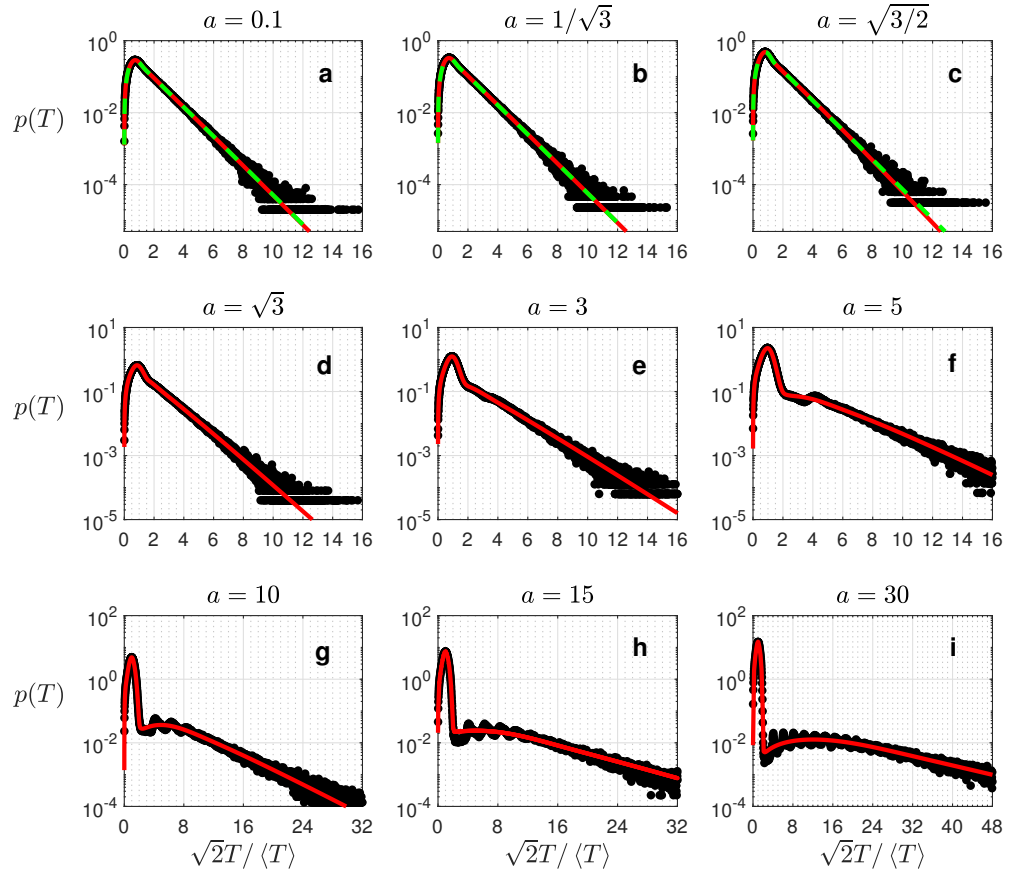


Figure 5.7.: Plots of the interval density for zero-crossing of the process ρ_{12} for values of the periodicity parameter $a > 0$. Histogrammed data are shown as black dots, and the density model (5.12) as solid red lines. In plots (a)–(c) the solid red lines represent the rescaled density $\sqrt{1+a^2}p_0(\sqrt{1+a^2}T)$ for when a is below the critical value $a = \sqrt{3}/2$. The density model (5.11) is displayed as a solid red line in plots (c)–(f). Also included as dashed green lines are plots of a finite mixture model *WEIB-GAM-EXPP* which are similar to the rescaled $p_0(\tau)$ density.

changes as a increases for processes ρ_{1j} . Just as the power spectrum reveals how frequencies (equivalently, periodicities) are distributed in the process $x(t)$, the latency density indicates how periodicity is represented in the zero-crossings of $x(t)$. For values of a in the class 0 regimes the means and variances of η are large—strong irregularity—whilst at large a the distribution significantly narrows—strong

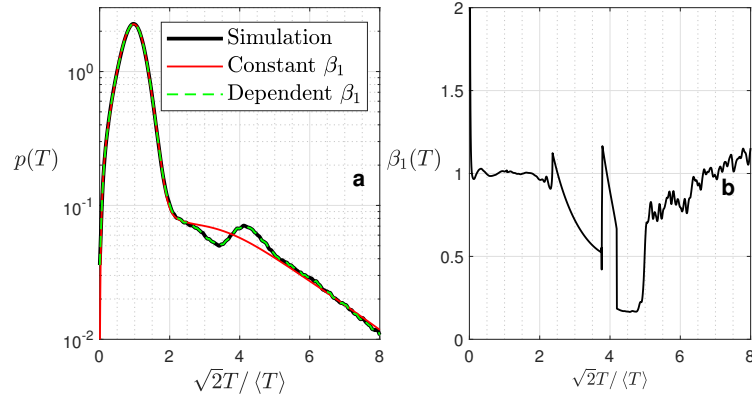


Figure 5.8.: (a) Plot of the interval density for the process ρ_{12} when $a = 5$, compared against the model (5.11) when nonlinear dependence is incorporated. (b) Plot of scale parameter $\beta_1(T)$.

regularity. We may even identify a variable for a since it is analogous to angular frequency:

$$\zeta = 2\pi\omega = 2\pi(1/2\eta) = \pi/\eta; \quad (5.17)$$

and above we referred to a symmetry in the crossing variable defined in (5.8) with respect to Rice's result: when $\beta_1 = 1$, $\beta_2 = 2$,

$$T(\tau, \eta) = T(\tau, \pi/\zeta) = \tau / \left(1 + (\tau\zeta/\pi)^2\right)^{1/2} \sim \pi/\zeta, \quad (5.18)$$

the last step using the small η (i.e. large ζ) simplification. This is another example of what we have referred to as 'stochastic periodicity', and will be explored further in the next chapter.

The latency density predicts tail behaviour. Appendix C derives the asymptotic forms of the general density model (5.11), and the behaviour is

$$p(T) \sim \begin{cases} p_0(T), & \text{if } T \ll \langle T \rangle, \\ \sqrt{T^{j-1}} f(T), & \text{if } T \gg \langle T \rangle, \end{cases} \quad (5.19)$$

using the $\beta_1 = 1$ form. (Refer to App. G for example parameter values for $f(\eta)$, and equation (C.15) for the exact forms.) As a grows, the mean interval length goes to zero, and the range of "small intervals" significantly shrinks, to the extent that it

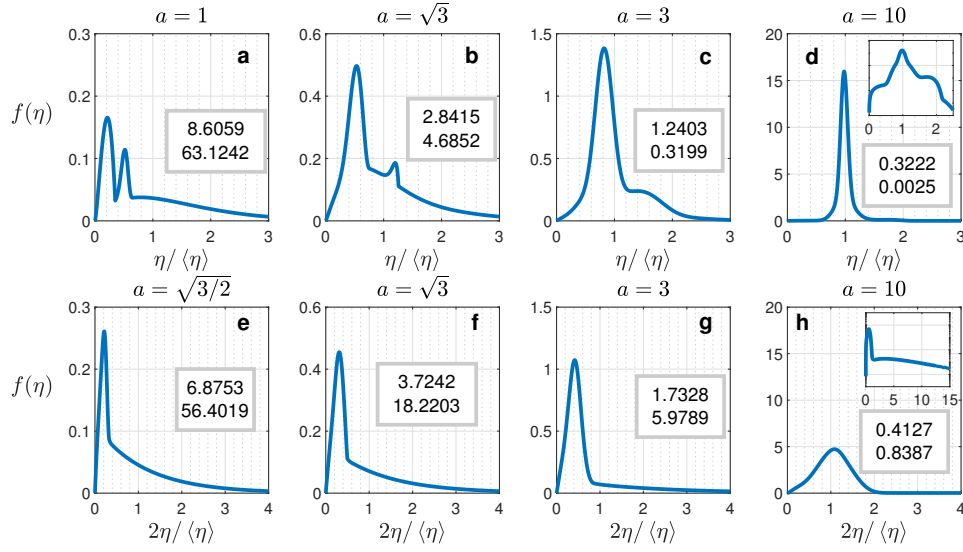


Figure 5.9.: Plots of the latency density as predicted by the model for the ρ_{11} process (a)–(d) and the ρ_{12} process (e)–(h). The boxes inset contain the mean (top) and variance (bottom) of each distribution.

is the second (large intervals) approximation that is key. Plots (a)&(b) of Fig. 5.10 indicate the region of T where (5.19) is valid when $a = 10$ for processes ρ_{1j} . The small intervals approximation is valid for both classes, implying such intervals occur with a similar frequency regardless of the class of process. This is slightly different for a sub-fractal process since from (5.14) $p(T) \sim \epsilon(a) p_0(T)$; that is, sub-fractal effects differ among the classes. Plots (a)&(b) further show that $p(T) \approx f(T)$ near the modal interval, and we discuss the symmetry in this interval range in Sec. 6.1. Note that the peak density is smaller by a factor of 10 for the class 2 case.

Turning now to the large $T > 2\langle T \rangle$, Fig. 5.10, plot (a) demonstrates the second row of (5.19) for a class 1 process, and so as $T \rightarrow \eta_M$, the tail is therefore a product of two multinomials:

$$p(T) \sim T^{v_M-1} (d_M - T)^{w_M-1}, \quad (5.20)$$

where $d_M = \eta_M$ is the largest range parameter for the *BETA* mixture, and the parameters v_M, w_M are the corresponding shape parameters for the contributing mixture component. For the class 2 case, plot (b) shows that for large T the density after the oscillations (refer to Fig. 5.7(g)) is approximately exponential, which is the oft quoted result in the literature for a nonnegative power-spectrum [97]. Further

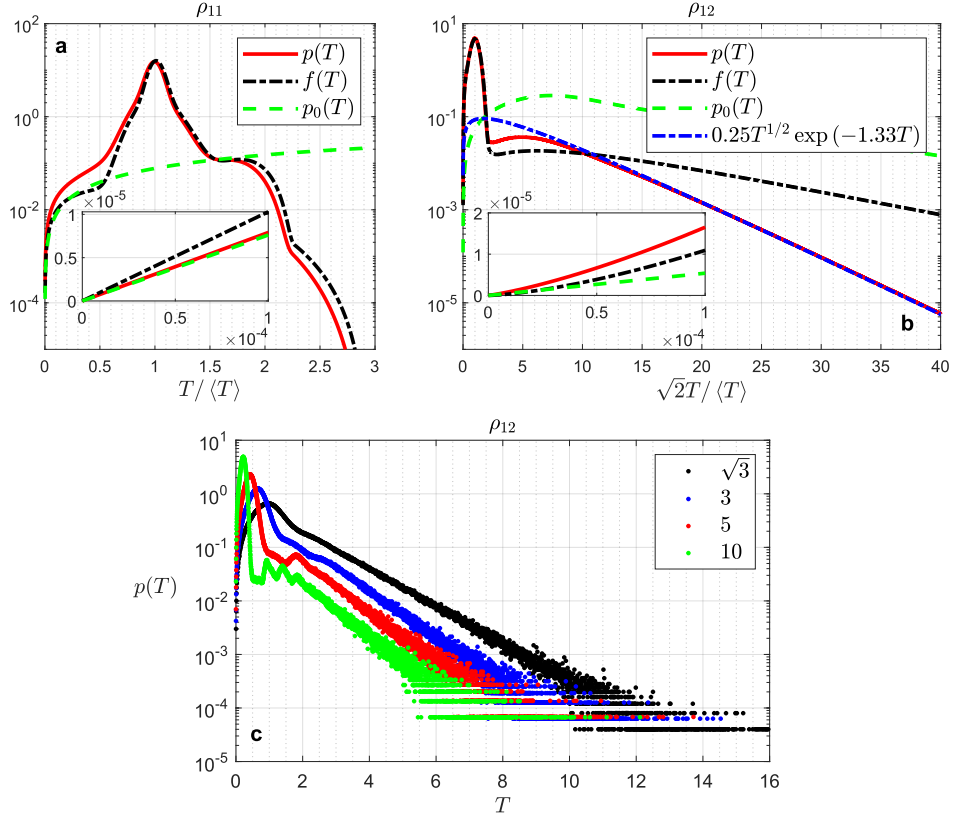


Figure 5.10.: (a)&(b): Plots illustrating tail behaviour of the interval density for processes ρ_{1j} when $a = 10$. (c): Plots showing the evolution of the interval density for the ρ_{12} process for varying a (values contained in legend).

comparison of the tail (Fig. 5.10(c)) shows a tail convergence that unlike in the class 1 case, does not depend on the mean $\langle T \rangle$. The definition for the persistence exponent (2.29) allows for the case where the density resembles that of a gamma distribution with non-unitary shape parameter. Therefore, the result

$$p(T) \sim T^{1/2} \exp\left(-\theta T \left(1 + (\theta b_M)^{-2/3}\right)^{3/2}\right), \quad (5.21)$$

agrees with the literature; θ is the persistence exponent when $a=0$, and b_M is the largest secondary scale parameter from the *EXPP* contributions to the latency density. Returning to the notion of the power spectrum as a distribution of frequencies ω in the process $x(t)$, $S_{12}(0;a)$ relates to the maximum periodicity ($\omega^{-1} \rightarrow \infty$ as $\omega \rightarrow 0$) and for $a > 2.8614$, $S_{12}(0;a) \approx \sqrt{\pi/2}$. This would explain why aside from scale changes there is little difference in the right tail of $p(T)$ as a increases.

Latency supports the sampling interpretation. The mixture models presented herein essentially say that crossings of a Gaussian process are analogous to a correlated sampling from a population of crossings, and for classes 1 and 2 processes there are additional nonlinearities and long range dependence. The Slepian regression solution method (Sec. 2.2.3.2) has the same perspective of not being concerned with the sequential propagation of crossings, but rather representing the long term features. It too involves an integral equation, though of far greater complexity and with more focus on the process $x(t)$. Ignoring sequential dependence, there is a reversibility between crossing intervals and their interval density for class 1 processes. Consider the random variable (5.8). The crossings of a Gaussian process ρ_{i1} leads to intervals T_m with distribution $p(T)$. In the opposite direction, uncorrelated variates τ_m and η_m from $p_0(\tau)$ and $f(\eta)$, respectively, are easily sampled using transformed uniform variates and/or acceptance-rejection methods (e.g. [100], Ch. 4), and then each T_m is obtained using (5.8). This reversibility is not as accessible for a class 2 process as $a \rightarrow \infty$, since β_1 in (5.8) depends on T (as seen in Fig. 5.8), highlighting again the strong, nonlinear dependence in this case.

In terms of the optimisation to find the interval density, a likelihood function that assumes a joint independence is sufficient for all the examples in this thesis. Following on from comments in Sec. 4.2.3, sequential dependence is not as important as mixing when computing the density for crossing intervals of a stationary Gaussian process. A Markov-chain model combined with our mixture models could in principle further demonstrate the correspondence between intervals derived from a stationary Gaussian process and intervals sampled from a mixture distribution, refer to [59]. The quality of mixture models that use MLE estimates depends on the size of sample data used in the optimisation; hence why the density model plots in Sec. 4.2 provided comparatively better agreement with simulations.

5.5 SUMMARY

The properties of classes 1 and 2 processes have been analysed and used to construct compound density models, the power spectrum providing insights on the connection between the process $x(t)$ and its crossings. The latency density is presented as a tool with which to move between classes of process, as proof of the doubly (or triply) stochastic nature of zero-crossings, and for finding expressions for the large T behaviour of the interval density. We have concentrated on additive, shift-type changes in the power spectrum of class 0 processes, but many other operations are possible, e.g. convolution, composition; and these may conceivably provide opportunities to use the generalised form of the density model.

Thus far we have been interested in long-term zero-crossing behaviour, studying dependence in the aggregate. The next chapter will investigate sequential dependence by measuring changes in varying time windows. A number of patterns emerge at extreme cases of the periodicity parameter a , not least the symmetries already seen in the interval density. More evidence will be provided for the idea of stochastic periodicity.

6

PATTERNS AND OTHER PROPERTIES OF THE CROSSING SEQUENCE

The preceding chapters have highlighted some of the intricacies to the zero-crossing problem, the two types of oscillatory correlation necessitating different density models. The transformation mixture model offers a mechanism for crossing propagation, and is obtained as an integral equation. Being an average, it does not directly assign any order to the intervals. Comparing classes 1 and 2 processes hints at the importance of the arrangement of crossings, given that the mean interval length is identical for both classes. This chapter demonstrates that the zero-crossing problem is also a geometrical problem, and accordingly, we use various measures for temporal and spatial point pattern formation. The analysis will concentrate on extreme cases of oscillatory correlation, specifically $a=0$ and $a=100$; but it should be understood that the sequential ordering of crossings is non-trivial for all values of a since crossings of a Gaussian process are dependent [85]. Again, central to the classification are simulation results which were in fact prefigured by long established general results [46, 49, 85]. Two graphical representations of the crossing interval sequence are introduced, and each are revealing of the notion of stochastic periodicity.

The limiting values of the power spectrum (3.12)–(3.14) demonstrate analytically that there is not much difference between processes within each class when a is large. This is supported empirically by simulated sample functions in Sec. 3.3.2 and corresponding interval density models in Sec. 5.3.1. Sub-fractality is suppressed and interval variances are approximately equal for smooth and sub-fractal cases.

Thus, in this chapter simulation plots will primarily be of processes ρ_{1j} and should be taken as representative of their respective classes. Except where indicated, all realisations are generated using the same random number generator (RNG) seed, $2^{31} - 1$.

6.1 ZERO-CROSSING TRACE

The Van Vleck arcsine law (2.16) connects memory in the process to memory of zero-crossing locations, and since the correlation in the former is global, so also is the correlation in the latter. Consequently, the crossing interval sequence \mathbf{T}_m , $1 \leq m \leq n_T$, is ordered in time. Using the notation of Sec. 3.2.3, $\mathbf{l}_{m+1}^{\Delta\Delta} := \Delta t (\mathbf{l}_{m+1} - 1)$ gives the time at the end of the crossing interval. The curve formed by the set of points $(\mathbf{l}_{m+1}^{\Delta\Delta}, \mathbf{T}_m)$ is the 'zero-crossing trace', denoted as $T(t)$, and plots of $T(t)$ below will be normalized by the mean interval length $\langle T \rangle$. For reference, the power spectrum of the processes under study is

$$S_{ij}(\omega; a) = \frac{(j-1)}{2} G_i(\omega) + \frac{1}{2j} \left(G_i \left(\omega + \frac{a}{\pi \sqrt{2^{3-j}}} \right) + G_i \left(\omega - \frac{a}{\pi \sqrt{2^{3-j}}} \right) \right). \quad (6.1)$$

6.1.1 Class 0

Beginning with Fig. 6.1, plots (a)&(c) show $T(t)$ for single realisations of the non-oscillatory processes g_1 and g_2 , (3.31), and plots (b)&(d) show the same but connected and over a shorter time duration. The zero-crossing traces support the simplification of the intervals being approximately independent. For the process g_1 , the modal interval length is approximately half the mean and this is somewhat reflected in the lower region of Fig. 6.1(a). The process g_2 was assigned a density model of hyperexponential type, i.e. maximal at zero and monotonic decreasing. This property is borne out in the trace plot, Fig. 6.1(c). Short sections of $T(t)$ identify more closely the variation in the interval sequence. Symmetricity about the

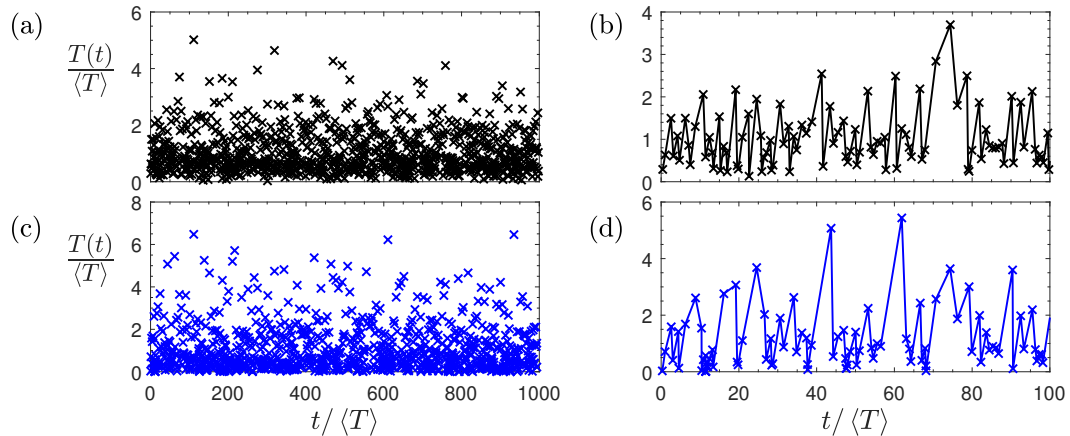


Figure 6.1.: Plots of the normalized zero-crossing trace for Gaussian processes g_1 (black crosses) and g_2 (blue crosses). Plots (a & c) reflect the skewness of the interval density (refer back to Figs. 4.1(a) and Figs. 4.2(b)). The connected traces in (b & d) respectively illustrate small negative and small positive correlation.

mean is seen in Fig. 6.1, plot(b), with alternating groups of long and short interval sizes, typical of a negative correlation coefficient (simulations give $\hat{\kappa}_1 \approx -0.0161$) and anti-bunching [47]. The trace in Fig. 6.1(d) displays clustering of small intervals, and large shifts in size predominately occur in pairs. This is again captured in the correlation coefficient (simulations give $\kappa_1 \approx 0.0478$) and is symbolic of bunching behaviour [47].

The process g_2 has a larger interval variance and smaller persistence exponent so that considering the full realisation would show there are on average more large intervals (relative to the mean) than for the g_1 case. The crossing intervals for each process may permit an independence assumption, but neither has zero correlation. This suggests the need for a global measure of the zero-crossing trace, one capable of accounting for minute differences between multiple processes. Hereafter only simulation plots of ρ_{1j} processes will be discussed.

6.1.2 Class 1 Processes: $a = 100$

The cos-wave process, Sec. 2.7.2, exemplifies a zero-crossing sequence absent of variability. The corresponding crossing trace is a horizontal line through the half-

period of the cosine. If we use a cos-wave process with mean $\langle T \rangle$, the crossing trace is then the limiting form a class 1 process approaches. Section 5.3.1 showed that as $a \rightarrow \infty$ the interval density closely resembles a delta-function, additionally with shoulders at 1.5 standard deviations from the mean, Fig. 5.5. The extent to which class 1 processes resemble a cos-wave process is illustrated in Fig. 6.2(a). The shoulders of the interval density are represented in the horizontal orange and yellow lines, and the trace $T(t)$ primarily traverses the narrow gap between these lines, narrow because the mean and variance are close to zero, with $\sigma_T^2 \ll \langle T \rangle$. The power spectrum is also narrow. On occasion, the trace also “jumps” outside the gap, but these are rare because the dominant frequencies in the process are at $\omega \sim \pm a/(2\pi)$.

It is especially useful to see the zero-crossing trace alongside the original sample function in cases of high oscillatory correlation. Figure 6.2(b) provides a closer look at the trace near a jump from its modal regime, and the corresponding region of sample function is given in Fig. 6.2(c). Large amplitudinal variation is accompanied by approximately regular intervals, whilst shorter amplitude changes are what cause crossing interval jumps outside the $\mu_T \pm 1.5\sigma_T$ window. Departures from regularity in the process are thus well accommodated in the zero-crossings, echoing the previous discussion on the periodicity density, Sec. 3.4.

6.1.3 Class 2: $a = 100$

Stochastic periodicity need not be as confined as in the class 1 case. Class 2 processes demonstrate most clearly the significance of the zero-crossing ordering, arising as a result of the two dominant time scales: $\sqrt{2}\langle T \rangle$ and $\sqrt{2a}\langle T \rangle \sim \sqrt{2}\pi$, as visible in Fig. 3.8(c). The trace $T(t)$ in Fig. 6.3(a) depicts what happens when the interval mean and variance are of similar order, and crossing intervals are arranged about the modal interval length, $\langle T \rangle/\sqrt{2}$, included as a horizontal black line. Recall the shape and model of the interval density in this case (Fig. 5.7) and how it reflects the dual nature of the crossing trace. Intervals falling between zero and twice the

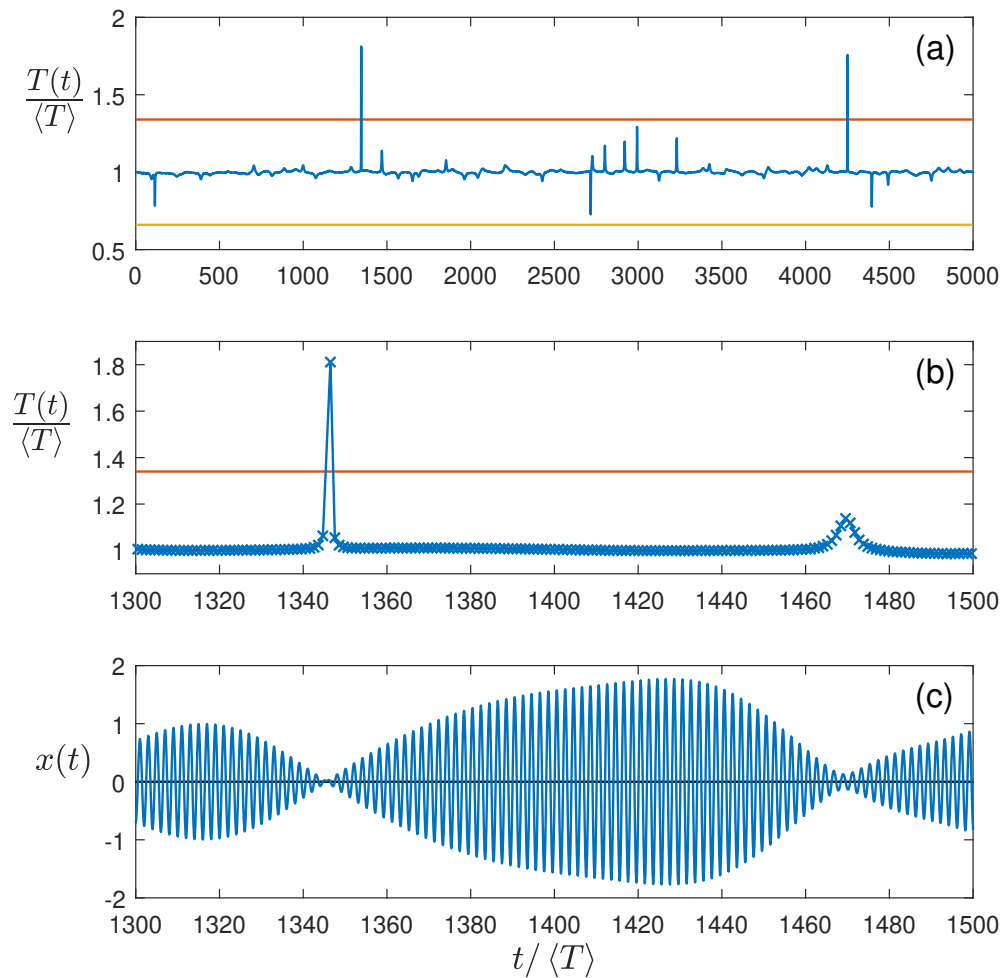


Figure 6.2.: Normalized zero-crossing trace and sample function for the process ρ_{11} when $a = 100$. Plot (a) gives the full $T(t)$ (blue line) for a single realisation, and horizontal orange/yellow lines represent plus/minus 1.5 standard deviations from the mean. A shorter region of the trace is given in (b), and the corresponding section of the sample function in (c).

mode are described by the *BETA* distribution contributions to the latency density $f(\eta)$. Rare but significantly large gaps in the trace are described by the *EXPP* distribution.

A smaller region of the crossing trace, and with marked crossings is shown in Fig. 6.3(b). The trace $T(t)$ is seen to in fact flip locally between the two branches disposed about the interval mode. The flipping must restart over sufficiently large

time scales because the correlation function decays to zero. Once again, a plot of the sample function is useful here, and this is given in Fig. 6.3(c) for the same time region as the trace in Fig. 6.3(b). The realisation alternates between oscillating towards, and then away from the zero-level. This effects patterns in the trace $T(t)$ caused by zero-crossings occurring near the extrema of the sample function. The fact that there are more turning points than crossings in any sufficiently large time window, (3.36), leads to epochs where there are no axis crossings, i.e. large excursions [86]. One such occurrence is indicated by the red-circles in Fig. 6.3(c). As seen in Fig. 6.3(a), these departures from the modal regime occur with more frequency than those seen in the class 1 case. These large excursions result in intervals that are up to 10^2 orders of magnitude larger than the mean interval length shared by both classes, as can be seen in Fig. 6.4.

6.2 LACUNARITY

The zero-crossing properties for extreme cases of classes 0, 1 and 2 processes can be investigated further using the lacunarity measure. The concept and various applications were discussed in Sec. 2.5, and here it will be shown that by quantifying the concentration of crossings at different time scales, lacunarity distinguishes the degree of randomness as well as the type of periodic modulation.

Let $\mathcal{N}(r)$ be the number of zero-crossings occurring in a time window (or box) of length r that moves along the time axis of a random process $x(t)$ in a contiguous fashion. Lacunarity is defined as

$$\Lambda(r) = \frac{\mathbb{E}[\mathcal{N}^2(r)]}{\mathbb{E}^2[\mathcal{N}(r)]} = 1 + \frac{\text{Var}[\mathcal{N}(r)]}{\mathbb{E}^2[\mathcal{N}(r)]}.$$

Here we focus on the analytical forms of the moments, and for the contiguous boxes counting method; the next chapter will evaluate estimation of Λ using the gliding boxes counting method, for which the analytical expressions are usually not known.

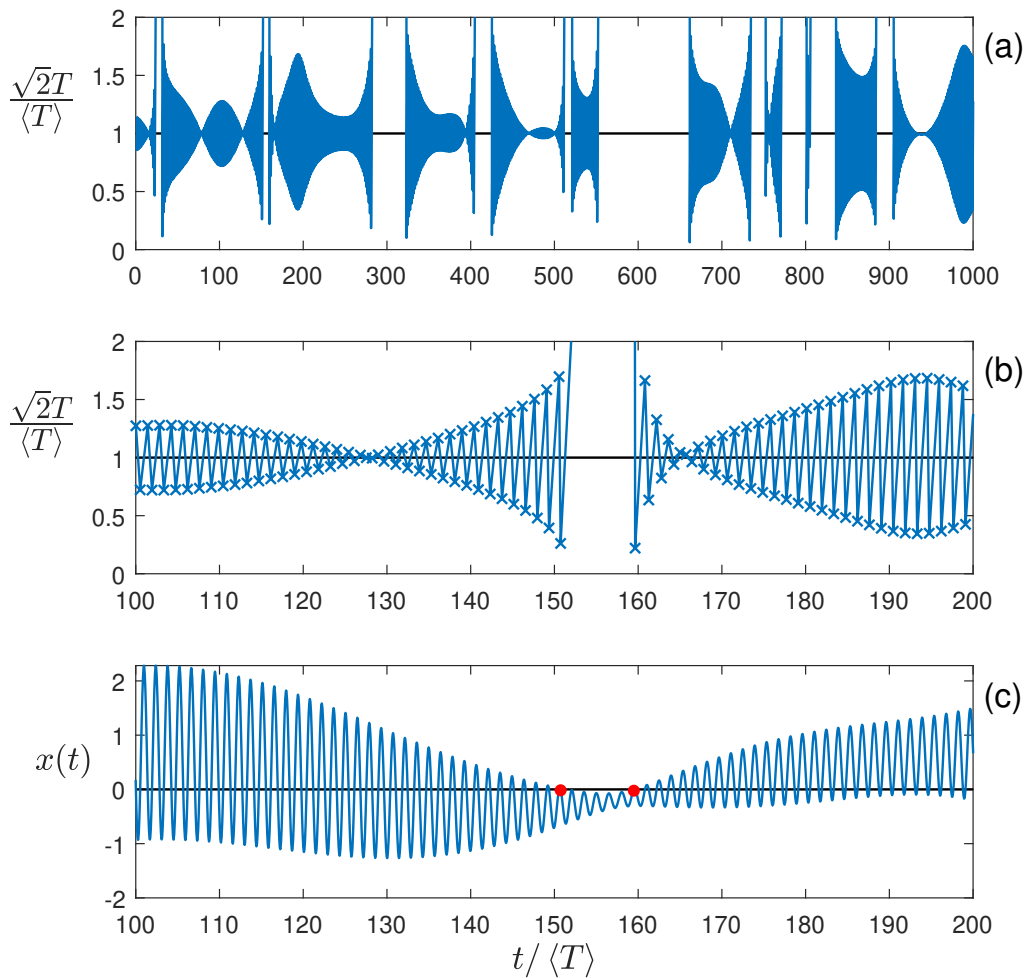


Figure 6.3.: Normalised zero-crossing trace and sample function for the process ρ_{12} when $a = 100$. Plot (a) gives the normalized trace (blue line) for one-fifth of a single realisation, and the trace is symmetric across the modal interval length $(\langle T \rangle / \sqrt{2})$ shown as a solid black line. Crossing intervals greater than twice the mode are located off-axis. A shorter region of the trace is given in plot (b) and the corresponding section of the sample function in plot (c).

As given in Sec. 2.2.1, the mean number of crossings is $\bar{R}r$, where \bar{R} is the crossing rate. The variance of crossing counts is (2.11)

$$\text{Var}[\mathcal{N}(r)] = \bar{R}r + 2\bar{R} \int_0^r (r - \tau)(U(\tau) - \bar{R}) d\tau. \quad (6.2)$$

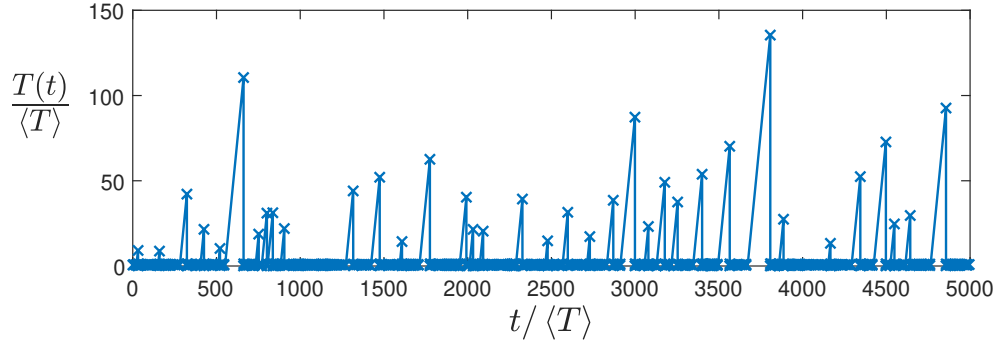


Figure 6.4.: Normalized zero-crossing trace over a full realisation of the process ρ_{12} when $a = 100$, with no restriction to the y-axis limit to emphasize the rarer and significantly large crossing intervals.

Rice's conditional density function $U(\tau)$, (2.12), tends to \bar{R} as $\tau \rightarrow \infty$, whence the variance (6.2) is linear at large box sizes.

The zero-crossing traces exhibit patterns relative to the mean interval length, therefore we will plot against $\log(\bar{R}r)$ lacunarity in the form

$$\log(\Lambda - 1) = \log(\text{Var}[\mathcal{N}(r)]) - 2 \log(\bar{R}r), \quad (6.3)$$

leading to the 'log-lacunarity slope'

$$\begin{aligned} \lambda(r) &= \frac{d \log(\Lambda - 1)}{d \log(r)} = \frac{r}{\text{Var}[\mathcal{N}(r)]} \frac{d \text{Var}[\mathcal{N}(r)]}{dr} - 2 \\ &= \frac{r \left(1 + 2 \int_0^r (U(\tau) - \bar{R}) d\tau \right)}{r + 2 \int_0^r (r - \tau)(U(\tau) - \bar{R}) d\tau} - 2, \end{aligned} \quad (6.4)$$

the last expression indicating it asymptotes to -1 in the limits $r \rightarrow 0$ and $r \rightarrow \infty$, the significance of which will be seen below. Logarithms are to base 10. To aid in the analysis we consider two reference cases, each extremes on the randomness scale: (i) the Poisson process derived from the random telegraph-wave, Sec. 2.7.1; (ii) a cosine wave, from Sec. 2.7.2 and without loss of generality we set the phase to zero.

6.2.1 Poisson Process

The Poisson process describes a counting process that is zero at time zero, possesses stationary and independent increments, and has events that follow a Poisson distribution with rate \bar{R} . For a strictly Poissonian interval sequence, the number of crossings in box size r has distribution

$$P_N(\mathcal{N}(r) = k) = e^{-\bar{R}r} (\bar{R}r)^k / k!, \quad (6.5)$$

and the mean and variance are $\bar{R}r$. From (6.3) and (6.4), it follows that

$$\log(\Lambda - 1) = -\log(\bar{R}r), \quad \lambda(r) = -1 \quad (6.6)$$

For a stationary Gaussian process, the counting process of zero-crossings is both stationary and dependent [49, 85].

6.2.2 Cosine Wave

Consider the deterministic function $x_d(t) = \cos(\sqrt{1+a^2}t)$. To speak of randomness we use the external monitoring scheme [101], under which the number of crossings does vary with box size. By inspection of a contiguous boxes setup, it follows that the counting distribution is

$$P_N(\mathcal{N}(r) = k) = \begin{cases} c + 1 - \bar{R}r, & \text{if } k = c, \\ \bar{R}r - c, & \text{if } k = c + 1, \\ 0 & \text{otherwise.} \end{cases} \quad (6.7)$$

where $c = \lfloor \bar{R}r \rfloor$; then

$$E[\mathcal{N}(r)] = \sum_{k=0}^{c+1} k P_N(\mathcal{N}(r) = k) = c(c + 1 - \bar{R}r) + (c + 1)(\bar{R}r - c) = \bar{R}r, \quad (6.8)$$

$$\begin{aligned}
\mathbb{E} [\mathcal{N}^2(r)] &= \sum_{k=0}^{c+1} k^2 P_N(\mathcal{N}(r) = k) = c^2(c+1 - \bar{R}r) + (c+1)^2(\bar{R}r - c) \\
&= \bar{R}r(2c+1) - c(c+1), \\
\text{Var} [\mathcal{N}(r)] &= (\bar{R}r - c) [1 - (\bar{R}r - c)] \equiv h(\bar{R}r) (1 - h(\bar{R}r)), \tag{6.9}
\end{aligned}$$

where $h(s) = s - [s]$ is a periodic function with period 1, and satisfies $0 \leq h(s) < 1$. The variance is therefore identical within integer multiples of \bar{R}^{-1} and bounded above by 1. In particular, if $0 \leq \bar{R}r < 1$,

$$\text{Var} [\mathcal{N}(r)] = \bar{R}r(1 - \bar{R}r), \tag{6.10}$$

$$\log(\Lambda - 1) = \log(1 - \bar{R}r) - \log \bar{R}r. \tag{6.11}$$

When $\bar{R}r > 1$, the first term in Eq. (6.3) oscillates within integer multiples of $\bar{R}r$, and the lacunarity slope (6.4) oscillates between $\pm\infty$.

6.2.3 Non-Oscillatory Gaussian Processes

Lacunarity curves for processes g_1 and g_2 are displayed in Fig. 6.5. The Poisson process is seen to be marginal between sub-fractal and smooth processes, and the crossing trace plots in Fig. 6.1 can now be distinguished using a statistic, and not just heuristically. At small box sizes the lacunarity is approximately equal for all three processes. The small box sizes property in fact holds for all stationary point processes ([3], Sec. 3.8): if $\mathcal{N}(r)$ (with $\mathcal{N}(0) = 0$) is a counting process with stationary increments,

$$\lim_{r \rightarrow 0} \frac{\Pr\{\mathcal{N}(r) > 0\}}{r} = \bar{R} \quad \Rightarrow \quad \Lambda = \frac{1}{P_N(\mathcal{N}(r) = 1)} \sim \frac{1}{\bar{R}r} \text{ as } r \rightarrow 0. \tag{6.12}$$

We have also seen that the periodicity density decays like η^{-2} for both Poisson and stationary Gaussian processes, Fig. 3.8. For box sizes r such that $10^{-1} < \bar{R}r < 1$, the smooth process has fewer than two crossings in a box with high probability and so the fluctuations are approximately binomially distributed [47], with $\Lambda(r)$ less

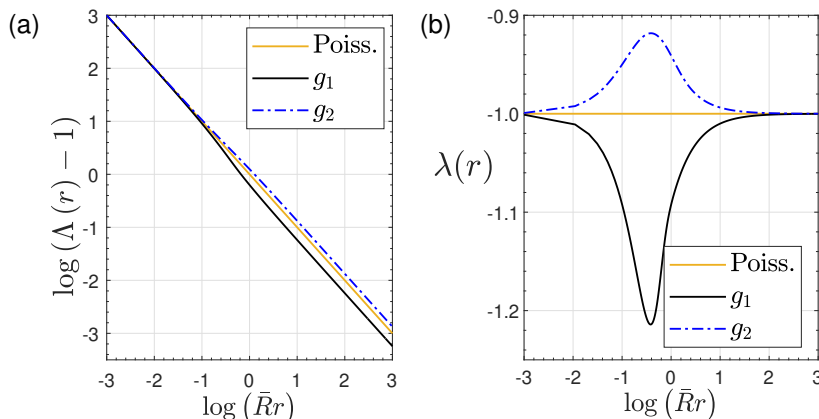


Figure 6.5.: Lacunarity and log-lacunarity slope for Gaussian processes g_1 and g_2 and the analogous Poisson process (Poiss.), which divides smooth and sub-fractal class 0 processes.

than the corresponding Poisson value and $\lambda(r) < -1$. The modal interval length is $\approx \pi/2$, meaning there is less variation in the crossing number close to this time scale, and this is evidenced in the lacunarity slope. At larger r the Poisson and binomial fluctuations become asymptotically similar and the slope returns to -1 , though the value of $\lambda(r)$ remains less than that for the Poisson process.

By contrast the fluctuations for the sub-fractal process are slightly greater than the Poisson case in the regime $10^{-1} < \bar{R}r < 1$ because clustering enables more than two crossings to occur within a box with higher probability than the smooth case, consistent with their being approximately negative-binomially distributed [47]. Consequently, $\lambda(r)$ exceeds -1 , but again the crossing behaviour scales asymptotically with the Poisson at larger r , now with $\Lambda(r)$ exceeding the Poisson value.

Describing class 0 processes as having independent intervals would belie the fact that correlation acts across all time scales. The constant lacunarity slope for the Poisson case illustrates true independence in the sense of translational invariance. Notwithstanding, the Markov-chain model is sufficient to obtain the mean and variance of interval lengths—refer to Fig. 3.6. However, when the arrangement of crossings become particularly important—e.g. modelling the correlation coefficient or the interval density—the Markov chain models are less accurate [5].

6.2.4 Oscillatory Gaussian Processes

Lacunarity curves for class 1 processes ρ_{i1} when $a = 100$ are provided in Fig. 6.6(a). The main figure displays the peak-to-peak value of $\Lambda(r)$ for the cosine wave when $\bar{R}r > 7/2$ (the third maximum point after $\bar{R} = 1$). All curves closely match at small and intermediate box sizes, which is expected given the sample function plot in Fig. 6.2(c). The inset in Fig. 6.6(a) better illustrates the oscillatory nature of the variance and thereby lacunarity signature. For the oscillatory Gaussian processes, the crossing number variances are small rather than vanish when the box size coincides with multiples of the mean interval length, leading to attenuating periodicities in $\Lambda(r)$.

With reference to Fig. 6.2(a), as the box size increases, extreme crossing interval sizes outside the $\mu_T \pm 1.5\sigma_T$ window are included in the counting, and the lacunarity is larger than that for the (deterministic) cosine wave. The associated lacunarity slopes are given in Fig. 6.6(c). For the cosine wave, only the peak-to-peak slope is plotted for $\bar{R}r > 7/2$, which is equivalent to isolating the second term in (6.3), whereupon $\lambda(r) = -2$. Aside from the periodicities, these lacunarity slopes resemble the g_1 case in Fig. 6.5(b). Notably, the sub-fractal case ρ_{21} approaches the Poisson limit from below just like the smooth ρ_{11} case. This further proves that sub-fractal effects can be suppressed by a large periodicity parameter, i.e. strong oscillatory correlation. In light of the truncation of the maximum interval size, this extreme of class 1 process is more closer to a binomial description than the smooth process g_1 ; in a short time window, crossings either do or do not occur, with little variation in their separation when they do.

Figure 6.6(b) provides an insightful classification of both the “gappiness” observed in the zero-crossing trace, Fig. 6.3(a), and the expanding and contracting modulation at smaller time scales, Fig. 6.3(b), in the class 2 variation. Also note the rescaling of box sizes by $\sqrt{2}$. Here it is more appropriate to use the Poisson process as a reference case. Box sizes close to $\bar{R}r/\sqrt{2}$ correspond to the flipping of the interval sequence about the mode, in essence approaching an asymptotic regularity;

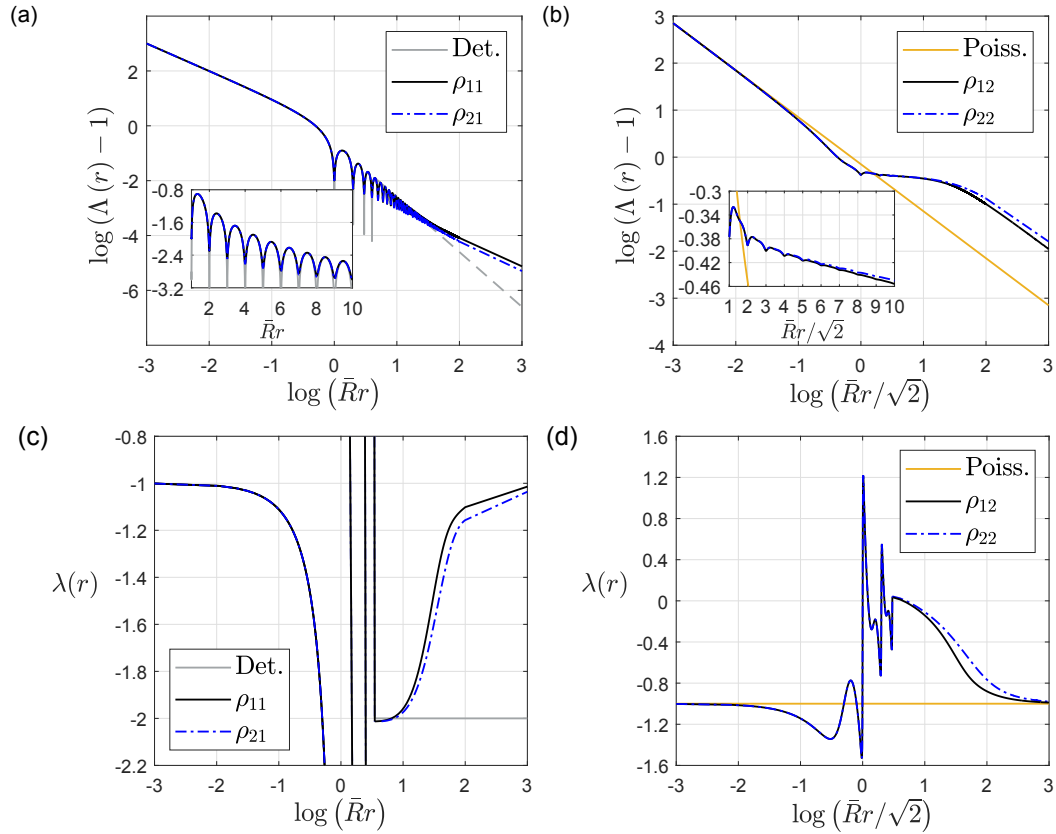


Figure 6.6.: Lacunarity and log-lacunarity slope for oscillatory Gaussian processes when $a = 100$, with results for a deterministic cosine wave (Det.) and a Poisson process (Poiss.) included for reference.

whence the lacunarity falls below that of the Poisson. There are again vestigial periodicities, indicated by the inset; but unlike the class 1 case, the oscillations are less symmetrical relative to multiples of the median crossing interval, $\approx \sqrt{2}\langle T \rangle$. The interval variance σ_T is larger, and the trace $T(t)$ has significant jumps to large values—refer back to Fig. 6.4. Lacunarity tracks these features, and identifies the periodicity time scales discussed in Sec. 3.4. At box sizes r less than $\sqrt{2}\langle T \rangle$, large crossing intervals result in many empty boxes that do not contribute to the moments of the lacunarity measure. Past this first timescale, large intervals begin to offset the small interval modulations, and the effect is a plateau-like form of lacunarity that continues till the second timescale ($a\sqrt{2}\langle T \rangle$) is reached. Thereafter, lacunarity asymptotes to the Poisson limit.

Figure 6.6(d) exemplifies the complexity of the periodic aspects of a class 2 extreme; rather than a series of equally spaced extrema as in the class 1 case, $\Lambda(r)$ addi-

tionally has inflection points not equally spaced, implying there are comparatively more changes at those time scales. The lacunarity slope is also seen to tend to the Poisson limit from above, slightly slower for the sub-fractal case. Super-Poisson behaviour connotes clustering of crossings, which holds true even for the smooth case given the significant jumps in interval size seen in plots of the crossing trace (refer back to Fig. 6.4).

In comparing lacunarity for the class 1 variant of the g_2 process, Fig. 6.6(a)&(c) show a reversal in the ordering of curves relative to their smooth counterparts. Figure 5.6 demonstrated that as a increases, the principal modal interval for the ρ_{21} process switches from the origin and asymptotes to the mean. Combined with the truncation of interval sizes, there is therefore a trio of properties— $p(0) \neq 0$, mode close to mean, and $P(T > 3\langle T \rangle) \approx 0$ —that would lead to a larger departure from the Poisson asymptote than in the smooth case. For the class 2 variants, the ordering of the class 0 processes is preserved. This agrees with our corresponding density model which has a support of infinity and an exponential tail, (5.21).

6.3 COUNTING DISTRIBUTIONS

Lacunarity is patently distinct for the three classes of Gaussian process, in spite of the shared linearity in the mean number of crossings. It is worth briefly making the comparison to Poisson and deterministic cases more explicit, and we do this by computing distributions of the counting process via simulations. The distributions are estimated from 10^3 realisations of the ρ_{1j} process. Smith [47] showed that smooth processes have binomially distributed zero-crossing counts as time $r \rightarrow \infty$. The binomial model enforces a maximum crossing count in fixed box sizes, which can be compared with simulations. For the analytical maximum count we fit the parameters of the binomial distribution using method of moments given the mean $\bar{R}r$ and variance (6.2). The counting distributions for the reference cases are first of all given in Fig. 6.7. For a Poisson process the idea of a maximum crossing count is not applicable because the counting process is independent, whilst for the cosine

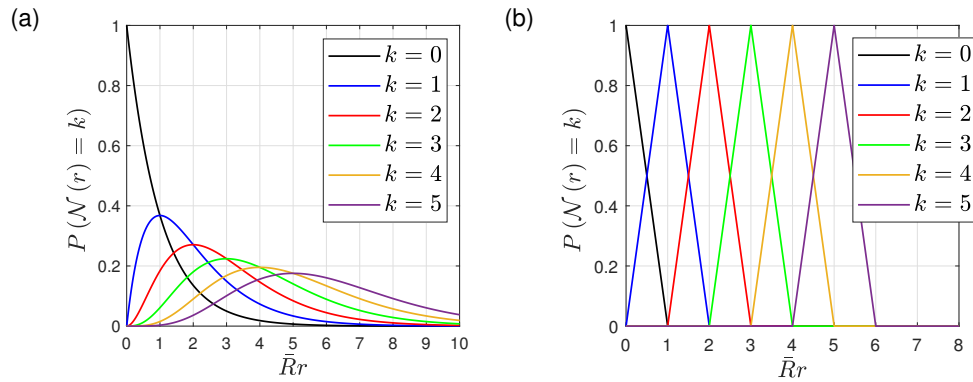


Figure 6.7.: Counting distributions for a Poisson process (a) and a cosine wave (b).

wave the maximum counts in box r is $\lceil \bar{R}r \rceil$.

Numerical estimates for the counting distribution $P_N(\mathcal{N}(r))$ for processes ρ_{1j} are supplied in Fig. 6.8, plots (a),(c)&(e). As in the plots of Fig. 6.7, the distributions for class 0 and class 1 processes have modes at approximately integer multiples of \bar{R}^{-1} , and for class 2 processes this is rescaled by $\sqrt{2}$. The distributions in Fig. 6.8(a) are skewed slightly more than their counterparts in Fig. 6.7(a), resulting in a smaller variance and therefore the lower lacunarity value for the g_1 process. Plot (c) of Fig. 6.8 again demonstrates the attenuation of periodicity in class 1 processes; the distributions slowly lose their triangular profile and the interquartile range expands.

The class 2 process has in diverse ways proven a complex embodiment of stochastic periodicity, and Fig. 6.8(e) reveals the distributions to have a dual nature. We have seen that the lacunarity has a plateau region, Fig. 6.6(b), owing to the presence of a large timescale contributed by the power spectrum having a maximum at the origin. Recall also the bimodality of sample function periodicities, Fig. 3.8(c). For reference, $P_N(\mathcal{N}(r) = 0) < 10^{-1}$ when $\bar{R}r > 36$. The distribution for positive even counts could almost be described as triangular as in the class 1 case, but here the tails are even more non-linear. The modes of the distributions for odd counts are at half-integer multiples of the rescaled mean, and like in the Poisson and class 0 processes, have less kurtosis.

The plots on the right in Fig. 6.8 provide another look at the counting process by plotting the average maximum number of crossings within a box. We have not

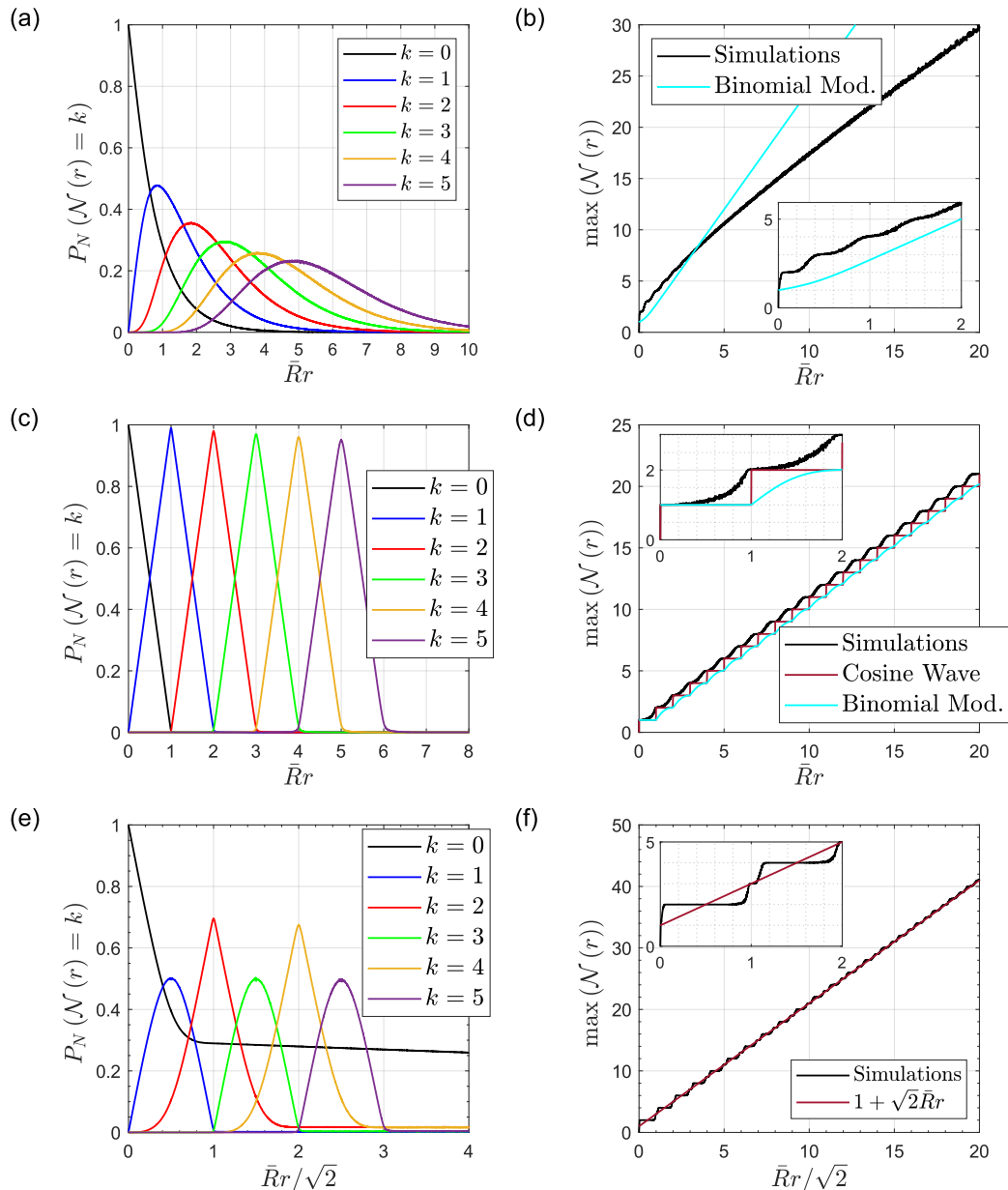


Figure 6.8.: Counting distributions and maximum crossing counts from simulations of the ρ_{1j} processes: (a & b) $a = 0$; (c & d) $j = 1$, $a = 100$; (e & f) $j = 2$, $a = 100$. The simulated maximum count is also compared with that of a binomial distribution, and in a cosine wave.

discussed the distribution of maximum counts, but the plots on the left of Fig. 6.8 would imply the distributions of the maximum are quite narrow, especially in the class 1 case where the crossing counts are asymptotically bounded above, due to concentration of the power spectrum at large frequencies. Furthermore, for large enough box sizes, the correlation between crossing locations is small, meaning the

crossing counts are approximately independent and the maximum count scales with Rice's result (3.4). Figure 6.8(b) shows that a binomial model that uses the analytical mean and variance of the crossing number is not appropriate for the g_1 process. In simulations there is a staircase feature, present in the oscillatory cases also. The cosine wave provides a lower bound for the extreme class 1 process over all time scales, plot (d). The fit from the binomial model may look better but we know that this is only approximately so from the plot opposite. For the extreme class 2 process a binomial fit is not possible because the variance of $\mathcal{N}(r)$ is much greater than the mean. Rather, the mean maximum count alternates either side of $1 + \sqrt{2\bar{R}r}$, which is essentially Rice's result with a different crossing rate.

Recall that the variance increases with r for Gaussian processes and is asymptotically parallel to the Poisson case; whence the counting distributions, should become rescaled Poisson distributions as r increases. A similar presentation could have been done for sub-fractal processes, and comparisons made with the negative-binomial distribution [47]. To be clear: these results do not contradict existing characterisations seen in [47]. Our contention is that the binomial model does not work for the specific form of the crossing number variance provided by Steinberg et al. [46], and that a characterisation with higher order complexity is required for oscillatory Gaussian processes when considering all possible time scales.

6.4 ZERO-CROSSING ORBITS

6.4.1 Phase Space Diagrams

We conclude this chapter by addressing dependence as determined by κ_1 , the correlation coefficient between adjacent intervals. Recall the definition:

$$\kappa_1 = \frac{\langle T_m T_{m+1} \rangle - \langle T \rangle^2}{\sigma_T^2}, \quad (6.13)$$

the subscript m being dropped for averages involving T_m alone. The product moment is what determines the sign of κ_1 , and we have seen that the ordering of

the intervals is non-trivial. Consider the path traced out by consecutive crossing interval pairs:

$$(T_1, T_2) \rightarrow (T_2, T_3) \rightarrow (T_3, T_4) \rightarrow \dots$$

Individually they form the terms for the product moment in (6.13), but together they give what we will term the ‘zero-crossing orbit’. The plots that follow give the orbits when the intervals are normalized by the mean interval length so that the “centre” of the resulting phase diagram is located at $(1, 1)$. This leads to four quadrants: bottom left, T_m, T_{m+1} both small; bottom right, T_m large and T_{m+1} small, and vice versa for the top left; top right, T_m, T_{m+1} both large. This division of crossing space is of more relevance at large a where the mode and median are approximately equal.

Plots (a)&(b) of Fig. 6.9, show the zero-crossing orbit when there is no oscillatory correlation. Plot (a) in fact obtains from a Poisson process, the orbit differing only slightly from plot (b) which results from a realisation of the g_1 process. The interval variances are large, and the bottom left region of the graphs are dense; hence the small correlation coefficients.

Moving on to the oscillatory cases, there is a distinctive structure. The orbit for ρ_{11} has a bow-tie structure oriented such that it goes through the line $T_{m+1} = T_m$, and therefore κ_1 is close to 1. Figure 6.9(d) shows the behaviour closer to the centre of the orbit, and there is a clear internal structure. Owing to the time discretisation and the fact that $P(T)$ is small both when $T \ll \langle T \rangle$ and $T > 2\langle T \rangle$, there is effectively a finite number of vertices the orbit can visit. Thus deterministic and stochastic periodicity in this case are not that far off. These observations are reminiscent of periodicity in dynamical systems—refer to Fig. 1.1.

Finally, for the process ρ_{12} , Fig. 6.9, plots (e)&(f) establish the intervals are negatively correlated, and again we see the $\sqrt{2}$ rescaling. In keeping with the dynamical systems analogy, the orbit does appear chaotic. It primarily moves along the line $T_{m+1} = \sqrt{2}\langle T \rangle - T_m$ with less but still fairly frequent movement above this diagonal, creating a horizontally reflected number four shape near the centre of the orbit. As indicated by Fig. 6.9(f), there are many contributions to the product moment

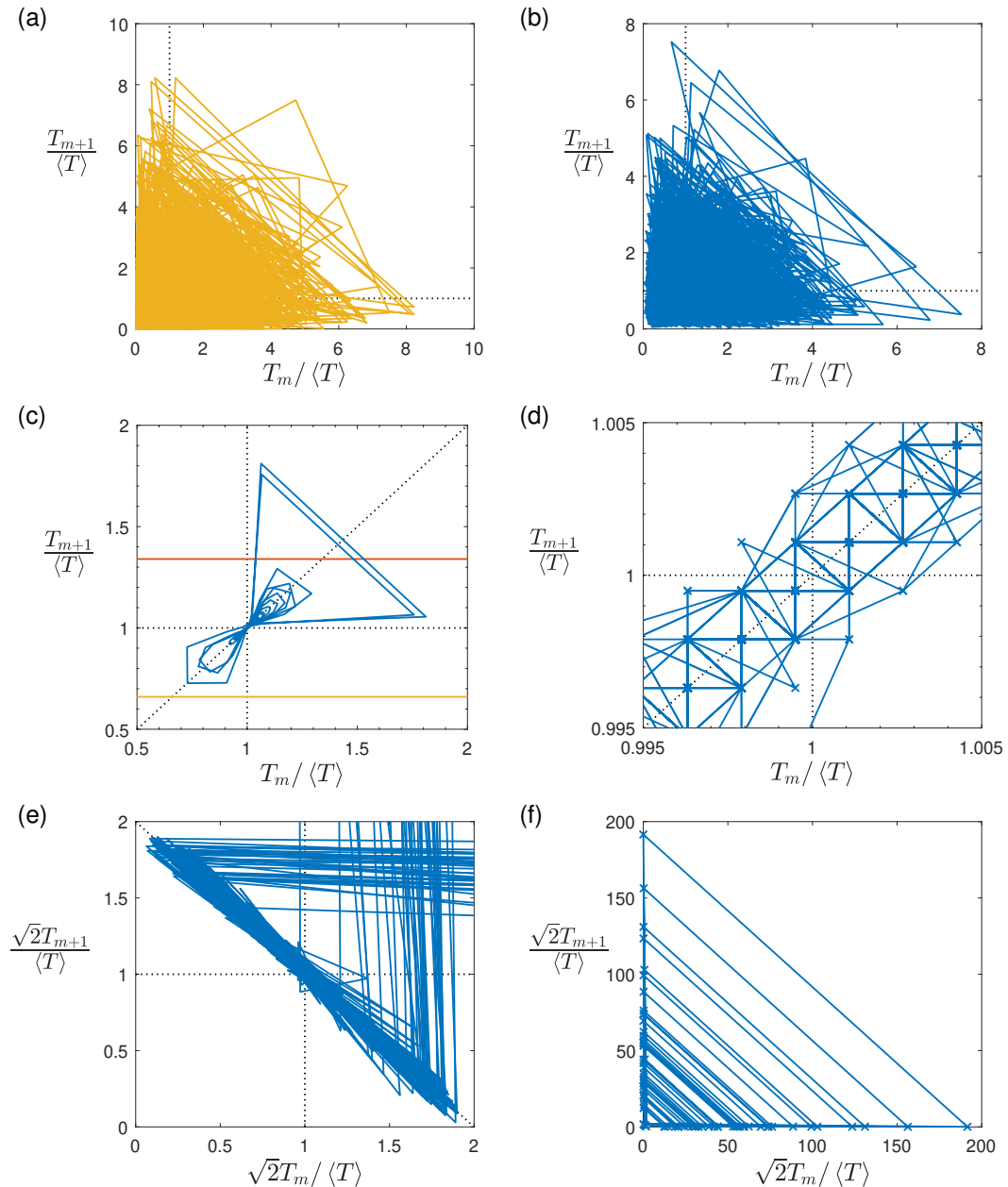


Figure 6.9.: Zero-crossing orbits for crossing intervals. (a) Poisson process. For Gaussian processes: (b) g_1 ; (c)&(d) ρ_{11} ; (e)&(f) ρ_{12} . Plot (c) has a bow-tie structure like the logistic map in Fig. 1.1, and (d) highlights the internal structure of the interval sequence. Plot (e) displays more variability due to the larger interval variance, but there are more returns to the “correlation line”. Unlike in plot (a), plots(c)&(e) have zones where interval pairs are hardly ever located. Plot (f) exemplifies the exponential tail of the interval density (5.21), and evidences the comments that as a consequence of (2.61), large crossing interval pairs of a stationary Gaussian process are unlikely.

where one of T_m and T_{m+1} is significantly large and the other significantly small. These are enough to result in a product moment that is close to the mean squared, resulting in κ_1 being negative but close to zero. Filtering out intervals greater than $\sqrt{2}\langle T \rangle$ (of which there are 36% for the data in Fig. 6.9(e)&(f)) leads to a correlation coefficient of -0.9357 as opposed to -0.0274 . The mean of the remaining data is the mode of the complete data since the large intervals are rare, and this can also be inferred from the symmetricity of the crossing trace in Fig. 6.3.

6.4.2 Correlation Coefficients

The correlation coefficient we have thus far been using is equivalent to Pearson's correlation coefficient, which is ideal for measuring linear dependence in adjacent intervals with small variations about the regression line. This however makes it susceptible to outliers. Kendall's tau coefficient¹ for crossing intervals, T_m , $m = 1, \dots, N - 1$, is given by

$$\kappa_\tau = \frac{2}{(N-1)(N-2)} \sum_{m=1}^{N-2} \sum_{n=m+1}^{N-1} \text{sign}\{(T_m - T_n)(T_{m+1} - T_{n+1})\}, \quad (6.14)$$

and is a more robust measure as all possible pairs of the ' $N - 1$ ' intervals are included in the computation. The coefficient κ_τ can be used to test for monotonic dependence that is not necessarily linear. Nonlinearity of the class 2 process has already been identified in the interval density (Fig. 5.8), and was also seen in plots of the crossing trace (Fig. 6.4). A plot of the Kendall's tau coefficient is included in Fig. 6.10 for processes ρ_{ij} , $i = 1, 2$, $j = 1, 2$, and this measure of serial correlation compliments the crossing orbit plots in Fig. 6.9(c)&(e). Even in processes with short-term dependence as defined in Sec. 2.1.2, strong positive correlation in the zero-crossing sequence is possible when the power spectrum is concentrated at high frequencies. When a process additionally has power dispersed near the zero frequency, two sufficiently separated time scales (or periodicities) result, leading to strong negative correlation in the interval sequence.

¹ See <https://uk.mathworks.com/help/stats/corr.html> and references thereat.

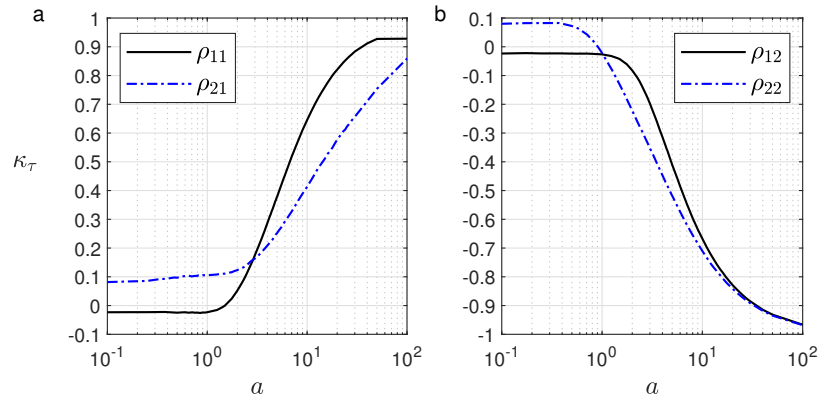


Figure 6.10.: Plots of Kendall's tau coefficient (6.14) for crossing intervals as a varies for (a) class 1 processes and (b) class 2 processes, computed using 100 realisations for each value of a . The plot for one class is almost a reflection in the x -axis of the other.

6.5 SUMMARY

The objective of this chapter was to illustrate the geometrical properties of the zero-crossing problem at extreme cases of oscillatory correlation, properties which exist, though to a lesser extent, at intermediary values of the periodicity parameter a . The zero-crossing trace and orbit respectively brought out the regularity in the crossing sequence for class 1 and class 2 processes, and the heuristic descriptions were quantified by the lacunarity measure. We also sought to unlock the intricacies to the lacunarity signatures by investigating the different counting distributions, and this especially revealed the higher order complexity when the periodicity parameter a is large. The exploration should also be viewed as an invitation to study dependent counting processes using level-crossings of correlated sample functions that can be reliably simulated, App. H. Alongside this, the two previous chapters showed how to model the inter-event times, and so we proffer dual tools of both simulation and parametric modelling.

All random processes $x(t)$ studied explicitly in this thesis have the same distribution, but it is the type of power spectrum that dictates the highly structured and varied behaviour of processes and sequences derived from $x(t)$. The next chapter will perform a zero-crossing analysis of real-world data which are approximately Gaussian.

Lacunarity is picked up again in terms of statistically and computationally efficient numerical estimation.

ZERO-CROSSING ANALYSIS IN PRACTICE

This thesis presents three tools for the analysis of zero-crossings of Gaussian processes, in addition to simulation procedures: a tripartite classification of the process, mixture models for the crossing intervals, and a demonstration that lacunarity captures the multi-scaling features in the zero-crossing sequence. Here we shall discuss box counting methods for computing the lacunarity measure, and thereafter perform a zero-crossing analysis that applies the tools of previous chapters.

7.1 LACUNARITY: CONTINUOUS VS GLIDING BOX METHODS

In Ch. 6 patterns in the zero-crossing sequence (obtained from simulations) were shown to complement analytical results for lacunarity, and this was possible due to the explicit definitions of the autocorrelation functions for the examples considered, which enabled substitution into Rice's conditional density and evaluation of the variance equation (6.2). When the autocorrelation is not known analytically or when experimental (as opposed to simulated) data is concerned, lacunarity must be determined numerically, and two methods for accumulating crossing counts in box sizes r have been used extensively. The first, the 'contiguous boxes method', involves non-overlapping boxes and is the definition traditionally used to analyse counting processes [3]. The second method does use overlapping or 'gliding boxes' and is particularly popular [32, 33, 102] in spite of various criticisms [34, 77, 103].

7.1.1 Criticisms of Gliding Box Lacunarity

Gliding box lacunarity in two-dimensions is affected by orientation, and this is dealt with in [77] through a self-referred box counting method that uses circular windows. Another issue with the gliding box method is the over-sampling of central data, and under-sampling at the edges. The sampling can be made even by “wrapping around” the extent of the data to include the opposite end [103], for example: computing lacunarity additionally using a box containing $x_{n_{\max}-2}, x_{n_{\max}-1}, x_{n_{\max}}, x_1$ if the box size is r_4 . Mitigating lacunarity bias has also been tackled by forming two binary sequences, and using a combined lacunarity measure. If Λ^+ is the lacunarity for the sequence z_n , with 1's at zero-crossing locations, a second lacunarity Λ^- can be obtained from the sequence $\mathbf{1}_n - z_n$, where $\mathbf{1}_n = 1, \forall n$. In [33], the normalised harmonic mean of the positive and negative lacunarity is then used for further analysis:

$$\frac{1}{\Lambda_H} = \frac{1}{\Lambda^+} + \frac{1}{\Lambda^-}. \quad (7.1)$$

Stationary Gaussian processes provide a non-trivial context to compare the two methods when analytical results are known. To the author's knowledge, analytical results for gliding box lacunarity exist primarily in deterministic contexts, some of which are described in for example [77, 81].

Appendix E contains derivations of formulae for the two lacunarity measures as applied to one-dimensional datasets. In testing the efficacy of the gliding box method, the main questions for a zero-crossing analysis are: does gliding box lacunarity distinguish between classes of Gaussian process?, and, can scale changes be easily detected and suitably interpreted?. We first consider the Poisson process, the simplest form of randomness as identified by the constant lacunarity slope when using contiguous boxes, Fig. 6.5. All simulation averages are taken over 10^3 realisations.

7.1.2 Comparisons in the Independent Case

From Fig. 7.1(a) one might assume the results are almost identical for all three methods, but plot (b) reveals the variance using the gliding box method diverges fairly quickly from the contiguous box case, attaining its maximum value at a box size close to half the maximum size, beyond which the variance is zero for the contiguous box method as only one disjoint box remains. Now, the authors of [76] do not state that the gliding box method should produce an unbiased estimate of the contiguous box method lacunarity statistic, and they do provide an interpretation for heterogeneity at all box sizes. However, lacunarity for the Poisson process is no longer simple. Contributions from gliding boxes are highly correlated, thus there is an added scale dependence for random data. Both lacunarity curves in plots (a)&(c) have the range of box sizes restricted to between 10^{-3} and 10^3 times the mean crossing interval length, the upper range corresponding here to approximately 20% of the maximum box-size. Plot (c) suggests we further restrict the range to $10^{-1} \leq \bar{R}r \leq 10^2$ so as to ignore the ambiguities outside this range for the gliding box method. They are ambiguous relative to the analytical log-lacunarity slope for a Poisson process, which is constant.

On the other hand, the reader will observe that the numerical derivative for the contiguous box lacunarity becomes quite volatile as the box size increases; the data from the box counts is noisy. In principle, this could be resolved by interpolating the lacunarity curve or incorporating more realisations. This would require a large range of box sizes and more data (i.e. more experiments or more simulation time) which may not always be practical—therefore an argument in favour of the gliding box method. Plot (d) is included as additional validation of the simulation procedure, and similar comments as for the Poisson process apply. Chiefly, the analytical and gliding-box variance differ. More importantly for any input data, the gliding box variance always curves back towards zero.

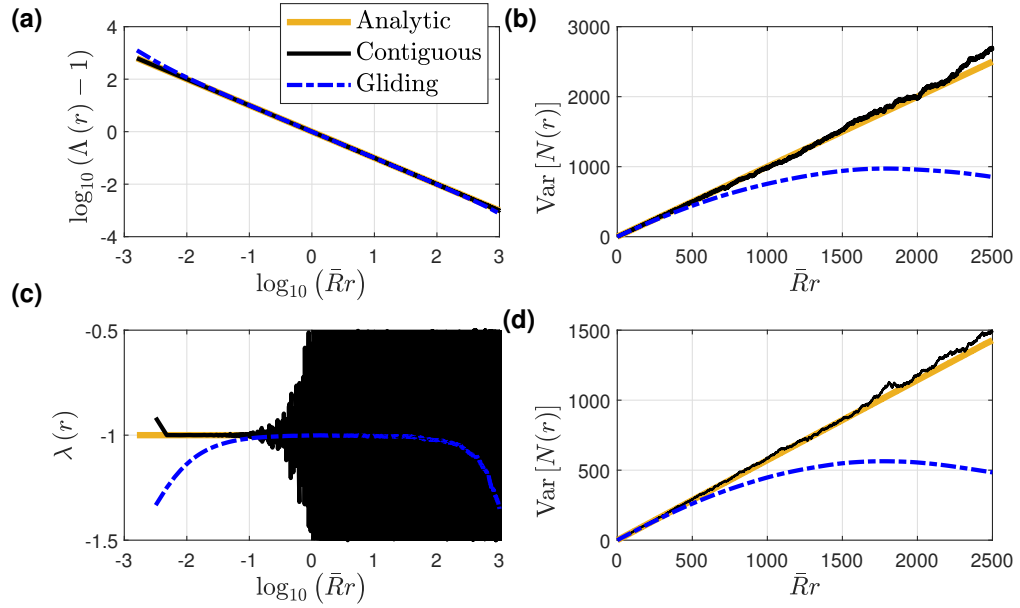


Figure 7.1.: Plots of numerical estimates for the lacunarity (a), variance (b) and lacunarity slope (c) for the Poisson process, and the variance (d) for the squared exponential process, g_1 . Also included are analytical results for the contiguous box method. The labelling in the legend of plot (a) also applies to the other plots.

7.1.3 Comparisons in the Dependent Case

Having commented on why and how to proceed with the gliding box method in spite of criticisms, we now focus on Gaussian random processes, and the results are somewhat satisfactory. In Fig. 7.2 the log-lacunarity slope is plotted for the squared exponential (g_1) and Wong (g_2 , $\gamma = \sqrt{3}$) processes, and the $\cos(a\tau)$ and $\cos^2(a\tau)$ modifications of the g_1 process with $a = 100$ —refer to Eq. (3.31). For the class 0 case, the Poisson process does divide the sub-fractal and smooth processes, similar to Fig. 6.5(b), and there is convergence towards the Poisson curve at the very small/large box sizes. There are also turning points approximately at the median crossing intervals, but here there is also an additional turning point for the smooth case.

For classes 1 and 2 processes, Fig. 7.2(b)&(c), there is not much difference here in comparison to the analytical results in the contiguous box case (Fig. 6.6(c)&(d)), and plot (d) is included to highlight the oscillations in (b) are smaller and fade

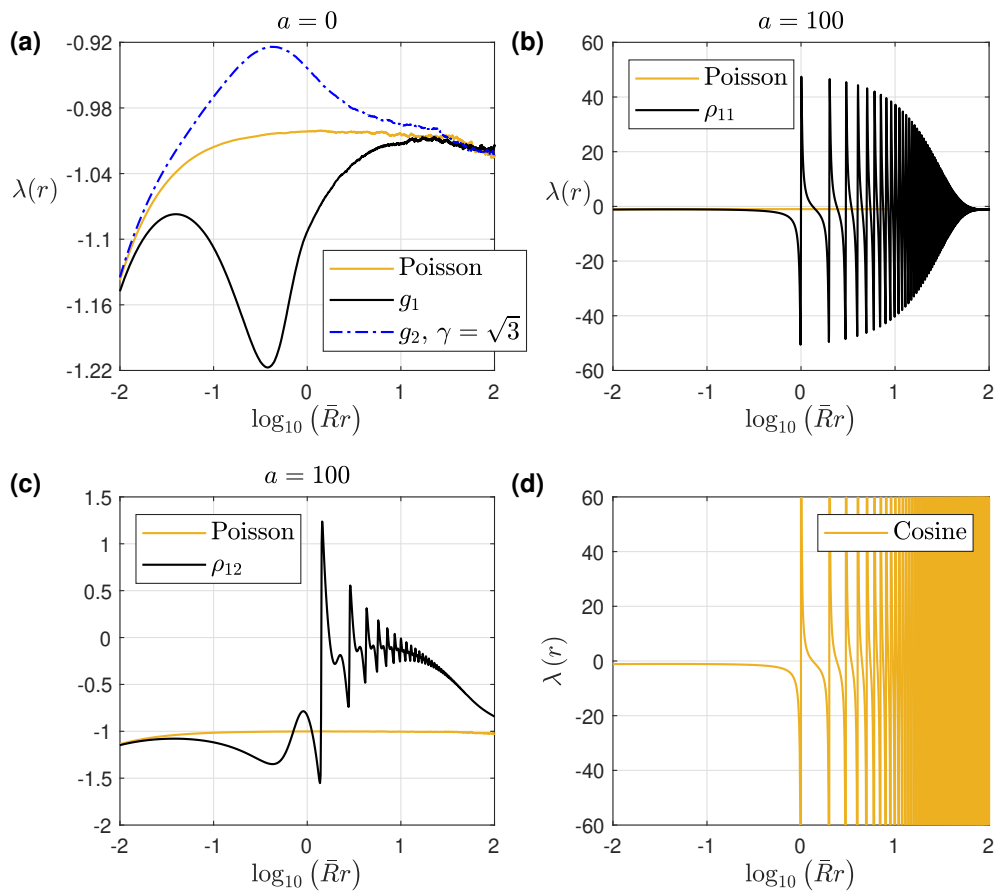


Figure 7.2.: Lacunarity slope for stationary Gaussian processes (a)–(c) and the cosine function (d) as estimated using the gliding box method.

for the Gaussian process. Note we did not need to plot the peak-to-peak values to see a “contained” lacunarity slope. Gliding box lacunarity appears to be most ideal when comparing distinctly different objects, which in our context would be extremes of the periodicity parameter. The user should however be aware that additional scaling signatures can be introduced, which makes it harder to draw out distinctive features for similar objects. It is important to have cases (such as the Poisson process) that are well understood as benchmarks—better still to perform analyses either alongside a contiguous box approach, or including refinements such as those mentioned above, Sec. 7.1.1.

7.2 CASE STUDY 4: MEG SIGNALS

To conclude this chapter we briefly describe an application of the tools we recommend for the zero-crossing analysis of stationary Gaussian processes, in a similar fashion to case study 2, Sec. 1.3.3. The experimental data¹ consists of 34 trials in which measurements of the magnetoencephalography (MEG) signal from the brain are made over 30 seconds with a sampling frequency of 600Hz. After the first 15 seconds each participant voluntarily presses a button. For the theoretical framework, experiment setup and data pre-processing, see [104]. Various experiments have revealed the brain is a network of functional connectivity, and that on small time scales hierarchical networks regularly form and dissolve in support of cognitive functions [104]. There is therefore a mixture of a continuous normative or base state, as well as transient states, and it is now possible to observe brain activity on millisecond time-scales. In particular, robust testing has demonstrated that significant changes in MEG signals are time-locked to the voluntary actions made by trial participants. For the MEG data we analyse, this translates to signals that are approximately stationary either side of the button press, in fact approximately Gaussian, as seen in Fig. 7.3. Our analysis seeks to establish a foundation for automatic detection of button press instants using zero-crossings of MEG signals. After the data is standardised (i.e. $x(t) \mapsto (x(t) - \langle x(t) \rangle) / \sqrt{\text{Var}[x(t)]}$), the zero-crossings are extracted and we find that there are clear differences relative to the button press.

In Fig. 7.5(a)&(b), we plot the variance to mean-squared ratio and the correlation coefficient κ_1 for zero-crossing intervals of the standardised MEG signals. For reference, the mean interval lengths respectively before and after the button press are approximately 0.0222 and 0.0191. Crossings after the button press are more regular, and go from being negatively correlated to being positively correlated. The linearity of the mean box counts seen in plot (c) supports the assumption of Gaussianity as

¹ MEG data provided courtesy of George C. O'Neill, formerly at the Sir Peter Mansfield Imaging Centre, School of Physics and Astronomy, University of Nottingham, University Park, Nottingham, UK.

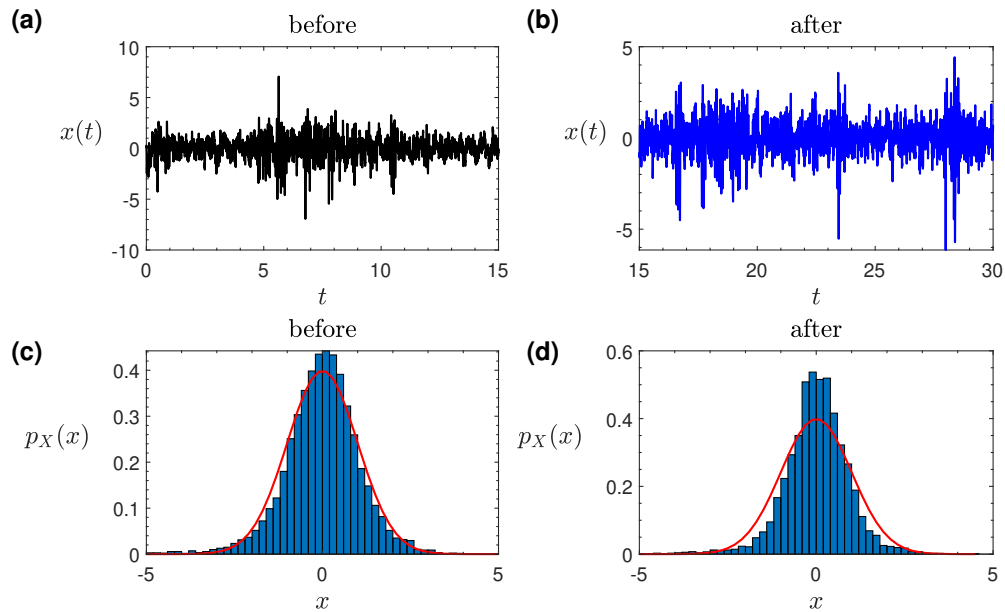


Figure 7.3.: Standardised realisation from one MEG trial partitioned into before and after the button press.

Rice's result (3.4) applies to all such processes. The variance and lacunarity curves in plots (d)&(e) contain prominent and persistent oscillations, possibly attributable to the quality of the data, but there is still a notable difference in before and after states. The oscillations thus suggest a class 1 type of process. Proposition 2 is based on the power spectrum and computing estimates using Eq. (3.21) suggests a class 1 power spectrum: there are gaps (approximately a minima) at the zero frequency: Fig. 7.4.

Finally, plotting the interval densities (Fig. 7.5(f)&(g)) reveals a profile characteristic of a sub-fractal class 1 process (refer to Fig. 5.6), plot (g) even displaying at least one non-trivial, non-zero mode, in contrast to the simpler density profile in the before state. The boundedness of the crossing intervals should be expected as the brain is constantly processing information; but note the observed range of intervals are similar relative to the respective mean interval lengths for both before and after MEG signals. In terms of the rapidity of these fluctuations and thus the significance of what we are saying is different relative to the button press, recall the highly structured patterns in Figs. 6.2&6.3 where the mean crossing interval has length $\approx \pi/100$. We would argue that this narrowing of crossing intervals near the

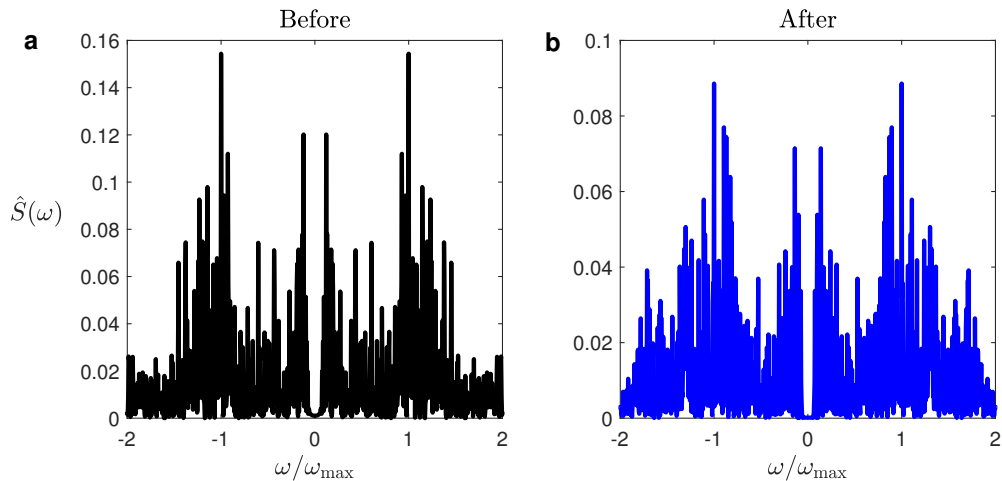


Figure 7.4.: Plots of the power spectrum estimate averaged over the 34 trials, with x -axes normalised by the peak frequencies. In (a), $\omega_{\max} \approx 6.9000$; in (b), $\omega_{\max} \approx 7.9333$.

mean/median length accompanies those previously seen patterns; indeed Fig. 6.2(a) is reminiscent of other medical data monitored in time (e.g. an electrocardiogram).

7.3 SUMMARY

The objective at this juncture was to connect the ideas of previous chapters and convey with reasonable confidence what can be inferred given only the autocorrelation or power spectrum of a stationary Gaussian process. This has always been the goal of the zero-crossing problem, and following on in the tradition of a simulation-driven approach at a solution, many of the essential features have been extracted and the espoused ideas repeatedly demonstrated, including in a practical context. The class subdivision of Gaussian processes is a useful first step in the analysis, in particular when seeking models for the interval densities.

Numerical estimates of the lacunarity statistic are especially important when considering real world data as no assumptions should be required about the distribution of crossing intervals. Results obtained using the gliding box method must be interpreted with caution, and ideally with reference cases for which related analytical results exist. In the first instance, the contiguous box method should be investi-

gated, though (as demonstrated in the literature) the gliding box method can still be suitably employed to compare and contrast heterogeneity [76].

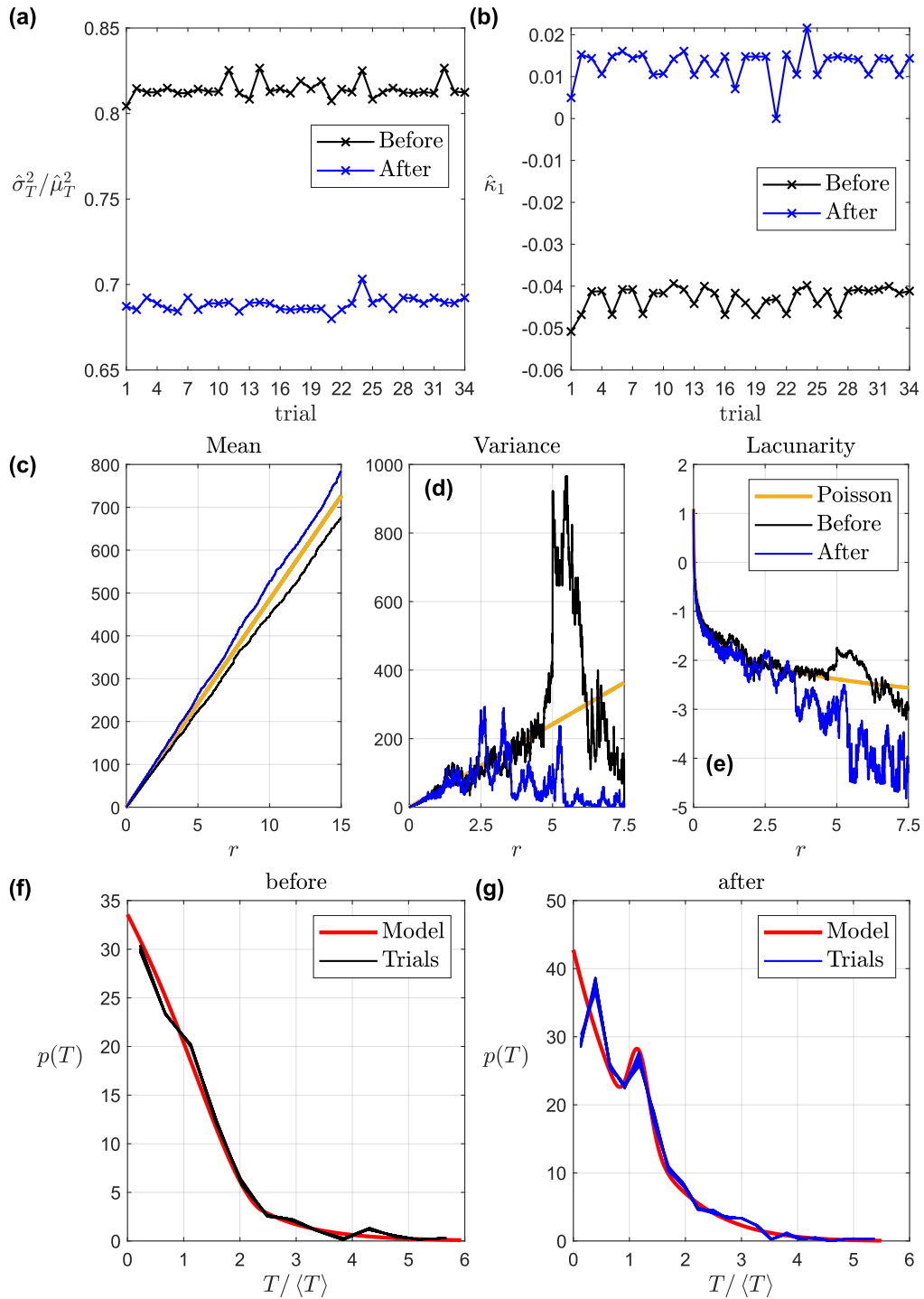


Figure 7.5.: Numerical results for MEG trials partitioned into before and after the button press. TOP: Variance to mean-squared ratio and correlation coefficient of (adjacent) crossing intervals. MIDDLE: Average mean, variance and lacunarity of box counts using contiguous boxes. The Poisson case uses the average of the interval means for before and after crossing intervals. (The legend in (e) also applies to (c)&(d).) BOTTOM: Interval densities for the crossing intervals. Both models are composed of two *BETA* densities.

CONCLUSION

8.1 DISCUSSION

Stationarity, Gaussianity and periodicity. Three simplifying assumptions that can yet supply a rich diversity of characteristics. If randomness is a continuum with the Poisson process and deterministic functions as extremes, studying the zero-crossings of stationary Gaussian processes has provided further insight into manifestations of correlated randomness between those extremes, both in terms of visual characteristics and statistical quantities. The message has been that three distinct power spectra preclude three distinct types of extremal behaviours, the which are encoded in zero-crossings. This recognition guided modelling approaches, particularly as it pertained to assignment and derivation of probability distributions.

As seen in the case studies (Sec. 1.3) and throughout this thesis, simulating a diverse range of data sets is an effective starting point for time series analysis when classification categories are few. Zero-crossing applications can benefit from the twin tools of mixture modelling and lacunarity analysis that extract characteristics not immediately obvious from power spectrum plots, and therefore form building blocks for deeper classification-based analysis. Note however that our modelling has been influenced by established analytical results, and this helps keep in mind the primary goal which is a causal understanding of zero-crossing formation, beyond observed associations.

Reflecting on the thesis title, how else could we have explored correlated randomness

and stochastic periodicity? Statistical randomness in count data can be quantified using measures of ‘variability’ and also of ‘predictability’. The former is concerned with averaging the random variable of counts, whilst the latter treats an associated distribution as itself a random variable. Concentrating on variability measures such as lacunarity [34], the Fano Factor [5] and intermittency [105]—all of which are directly related by virtue of their definitional equations—enables reliable comparison with existing analytical results. That being said, the other interpretation of randomness appears frequently when searching the literature for related research covering time series, binary sequences, zero-crossing aided machine learning, and geometries with stochastic elements. Predictability is often measured using ‘entropy’ and its generalisations [106], the task being to quantify information or surprise as data accumulates. The standard expression for (Shannon) entropy of count data is [107]

$$H_N(\mathcal{N}(r)) = - \sum_n P_N(\mathcal{N}(r) = n) \log(P_N(\mathcal{N}(r) = n)). \quad (8.1)$$

High entropy means a high degree of uncertainty in predicting future randomness, low entropy means less uncertainty. Entropy measures typically depend heavily on abundance or diversity in count data; the true value of the richness (maximum count possible) is usually unknown. It is well known that numerical estimates of entropy are always biased [108]. The high dependence on $P_N(\mathcal{N}(r))$ additionally makes entropy estimation comparatively more computationally demanding than using lacunarity or the Fano factor. (Consult App. E.3 to see how the count distribution is implicit rather than explicit in these latter box-mass moments.) The use of entropy is therefore always a trade-off between bias reduction and variance minimisation—see further [109, 110, 111].

Accumulating additional metrics in the time-domain is beneficial for feature based time series analysis as discussed in Sec. 1.2. Given zero-crossings and the lacunarity values computed via the contiguous-box method, one may compute a vector consisting of the mean, variance, and median lacunarity, and lacunarity values at critical box sizes. This feature vector could then be extended using the Fano factor,

gliding-box lacunarity, and an entropy measure that limits bias. One such example is the ‘relative binary entropy’ [111]:

$$\mathbf{H}(\mathbf{r}_n) = \sum_{j=1}^2 \mathbf{p}_{jn} \log_2 \left(\frac{\mathbf{q}_{jn}}{\mathbf{p}_{jn}} \right), \quad (8.2)$$

where \mathbf{p}_{1n} and \mathbf{q}_{1n} are respectively proportions of non-empty boxes of size \mathbf{r}_n in the target signal and a reference signal with known randomness features (e.g. the Poisson process), with $\mathbf{p}_{2n} = 1 - \mathbf{p}_{1n}$, $\mathbf{q}_{2n} = 1 - \mathbf{q}_{1n}$. Note that due to stationarity and the fact that $\mathbf{p}_{1n} = \Pr\{\mathcal{N}(\mathbf{r}_n) = 0\} \rightarrow 0$ as the box size increases, there is an \mathbf{r}_* such that all boxes are non-empty for $\mathbf{r}_n \geq \mathbf{r}_*$.

In order to extend a feature extraction schema to nonstationary time series, it is necessary to account for ‘subsequence features’, patterns that are specific to particular windows of time. Applied to the MEG signals in Sec. 7.2, this would help identify instances of the button press *a posteriori*, which can then be fed into a machine learning procedure for unsupervised recognition of pre- and post-button press brain states. Given the realisation \mathbf{x}_n , its ‘recurrence matrix’ is

$$\mathbf{R}_{mn} = \begin{cases} 1 & \text{if } \|\mathbf{x}_m - \mathbf{x}_n\| \leq c_\epsilon, \\ 0 & \text{if } \|\mathbf{x}_m - \mathbf{x}_n\| > c_\epsilon, \end{cases} \quad (8.3)$$

for $1 \leq m, n \leq n_{\max}$, and where $c_\epsilon > 0$ is the vicinity threshold chosen to detect meaningful regime transitions [112]. The matrix can be represented visually as a binary image of black and white dots, and thereby amenable to a lacunarity analysis of a two-dimensional image. Depending on the value of n_{\max} , computing resources may require the data be further segmented, and the authors of [112] show that even with short time series recurrence lacunarity is a powerful detection tool. Alternatively, the analysis could be performed on the much shorter zero-crossing sequence \mathbf{T}_k , $1 < k < n_T$, for which we have already observed patterns in the zero-crossing orbit 6.4

The language of stochastic periodicity encapsulates the idea that randomness can be locked in with periodic behaviour. The prevalence of this phenomena is wit-

nessed in ‘cyclostationary processes’ [113], whereby a random signal is implicitly modulated because of measurement methods, mechanical aspects such as rotation, or seasonality. Any signal can be decomposed into a predictable part that embodies the periodic elements, and a residual part that describes the aperiodic randomness. Reviewing additional definitions for cyclostationary processes reveals an overlap with stationary processes that have periodic autocorrelation, though the former usually applies when first and second-order moments are periodic. This makes cyclostationarity an ideal stepping stone from the thesis, and would extend the applicability to non-stationary processes that contain transient, as opposed to constant, periodic dependence.

Further directions for continuing research are provided after the chapter summaries to follow.

8.2 CHAPTER SUMMARIES

Chapter 3 introduced the idea that the general stationary Gaussian process can be divided into three classes, a proposition investigated by this thesis using a parametrised process with an oscillatory autocorrelation function: $\rho_{ij}(\tau) = g_i(\tau) \cos^j(a\tau / \sqrt{j})$. The autocorrelation $g_i(\tau)$ prescribes a class 0 process and determines the smoothness. The periodicity parameter a controls periodic memory in the process and, owing to critical points $a = a_c$, the switching between classes. Realisations of the processes were reliably simulated using the iterative Fourier filtering method (iFFM), and zero-crossing statistics easily computed then compared with existing results on crossing interval moments. When the periodicity parameter a is zero, the distinction between smooth and sub-fractal processes is apparent, the latter displaying greater fluctuation in sample functions, in turn reflected in the greater variability in crossing interval sizes. As a increases there is a homogenisation in sample function characteristics; sub-fractality is suppressed and the timescale accompanying periodic modulation dominates. Two different kinds of regularisation are observed. For class 1 cases ($\cos(a\tau)$), sample functions begin to resemble a sinusoidal wave

as variability in the extrema almost match that at the zero-level. In the class 2 case ($\cos^2(a\tau/\sqrt{2})$), sample function oscillations ostensibly superimpose a slower varying function of time resulting in long sequences of small crossings and large epochs where there are no zero-crossings.

Chapter 4 explored added forms of autocorrelation $g_i(\tau)$, many of which feature in early literature on the zero-crossing problem, and prescribe processes where the crossing intervals are approximately independent, as judged by the linear correlation coefficient, κ_1 . The main goal was to demonstrate the similarity of class 0 processes using finite mixture (FM) models for the interval density function $p(T)$. A new distribution family was introduced, Eq. (4.5), its probability density function acting as a basis function for the interval density of class 0 processes, with special cases (*EXP* and *EXPP*) suited to capture previously predicted tail behaviour. Maximum likelihood under an independent and identically distributed (IID) intervals assumption was successfully used to estimate mixture parameters, and where alternative solution methods (Talbot inversion of McFadden's model, and a Slepian regression model) were possible, the FM models compared favourably, yielding similar estimates of the persistence exponent. For processes with oscillatory correlation, the additional periodicities though mild often led to multi-modalities in the interval density, necessitating additional density components. More generally, this should be understood as a consequence of additional effective time scales. For most of the processes, the FM models consisted of no more than three components. A similarity to the Poisson process was most demonstrated in those sub-fractal processes with interval density modelled as a two component mixture, one being the *EXP* density function. The FM model approach provides a measure of crossing interval dependence; for class 0 processes the long term behaviour of crossing intervals is analogous to sampling from a fixed number of *GEXPP* distributions.

Having established the similarity of class 0 processes, we returned in chapter 5 to the more general autocorrelation $\rho_{ij}(\tau)$ and investigated changes in the interval density as the periodicity parameter a increases. We used as class 0 input autocorrelations a squared exponential and an exponential sum, Eq. (3.31). The former

defines a smooth process and is the limiting form of other smooth and sub-fractal cases; the latter is a sub-fractal example and the only process for which the interval density is known explicitly, App. B.8. The power spectrum $S_{ij}(\omega; a)$, Eq. (5.3), was explored in more detail, leading to critical values a_c as calculated by turning points of $S_{ij}(0; a)$ that signify the transition out of class 0. For values of $a > a_c$, the spectrum prescribes a class 1 process if $S_{ij}(\omega)$ has a minimum at the origin, and maxima occurring away from the origin. The spectrum prescribes a class 2 process if $S_{ij}(\omega)$ has a maximum at the origin and either additional maxima, or inflection points, away from the origin.

The remainder of chapter 5 advanced a compound mixture (CM) model connecting the interval density $p_0(\tau)$ of processes g_i to the density $p(T)$ of processes ρ_{ij} , a transformation different from a correlated Markov chain model [5]. This introduced a latency variable η , interpreted as an additional stochasticity induced by the periodicity parameter a . For class 1 cases, the model took the form $p(T) = \int_T^{\eta_M} (\tau/T)^3 p_0(\tau) f(\eta) d\eta$, with $f(\eta)$ a mixture of *BETA* density functions. These helped capture the inflection properties of the density at large a , and $2\langle T \rangle < \eta_M < \infty$, $\eta_M \rightarrow 0$, captured the contraction of the range of interval sizes. For class 2 cases, the density model was $p(T) = \int_{\beta_1^{1/2} T}^{\infty} (\tau/T)^3 p_0(\tau) f(\eta) d\eta$, with $f(\eta)$ a mixture of *BETA* and *GEXPP* density functions, essentially a combination of the class 1 mixture form and the class 0 basis function; and $\beta_1 = \beta_1(T) \rightarrow 1$ as $T \rightarrow 0$ and $T \rightarrow \infty$. These functional forms of the interval density enabled derivation of tail behaviour; for class 1 processes, it is multinomial like a *BETA* density, whilst for class 2 processes it is exponential like a *GAM* density with non-unit shape parameter.

The zero-crossing intervals of stationary Gaussian processes are 'dependent and identically distributed', and in chapter 6 this dependence was tracked by analysis of the crossing sequence and its derived counting process at different time scales. The contrast arising from strong oscillatory correlation was emphasised through the comparison of extreme cases of periodicity ($a=0$ and $a=100$). Two ways of viewing the time-dependent interval sequence were introduced: the crossing trace (effectively a

plot of $T(t)$) and the crossing orbit (a plot of adjacent interval pairs contributing to the product moment $\langle T_1 T_2 \rangle$). For a class 0 process the crossing trace displays broad variability relative to the mean, resembling the visualisation of a non-terminating random walk, though $T(t)$ is stationary like the original process $x(t)$. For a class 1 process the crossing trace is almost horizontal with intermittent-like departures, indicative of the contraction property of the interval sizes and asymptotic convergence of sample functions towards a deterministic sinusoid as $a \rightarrow \infty$. An even more intricate structure is seen in the class 2 case; the trace oscillates about the modal interval, forming a helix of varying width. The crossing orbits provide a visual critique of the correlation coefficient κ_1 when there is strong oscillatory correlation, and for class 2 processes the Kendal tau coefficient κ_τ proves a more informative measure as it is less affected by outliers. We showed that nonnegative periodic modulation can lead to a correlation coefficient that approaches -1 as $a \rightarrow \infty$. Conversely, when the periodic modulation does assume negative values, $\kappa_\tau \rightarrow 1$ as $a \rightarrow \infty$. These facts reflect the attractor-like behaviour played by the diagonals with positive or negative slope in the zero-crossing orbits, Fig. 6.9.

The lacunarity curve (LC) and lacunarity slope (LS) provided a way to quantify the heterogeneity displayed in the crossing traces, and enabled further comparison with the Poisson process and deterministic sinusoid, each extremes of correlated randomness. In the same way that the hazard function is constant for an exponential distribution [3], the LS is constant for a Poisson process, and for Gaussian processes it converges to the Poisson case at both the very small and very large time scales, in agreement with them having the same asymptotic decay in the periodicity density, Fig. 3.8. For class 0 processes, the LC has no turning points, and the LS falls either above/below the Poisson case when the interval variance is greater/less than the interval mean. This invariably translates to sub-fractal/smooth process having supra-/sub-lacunarity signatures relative to a Poisson process. For class 1 processes, similarity to a deterministic sinusoid was demonstrated by the almost identical oscillations in the LC at intermediate time scales (within 1 and 10^2 times the mean interval). For class 2 processes, the long range and repeating helical structure of the crossing trace is quantified in the lacunarity curve by the unique

inflection points and the much slower approach to the Poisson case. Thus, the concept of lacunarity is particularly useful for examining crossing interval dependence at different time scales.

As described in Sec. 2.5, gliding box lacunarity is used widely and not always alongside the contiguous box lacunarity. The latter should be the preferred method as it enables direct comparison with well-established analytical results for counting processes, and the user can be certain that correlation features are not exaggerated by the resampling of the gliding box setup. The resampling uses more data to compute the box moments, thereby yielding lacunarity curves that are smoother and more amenable to estimating the lacunarity slope. However, there still remain issues of standardisation relative to a Poisson process—the paradigmatic example of time independent events—and the strong dependence on sample length. The user can *a priori* limit the range of time scales for which the gliding box lacunarity or lacunarity slope will be used, as practised and carefully revised by some authors [77, 81], or try to combine multiple lacunarity measures of the same data set [33].

Chapter 7 ended with a real-world test case of the analytical tools of previous chapters. The recorded one-dimensional magnetoencephalography (MEG) data signals were approximately Gaussian and stationary once segmented into before and after the change in state. The change was triggered by the participant pressing a button at the halfway point of each signal data. After the button press the lengths of zero-crossing intervals varied less and were more correlated. Under the nomenclature we propose, the signals were deemed to be of class 1 type and sub-fractal. The interval densities are reliably modelled as a finite mixture of *BETA* density functions, and the bimodal density for crossing intervals after the button press were reminiscent of the change in $p(T)$ for a periodically modulated sub-fractal process as the periodicity parameter is increased. The next stage in such an analysis would be to identify unspecified change points of such signal data algorithmically. Finally, we note that the test case of our zero-crossing analysis approach applied to real-world data demonstrates that a compound mixture model may not be necessary for non class 0 processes.

8.3 FUTURE WORK

8.3.1 *Additional Processes*

That stationary Gaussian processes belong to one of three classes is true with respect to the power spectrum only assuming three forms. With the exception of the sinc type 1 process ($G_3(\omega; \gamma)$ in App. A.2), we have not explicitly considered spectra that have more than one local maxima away from the origin, e.g. [114]. Such multimodal spectra arise in ocean wave analysis (refer to Sec. 2.3 in [30] for examples with empirical data), and is also achieved by a superposition of power spectra (see App. B in [30]) and/or by introducing shifts in the frequency domain to widen the gap between peak frequencies. This is exactly the effect of periodic modulation of an autocorrelation function (refer to (5.3)); and as for cases with more than two peak frequencies, the top-hat spectrum ($G_3(\omega, 1)$) can be regarded as a limiting form of either a class 1 or 2 process since there is a whole range of frequencies (including the origin) for which the spectrum is maximal, and this is reflected in the interval density shape, Fig. 4.3. Moreover, since as $\gamma \rightarrow \infty$ $\log(\cos(a\tau/\sqrt{\gamma})) \sim \log(1 - a^2\tau^2/(2\gamma)) \sim -a^2\tau^2/(2\gamma)$, it follows that

$$\lim_{\gamma \rightarrow \infty} g_i(\tau) \cos^\gamma(a\tau/\sqrt{\gamma}) = g_i(\tau) \exp(-a^2\tau^2/2);$$

hence periodic modulation of an autocorrelation $g_i(\tau)$ using $\cos^\gamma(a\tau/\sqrt{\gamma})$, $\gamma \in \mathbb{N}$, converges as $\gamma \rightarrow \infty$ to an autocorrelation with faster decay. Thus, there are good reasons for maintaining our tripartite classification of stationary processes, and regarding as sufficiently representative the forms of autocorrelation we have considered.

The iterative Fourier filtering method for generating correlated random processes can take as input any distribution (see App. H), and so a natural extension is to simulate non-Gaussian processes and perform zero-crossing analyses using the tools presented here. This may require switching to level-crossings depending on the chosen distribution, or incorporating the work on transformation to Gaussianity of

non-Gaussian processes (see [115]). We would expect to observe similar behaviour relative to the median of the process, and verification of results will require evaluating Rice's general result for the rate of crossings of a level $c \in \mathbb{R}$ by a stationary process $x(t)$ [37]:

$$\bar{R} = \int_0^\infty z f_{x(0),x'(0)}(c, z) dz,$$

for almost any c , and if the joint density exists. Evaluating the integral has been described for gamma [47] and Laplace [116] processes.

A related avenue would be to consider curve crossings of Gaussian processes, i.e. trend stationary Gaussian processes. The case involving an oscillatory curve [117] will be an interesting comparator to the oscillatory stationary Gaussian process studied here. Given a mixed process $y(t) = x(t) + \cos(at)$, where $x(t)$ is Gaussian and has a non-oscillatory autocorrelation, one might expect the level-crossings of $y(t)$ to admit a mixture model, possibly even a compound model that maps from the level crossings of $x(t)$. This is a basic example of cyclostationary process discussed earlier, Sec. 8.1. The relevance of such considerations can be seen in foreign exchange data, which are non-Gaussian but may exhibit oscillatory correlation as illustrated in Fig. 8.1.

8.3.2 Count Distributions

We have seen that for processes ρ_{ij} with strong oscillatory correlation zero-crossings have strong dependence, particularly at time scales $10^{-1} < \bar{R}r < 10^2$ where lacunarity curves show the crossing sequence is more complicated than what a known standard distribution (i.e. not a mixture) of crossing counts could represent. For the $\cos(a\tau)$ or class 1 case (refer to Figs. 6.7–6.8) there is a similarity to a deterministic cosine function $x_d(t)$, a similarity that vanishes as the time window r increases. For the $\cos^2(a\tau/\sqrt{2})$ or class 2 case (refer to Fig. 6.8) there is an additional dependence on the parity of the counts, but again the crossing distributions show a slow divergence from those of the process $x_d(t)$.

Given that independent of the class of process the limiting value of the lacunarity

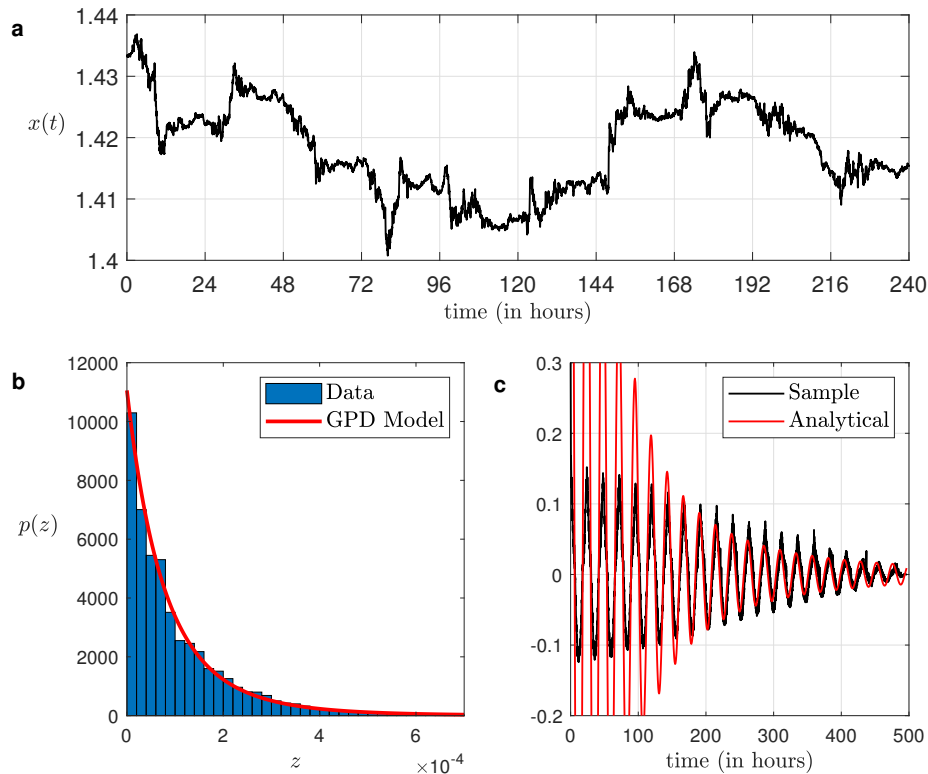


Figure 8.1.: Plots relating to the derived process $z(t) = |\log(x(t+1)/x(t))|$, the absolute log return of $x(t)$ which represents GBP:USD exchange data (sampled at 1-minute intervals) for the month of April 2016 [118]. (a): Original sample data. (b): The distribution of $z(t)$ fitted with a generalised Pareto distribution with shape and scale parameters respectively equal to 0.1704 and 0.0001 to 4.d.p., found using maximum likelihood. (c): The sample autocorrelation of $z(t)$ and a class 1 correlation function $\rho_{51}(\tau; a, L) = \left(1 + (\tau/(2L))^2\right)^{-1} \cos(a\tau)$, $a = 11$, $L = 2500$.

slope is that of a Poisson process, a mixture model approach that accounts for this could prove fruitful. The simpler class 1 case suggests a mixture of the count distributions for a Poisson process, (6.5), and a cosine wave, (6.7), with a mixing parameter that depends on r . For the class 2 case, one could pursue a modified negative binomial model in which the ‘number of failures’ and/or ‘success probability’ are themselves random variables, as described in Sec. 8.3 of [62]. In renewal theory, the following rule links event counts with the inter-event times [3]:

$$\mathcal{N}(r) \geq k \Leftrightarrow \hat{T}_k \leq r,$$

where \hat{T}_k is the sum of $k+1$ consecutive inter-event times, from which it follows that

$$\Pr\{\mathcal{N}(r) = k\} = \Pr\{\hat{T}_k \leq r\} - \Pr\{\hat{T}_{k+1} \leq r\}.$$

Thus to advance a mixture model for the crossing intervals \hat{T}_q is to assume that one also exists for the crossing counts $\mathcal{N}(r)$. We have already seen for example that the compound model connecting intervals of processes g_i and ρ_{ij} also applies to these higher order intervals (refer to Fig. D.1). The simulated sequence \mathbf{z}_n , (3.23), indicates crossing occurrence and is essentially a sequence of correlated Bernoulli trials. Treated as such, the Conway-Maxwell-binomial distribution [119] which models sums of Bernoulli trials with positive or negative association, could be appropriate. Whichever model is chosen, it is partly simplified by knowledge of the mean and variance of $\mathcal{N}(r)$ [9, 46]. Further investigation into the counting process will highlight the possible relevance to other research areas, especially given the ease of numerical simulation.

8.3.3 Stochastic Periodicity

Finally, the patterning seen in the crossing trace and orbit are examples of stochastic periodicity—randomness and periodicity that are jointly persistent (in time). This has already been proven by the lacunarity signatures. In addition, the crossing orbits are reminiscent of chaos in dynamical systems as seen in the classic logistic map (see Sec. 10 in [6]); within Fig. 6.9, plots (c)&(e) there is a diagonal that the iterates (here the crossing sequence) surround, as well as an “unstable centre”. For the class 1 case there is a distinctive bowtie structure, and orbits for both classes 1 and 2 cases contain periodic encircling of an attractor, though it is more contained in the former. In [120], well-known circle maps are revisited with the assumption that the iterates form a Markov-chain. Stochastic periodicity is equivocated to ‘phase-locking’, and we have already seen that crossing interval sizes can be trapped within a certain range containing the modal interval, with rare escapes. It will be interesting to further investigate whether zero-crossings of random processes form true dynamical

systems and test the applicability of formalisms such as described in [121], the which considers deterministic systems with Gaussian excitation, employing results on the up-crossings of Gaussian processes. The logistic map described in Sec. 1 has an arcsin distribution when in the chaotic regime [122], meaning it has infinite variance. This differs from a differentiable stationary Gaussian process as the variance of the crossing trace (Sec. 6.1) is finite. Stochastic periodicity in Gaussian processes is not chaotic. The connection yet remains due to the mixture models (Sec. 5.3) that included beta distributions, of which the arcsin distribution is a special case.

We have explored lacunarity of zero-crossings as a measure of dependence, and for a stationary Gaussian process the zero-crossings are the most important returns. The dependence analysis may be extended by considering all returns as expressed in the ‘unwrapped phase’, $\varphi_u(t) = \varphi(0) + \int_0^t \psi(t') dt'$. The function $\psi(t)$ is known as the instantaneous frequency and can be evaluated using the analytical signal, (2.49):

$$\psi(t) = \frac{d}{dt} \varphi(t) = \frac{1}{A^2(t)} \left(x(t) \frac{d}{dt} x_q(t) - x_q(t) \frac{d}{dt} x(t) \right).$$

To illustrate the merits of the unwrapped phase, Fig. 8.2 contains plots of $\varphi_u(t)$ for realisations of the process ρ_{1j} when $a = 100$, as well as plots of the sample function and crossing trace in the same time region. The phase is seen to be approximately linear at significant jumps in the crossing trace. Most noticeable is that when $j = 1$, the gradient of the phase has little variation, another indicator of similarity to a deterministic cosine wave (refer to [123]). Conversely, when $j = 2$, the phase varies significantly and progresses like a series of step-functions, a structure also present in the maximum crossing count at box size r (Fig. 6.8(f)). Such complexities therefore warrant further investigation. Truly, zero-crossings of stationary Gaussian processes exhibit correlated randomness and stochastic periodicity.

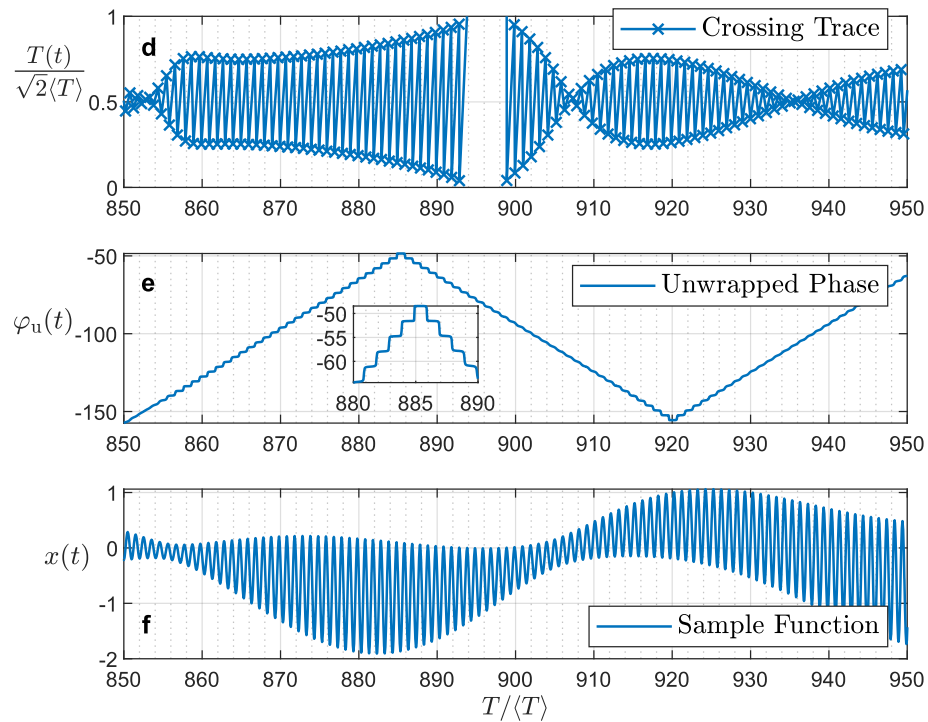
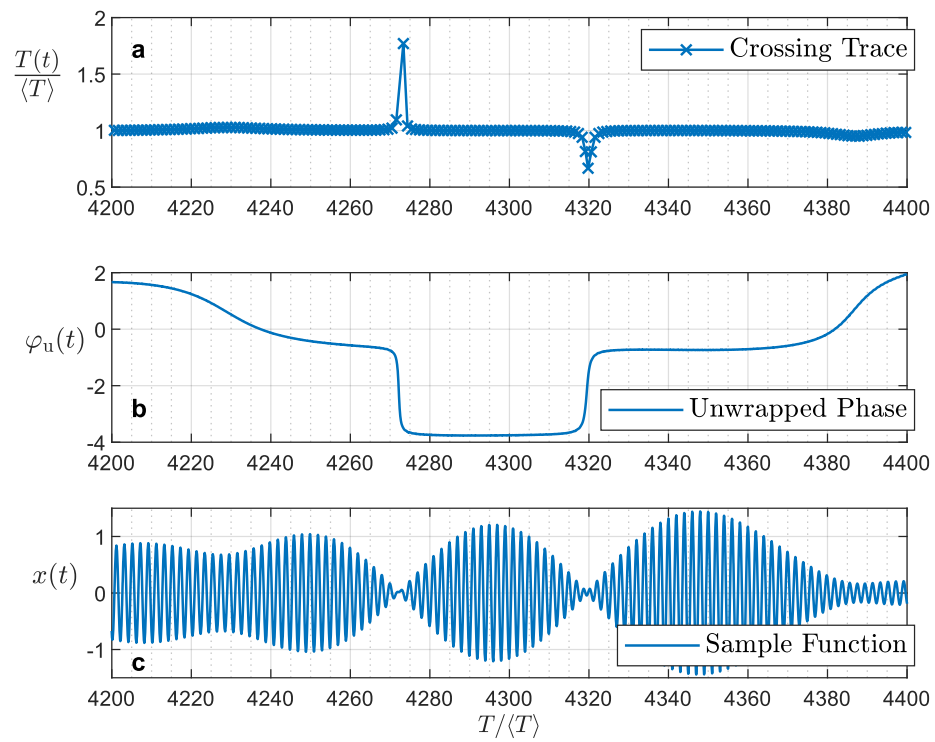


Figure 8.2.: Plots of the unwrapped phase for stationary Gaussian processes ρ_{1j} ($a = 100$) with strong oscillatory correlation demonstrating phase related changes in the crossing trace and sample function. The unwrapped phase is computed using Fourier transform methods as outlined in [124]. (a)–(c): $j=1$. (d)–(f): $j=2$.

POWER SPECTRA OF CLASS 0 PROCESSES

A.1 SPECIAL FUNCTIONS

- Gamma function: $\Gamma(z) = \int_0^\infty t^{z-1} e^{-t} dt$, $\Re(z) > 0$
- Heaviside step function: $H(z) = 1 (z > 0), 0 (z \leq 0)$;
- Modified Bessel function of the second kind ([125], Eq. 10.32.9):
 $K_\nu(z) = \int_0^\infty \exp(-z \cosh(t)) \cosh(\nu t) dt$, $|\arg z| < \pi/2$.

A.2 SMOOTH PROCESSES

$$G_1(\omega) = \sqrt{2\pi} \exp(-2\pi^2 \omega^2);$$

$$G_3(\omega, 1) = \frac{\pi}{\sqrt{3}} \left(H\left(|\omega| + \frac{\sqrt{3}}{2\pi}\right) - H\left(|\omega| - \frac{\sqrt{3}}{2\pi}\right) \right),$$

$$G_3(\omega, \gamma \in \mathbb{N}_{\geq 2}) = \frac{\pi \gamma^{3/2}}{2^{\gamma-1} \sqrt{3}} H\left(\frac{\sqrt{3}\gamma}{2\pi} - |\omega|\right) \\ \times \sum_{j=1}^{\lfloor \pi \sqrt{\gamma/3} |\omega| + \gamma/2 \rfloor} (-1)^j \frac{(2\pi \sqrt{\gamma/3} |\omega| + \gamma - 2j)^{\gamma-1}}{j!(\gamma-j)!};$$

$$G_5(\omega, \gamma \in \mathbb{R}_{>1/2}) = 2(2\gamma)^\gamma \frac{\sqrt{\pi}}{\Gamma(\gamma)} \left(\frac{\pi |\omega|}{\sqrt{2\gamma}}\right)^{\gamma-1/2} K_{\gamma-1/2}(2\pi \sqrt{2\gamma} |\omega|);$$

$$G_7(\omega, \gamma \in \mathbb{R}) = \frac{(2\pi\gamma') \cos(\pi\gamma'/2) \cosh(\pi^2\gamma'\omega)}{2 \cosh^2(\pi^2\gamma'\omega) + \cos(\pi\gamma\gamma') - 1},$$

$$\gamma' = 1/\sqrt{1 + \gamma^2};$$

$$G_9(\omega) = \frac{3\pi}{10\sqrt{5}} (5 - 4\pi^2\omega^2) H\left(\frac{\sqrt{5}}{2\pi} - |\omega|\right).$$

See [99] for G_3 (Eq. 1.6.11) and G_9 (Eq. 1.3.7). For reference,

$$G_3(\omega, 2) = \frac{\pi}{3} (\sqrt{6} - 2\pi|\omega|) H\left(\frac{\sqrt{6}}{2\pi} - |\omega|\right),$$

$$G_3(\omega, 3) = \frac{\pi}{8} \left(2(3 - 4\pi^2\omega^2) H\left(\frac{1}{2\pi} - |\omega|\right) \right. \\ \left. + (3 - 2\pi|\omega|)^2 H\left(|\omega| - \frac{1}{2\pi}\right) H\left(\frac{3}{2\pi} - |\omega|\right) \right), \text{ etc.}$$

$G_3(\omega, \gamma)$ is a polynomial of order $\gamma - 1$ for $|\omega| < \sqrt{3\gamma}/(2\pi)$, and 0 otherwise. Likewise, when $\gamma \in \mathbb{N}$, $G_5(\omega, \gamma)$ forms a sequence of functions of polynomial type, and with exponential decay:

$$G_5(\omega, 1) = \sqrt{2}\pi \exp(-2\sqrt{2}\pi|\omega|),$$

$$G_5(\omega, 2) = \pi(1 + 4\pi|\omega|) \exp(-4\pi|\omega|), \text{ etc.}$$

A.3 SUB-FRACTAL PROCESSES

$$G_2(\omega, \gamma \in \mathbb{N}_{>1}) = \frac{2\gamma(1 + \gamma^2)}{(\gamma^2 + 4\pi^2\omega^2)(1 + 4\pi^2\gamma^2\omega^2)};$$

$$G_4(\omega) \approx \frac{2(\pi - 1)}{(1 + \pi^4\omega^2)(1 + (\pi - 2)^2\pi^2\omega^2)};$$

$$G_6(\omega, \gamma \in \mathbb{N}) = \frac{(\Gamma(\gamma + 1))^2}{\Gamma(2\gamma + 1)} \frac{(2\sqrt{2\gamma - 1})^{2\gamma+1}}{(2\gamma - 1 + 4\pi^2\omega^2)^{\gamma+1}};$$

$$G_8(\omega) = \frac{2\sqrt{2}}{1 + 16\pi^4\omega^4};$$

$$G_{10}(\omega) = \frac{14 \sin(\pi/14)}{\bar{\gamma}(1 + 16384\pi^{14}\omega^{14}/\bar{\gamma}^{14})},$$

$$\tilde{\gamma}^{-2} = -\sin(\pi/14) \left(1 + 2 \sum_{j=1}^3 \cos(3j\pi/7) \right).$$

For $G_6(\omega, \gamma)$ and the corresponding autocorrelation function when $\gamma \notin \mathbb{N}$ see [39].

The autocorrelation has the same form as $G_5(\omega, \gamma)$ above.

B

PROBABILITY DISTRIBUTIONS

Moments are taken about zero. Abbreviations: PDF (probability density function), CDF (cumulative density function), MGF (moment generating function). \bar{m} is the median of the random variable. $\operatorname{erf}(z) = (2/\sqrt{\pi}) \int_0^z e^{-t^2} dt$ is the error function. $\Gamma_i(z; \nu) = \int_z^\infty t^{\nu-1} e^{-t} dt$ is the upper incomplete gamma function. $H(z) = 0\{z < 0\}, 1\{z \geq 0\}$ is the Heaviside step function. $B_i(z; \nu, w) = \int_0^z t^{\nu-1} (1-t)^{w-1} dt$ is the incomplete beta function, its inverse is $B_i^{-1}(z; \nu, w)$, and $B(\nu, w) \equiv B_i(1; \nu, w)$ is the beta function. Unless specified below, the support for all distributions is $\mathbb{R}_{\geq 0}$. All distribution parameters are nonnegative, except for μ in $NORM(\mu, \sigma^2)$ and c, d in $UNI(c, d)$.

B.1 NORMAL DISTRIBUTION, $NORM(b)$

Support : $(-\infty, \infty)$

PDF : $\frac{1}{\sqrt{2\pi\sigma^2}} \exp\left(-\frac{(T-\mu)^2}{2\sigma^2}\right)$

CDF : $\frac{1}{2} \left(1 - \operatorname{erf}\left(\frac{\mu - T}{\sqrt{2\sigma^2}}\right)\right)$

Central Moments : $\sigma^r (1 + (-1)^r) (r-1)!!$

MGF : $\exp\left(-\mu s + \sigma^2 s^2 / 2\right)$

Mode : μ

Median : μ

B.2 UNIFORM DISTRIBUTION, $UNIF(c, d)$

$$\begin{aligned}
\text{Support :} & \quad (c, d) \\
\text{PDF :} & \quad (d - c)^{-1} \\
\text{CDF :} & \quad H(T - c) H(d - T) \\
\text{Moments :} & \quad (d - c)^{-1} (r + 1)^{-1} (d^{r+1} - c^{r+1}) \\
\text{MGF :} & \quad s^{-1} (d - c)^{-1} (e^{-cs} - e^{-ds}) \\
\text{Mode :} & \quad (c, d) \\
\text{Median :} & \quad (c + d) / 2
\end{aligned}$$

B.3 EXPONENTIAL DISTRIBUTION, $EXP(b)$

$$\begin{aligned}
\text{PDF :} & \quad \frac{1}{b} \exp\left(-\frac{T}{b}\right) \\
\text{CDF :} & \quad 1 - \exp\left(-\frac{T}{b}\right) \\
\text{Moments :} & \quad r! b^r \\
\text{MGF :} & \quad (1 + bs)^{-1} \\
\text{Mode :} & \quad 0 \\
\text{Median :} & \quad b \ln 2
\end{aligned}$$

B.4 GAMMA DISTRIBUTION, $GAM(c, b)$

$$\begin{aligned}
\text{PDF :} & \quad \frac{1}{\Gamma(c) b} \left(\frac{T}{b}\right)^{c-1} \exp\left(-\frac{T}{b}\right) \\
\text{CDF :} & \quad 1 - \Gamma_i(b^{-1}T; c) / \Gamma(c) \\
\text{Moments :} & \quad b^r \Gamma(r + c) / \Gamma(c)
\end{aligned}$$

$$\begin{aligned} \text{MGF :} & \quad (1 + bs)^{-c} \\ \text{Mode :} & \quad b(c - 1) \\ \text{Median, } \bar{m} : & \quad \bar{m}(c, b) - \frac{1}{3} < \bar{m}(c, 1) \leq \bar{m}(c, b) \end{aligned}$$

B.5 WEIBULL DISTRIBUTION, WEIB(c, b)

$$\begin{aligned} \text{PDF :} & \quad \frac{c}{b} \left(\frac{T}{b}\right)^{c-1} \exp\left(-\left(\frac{T}{b}\right)^c\right) \\ \text{CDF :} & \quad 1 - \exp\left(-\left(\frac{T}{b}\right)^c\right) \\ \text{Moments :} & \quad b^r \Gamma(1 + r/c) \\ \text{MGF :} & \quad \sum_{r=0}^{\infty} s^r b^r \Gamma(1 + r/c) \\ \text{Mode :} & \quad b \left(\frac{c-1}{c}\right)^{1/c} H(c-1) \\ \text{Median :} & \quad b(\ln 2)^{1/c} \end{aligned}$$

B.6 EXPONENTIAL PRODUCT DISTRIBUTION, EXPP(a, b)

$$\begin{aligned} \text{PDF :} & \quad b^{-2}(a + b) \exp\left(-\frac{T}{b}\right) \left(1 - \exp\left(-\frac{T}{a}\right)\right) \\ \text{CDF :} & \quad 1 - \exp\left(-\frac{T}{b}\right) \left(1 + \frac{a}{b} \left(1 - \exp\left(-\frac{T}{a}\right)\right)\right) \\ \text{Moments :} & \quad r! b^{r-1} (a + b)^{-r} \left((a + b)^{r+1} - a^{r+1}\right) \\ \text{MGF :} & \quad (1 + bs)^{-1} \left(1 + \frac{abs}{a + b}\right)^{-1} \\ \text{Mode :} & \quad c \ln(1 + b/a) \\ \text{Median } \bar{m} : & \quad b \ln 2 \leq \bar{m}(a, b) \leq b \ln(2(1 + a/b)) \end{aligned}$$

B.7 BETA DISTRIBUTION, $BETA(v, w, d)$

$$\begin{aligned}
\text{Support :} & \quad (0, d) \\
\text{PDF :} & \quad \frac{T^{v-1}(d-T)^{w-1}}{B(v, w) d^{v+w-1}} \\
\text{CDF :} & \quad B_i(d^{-1}T; v, w) / B(v, w) \\
\text{Moments :} & \quad d^r B(v+r, w) / B(v, w) \\
\text{MGF :} & \quad \frac{1}{B(v, w)} \sum_{r=0}^{\infty} (ds)^r B(v+r, w) \\
\text{Mode :} & \quad (0, d), \quad \text{if } v=w=1; \\
& \quad \frac{d(v-1)}{v+w-2}, \quad \text{if } v, w > 1; \\
& \quad (d+1)H(v-1) + H(w-1) - 1, \quad \text{otherwise} \\
\text{Median :} & \quad dB_i^{-1}(B(v, w) / 2; v, w)
\end{aligned}$$

B.8 WONG'S DENSITY FUNCTION [35]

$$\begin{aligned}
p_w(T) = \frac{\sqrt{3}}{4\pi} & \left(\frac{(1-2r^2(T))^{1/2}}{(1-r^2(t))(1+2r^2(t))} E(r(t)) + \frac{(1-2r^2(t))}{(3-2r^2(t))} D(r(t)) \right. \\
& \left. + \frac{8(1-2r^2(t))^{3/2}}{(3-2r^2(t))^2(1+2r^2(t))} \left(\Pi\left(\frac{3}{4} - \frac{1}{2}r^2(t), r(t)\right) - K(r(t)) \right) \right),
\end{aligned} \tag{B.1}$$

where

$$r^2(t) = \left(1 - e^{-T/\sqrt{3}}\right) / 2, \tag{B.2}$$

and

$$E(k) = \int_0^{\pi/2} \sqrt{1 - k^2 \sin^2(\varphi)} d\varphi,$$

$$\begin{aligned}
K(k) &= \int_0^{\pi/2} \frac{1}{\sqrt{1 - k^2 \sin^2(\varphi)}} d\varphi, \\
D(k) &= \int_0^{\pi/2} \frac{\sin^2(\varphi)}{\sqrt{1 - k^2 \sin^2 \varphi}} d\varphi, \\
\Pi(v^2, k) &= \int_0^{\pi/2} \frac{1}{(1 - v^2 \sin^2(\varphi)) \sqrt{1 - k^2 \sin^2(\varphi)}} d\varphi \quad (\text{B.3})
\end{aligned}$$

are complete elliptic integrals (see [125], Eqn. 19.2).

TAIL BEHAVIOUR OF THE INTERVAL DENSITY

For processes with autocorrelation $\rho_{ij}(\tau) = g_i(\tau) \cos^j(a\tau/\sqrt{2^{j-1}})$, where $j=1,2$, and $g_i(\tau)$ prescribes a class 0 process, the density model for intervals between zero-crossings is

$$p(T) = \int_{\beta_1^{1/\beta_2} T}^{\eta_M} \frac{1}{\left(1 - \beta_1(T/\eta)^{\beta_2}\right)^{1+1/\beta_2}} p_0\left(\frac{T}{\left(1 - \beta_1(T/\eta)^{\beta_2}\right)^{1/\beta_2}}\right) f(\eta) d\eta, \quad (\text{C.1})$$

where $f(\eta)$ is the latency density and $p_0(\tau)$ the interval density of the original class 0 process.

Left tail

Under the substitution $\tau = T/\left(1 - \beta_1(T/\eta)^{\beta_2}\right)^{1/\beta_2}$,

$$\eta = \frac{\beta_1^{1/\beta_2} T}{\left(1 - (T/\tau)^{\beta_2}\right)^{1/\beta_2}}, \quad \frac{d\eta}{d\tau} = -\frac{\beta_1^{1/\beta_2} (T/\tau)^{1+\beta_2}}{\left(1 - (T/\tau)^{\beta_2}\right)^{1+1/\beta_2}},$$

and (C.1) becomes

$$p(T) = \beta_1^{1/\beta_2} \int_{\tau_M}^{\infty} \frac{1}{\left(1 - (T/\tau)^{\beta_2}\right)^{1+1/\beta_2}} f\left(\frac{\beta_1^{1/\beta_2} T}{\left(1 - (T/\tau)^{\beta_2}\right)^{1/\beta_2}}\right) p_0(\tau) d\tau, \quad (\text{C.2})$$

$$\tau_M = T / \left(1 - \beta_1(T/\eta_M)^{\beta_2}\right)^{1/\beta_2}. \tag{C.3}$$

For small values of T , $T \ll \langle T \rangle$, say, (C.1) and (C.2) respectively approximate as

$$p(T) \approx \int_{\beta_1^{1/\beta_2} T}^{\eta_M} p_0(T) f(\eta) d\eta, \quad p(T) \approx \beta_1^{1/\beta_2} \int_{\tau_M}^{\infty} f\left(\beta_1^{1/\beta_2} T\right) p_0(\tau) d\tau;$$

thus the model necessarily has the boundary condition

$$p(T) \approx p_0(T) \approx \beta_1^{1/\beta_2} f\left(\beta_1^{1/\beta_2} T\right) \quad \text{as } T \rightarrow 0. \tag{C.4}$$

Specifically, from (4.1), as $T \rightarrow 0$, $p_0(T)$ is $\mathcal{O}(T)$ for a smooth process, or $\mathcal{O}(1)$ for a sub-fractal process with an autocorrelation $g_i(\tau)$ such that $g'''(0) \neq 0$. These transfer to $p(T)$ and Eq. (C.4) acts as a continuity condition.

Right tail

The integration range in (C.1) contracts as T increases. Consider $T \gg \langle T \rangle$ and let $s = \left(1 - \beta_1(T/\eta)^{\beta_2}\right)^{1/\beta_2}$, giving

$$\eta = \frac{\beta_1^{1/\beta_2} T}{(1 - s^{\beta_2})^{1/\beta_2}}, \quad \frac{d\eta}{ds} = \frac{s^{\beta_2-1} \beta_1^{1/\beta_2} T}{(1 - s^{\beta_2})^{1+1/\beta_2}}, \quad s_M = \left(1 - \beta_1(T/\eta_M)^{\beta_2}\right)^{1/\beta_2}. \tag{C.5}$$

Substitution into (C.1) leads to

$$\begin{aligned} p(T) &= \beta_1^{1/\beta_2} T \int_0^{s_M} \frac{1}{s^2 (1 - s^{\beta_2})^{1+1/\beta_2}} p_0\left(\frac{T}{s}\right) f\left(\frac{\beta_1^{1/\beta_2} T}{(1 - s^{\beta_2})^{1/\beta_2}}\right) ds \\ &\approx A \beta_1^{1/\beta_2} T \int_0^{s_M} \frac{1}{s^2 (1 - s^{\beta_2})^{1+1/\beta_2}} \exp\left(-\frac{\theta T}{s}\right) f\left(\frac{\beta_1^{1/\beta_2} T}{(1 - s^{\beta_2})^{1/\beta_2}}\right) ds, \end{aligned} \tag{C.6}$$

where from (4.2) the large T form of $p_0(T)$ has been substituted; A is a constant scale factor and θ the persistence exponent.

For processes ρ_{i1} , $f(\eta)$ is modelled as a *BETA* mixture and $T < \eta_M < \infty$, whereupon the integration range in (C.6) is contained in $[0, 1)$. Then as $T \rightarrow \eta_M^-$, from (C.5), $s_M \rightarrow 0^+$, and the approximation (C.6) further reduces to

$$\begin{aligned} p(T) &\approx A\beta_1^{1/\beta_2} T \int_0^{s_M} \frac{1}{s^2} \exp\left(-\frac{\theta T}{s}\right) f\left(\beta_1^{1/\beta_2} T\right) ds \\ &= \frac{A\beta_1^{1/\beta_2}}{\theta} \exp\left(-\frac{\theta T}{s_M}\right) f\left(\beta_1^{1/\beta_2} T\right) \\ &\approx A_1 T^{v_M-1} \left(\eta_M - \beta_1^{1/\beta_2} T\right)^{w_M-1}, \end{aligned} \tag{C.7}$$

substituting the beta mixture component of $f(T)$ with range parameter η_M . Since $\exp(-\theta T/s_M) \ll 1$, the exponential term and the remaining constant prefactors may be absorbed into a single constant A_1 .

For processes ρ_{i2} , $f(T)$ is modelled as a mixture of two *BETA*'s and two *GEXPP*'s, so that $\eta_M = \infty$. Consider T larger than the range parameter for the *BETA* density components. The asymptotic form of $f(T)$ is then given by the *GEXPP* component with the slowest decay, i.e. $f(T) \approx \alpha_M T^{c_M-1} \exp(-b_M^{-1} T)$. From (C.5), $s_M = 1$, and (C.6) becomes

$$\begin{aligned} p(T) &\approx A\alpha_M \beta_1^{c_M/\beta_2} T^{c_M} \int_0^1 \frac{1}{s^2(1-s\beta_2)^{1+c_M/\beta_2}} \exp\left(-\frac{\theta T}{s} - \frac{b_M^{-1} \beta_1^{1/\beta_2} T}{(1-s\beta_2)^{1/\beta_2}}\right) ds \\ &\equiv A\alpha_M \beta_1^{c_M/\beta_2} T^{c_M} \int_0^1 \psi(s) \exp\left(\beta_1^{1/\beta_2} T \phi(s)\right) ds. \end{aligned} \tag{C.8}$$

The integral may be evaluated using Laplace's method [126]. First, replace $\phi(s)$ with a Taylor series approximation $\phi(s_0) + (s - s_0)^2 \phi''(s_0) / 2$, where $s_0 \in (0, 1)$ is the maximum point of $\phi(s)$; then for some $\epsilon \ll 1$, as $T \rightarrow \infty$

$$\begin{aligned} &\int_0^1 \psi(s) \exp\left(\beta_1^{1/\beta_2} T \phi(s)\right) ds \\ &\approx \psi(s_0) \int_{s_0-\epsilon}^{s_0+\epsilon} \exp\left(\beta_1^{1/\beta_2} T \left(\phi(s_0) + (s - s_0)^2 \phi''(s_0) / 2\right)\right) ds \end{aligned}$$

$$\begin{aligned} &\approx \psi(s_0) \exp\left(\beta_1^{1/\beta_2} T \phi(s_0)\right) \int_{-\infty}^{\infty} \exp\left(\beta_1^{1/\beta_2} T (s - s_0)^2 \phi''(s_0) / 2\right) ds \\ &= \frac{\sqrt{2\pi} \psi(s_0)}{\sqrt{-\beta_1^{1/\beta_2} T \phi''(s_0)}} \exp\left(\beta_1^{1/\beta_2} T \phi(s_0)\right), \end{aligned}$$

provided $\phi''(s_0) < 0$. From (C.8),

$$\phi(s) = -\frac{\theta}{\beta_1^{1/\beta_2} s} - \frac{b_M^{-1}}{(1 - s^{\beta_2})^{1/\beta_2}} < 0; \quad (\text{C.9})$$

$$\phi'(s) = \frac{\theta}{\beta_1^{1/\beta_2} s^2} - \frac{b_M^{-1} s^{\beta_2 - 1}}{(1 - s^{\beta_2})^{1+1/\beta_2}}; \quad (\text{C.10})$$

$$\phi''(s) = -\frac{2\theta}{\beta_1^{1/\beta_2} s^3} - \frac{b_M^{-1} s^{\beta_2 - 2} (\beta_2 - 1)}{(1 - s^{\beta_2})^{1+1/\beta_2}} - \frac{b_M^{-1} s^{2(\beta_2 - 1)} (1 + \beta_2)}{(1 - s^{\beta_2})^{2+1/\beta_2}} < 0, \quad (\text{C.11})$$

the last inequality being true for all $s \in (0, 1)$ if $\beta_2 \geq 1$. It follows that

$$p(T) \approx A_2 T^{c_M - 1/2} \exp\left(-\beta_1^{1/\beta_2} T |\phi(s_0)|\right), \quad (\text{C.12})$$

once again absorbing the constant prefactors into the constant A_2 . Note: the *GEXPP* distribution goes like $\mathcal{O}(T^{c_M})$ as $T \rightarrow 0$, and thus the condition (C.4) means only $c_M \geq 1$ is admissible. In Sec. 5.3.2 the optimisation gives, $c_M = 1$ for the processes considered. When $\beta_1 = 1, \beta_2 = 2$, equations (C.10)&(C.11) imply s_0 exists, and

$$\phi'(s_0) = 0 \quad \Rightarrow \quad (\theta b_M)^2 (1 - s_0^2)^3 = s_0^6.$$

This is a cubic equation for $x = s_0^2$ and simplifies to

$$x^3 + \lambda(-3x^2 + 3x - 1) = 0, \quad \lambda = \frac{(\theta b_M)^2}{1 + (\theta b_M)^2} < 1. \quad (\text{C.13})$$

The substitution $x = y + \lambda$ leads to the reduced cubic equation

$$y^3 + \mathcal{P}y + \mathcal{Q} = 0, \quad \mathcal{P} = 3\lambda(1 - \lambda), \quad \mathcal{Q} = \lambda(1 - \lambda)(2\lambda - 1).$$

According to Cardano's method ([127], Sec. 2.1) the determinant is

$$\Delta = \mathbb{Q}^2 + \frac{4\mathcal{P}^3}{27} = \lambda^2(1 - \lambda)^2 > 0,$$

which implies there is one real solution given by

$$\begin{aligned} x = y + \lambda &= \left(\frac{1}{2}(-\mathbb{Q} + \sqrt{\Delta}) \right)^{1/3} + \left(\frac{1}{2}(-\mathbb{Q} - \sqrt{\Delta}) \right)^{1/3} + \lambda \\ &= \lambda^{2/3}(\lambda - 1)^{1/3} + \lambda^{1/3}(\lambda - 1)^{2/3} + \lambda \\ &= \lambda^{1/3} \left(\lambda^{1/3}(\lambda - 1)^{1/3} + (\lambda - 1)^{2/3} + \lambda^{2/3} \right) \\ &= \frac{\lambda^{1/3}}{\lambda^{1/3} - (\lambda - 1)^{1/3}} \quad \text{using } \frac{a^3 - b^3}{a - b} \equiv a^2 + ab + b^2 \\ &= \frac{1}{1 - (1 - \lambda^{-1})^{1/3}}; \end{aligned}$$

and substituting for λ from (C.13)

$$s_0 = \sqrt{x} = \left(1 + (\theta b_M)^{-2/3} \right)^{-1/2} < 1, \quad (\text{C.14})$$

which may then be substituted into (C.11). Note: for the density model shown in Fig. 5.10(b), $s_0 = 0.6838\dots$

In summary, as $T \rightarrow \infty$, the interval density model for processes ρ_{ij} decays as

$$p(T) \sim \begin{cases} T^{v-1}(\eta_M - T)^{w-1}, & \text{if } j = 1, \\ T^{1/2} \exp\left(-\theta T \left(1 + (\theta b)^{2/3}\right)^{3/2}\right), & \text{if } j = 2, \end{cases} \quad (\text{C.15})$$

for constants v, w, b determined by the latency density, $f(\eta)$. In the $j = 1$ case η_M is retained to emphasize the connection between the supports of the latency density, $f(\eta)$, and the compound density, $p(T)$. In the $j = 2$ case the exponent remains dependent on θ , the persistence exponent of the base density, $p_0(\tau)$.

D

HIGHER ORDER DISTRIBUTIONS

The mixture paradigm we advocate transfers to distributions of sums of consecutive intervals, constructed as

$$\hat{T}_q = \sum_{m=0}^q T_m; \quad (\text{D.1})$$

so, $\hat{T}_0 \equiv T$ is the variable for adjacent crossing intervals; \hat{T}_1 applies to the time between crossings where the sample function derivative has the same sign; and so on. Note: the variable \hat{T}_q is formed by contiguous intervals, as opposed to overlapping groupings of adjacent intervals. This latter grouping is used in computing the correlation coefficients $\kappa_{m,m+j}$, given in (2.26).

Known results

Taking the expectation of (D.1) gives a rescaling of Rice's result: $\langle \hat{T}_q \rangle = (q+1)\langle T \rangle$. From [53], the density $p_q(\hat{T}_q)$ is always $\mathcal{O}(1)$ as $T \rightarrow 0$ for a sub-fractal process that is only once differentiable. (Intuitively, there is no difference between one and arbitrarily many tangent crossings occurring in an instant.) However, for a smooth process,

$$p_q(\hat{T}_q) = \mathcal{O}\left(\hat{T}_q^{1+q(q+5)/2}\right), \quad (\text{D.2})$$

as $\hat{T}_q \rightarrow 0$. The results provided by [53] are not as easily summarised when the process is sub-fractal and at least twice differentiable; each case of differentiability must be pursued separately.

By definition, $\hat{T}_q \geq \hat{T}_{q-1} \geq \dots \geq \hat{T}_0$, whence $\Pr\{T' \geq \hat{T}_q\} \geq \Pr\{T' \geq \hat{T}_{q-1}\}$, $\forall q \geq 1$; therefore the asymptotic decay at large \hat{T}_q is slower for each successive density function $p_q(T)$, $q \geq 0$. Recall also that the processes under consideration have short-range dependence, and that according to Sec. 3.4, variation in \hat{T}_q is constrained by the sample function periodicities. Therefore, an increase in central tendency is expected.

Preliminary models

Given a class 0 process, as a first modelling step, *GAM* densities can be used to probe the forms of $p_q(\hat{T})$ without making further assumptions about tail behaviour. In figure D.1, plots (a)&(b) show $p_1(\hat{T})$ and $p_2(\hat{T})$ for the squared exponential process (4.11). We observe that the densities become less skewed, and the intervals \hat{T}_q are less dispersed as q increases.

Turning to classes 1 and 2 extensions of the process g_i , the transform principle can again be employed using a modified compound mixture model. Equation (5.11) becomes

$$p_q(\hat{T}_q) = \int_{\beta_1^{1/\beta_2} \hat{T}_q}^{\eta_M} \frac{1}{\left(1 - \beta_1(\hat{T}_q/\eta)^{\beta_2}\right)^{1+1/\beta_2}} p_{0,q} \left(\frac{\hat{T}_q}{\left(1 - \beta_1(\hat{T}_q/\eta)^{\beta_2}\right)^{1/\beta_2}} \right) f_q(\eta) d\eta. \quad (\text{D.3})$$

where $p_{0,q}(\hat{T})$ gives the density of summed intervals for the original class 0 process. The latency density also changes with the value of q , but the basis distributions should remain the same since the variation is constrained by the modal periodicities. Provided only linear exponentials are used in the mixture models for $p_{0,q}(T)$, and $f_q(\eta)$ in class 2 cases, the derivation of tail behaviours for (D.3) when $q \geq 1$ will resemble App. C. Whence, the right tail is expected to have either multinomial (class 1) or exponential (class 2) decay, similar to the forms in (C.15).

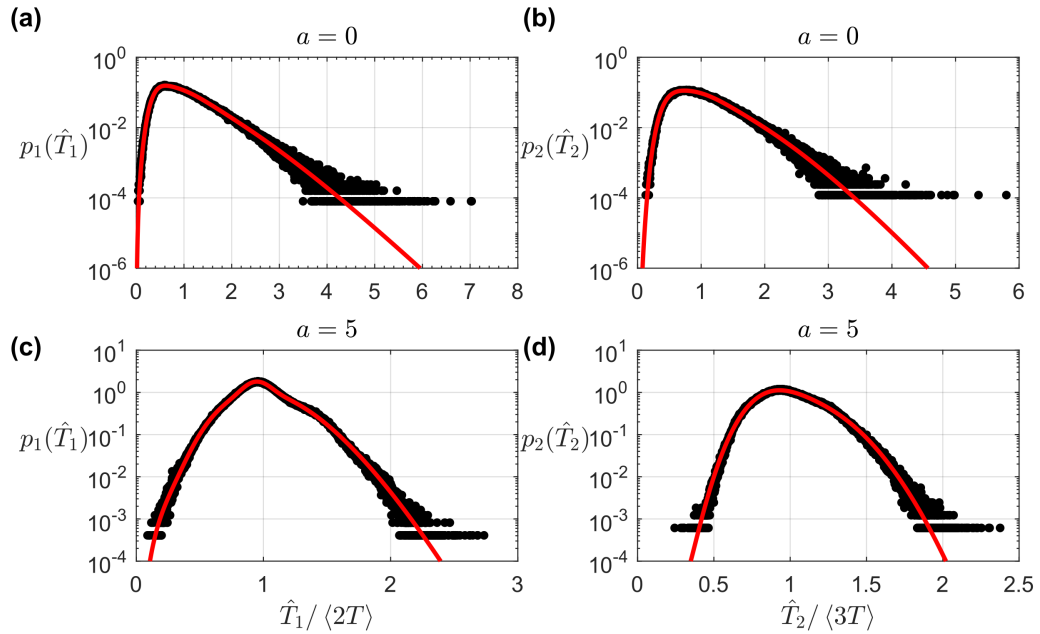


Figure D.1.: Plots of the distribution of crossing intervals \hat{T}_q when $q = 1$ for the process with autocorrelation $\rho_{11}(\tau) = \exp(-\tau^2/2) \cos(a\tau)$. Plots (a)&(b) result from mixture models of three *GAM* distributions. These are reused as base distributions for the compound mixture model (D.3), alongside *BETA* tri-mixtures for the latency densities, leading to plots (c)&(d). As in Sec. 5.3, fixing $\beta_1 = 1$ and $\beta_2 = 2$ is sufficient for class 1 processes.

Figures D.1(c)&(d) show the first two additional densities for the process ρ_{11} when $a = 5$. In comparison to Fig. 5.5(f), the “shoulder” of the distribution begins to disappear as q increases, and it is conceivable that for sufficiently large q the latency density may have only one component.

The mixture models plotted in Fig. D.1 are presented without a detailed analysis of tail behaviour as in App. C. The message here is that mixture models coupled with maximum likelihood estimation can be used to recover (or discover) previously known (or unknown) analytical behaviours in the interval density. For reference, the parameter estimates corresponding to the density plots in Fig. D.1 are provided below (to 4 decimal places). Refer back to App. B for the role of each parameter.

g1:

Mixture model is three *GAM* distributions, with parameters

$$[\alpha_1, c_1, b_1, \alpha_2, c_2, b_2, \alpha_3, c_3, b_3].$$

$$p_1(T): [0.3968, 4.4168, 1.8507, 0.1475, 10.2368, 0.3329, 5.8410, 0.9530]$$

$$p_2(T): [0.3545, 7.2041, 1.6986, 0.4798, 9.5403, 0.9101, 13.4067, 0.4142]$$

ρ_{11} , $a = 5$:

Mixture model for η is three *BETA* distributions, with parameters

$$[\alpha_1, v_1, w_1, d_1, \alpha_2, v_2, w_2, d_2, v_3, w_3, d_3].$$

$$p_1(T): [0.0166, 6.2352, 1090.5217, 174.1114, 0.7544, 12.8003, 126.1411, 14.3807, 68.6538, 95.2248, 2.8967].$$

$$p_2(T): [3.5227e-05, 2.8443, 618.1227, 323.3428, 0.5415, 17.1531, 40.4280, 7.0458, 29.6971, 106.4313, 7.8482].$$

E

FORMULAE FOR CONTIGUOUS AND GLIDING BOX COUNT METHODS

The notation used here is from Sec. 3.2. For the realisation \mathbf{x}_n , with $n = 1, \dots, n_{\max}$, the vector \mathbf{z}_n equals one if there is a crossing in the time interval $[\mathbf{t}_{n-1}, \mathbf{t}_n]$, and let \mathbf{N}_n represent the counting process for crossings up to and including time \mathbf{t}_n . The box size r can be discretised as

$$\mathbf{r}_n = (n - 1) \Delta t, \quad n = 1, \dots, n_{\max}, \quad \mathbf{r}_{n_{\max}} \equiv t_{\max}. \quad (\text{E.1})$$

The numerical lacunarity estimate $\Lambda(\mathbf{r}_n)$ measures the variation in box mass $\mathbf{M}_j(\mathbf{r}_n)$ of crossing counts, and is defined by

$$\Lambda(\mathbf{r}_n) = 1 + \frac{\text{Var}[\mathbf{M}_j(\mathbf{r}_n)]}{(\mathbb{E}[\mathbf{M}_j(\mathbf{r}_n)])^2}. \quad (\text{E.2})$$

E.1 CONTIGUOUS BOXES

When the contiguous boxes method is applied the box masses accumulate disjointly:

$$\mathbf{M}_j(\mathbf{r}_n) = \begin{cases} \mathbf{N}_n, & j = 1, \\ \mathbf{N}_{j(n-1)+1} - \mathbf{N}_{(j-1)(n-1)+1}, & 2 \leq j \leq j_{\max}, \end{cases} \quad (\text{E.3})$$

$$j_{\max} = \begin{cases} n_{\max}, & n = 1, \\ \lfloor (n_{\max} - 1) / (n - 1) \rfloor, & 2 \leq n \leq n_{\max}. \end{cases} \quad (\text{E.4})$$

For $n > 1$, this leads to

$$\begin{aligned} \mathbb{E}[M_j(\mathbf{r}_n)] &= \frac{1}{j_{\max}} \sum_{j=1}^{j_{\max}} M_j(\mathbf{r}_n) = \frac{1}{j_{\max}} \left(\sum_{j=1}^{j_{\max}} N_{j(n-1)+1} - \sum_{j=1}^{j_{\max}-1} N_{j(n-1)+1} \right) \\ &= \frac{1}{j_{\max}} N_{j_{\max}(n-1)+1}, \\ \text{Var}[M_j(\mathbf{r}_n)] &= \frac{1}{j_{\max} - 1} \left(\sum_{j=1}^{j_{\max}} M_j^2(\mathbf{r}_n) + \frac{1}{j_{\max}} \left(\sum_{j=1}^{j_{\max}} M_j(\mathbf{r}_n) \right)^2 \right) \\ &= \frac{2}{j_{\max} - 1} \sum_{j=1}^{j_{\max}} N_{j(n-1)+1} \left(N_{j(n-1)+1} - N_{(j+1)(n-1)+1} \right) \\ &\quad - \frac{j_{\max} + 1}{j_{\max}(j_{\max} - 1)} N_{j(n-1)+1}^2. \end{aligned} \quad (\text{E.5})$$

Note: the simplification of the first moment virtually guarantees it is an unbiased estimate of the mean box mass since the index $j_{\max}(n-1)+1 > n_{\max}/2$ for $n \neq 1$. By the stationarity property, this means that at least half of the total number of crossing events are included. The variance of box counts is not so easily simplified, though for $n > n_{\max}/2$ there is only one disjoint box of size \mathbf{r}_n meaning the variance is zero.

E.2 GLIDING BOXES

In the gliding box method the boxes slide through the discretisation one point at a time, and the box masses are

$$M_j(\mathbf{r}_n) = \begin{cases} N_n, & j = 1, \\ N_{j+n-1} - N_{j-1}, & 2 \leq j \leq n_{\max} - k + 1. \end{cases} \quad (\text{E.6})$$

Further define the first and second order cumulants $\mathbf{S}_i^{(1)} = \sum_{j=1}^i \mathbf{N}_j$, $\mathbf{S}_i^{(2)} = \sum_{j=1}^i \mathbf{N}_j^2$.

Then for $n > 1$ the mean and variance are

$$\begin{aligned} \mathbb{E}[\mathbf{M}_j(\mathbf{r}_n)] &= \frac{1}{n_{\max} - n + 1} \sum_{j=1}^{n_{\max} - n + 1} \mathbf{M}_j(\mathbf{r}_n) = \frac{\boldsymbol{\phi}_1(\mathbf{r}_n)}{n_{\max} - n + 1}, \\ \text{Var}[\mathbf{M}_j(\mathbf{r}_n)] &= \frac{1}{n_{\max} - n} \left(\sum_{j=1}^{n_{\max} - n + 1} \mathbf{M}_j^2(\mathbf{r}_n) \right. \\ &\quad \left. + \frac{1}{n_{\max} - n + 1} \left(\sum_{j=1}^{n_{\max} - n + 1} \mathbf{M}_j(\mathbf{r}_n) \right)^2 \right) \\ &= \frac{1}{n_{\max} - n} \left(\boldsymbol{\phi}_2(\mathbf{r}_n) - 2\boldsymbol{\phi}_3(\mathbf{r}_n) - \frac{\boldsymbol{\phi}_1^2(\mathbf{r}_n)}{n_{\max} - n + 1} \right), \end{aligned} \quad (\text{E.7})$$

where

$$\begin{aligned} \boldsymbol{\phi}_1(\mathbf{r}_n) &= \mathbf{S}_{n_{\max}}^{(1)} - \mathbf{S}_{n_{\max} - n}^{(1)} - \mathbf{S}_{n-1}^{(1)}, \\ \boldsymbol{\phi}_2(\mathbf{r}_n) &= \mathbf{S}_{n_{\max}}^{(2)} - \mathbf{S}_{n_{\max} - n}^{(2)} - \mathbf{S}_{n-1}^{(2)}, \\ \boldsymbol{\phi}_3(\mathbf{r}_n) &= \sum_{j=1}^{n_{\max} - n} \mathbf{N}_j \mathbf{N}_{j+n}. \end{aligned} \quad (\text{E.8})$$

Calculating $\boldsymbol{\phi}_3$ directly from the expression above is computationally costly, and so like other practitioners (see [102]) we seek an accurate and efficient estimate. Suppose the first crossing occurs at time t_K ; then $\mathbf{N}_{n < K} = 0$, $\mathbf{N}_K = 1$, and for $0 \leq c \leq K$,

$$\begin{aligned} \boldsymbol{\phi}_3(\mathbf{r}_{n_{\max} - K + c}) &= \sum_{j=1}^{K-c} \mathbf{N}_j \mathbf{N}_{j+n_{\max} - n + c} \\ &= \mathbf{N}_1 \mathbf{N}_{n_{\max} - K + c + 1} + \cdots + \mathbf{N}_{K-c} \mathbf{N}_{n_{\max}} \\ &= \delta_{0c} \mathbf{N}_{n_{\max}}. \end{aligned}$$

The numerical autocorrelation is

$$\hat{\rho}(\mathbf{r}_n) = \frac{1}{n_{\max} \hat{\sigma}^2} \sum_{j=1}^{n_{\max} - n} (\mathbf{N}_j - \hat{\mu})(\mathbf{N}_{j+n} - \hat{\mu}),$$

$$\hat{\mu} = \frac{1}{n_{\max}} \mathcal{S}_{n_{\max}}^{(1)}, \quad \hat{\sigma}^2 = \frac{1}{n_{\max}^2} \left(n_{\max} \mathcal{S}_{n_{\max}}^{(2)} - \left(\mathcal{S}_{n_{\max}}^{(1)} \right)^2 \right), \quad (\text{E.9})$$

and for $n < n_{\max} - K$ this can be rearranged to give a sufficiently accurate estimate of ϕ_3 (relative error of at most 10^{-7}):

$$\phi_3(\mathbf{r}_n) \approx (n_{\max} + 1) \hat{\sigma}^2 \hat{\rho}(\mathbf{r}_n) + \hat{\mu} \left(\mathcal{S}_{n_{\max}-n}^{(1)} - \mathcal{S}_n^{(1)} \right) + n \hat{\mu}^2. \quad (\text{E.10})$$

The lacunarity value at box size \mathbf{r}_1 is identical for both box counting methods and depends entirely on the discretisation of the process. The mean crossing count is $N_{n_{\max}}/n_{\max}$, and the variance is $N_{n_{\max}}(1 - N_{n_{\max}}/n_{\max})/n_{\max}$. Therefore,

$$\Lambda(\mathbf{r}_1) = \frac{n_{\max}}{N_{n_{\max}}} \approx 628.32, \quad (\text{E.11})$$

substituting $N_{n_{\max}} \approx 5 \times 10^3$ and $n_{\max} = 3.1416 \times 10^6$.

The lacunarity slope may be computed as

$$\lambda(\mathbf{r}_n) = \mathbf{r}_n \frac{d\text{Var}[\mathbf{M}_j(\mathbf{r}_n)]}{d\mathbf{r}_n} \text{Var}[\mathbf{M}_j(\mathbf{r}_n)] - 2, \quad (\text{E.12})$$

where the derivative is evaluated using finite differences. In the text we use the four-point centred estimate, which for a continuous function $f(t)$ gives the first derivative as

$$f'(t_k) \approx \frac{f_{k-2} - 8f_{k-1} + 8f_{k+1} - f_{k+2}}{12h}, \quad (\text{E.13})$$

where $f_k = f(t_k)$ and $h = t_{k+1} - t_k > 0$ is the discretisation length Δt .

E.3 RELATION TO COUNTING DISTRIBUTIONS

For each sequence of crossings, and its box masses $\mathbf{M}_j(\mathbf{r}_n)$, $j = 1, \dots, b(\mathbf{r}_n)$, the raw moments for the counting process $\mathcal{N}(\mathbf{r}_n)$ are

$$\langle \mathcal{N}^q(\mathbf{r}_n) \rangle \approx \frac{1}{b(\mathbf{r}_n)} \sum_{j=1}^{b(\mathbf{r}_n)} \mathbf{M}_j(\mathbf{r}_n)$$

$$\begin{aligned}
&= \frac{1}{b(\mathbf{r}_n)} \sum_{j=1}^{b(\mathbf{r}_n)} \sum_{m=0}^{m_{\max}} m^q \hat{\delta}_m(\mathbf{M}_j(\mathbf{r}_n)) \\
&= \frac{1}{b(\mathbf{r}_n)} \sum_{m=0}^{m_{\max}} m^q \sum_{j=1}^{b(\mathbf{r}_n)} \hat{\delta}_m(\mathbf{M}_j(\mathbf{r}_n)) \\
&= \sum_{m=0}^{m_{\max}} m^q \frac{B(m, \mathbf{r}_n)}{b(\mathbf{r}_n)} \approx \sum_{m=0}^{\infty} m^q P_N(\mathcal{N}(\mathbf{r}_n) = m), \quad (\text{E.14})
\end{aligned}$$

where $B(m, \mathbf{r}_n)$ is the total number of boxes of size \mathbf{r}_n with m counts, so that $B(m, \mathbf{r}_n) / b(\mathbf{r}_n)$ is an estimate for the distribution of counts given a particular box-counting method.

PARAMETER VALUES AND ADDITIONAL STATISTICS:
CLASS 0 DENSITIES

The parameter values here are representative of the processes in Tables 4.1&4.2. The expressions of probability density functions given in App. B show the role of each parameter, and for convenience only the letters c and b are used below. Each density model's mixture parameters is represented as a vector, with the final mixture parameter (given by $\alpha_K = 1 - \sum_{k=1}^{K-1}$) omitted. For example, for the g_1 process the density model is $[WEIB_{\{1\}}, GAM_{\{2\}}, EXPP_{\{3\}}]$, which translates to $[\alpha_1, c_1, b_1, \alpha_2, c_2, b_2, c_3, b_3]$. Decimals are given to 4 decimal places.

$$g_1: [WEIB_{\{1\}}, GAM_{\{2\}}, EXPP_{\{3\}}]$$

$$[0.1836, 2.6859, 1.7875, 0.1086, 5.5100, 0.5214, 2.6105, 2.3498]$$

$$g_2, \gamma = \sqrt{3}: [EXP_{\{1,2\}}]$$

$$[0.1095, 0.5845, 3.4562]$$

$$g_3, \gamma = 1: [WEIB_{\{1,2,3\}}, GAM_{\{4,5,6,7,8\}}, EXPP_{\{9\}}]$$

$$[0.4901, 3.6845, 2.5536, 0.0626, 7.3623, 5.8556, 0.0437, 6.7198, 2.4578, 0.0064, 162.8764, 0.0567, 0.0009, 407.4457, 0.0316, 0.0002, 497.5011, 0.0329, 4.4901e-05, 559.4911, 0.0354, 1.2010e-05, 568.9751, 0.0412, 7.3180, 2.1234]$$

$$g_4: [EXP_{\{1,2\}}]$$

$$[0.9498, 0.7158, 3.2876]$$

$$g_5: [WEIB_{\{1\}}, GAM_{\{2\}}, EXPP_{\{3\}}]$$

$$[0.0522, 2.1821, 2.6106, 0.1148, 3.4437, 0.3296, 0.4903, 3.0478]$$

$$\underline{g_6, \gamma=1}: [EXP_{\{1\}}, EXP_{\{2\}}]$$

$$[0.2973, 0.8387, 1.4868, 3.1323]$$

$$\underline{g_6, \gamma=2}: [GAM_{\{1\}}, EXP_{\{2\}}]$$

$$[0.0198, 2.3087, 0.2008, 0.7256, 2.6289]$$

$$\underline{g_7, \gamma=0}: [GAM_{\{1,2\}}, EXP_{\{3\}}]$$

$$[0.0806, 3.4844, 0.3334, 0.0150, 4.0573, 0.5477, 0.8862, 2.6678]$$

$$\underline{g_7, \gamma=3}: [GAM_{\{1,2,3,4\}}, EXP_{\{5\}}]$$

$$[0.3204, 2.5212, 0.1612, 0.1746, 2.0176, 1.1080, 0.1482, 3.7264, 0.2847, 0.0016,$$

$$27.9454, 0.0090, 0.0132, 6.9335]$$

$$\underline{g_8}: [WEIB_{\{1\}}, GAM_{\{2\}}, EXP_{\{3\}}]$$

$$[0.0679, 2.0024, 6.4976, 0.2116, 4.4366, 0.7736, 2.8287]$$

$$\underline{g_9}: [WEIB_{\{1,2\}}, GAM_{\{3,4\}}, EXP_{\{5\}}]$$

$$[0.3988, 3.5135, 2.2916, 0.0616, 5.6863, 4.9436, 0.0054, 152.5598, 0.0508, 0.0005,$$

$$473.0579, 0.0224, 5.0806, 2.1940]$$

$$\underline{g_{10}}: [WEIB_{\{1,2\}}, GAM_{\{3,4\}}, EXP_{\{5\}}]$$

$$[0.3764, 3.2198, 2.4159, 0.0710, 4.4883, 5.3533, 0.1155, 19.5102, 0.1286, 0.0040,$$

$$73.8112, 0.1166, 109.2310, 1.9272]$$

Process	γ	$\hat{\sigma}_T^2$	σ_T^2	$\hat{\kappa}_1$	κ_1	κ_τ	p -value
g_1	-	5.8200	5.8201	-0.0148	-0.0153	-0.0221	1.0000
g_3	1	4.4048	4.6404	-0.0071	0.0069	-0.0444	0.9995
	2	5.5943	7.3468	-0.0261	0.0961	-0.0414	0.9995
	3	5.5138	7.5715	-0.0155	0.1420	-0.0246	0.9992
	4	5.6105	7.9221	-0.0170	0.1533	-0.0262	0.9989
g_5	1	8.6339	9.1108	-0.0266	-0.0451	-0.0253	0.9980
	2	7.1002	7.1296	-0.0124	-0.0129	-0.0160	0.9999
	3	6.6375	6.6403	-0.0105	-0.0110	-0.0154	0.9964
	4	6.4079	6.4159	-0.0116	-0.0113	-0.0166	0.9965
g_7	0	7.2453	7.2509	-0.0057	-0.0053	-0.0085	0.9982
	1	10.8532	10.8970	-0.0135	-0.0141	-0.0304	0.9999
	2	18.0317	18.1129	-0.0149	-0.0154	-0.0278	0.9954
	3	26.0804	26.1570	-0.0135	-0.0122	-0.0304	0.9998
g_9	-	4.9671	5.0380	-0.0169	-0.0136	-0.0343	0.9993

Table F.1.: Moments of smooth class 0 processes considered in Sec. 4.2.1. $\hat{\sigma}_T^2$ and $\hat{\kappa}_1$ are respectively the variance and correlation coefficient obtained from simulations, while σ_T^2 and κ_1 are corresponding quantities as predicted by McFadden's equations (3.26) and (3.30). Additionally, the last two columns include Kendall's tau correlation coefficient (from simulations), as well as the maximum p -value of the Kolmogorov-Smirnov test assuming the mixture model is the true distribution for the interval data from each realisation (out of 1000).

Process	γ	$\hat{\sigma}_T^2$	σ_T^2	$\hat{\kappa}_1$	κ_1	κ_τ	p -value
g_2	$\frac{1+\sqrt{3}}{2}$	10.5560	10.8338	0.0497	0.0576	0.0795	0.9963
	$\sqrt{3}$	11.4906	11.7807 11.4783	0.0476	0.0552	0.0800	0.9971
	2	12.3576	12.6321	0.0463	0.0532	0.0811	0.9984
	$2\sqrt{3}$	17.9075	18.1875	0.0362	0.0425	0.0814	0.9884
g_4	-	10.6098	10.8901	0.0415	0.0492	0.0692	0.9984
g_6	1	10.1047	10.3930	0.0503	0.0587	0.0785	0.9991
	2	7.2730	7.2872	0.0045	0.0046	0.0069	0.9995
	3	6.6848	6.6892	-0.0046	-0.0047	-0.0061	0.9995
	4	6.4247	6.4369	-0.0085	-0.0083	-0.0117	0.9994
g_8	-	7.4769	7.7363	0.0562	0.0656	0.0746	0.9963
g_{10}	-	4.457	4.5083	-0.0200	-0.0183	-0.0422	0.9991

Table F.2.: Moments of sub-fractal class 0 processes considered in Sec. 4.2.2. $\hat{\sigma}_T^2$ and $\hat{\kappa}_1$ are respectively the variance and correlation coefficient obtained from simulations, while σ_T^2 and κ_1 are corresponding quantities as predicted by McFadden's equations (3.26) and (3.30). Additionally, the last two columns include Kendall's tau correlation coefficient (from simulations), as well as the maximum p -value of the Kolmogorov-Smirnov test assuming the mixture model is the true distribution for the interval data from each realisation (out of 1000). For the process g_2 with $\gamma = \sqrt{3}$, the second tabulated value for σ_T^2 is the variance computed using Wong's pdf App. B.8.

PARAMETER VALUES: CLASSES 1 AND 2 DENSITIES

This appendix uses the same notation for representing mixtures as in App. F. I_0 denotes the class 0 regime as described in Sec. 5.1.1. For the sub-fractal process ρ_{21} , $\epsilon = 2\alpha_1 / (c_1 p_0(0))$, $p_0(0) = 37 / (48\sqrt{3})$. Refer back to App. B for the *BETA* (B.7), *EXP* (B.3), and *EXPP* (B.6) distributions. The *GEXPP* density is defined in Eq. (4.5). Decimals are given to 4 decimal places.

$\underline{\rho}_{11}$: $I_0 = [0, 1]$

$[WEIB_{\{1\}}, GAM_{\{2\}}, EXP_{\{3\}}]$:

$a = 1/10$: [0.1598, 2.7220, 1.7923, 0.1276, 4.4661, 0.6011, 2.4373, 2.3518].

$a = 1/\sqrt{3}$: [0.0184, 3.9743, 3.9372, 0.2300, 6.1972, 0.2696, 2.0075, 2.0107].

$[BETA_{\{1,2,3\}}]$:

$a = 1$: [0.8282, 2.0000, 16.3109, 112.6334, 0.1677, 3.1761, 1.5475, 2.3621, 19.3086, 8.4426, 5.9194].

$[BETA_{\{1,2,3,4\}}]$:

$a = \sqrt{3}$: [0.4839, 2.0000, 24.5646, 51.3375, 0.2459, 7.7256, 3.9441, 2.1629, 0.0251, 25.3048, 2.0651, 3.5718, 2.3014, 6.4738, 8.3416].

$a = 3$: [0.2036, 2.0000, 6.3377, 6.3000, 0.5119, 16.7196, 17.3312, 2.0810, 0.1328, 5.4058, 16.0876, 3.7981, 11.7310, 11.3219, 3.6630].

$a = 10$: [0.0121, 2.0000, 4.3504, 0.9238, 0.3184, 30.2040, 122.5852, 1.6241, 0.6490, 197.4417, 518.0396, 1.1473, 12.4905, 4.0968, 0.7108].

$[BETA_{\{1,2,3,4,5\}}]:$

$a = 30: [0.0005, 2.0000, 2.0833, 0.0740, 0.7898, 695.0213, 535.5000, 0.1856, 0.1877, 96.5437, 118.4701, 0.2347, 0.0012, 19.3160, 2.5205, 0.2130, 14.1546, 53.6417, 0.5242].$

$\rho_{21}: I_0 = [0, 0.3295]$

$[EXP_{\{1,2\}}]:$

$a = 1/10: [0.9168, 0.5195, 3.3846].$

$[BETA_{\{1,2,3,4\}}]:$

$a = 0.3295: [2.3318e-13, 1.000, 2.0000, 1.1972e-12, 2.7282e-09, 2.0000, 2.7708, 0.0010, 0.7410, 3.8512, 13.3109, 233.8229, 7.7730, 26.0805, 50.2527].$

$a = 1/\sqrt{3}: [8.0500e-11, 1.000, 2.0000, 5.5769e-10, 0.0105, 2.0000, 20.2268, 3.0827, 0.6134, 5.1974, 15.4439, 85.1955, 5.6789, 15.1076, 29.1582].$

$a = \sqrt{\sqrt{40/3} - 3}: [3.0401e-11, 1.000, 2.0000, 2.6085e-10, 0.0068, 2.0000, 21.0639, 2.5186, 0.5876, 3.6778, 9.5951, 42.8109, 6.9841, 17.1156, 17.2611].$

$a = \sqrt{3}: [5.9300e-12, 1.000, 2.0000, 1.2325e-10, 7.6607e-06, 2.0000, 2.0002, 0.0647, 0.3944, 5.0353, 25.3551, 20.9023, 16.4132, 51.8368, 8.2977].$

$a = 3: [2.9743e-12, 1.000, 2.0000, 1.5349e-10, 1.7576e-09, 2.0000, 2.3758, 0.0287, 0.2984, 6.1891, 36.9340, 10.7180, 30.5124, 68.6987, 3.5759].$

$[BETA_{\{1,2,3,4,5\}}]:$

$a = 10: [1.5792e-14, 1.000, 2.0000, 5.5357e-12, 1.5651e-11, 2.0000, 2.1532, 0.0289, 0.0682, 9.1491, 68.5631, 3.2836, 0.3462, 43.2735, 55.5014, 0.7382, 173.1249, 140.1934, 0.5715].$

For $a \geq 0.3295\dots$, the surrogate density is a *WEIB-GAM-EXPP* mixture, with parameters $[1.7090e-05, 3.1263, 1.3539, 0.0859, 5.5880, 0.6097, 2.0573, 2.0819].$

Its mean and variance are respectively π and 5.1257. The parameters were found by performing the optimisation for both the τ and η variables when $a = 0.3295\dots$

$$\underline{\rho}_{12}: I_0 = [0, \sqrt{3/2}]$$

$$[WEIB_{\{1\}}, GAM_{\{2\}}, EXP_{\{3\}}]:$$

$$a = 1/10: [0.1199, 2.9781, 1.8293, 0.1592, 3.6277, 0.6632, 2.3775, 2.3525].$$

$$a = 1/\sqrt{3}: [0.1373, 2.9586, 1.6026, 0.1526, 3.7878, 0.5803, 2.1189, 2.0425].$$

$$[BETA_{\{1,2\}}, GEXPP_{\{3\}}, EXPP_{\{4\}}]:$$

GEXPP with $d = 1$.

$$a = \sqrt{3/2}: [0.1456, 4.0657, 2.8826, 2.2463, 0.0269, 27.0776, 161.3178, 11.2652, 0.0144, 2.1553, 0.6598, 0.3272, 1.0000, 0.3940, 7.7765].$$

$$a = \sqrt{3}: [0.2623, 3.1449, 2.2987, 1.8541, 0.0553, 11.4677, 20.0336, 3.2867, 0.0463, 1.4271, 0.4796, 2.4207, 1.0000, 0.2910, 4.7660].$$

$$a = 3: [0.4585, 5.1081, 6.2059, 1.6493, 0.0665, 13.3476, 16.2025, 1.6961, 0.1012, 2.0537, 68.5985, 0.1739, 1.0000, 0.0964, 3.3482].$$

$$a = 10: [0.7721, 5.4956, 6.7980, 0.5149, 0.0245, 24.1277, 16.0693, 0.3800, 0.1312, 1.5472, 1.4929, 0.0550, 1.0000, 2.0393, 1.9335].$$



MATLAB CODE FOR SIMULATING A CORRELATED RANDOM PROCESS

```
function simdat=randprocsim(n,dti,pd,pdT,lc,powcor,sim,rep...
    seed,gen,SI,s)
% randprocsim  Simulates a random process using the iterative
%              Fourier Filtering Method (iFFM) and computes
%              level-crossing statistics.
%
% FORMAT:
%   simdat=randprocsim(n,dti,sim,powcor,rep,seed,gen,SI,s,rel)
%
% INPUTS:
% n      length of realisation (should be even)
% dti    dti=1/dt, dt is the discretisation length
% pd     probability distribution object (create with 'makedist')
% pdT    distribution transformation function ([] or @(u)f(U))
% lc     level (to find crossings of)
% powcor power spectrum or normalised autocorelation function
% sim    1 (for power sepctrum), 2 (for autocorrelation)
% rep    number of repeats for iterative step
% seed   for random number generator ('shuffle' for random seed)
% gen    generator algorithm
% SI     true if generator supports substreams, false otherwise
% s      number of simulations to run
```

```

%-----
% Example power spectrum (sim=1): @(w)sqrt(2*pi)*exp(-2*(pi*w).^2)
% Example autocorrelation(sim=2): @(t)exp(-(t/2).^2);
% Example transformation: Uniform ---> Laplace
%           pd=makedist('uniform','lower',-1/2,'upper',1/2);
%           mu0=1/sqrt(2); mu1=0;
%           pdT=@(U)mu1-mu0*sign(U).*log(1-2*abs(U));
% Example values for other inputs:
% n=3.1416e6; dti=200; lc=0; rep=30; seed=0; gen='mt19937ar';
% SI=false; s=1;
%-----
% OUTPUTS: all inputs and...
%   For first simulation only:
%   simdat.
%       N1      crossing count
%       taub1   crossing intervals
%       betas1  crossing locations
%       x1      realisation
%       zetas1  crossing indicator
%   For all simulations:
%   simdat.
%       seedz   random number generator seeds
%       BETAZ   location of first-crossings
%       TAUZ   crossing intervals
%       Nci    crossing interval counts
%       MTAU   (non-discretised) interval means
%       VARTAU (non-discretised) interval variances
%       KAPPA1 linear correlation coefficient
%       KTAU   rank correlation coefficient
%       TAUB12 interval product moments
%
% Requires 'Statistics and Machine Learning Toolbox'.
%-----

```

```

if SI==false && s>1
    seed='shuffle'; % Necessary for non-uniform/non-Gaussian cases
end
%-----
if isempty(pdT) % Check if transformation function is empty.
    pdT=@(U)U; % Define as identity function.
end
%-----
% Store inputs.
simdat.n=n;      simdat.dti=dti;      simdat.pd=pd;
simdat.pdT=pdT; simdat.lc=lc;      simdat.powcor=powcor;
simdat.sim=sim; simdat.rep=rep;      simdat.seed=seed;
simdat.gen=gen; simdat.SI=SI;      simdat.s=s;
%-----
% Predefine the seeds, first-crossing locations, and interval
% sequence, counts and averages.
seedz=zeros(s,1);  BETAZ=zeros(s,1);  TAUZ=zeros(4800*s,1);
Nci=zeros(s,1);   MTAU=zeros(s,1);   M2TAU=zeros(s,1);
TAUB12=zeros(s,1); KTAU=zeros(s,1);
%-----
nci=0; % for counting total crossing intervals
%-----
% FOURIER FILTERING
%-----
% 1. Compute filter...
if sim==1 % ...using power spectrum.
    omega=(dti*(0:(n/2))/n)'; % frequencies
    sm=zeros(n,1);
    sm(1:n/2+1)=powcor(omega);
    sm(n/2+2:n)=flip(sm(2:n/2));
    Wm=sqrt(dti*sm); % filter
elseif sim==2 % ...using the autocorrelation function.
% Zero-padding is used to improve Fourier transform output.

```

```

zpad=2*(ceil(n*1e-3/4));
T=2*(ceil(n/2))-zpad;
tau=abs(-T/2:T/2)'/dti;      % delay times
rho=powcor(tau);
rhop=[rho;zeros(zpad-1,1)];
Wm=sqrt(abs(fft(rhop) ) );   % filter
end
%-----
% SIMULATIONS
%-----
% Run first simulation.
[N,sumz,taub,betas,x,zetas,seedz(1)]=randsimk(n,pd,pdT,lc,Wm,...
                                               rep,seed,gen,SI,s,1);
%-----
if min(x)>lc || max(x)<lc
    error('level must lie between minimum and maximum of process');
end
%-----
% Store crossing count, intervals and locations, and the
% realisation and its crossing indicator.
simdat.N1=N; simdat.taub1=taub;  simdat.betas1=betas;
simdat.x1=x+lc; simdat.zetas1=zetas;
%-----
% Compute Kendall's rank correlation coefficient.
ktau=corr([taub(1:N-2),taub(2:N-1)],'type','Kendall');
KTAU(1)=ktau(1,2);
%-----
BETAZ(1)=betas(1); TAUZ(nci+1:nci+N-1)=taub; Nci(1)=N-1;
MTAU(1)=sumz(1); M2TAU(1)=sumz(2); TAUB12(1)=sumz(3);
nci=nci+N-1;
%-----
if s>1 % Run remaining simulations.
for k=2:s

```

```

[N,sumz,taub,betas,~,~,seedz(k)]=randsimk(n,pd,pdT,lc,Wm,...
                                           rep,seed,gen,SI,s,k);
%-----
% Store crossing interval data and moment sums:
    BETAZ(k)=betas(1); TAUZ(nci+1:nci+N-1)=taub;
    Nci(k)=N-1; nci=nci+N-1;
    MTAU(k)=sumz(1); M2TAU(k)=sumz(2); TAUB12(k)=sumz(3);
%-----
% Compute and store Kendall's rank correlation coefficient.
    ktau=corr([taub(1:N-2),taub(2:N-1)],'type','Kendall');
    KTAU(k)=ktau(1,2);
%-----
    clc; fprintf('Simulation %d complete\n\n',k);
%-----
end
end
%-----
% AVERAGES
%-----
% Compute (non-discretised) averages of the mean and variance, and
% the linear correlation coefficient.
VARTAU=(M2TAU-MTAU.^2./Nci)./(Nci-1);
KAPPA1=(TAUB12./(Nci-1)-MTAU.^2./Nci.^2)./VARTAU;
MTAU=MTAU./Nci;    TAUB12=TAUB12./(Nci-1);
%-----
TAUZ=TAUZ(1:nci); % (redefinition in case of extra zero entries)
%-----
% FINAL STORAGE
%-----
% Store all first-crossing locations, (non-discretised) crossing
% intervals, means, variances, product moment, correlation
% coefficients and generator seeds:
simdat.BETAZ=BETAZ;    simdat.TAUZ=TAUZ;    simdat.Nci=Nci;

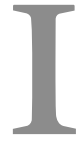
```

```

simdat.MTAU=MTAU;          simdat.VARTAU=VARTAU;
simdat.TAUB12=TAUB12;    simdat.KAPPA1=KAPPA1;    simdat.KTAU=KTAU;
simdat.seedz=seedz;
%-----
fprintf(...
' [mean,var,kappa1,kappatau] = [%.4f,%.4f,%.4f,%.4f]\n\n',...
[mean(TAUZ)/dti,mean(VARTAU)/dti^2,mean(KAPPA1),mean(KTAU)]);
%-----
%-----
function [N,sumz,taub,betas,y,zeta,seed]=randsimk(n,pd,pdT,...
lc,Wm,rep,seed,gen,SI,s,k)
%-----
% FOURIER FILTERING (continued)
%-----
% 2. Generate uncorrelated sequence of random numbers, and apply
% distribution transformation, pdT:
if SI % (multiple independent streams)
    strm=RandStream.create(gen,'NumStreams',s,...
                           'StreamIndices',k,'Seed',seed);
    seed=strm.Seed;
    y=pdT(randn(strm,n,1)); % uncomment for standard normals
    %y=pdT(rand(strm,n,1)); % uncomment for uniform variates
else % (variates from MATLAB supported distributions)
    sd=rng(seed,gen);
    seed=sd.Seed;
    y=pdT(random(pd,n,1));
end
%-----
for jj=1:rep+1
    ym=fft(y);
%-----
% 3. Enforce the original power spectrum on y:
    zm=Wm.*ym./abs(ym); z=ifft(zm);

```

```
%-----  
% 4. Rank replace z with y:  
    [~,Iz]=sort(z,'descend'); [~,Iy]=sort(y,'descend');  
    z(Iz)=y(Iy);  
    y=z;  
%-----  
    end  
%-----  
    y=real(y)-lc; % subtract level (for crossings)  
%-----  
% ZERO CROSSINGS  
%-----  
% 1. Identify zero crossings (value 1 entries of zeta below):  
    zeta=[0;(1- ( sign(y(1:n-1)).*sign(y(2:n)) ) )/2];  
    N=sum(zeta); % Total number of crossings:  
% 2. Find crossing locations:  
    betas=find(zeta);  
% 3. Determine (non-discretised) intervals between crossings:  
    taub=betas(2:N)-betas(1:N-1);  
% 4. Calculate sums for the first, second and product moments:  
    sumz=[sum(taub),dot(taub,taub),dot(taub(1:N-2),taub(2:N-1))];  
end  
%-----  
%-----  
end
```



MATLAB CODE FOR COMPUTING LACUNARITY

```
function simlac=lacunarityCG(zetas,dt,CG)
%lacunarityCG Computes the lacunarity measure of a
% one-dimensional object given a zero-crossing indicator vector
%
% INPUTS:
%   zetas   zero-crossing indicator vector
%   CG      box counting method: 1 (contiguous), 2 (gliding)
%   dt      discretisation length
% OUTPUTS:  (at time-scales r_[m]=(m-1)*dt)
%   simlac.
%   L       Lacunarity
%   mN1     Mean crossing counts
%   varN2   Variance of crossing counts
%   r       time scales
%   dL      Lacunarity slope
%   rd      time scales dL is computed at (r_[3] to r_[n-2])
%
% Requires Econometrics Toolbox
%-----
n=numel(zetas);
%-----
Ni=cumsum(zetas);
%-----
```

```

if CG==1
%-----
% CONTIGUOUS BOX LACUNARITY
%-----
    mN2=zeros(n,1);    varN2=zeros(n,1);    L=zeros(n,1);
    maxjs=[n;floor((n-1)./(1:n-1)')];
%-----

    mN2(1)=Ni(n);
    nn=ceil(n/2);
    for jj=2:nn
        maxj=maxjs(jj);
        jz=(jj-1)*(2:maxj)+1;
        Nicj=[Ni(jj);Ni(jz) - Ni(jz-jj+1)];
        mN2(jj)=sum(Nicj.^2);
    end
%-----

    mN1=[Ni(n);Ni( ((2:n)')-1).*maxjs(2:n)+1 )];
    mN2(nn+1:end)=Ni(nn+1:end).^2;
%-----

    varN2(1)=Ni(n)*(1-Ni(n)/n)/n;
    varN2(2:nn)=(mN2(2:nn)-mN1(2:nn).^2./maxjs(2:nn))./...
                                                    (maxjs(2:nn)-1);
    L(1:nn)=varN2(1:nn)./mN1(1:nn).^2.*maxjs(1:nn).^2;
    L=L+1;
    mN1=mN1./maxjs;
%-----

elseif CG==2
%-----
% GLIDING BOX LACUNARITY
%-----

    riz=(1:n-1)';
%-----

    Si1=cumsum(Ni);    Si2=cumsum(Ni.^2);

```

```

%-----
    phi1=Si1(n) - Si1(n-riz) - Si1(riz) + Ni(riz);
    phi2=Si2(n) + Si2(n-riz) - Si2(riz) + Ni(riz).^2;
%-----
    rho=autocorr(Ni,n-1); rho=[rho(2:end);0];
    mu=Si1(n)/n; sig2=(n*Si2(n)-Si1(n)^2)/n^2;
    c1=find(Ni>0,1);
    phi3=n*sig2*rho(riz) +mu*( Si1(n-riz) - Si1(riz) ) +mu^2*riz;
    phi3(n-c1)=Ni(end);
    phi3(n-c1+1:n-1)=0;
%-----
    mN1=phi1./(n+1-riz);
    varN2=( phi2 - 2*phi3(1:n-1) - phi1.^2./(n+1-riz) )./(n-riz);
    L=1+varN2./mN1.^2;
%-----
    L=[L;1];    mN1=[mN1;Ni(n)];    varN2=[varN2;0];
end
%-----
simlac.L=L;    simlac.mN1=mN1;    simlac.varN2=varN2;
rz=dt*linspace(0,n-1,n)';
%-----
% LACUNARITY SLOPE
%-----
dL=rz(3:n-2).*deriv1(log10(varN2./mN1.^2),dt);
%-----
simlac.dL=dL;    simlac.r=rz;    simlac.rd=rz(3:n-2);
%-----
%-----
function df=deriv1(f,h) % Fourth-order centred derivative
                        % estimate
    N=length(f);
    f2m=f(1:N-4);    f1m=f(2:N-3);
    f1=f(4:N-1);    f2=f(5:N);

```

```
df=(f2m - 8*f1m + 8*f1 -f2)./(12*h);  
end  
%-----  
%-----  
end
```



MATLAB CODE FOR COMPUTING THE INTERVAL DENSITY AND CROSSING COUNT DISTRIBUTIONS

```
function [pb,Tb]=rebinpdf(TAUZ,dti,bin)
% rebinpdf Estimates the interval density using frequency
%           binning.
%
%INPUTS:
%  TAUZ = non-discretised intervals
%  dti  = reciprocal of discretisation length
%  bin  = desired grouping of adjacent interval sizes
%
% OUTPUTS:
%  pb = estimate of interval density
%  Tb = crossing interval values associated with pb
%-----
[p,np]=simpdff(TAUZ); m=ceil(np/bin); pb=zeros(m,1);
%-----
for jj=1:m-1
    pb(jj)=sum(p(bin*(jj-1)+1:bin*jj));
end
pb(m)=sum(p(bin*(m-1)+1:np));
%-----
pb=dti*pb/sum(pb)/bin;
Tb=(bin/2:bin:bin*(m-1/2))'/dti;
```

```

%-----
function [p,np]=simpdff(x)
% simpdff Finds the frequencies for the values (positive
% integers) in the vector x, from 1 to max(x).

np=max(x); p=zeros(np,1); nx=numel(x);
for i=1:nx
    j=x(i);
    p(j)=p(j)+1;
end
end
end

```

```

function PN=boxmassdistCGrN(r,zetas,CG)
% boxmassdistCGrN Computes box mass distribution for fixed r.
%
% INPUTS:
% r non-discretised box size
% zetas zero-crossing indicator vector
% CG box counting method: 1 (contiguous), 2 (gliding)
%-----
n=numel(zetas);
%-----
% Define counting process.
Nic=cumsum(zetas);
%-----
% Calculate box counts.
%-----
if r==1
    Nc=sum(zetas);
    PN=[n-Nc,Nc];
else

```

```

if CG==1 %-----CONTIGUOUS BOXES-----
    nn=ceil(n/2);
    if r<=nn
        maxj=floor((n-1)/r);
        jz=(r-1)*(2:maxj)+1;
        Nicj=[Nic(r);Nic(jz) - Nic(jz-r+1)];
        elseif r>nn
            Nicj=Nic(r);
        end
    elseif CG==2 %-----GLIDING BOXES-----
        Nicj=[Nic(r);Nic(1+r:n)-Nic(1:n-r)];
    end
%-----
% Calculate count frequencies.
    PN=prbmf(Nicj);
end
%-----
%-----

function p=prbmf(x) % Bins frequencies of values in x,
                    % from 0 to max(x).

    p=zeros(max(x)+1,1);
    mx=length(x);
    for i=1:mx
        j=x(i);
        p(j+1)=p(j+1)+1;
    end
end
%-----
%-----
end

```

```

function PN=boxmassdistCGNr(N,maxr,zetas,CG)

```

```

% boxmassdistCGNr Computes box mass distribution for fixed N.
%
% INPUTS:
%   N          counts
%   maxr       maximum non-discretised box-size for calculation
%   zetas      zero-crossing indicator vector
%   CG         box counting method: 1 (contiguous), 2 (gliding)
%
%Assumes N < maxr
%-----
n=numel(zetas);   PN=zeros(maxr,1);
%-----
% Define counting process.
Nic=cumsum(zetas);
%-----
PN(1)=sum(zetas==N); % Calculate counts at size 1.
%-----
if CG==1 %-----CONTIGUOUS BOXES-----
    maxjs=[n;floor((n-1)./(1:n-1)')]; % number of boxes
    nn=ceil(n/2); cmaxr=min(nn,maxr);
%-----
% Calculate box counts.
    for r=2:cmaxr
        maxj=maxjs(r);
        jz=(r-1)*(2:maxj)+1;
        Nicj=[Nic(r);Nic(jz) - Nic(jz-r+1)];
        PN(r)=sum(Nicj==N);
    end
    if maxr>nn
        PN(cmaxr+1:maxr)=Nic(cmaxr+1:maxr);
    end
% Normalise by number of boxes.
    PN=PN./maxjs(1:maxr);

```

```
elseif CG==2 %-----GLIDING BOXES-----
    for r=2:maxr
%-----
% Calculate box counts.
        Nicj=[Nic(r);Nic(1+r:n)-Nic(1:n-r)];
%-----
% Calculate count frequencies.
        PN(r)=sum(Nicj==N);
%-----
    end
% Normalise by number of boxes.
    rz=(1:maxr)';
    PN=PN./(n+1-rz);
end
%-----
end
```

REFERENCES

- [1] I. Florescu and C. A. Tudor, *Handbook of Probability*. New York, Wiley, 2014.
- [2] G. Lindgren and I. Rychlik, Slepian models and regression approximations in crossing and extreme value theory. *International Statistical Review*, **59**(2): 195–225, 1991.
- [3] S. M. Ross, *Introduction to Probability Models, Ninth Edition*. Academic Press, London, 2007.
- [4] J. F. Eichner, J. W. Kantelhardt, A. Bunde, S. Havlin, Statistics of return intervals in long-term correlated records. *Physical Review E*, **75**: 011128, 2007.
- [5] L. R. M. Wilson and K. I. Hopcraft. Periodicity in the autocorrelation function as a mechanism for regularly occurring zero crossings or extreme values of a Gaussian process. *Physical Review E*, **96**: 062129, 2017.
- [6] S. H. Strogatz, *Nonlinear Dynamics and Chaos: With Applications to Physics, Biology, Chemistry, and Engineering*. Westview Press, Philadelphia, 2014.
- [7] E. W. Weisstein, Sequence A086181 in *The On-Line Encyclopedia of Integer Sequences*, published electronically at <https://oeis.org>. [Accessed October 2020].
- [8] H. Zhao, Z-H. Zheng. Random periodic solutions of random dynamical systems. *Journal of Differential Equations*, **246**(5): 2020–2038, 2009. DOI: 10.1016/j.jde.2008.10.011.
- [9] S. O. Rice. Mathematical analysis of random noise. *Bell System Technical Journal*, **23**(3): 282–332, 1944.

- [10] S. O. Rice. Mathematical analysis of random noise. *Bell System Technical Journal*, **24**(1): 46–156, 1945. DOI: 10.1002/j.1538-7305.1945.tb00453.x.
- [11] R. Vijayan and M. Holtzman. Foundations for level crossing analysis of handoff algorithms. *Proceedings of the IEEE International Conference on Communications*, **2**: 935–939, 1993. DOI: 10.1109/ICC.1993.397408.
- [12] S. Agarwal and J. M. Holtzman. Modelling and analysis of handoff algorithms in multi-cellular systems. *IEEE 47th Vehicular Technology Conference*, **1**: 300–304, 1997. DOI: 10.1109/VETEC.1997.596368.
- [13] S. Souissi, O. Ben Rhouma, and C. Rebai. Statistical modeling of mains zero crossing variation in powerline communication. *Measurement*, **90**: 158–167, 2016.
- [14] V. Veeramsetty, B. R. Edudodla, and S. R. Salkuti. Zero-Crossing Point Detection of Sinusoidal Signal in Presence of Noise and Harmonics Using Deep Neural Networks. *Algorithms*, **14**: 329, 2021. DOI: 10.3390/a14110329.
- [15] P. H. Brill. An Embedded Level Crossing Technique for Dams and Queues. *Journal of Applied Probability*, **16**(2): 174–186, 1979.
- [16] G. Lindgren. Wave analysis by Slepian models. *Probabilistic Engineering Mechanics*, **15**(1): 49–57, 2000.
- [17] P. J. Edwards and R. B. Hurst. Level-crossing statistics of the horizontal wind speed in the planetary surface boundary layer. *Chaos*, **11**: 611. DOI: 10.1063/1.1379310.
- [18] D. Cava, G. G. Katul, A. Moliini and C. Elefante. The role of surface characteristics on intermittency and zero-crossing properties of atmospheric turbulence. *Journal of Geophysical Research: Atmospheres*, **117**(D1), 2012. DOI: 10.1029/2011JD016167.
- [19] C. Santamaria, M. Bober and W. Szajnowski. Texture analysis using level-crossing statistics. *Proceedings of the 17th International Conference on Pattern Recognition*, **2**: 712–715, 2004. DOI: 10.1109/ICPR.2004.1334358.

- [20] M. Mazruei, S. Sanati, A. N. Sarcheshmeh, and M. S. Tarzjan. A new algorithm for edge detection based on edge following. *Conference: 3rd International Conference on Applied Research in Computer & Information Technology*, 2016.
- [21] A. Tabesh. Zero-crossing rates of wavelet frame representations for texture classification. *Electronics Letters*, **38**(22): 1340–1341, 2002. DOI: 10.1049/el:20020887.
- [22] B. D. Fulcher. Feature-based time-series analysis. arXiv:1709.08055v2, 2017.
- [23] R. C. Guido. ZCR-aided neurocomputing: A study with applications. *Knowledge-Based Systems*, **105**: 248–269, 2016. DOI: 10.1016/j.knosys.2016.05.011.
- [24] I. Agranat. Bat Species Identification from Zero Crossing and Full Spectrum Echolocation Calls using HMMs, Fisher Scores, Unsupervised Clustering and Balanced Winnow Pairwise Classifiers. *Wildlife Aquatic inc 2012*: 1–27.
- [25] B. Gomez and U. Kadri. Earthquake source characterization by machine learning algorithms applied to acoustic signals. *Scientific Reports*, **11**: 23062, 2021. DOI:10.1038/s41598-021-02483-w.
- [26] P. H. Brill and M. J. M. Posner. The system point method in exponential queues: a level crossing approach. *Mathematics of Operations Research*, **6**(1): 31–49, 1981.
- [27] H. Cramer and M. R. Leadbetter, *Stationary and Related Stochastic Processes: Sample Function Properties and Their Applications*. Wiley, New York, 1967.
- [28] J. Masoliver. The level-crossing problem: First-passage, escape and extremes. *Fluctuation and Noise Letters*, **13**:4, 1430001, 2014. DOI: 10.1142/S0219477514300018.
- [29] A. J. Bray, S. N. Majumdar, and G. Schehr. Persistence and first-passage properties in nonequilibrium systems. *Advances in Physics*, **62**(3): 225–361, 2013. DOI: 10.1080/00018732.2013.803819.

- [30] WAFO-Group. *WAFO - a MATLAB Toolbox for Analysis of Random Waves and Loads - Tutorial for WAFO version 2017*. [Online]. Available from: <https://www.maths.lth.se/matstat/wafo/documentation/index.html>. [Accessed October 2018].
- [31] W. Huang and S. Dong. Probability distribution of wave periods in combined sea states with finite mixture models. *Applied Ocean Research*, **92**: 101938, 2019. DOI: 10.1016/j.apor.2019.101938.
- [32] A. Roy, E. Perfect, W. M. Dunne, and L. D. McKay. A technique for revealing scale-dependent patterns in fracture spacing data. *Journal of Geophysical Research: Solid Earth*, **119**: 5979–5986, 2014. DOI: 10.1002/2013JB010647.
- [33] A. Chornet-Lurbe, J. A. Oteo, and J. Ros. Statistical geometric affinity in human brain electric activity. *Physical Review E*, **75**: 051918, 2007. DOI: 10.1103/PhysRevE.75.051918.
- [34] A. Ogunshemi, K. I. Hopcraft and S. P. Preston. Lacunarity of the zero crossings of Gaussian processes. *Physical Review E*, **99**, 062109, 2019.
- [35] E. Wong. Some results concerning the zero-crossings of Gaussian noise. *SIAM Journal on Applied Mathematics*, **14**(6): 1246–1254, 1961.
- [36] L. R. M. Wilson. *The Impact of Periodicity on the Zero-Crossings of Random Functions*. PhD thesis, University of Nottingham, 2015.
- [37] G. Lindgren. *Stationary Stochastic Processes - Theory and Applications*. Chapman & Hall/CRC, Boca Raton, 2013.
- [38] J. W. Goodman, *Statistical Optics*. Wiley, New York, 1984.
- [39] C. E. Rasmussen and C. K. I. Williams, *Gaussian Processes for Machine Learning*, MIT Press, Cambridge, 2006.
- [40] I. N. Bronshtein, K. A. Semendyayev, G. Musiol and H. Mühlig, *Handbook of Mathematics - Sixth Edition*. Springer Berlin, Heidelberg, 2015.

- [41] J.-M. Azais and M. Wschebor. *Level sets and extrema of random processes and fields*. Wiley, New York, 2009.
- [42] J. Beran, Y. Feng, S. Ghosh and R. Kulik, *Long-Memory Processes*. Springer, Berlin, 2013.
- [43] A. Bunde and S. Lennartz. Long-Term Correlations in Earth Sciences. *Acta Geophysica*, **60**(3): 562–588, 2012. DOI: 10.2478/s11600-012-0034-8.
- [44] J. Blackledge, D. Kearney, M. Lamphiere, R. Rani, and P. Walsh. Econophysics and fractional calculus: Einstein’s evolution equation, the fractal market hypothesis, trend analysis and future price prediction. *Mathematics*, **7**: 1057, 2019. DOI: 10.3390/math71110572019.
- [45] M. R. Leadbetter. On crossings of arbitrary curves by certain Gaussian processes. *Proceedings of the American Mathematical Society*, **16**(1): 60–68, 1965.
- [46] H. Steinberg, P. M. Schultheiss, C. A. Wogrin and F. Zweig. Short-time frequency measurement of narrow-band random signals by means of a zero counting process. *Journal of Applied Physics*, **26**(2): 195–201, 1955.
- [47] J. M. Smith. *Discrete Properties of Continuous, non-Gaussian Random Processes*. PhD thesis, University of Nottingham, 2008.
- [48] J. McFadden, The axis-crossing intervals of random functions—II. *IEEE Transactions on Information Theory*, **4**(1): 14–24, 1958.
- [49] J. H. Van Vleck and D. Middleton. The spectrum of clipped noise *Proceedings of the IEEE*, **54**(1): 2–19, 1966.
- [50] T. Mimaki, Zero-crossing intervals of Gaussian processes. *Journal of Applied Physics*, **44**(1): 477–485, 1973.
- [51] J. McFadden, The axis-crossing intervals of random functions. *IEEE Transactions on Information Theory*, **2**(4): 146–150, 1956. DOI: 10.1109/TIT.1956.1056822.

- [52] G. Lindgren. Gaussian integrals and Rice series in crossing distributions—to compute the distribution of maxima and other features of Gaussian processes. *Statistical Science*, **34**(1): 100–128, 2019. DOI:10.1214/18-STS662.
- [53] M. S. Longuet-Higgins. Bounding approximations to the distribution of intervals between zeros of a stationary Gaussian process, pp.63–88; D. Slepian. On the zeros of Gaussian Noise, pp.104–115. In: *Time Series Analysis*. Edited by M. Rosenblatt. Wiley, New York, 1963.
- [54] G. F. Newell and M. Rosenblatt. Zero crossing probabilities for Gaussian stationary processes *Annals of Mathematical Statistics*, **33**(4): 1306–1313, 1962.
- [55] A. Dembo and S. Mukherjee. No zero-crossings for random polynomials and the heat equation. *The Annals of Probability*, **43**(1): 85–118, 2015. DOI:10.1214/13-AOP852.
- [56] N. D. Feldheim and O. N. Feldheim. Long Gaps Between Sign-Changes of Gaussian Stationary Processes. *International Mathematics Research Notices*, **2015**(11): 3021–3034, 2015. DOI:10.1093/imrn/rnu020.
- [57] G. Lindgren, K. Podgorski and I. Rychlik. Effective computations of joint excursion times for stationary Gaussian processes. arXiv:2007.14220, 2020.
- [58] T. McClure. *Numerical Inverse Laplace Transform*. [Online]. Available from: uk.mathworks.com/matlabcentral/fileexchange/39035-numerical-inverse-laplace-transform. [Accessed July 2016].
- [59] G. McLachlan and D. Peel, *Finite Mixture Models*. Wiley, New York, 2000.
- [60] D. M. Titterton, A. F. M. Smith and U. E. Makov, *Statistical Analysis of Finite Mixture Distributions*. Wiley, New York, 1985.
- [61] F. Nielsen and V. Garcia. Statistical exponential families: A digest with flash cards. arXiv:0911.4863v2, 2011.
- [62] N. L. Johnson, A. W. Kemp and S. Kotz, *Univariate Discrete Distributions, 3rd Edition*. Wiley, New Jersey, 2005.

- [63] B. G. Lindsay. Mixture Models: Theory, Geometry and Applications. *NSF-CBMS Regional Conference Series in Probability and Statistics* **5**: I–163, 1995.
- [64] W. Feller, *An Introduction to Probability Theory and its Applications, Vol 2, 2nd Edition*. Wiley, New York, 1971.
- [65] R. Winkelmann, Duration dependence and dispersion in count-data models. *Journal of Business & Economic Statistics*, **13**(4): 467–474, 1995. DOI: 10.1080/07350015.1995.10524620.
- [66] B. McShane, M. Adrian, E. T. Bradlow and P. S. Fader, Count models based on Weibull interarrival times. *Journal of Business & Economic Statistics*, **26**(3): 369–378, 2008. DOI: 10.1198/073500107000000278.
- [67] Y. C. Low and S. H. Ong, Count distribution for mixture of two exponentials as renewal process duration with applications. *AIP Conference Proceedings*, **1739**: 020078, 2016. DOI: 10.1063/1.4952558.
- [68] W. Huang and S. Dong. Joint distribution of significant wave height and zero-up-crossing wave period using mixture copula method. *Ocean Engineering*, **219**: 108305, 2019. DOI: 10.1016/j.oceaneng.2020.108305.
- [69] T. Liu, J. Chen, and G. Dong. Zero crossing and coupled hidden Markov model for a rolling bearing performance degradation assessment. *Journal of Vibration and Control*, **20**(16): 2487–2500, 2014. DOI:10.1177/1077546313479992.
- [70] B. S. Everitt and D. J. Hand, *Finite Mixture Distributions*. Chapman and Hall, London, 1981.
- [71] T. T. Nguyen, H. D. Chamroukhi and G. J. McLachlan. Edited by L. Liu. Approximation by finite mixtures of continuous density functions that vanish at infinity. *Cogent Mathematics & Statistics*, **7**(1): 1750861. DOI: 10.1080/25742558.2020.1750861.
- [72] I. S. Gradshteyn and I. Ryzhik's, *Table of Integrals, Series, and Products - Seventh Edition*. Edited by A. Jeffrey and D. Zwillinger. Elsevier, Amsterdam, 2007.

- [73] J. C. Lagarias, J. A. Reeds, M. H. Wright, and P. E. Wright. Convergence properties of the Nelder-Mead simplex method in low dimensions. *SIAM Journal of Optimization*, **9**(1): 112–147, 1998.
- [74] S. Singer and J. Nelder, Nelder-Mead algorithm. *Scholarpedia*, **4**(7): 2928, 2005.
- [75] M. R. Espejo, M. D. Pineda and S. Nadarajah. Optimal unbiased estimation of some population central moments. *Metron*, **71**(1): 39–62, 2013.
- [76] R. E. Plotnick, R. H. Gardner, W. W. Hargrove, K. Prestegard, M. Perlmutter, Lacunarity analysis: A general technique for the analysis of spatial patterns. *Physical Review E*, **53**(5): 5461, 1996.
- [77] E. P. Rodrigues, M. S. Barbosa and L. F. Costa. Self-referred approach to lacunarity. *Physical Review E*, **72**: 016707, 2005. DOI: 10.1103/PhysRevE.72.016707.
- [78] B. Mandelbrot, *The Fractal Geometry of Nature*. Freeman, New York, 1983).
- [79] J. Blackledge, *Digital Signal Processing (Second Edition)*. Horwood Publishing, 2006.
- [80] K. I. Hopcraft, P. C. Ingrey and E. Jakeman. Power-law-distributed level crossings define fractal behavior. *Physical Review E*, **76**: 031134, 2007.
- [81] C. Allain, M. Cloitre, Characterizing the lacunarity of random and deterministic fractal sets. *Physical Review A*, **44**(6): 3552, 1991.
- [82] M. A. Reiss, B. Lemmerer, A. Hanslmeier and H. Ahammer. Tug-of-war lacunarity—A novel approach for estimating lacunarity. *Chaos*, **26**: 113102, 2016. DOI: 10.1063/1.4966539.
- [83] D. E. Knuth, *The Art of Computer Programming (Third Edition)*. Addison Wesley, Boston, 1997.

- [84] R. Kumerasan. Encoding Bandpass Signals Using Zero/Level Crossings: A Model-Based Approach. *IEEE Transactions on Audio, Speech, and Language Processing*, **18**(1): 17–33, 2010.
- [85] J. McFadden, The fourth product moment of infinitely clipped noise. *IEEE Transactions on Information Theory*, **4**(4): 159–162, 1958. DOI:10.1109/IRETIT.1958.6741950.
- [86] V. M. Nguyen. Some properties of large excursions of a stationary Gaussian process. arXiv:1205.4126v2, 2014.
- [87] H. A. Makse, S. Havlin, M. Schwartz, S. H. Eugene, Method for generating long-range correlations for large systems. *Physical Review E*, **53**(5): 5445–5449, 1996. DOI: 10.1103/PhysRevE.53.5445.
- [88] G. R. Cooper, C. D. McGillem, *Probabilistic Methods of Signal and System Analysis, 3rd Edition*. Oxford University Press, New York, 1998.
- [89] MathWorks. *One-Sample Kolmogorov-Smirnov Test*. [Online]. Available from: <https://uk.mathworks.com/help/stats/kstest.html>. [Accessed March 2020].
- [90] C. B. Moler. *Numerical Computing with MATLAB*. [Online]. Available from: <https://uk.mathworks.com/moler/chapters.html>. [Accessed February 2019].
- [91] M. Matsumoto and T. Nishimura. Mersenne Twister: A 623-Dimensionally Equidistributed Uniform Pseudorandom Number Generator. *ACM Transactions on Modeling and Computer Simulation*, **8**(1): 3–30, 1998.
- [92] G. Marsaglia and W. W. Tsang. The ziggurat method for generating random variables. *Journal of Statistical Software*, **5**: 1–7, 2000.
- [93] D. Slepian. The one-sided barrier problem for Gaussian noise. *The Bell System Technical Journal*, **41**(2): 463–501, 1962.

- [94] D. R. Cox and D. Oakes, *Analysis of Survival Data*. Chapman & Hall, Cambridge, 1984.
- [95] M. Pal, M. M. Ali and J. Woo. Exponentiated Weibull distribution. *Statistica*, **66**(2): 139–147, 2006.
- [96] J. Antezana, J. J. M. Buckley and J. -F. Olsen. Gap probabilities for the cardinal sine. *Journal of Mathematical Analysis and Applications*, **396**(2): 466–472, 2012.
- [97] S. N. Majumdar and A. J. Bray, Persistence with partial survival. *Physical Review Letters*, **81**(13): 2626–2629, 1998.
- [98] R. .N. Miroshin, The use of Rice series. *Theory of Probability and its Applications*, **28**(4): 714–726, 1984.
- [99] H. Bateman, *Tables of integral transforms - Volume I - Based, in part, on notes left by Harry Bateman and compiled by the staff of the Bateman Manuscript Project*. McGraw-Hill, New York, 1954.
- [100] W. L. Martinez and A. R. Martinez, *Computational Statistics with MATLAB[®] - Third Edition*. Chapman & Hall/CRC, Boca Raton, 2016.
- [101] K. I. Hopcraft, E. Jakeman and K. D. Ridley, *The Dynamics of Discrete Populations and Series of Events*. CRC Press, Boca Raton, 2014.
- [102] C. R. Tolle, T. R. McJunkin, D. J. Gorsich, An efficient implementation of the gliding box lacunarity algorithm. *Physica D*, **237**(3): 306–315, 2008.
- [103] R. A. Feagin, X. B. Wu and T. Feagin. Edge effects in lacunarity analysis. *Ecological Modelling*, **201**(3): 262–268, 2007. DOI:10.1016/j.ecolmodel.2006.09.019.
- [104] G. C. O'Neill, P. K. Tewarie, G. L. Colclough, L. E. Gascoyne, B. A. E. Hunt, P. G. Morris, M. W. Woolrich, M. J. Brookes. Measurement of dynamic task related functional networks using MEG. *NeuroImage*, **146**: 667–678, 2017.

- [105] D. R. Bickel. Estimating the intermittency of point processes with applications to human activity and viral DNA. *Physica A: Statistical Mechanics and its Applications*, **265**: 634–648, 1999.
- [106] R. K. Peet. The measurement of species diversity. *Annual Review of Ecological and Systematics*, **5**: 285–307, 1974. DOI: 10.1146/annurev.es.05.110174.001441.
- [107] C. E. Shannon. A mathematical theory of communication. *The Bell System Technical Journal*, **27**(3): 379–423, 1948. DOI: 10.1002/j.1538-7305.1948.tb01338.x.
- [108] L. Paninski. Estimation of entropy and mutual information. *Neural Computation*, **15**: 1191–1253, 2003.
- [109] K. Rajdl, P. Lansky and L. Kostal. Entropy factor for randomness quantification in neuronal data. *Neural Networks*, **95**: 57–65, 2017. DOI: 10.1016/j.neunet.2017.07.016.
- [110] Y. Gao, I. Kontoyiannis and E. Bienenstock. Estimating the Entropy of Binary Time Series. Methodology, Some Theory and a Simulation Study. *Entropy*, **10**: 71–99. DOI: 10.3390/entropy-e10020071.
- [111] J. M. Blackledge and N. Mosola. A statistically significant test to evaluate the order or disorder of a binary string. *2020 31st Irish Signals and Systems Conference (ISSC)*: 1–6, 2020. DOI: 10.1109/ISSC49989.2020.9180178.
- [112] T. Braun, V. R. Unni, R. I. Sujith, J. Kurths and N. Marwan. Detection of dynamical regime transitions with lacunarity as a multiscale recurrence quantification measure. *Nonlinear Dynamics*, **104**: 3955–3973, 2021. DOI: 10.1007/s11071-021-06457-5.
- [113] J. Antoni. Cyclostationarity by examples. *Mechanical Systems and Signal Processing*, **23**: 987–1036, 2009. DOI: 10.1016/j.ymsp.2008.10.010.

- [114] G. R. Toro and C. A. Cornell. Extremes of Gaussian processes with bimodal spectra. *Journal of Engineering Mechanics*, **112**(5): 465–484, 1986.
- [115] M. Grigoriu, Crossings of non-Gaussian translation processes. *Journal of Engineering Mechanics*, **110**(4): 610–620, 1984.
- [116] T. J. Kozubowski and K. Podgórski. Laplace Probability Distributions and Related Stochastic Processes, 105–145. In: *Probability: Interpretation, Theory and Applications*. Edited by Y. S. Shmaliy. Nova Science Publishers, 2011.
- [117] S. M. Cobb, The distribution of intervals between zero crossings of sine wave plus random noise and allied topics. *IEEE Transactions on Information Theory*, **11**(2): 220–233, 1965. DOI: 10.1109/TIT.1965.1053743.
- [118] HistData.com - Free Forex Historical Data. *Microsoft Excel GBP/USD M1 (1 Minute Bar) Data 2016*. [Online]. Available from: <https://www.histdata.com/download-free-forex-historical-data/?/excel/1-minute-bar-quotes/gbpusd/2016>. [Accessed August 2020].
- [119] J. B. Kadane, Sums of possibly associated Bernoulli variables: the Conway-Maxwell-Binomial distribution. *Bayesian Analysis*, **11**(2): 403–420. DOI: 10.1214/15-BA955.
- [120] A. Borisyuk and F. Rassoul-Agha, Quasiperiodicity and phase locking in stochastic circle maps: A spectral approach, *Physica D: Nonlinear Phenomena*, **288**: 30–44, 2014.
- [121] E. Simiu, *Chaotic Transitions in Deterministic and Stochastic Dynamical Systems*. Princeton University Press, Princeton, 2002.
- [122] B. T. y. Widemann. Kumaraswamy and beta distribution are related by the logistic map. arXiv:1104.0581, 2011.
- [123] L. Rossi and G. Girolami. Instantaneous frequency and short term Fourier transforms: Application to piano sounds. *The Journal of the Acoustical Society of America*, **110**: 2412, 2001. DOI: 10.1121/1.1409372.

- [124] J. M. Blackledge, R. E. Burge and N. R. Barratt. Phase imaging by real-zero conversion and its application to synthetic aperture radar. *Journal of Physics D: Applied Physics*, **20**: 1438–1444, 1987.
- [125] DLMF. *NIST Digital Library of Mathematical Functions*. <http://dlmf.nist.gov/>, Release 1.0.20 of 2018-09-15. F. W. J. Olver, A. B. Olde Daalhuis, D. W. Lozier, B. I. Schneider, R. F. Boisvert, C. W. Clark, B. R. Miller, and B. V. Saunders, eds.
- [126] C. M. Bender and S. A. Orszag, *Advanced Mathematical Methods for Scientists and Engineers I*. McGraw-Hill, New York, 1978.
- [127] H. Cohen, *Numerical Approximation Methods*. Springer, New York, 2011.